EXPERIMENTAL AND COMPUTATIONAL STUDY OF PERFORMANCE OF HIGHWAY EMBANKMENTS

by

Mehrdad Hassani

A dissertation submitted to the faculty of
the University of North Carolina at Charlotte
in partial fulfillment of the requirements
for the degree of Doctor of Philosophy in
Civil Engineering

Charlotte

2021

Approved by:

____
Dr. Miguel A. Pando

____
Dr. Rajaram Janardhanam

____
Dr. Vincent Ogunro

____
Dr. Lisa Schulkind

____
Dr. Jeff Kimble

ABSTRACT

MEHRDAD HASSANI. Experimental and computational study of performance of highway embankments. (under the direction of DR. MIGUEL A. PANDO)

Highway embankments require careful selection of the borrow material and construction practices. Most highway agencies in North America specify the soil selection criteria based on gradation or Atterberg limits. Furthermore, current construction practices also include specifications for the placement and compaction of the selected borrow materials. However, embankment material selection criteria and embankment construction specifications were discovered to be variant among the agencies. Some agencies use plasticity index requirement as the only specification regarding selection of embankment material. Some other agencies specify using dry unit weight of the compacted soil in the form of a ratio known as relative compaction (RC), as their main construction requirement. Although this traditional approach has resulted for the most part in safe embankments, there have been unsatisfactory performances in some cases. For example, longitudinal cracking and shallow slope failures have been reported for some embankments, despite the fact that material selection criteria and material placement criteria were met. Review of the literature reveals that in the process of embankment design, for the most part, no information is provided regarding embankment slope stability or, embankment allowable settlement.

In this dissertation, an alternative approach for the selection and placement of borrow soils for highway embankments has been investigated. The alternative approach is a performance-based methodology where the selection and placement of the candidate

borrow soil must meet performance criteria for slope stability and deformation levels. The study focused on five test soils from the Piedmont region of North Carolina. For each test soil, extensive laboratory testing was performed to allow assessment of the aforementioned performance criteria. This includes a series of analyses to assess slope stability and deformation levels both short-term and long-term. To investigate performance of embankments, soil strength parameters obtained from both total stress analysis (TSA) or undrained conditions and effective stress analysis (ESA) or drained conditions have been considered. A set of unconsolidated-undrained (UU) triaxial tests was used to obtain total stress soil strength properties, and a set of consolidated-undrained (CU) triaxial tests with pore pressure measurements was considered to achieve effective stress soil strength properties. Moreover, a set of one-dimensional creep compression tests were considered to study long-term deformation characteristics of embankment soil materials. Sixteen embankment geometric sections have been considered in total for the study. For the highway embankment deformation analysis, two-dimensional plane strain conditions were assumed. It is noted that the scope of this study considers only failures and settlements related to the highway embankment and not due to poor foundation soil conditions.

The study found that the proposed performance-based criteria is generally a viable alternative to the traditional approach. No cases showed that the TSA factor of safety was lower than the minimum value of 1.3. In many of the TSA cases, FS was well above the minimum value. However, in the effective stress stability analysis many cases were found to have FS lower than 1.3. Observed modes of failure consisted of non-shallow mode, local mode, and shallow mode. For the effective stress slope stability analysis, shallow failure (infinite) must be checked as there is a high likelihood for this mode of failure.

Some findings might give ground to the idea that soils with higher PI, such as Soil 2 (A-7-6 class), perform slightly better under saturated conditions. This finding may cast doubt on specifications set by some agencies to limit Atterberg limits of embankment material as a selection criterion. This fact may also reject the specifications which abandon using A-7 group soil as embankment material. Providing suitable vegetation cover as well as drainage systems (to reduce infiltration and promote runoff, respectively) for the highway embankments could be useful measures in avoiding the detrimental effects of the water presence in the body of embankment. There was no strong evidence indicating that the soils with higher PI had a higher creep rate. The creep rate of 6×10^{-6} %/min may be introduced as a rough number for the silty soils compacted at optimum moisture content which were studied in this research.

ACKNOWLEDGMENTS AND DEDICATION

First, I would like to thank my family and friends; whom without their support and encouragement this could not be possible.

This research is associated with a project funded by the North Carolina Department of Transportation; NCDOT's support is appreciated.

Many thanks are due to Dr. Miguel Pando who has been an incredible advisor throughout this research. Dr. Rajaram Janardhanam's patience and support as the Principal Investigator (PI) of the project and a committee member is highly appreciated. I would also like to thank other committee members Dr. Vincent Ogunro, Dr. Lisa Schulkind, and Dr. Jeff Kimble.

This work is dedicated to Imam Hussain, his brother Abbas, and his loyal companions who fought to death to support justice in 680 A.D. in Karbala, Iraq, and to my lord, MAHDI.

TABLE OF CONTENTS

CHAPTER 3: RESEARCH METHODOLOGY

CHAPTER 4: LABORATORY TESTING PROGRAM

CHAPTER 5: SLOPE STABILITY ANALYSIS

CHAPTER 6: DEFORMATION ANALYSIS

CHAPTER 7: FINAL ACCEPTANCE ZONES

CHAPTER 8: SUMMARY AND CONCLUSIONS

LIST OF FIGURES

LIST OF TABLES

LIST OF SYMBOLS AND ABBREVIATIONS

FHWA	Federal Highway Administration
AASHTO	American Association of State Highway and Transportation Officials
ASTM	American Society for Testing and Materials
USDOT	United States Department of Transportation
NCDOT	North Carolina Department of Transportation
NC	North Carolina
MC	moisture content (same as water content) of soil sample, also denoted by w, unit: %
w	moisture content of soil sample, unit: %
OMC	optimum moisture/water content obtained in a standardized laboratory compaction test, unit: %, also denoted by w_{opt}
g_m	total / moist unit weight of material, unit: kN/m^3
g_d	dry unit weight of material, unit: kN/m^3
$g_{d\max}$	maximum dry unit weight obtained in a standardized laboratory compaction test, unit= kN/m^3
MDD	maximum dry density (expressed in terms of mass per unit volume) obtained in a standardized laboratory compaction test, unit: kg/m^3, $g_{d\max}$ = MDD*g (g= gravity acceleration= 9.807 m/s^2)
RC	relative compaction which is the ratio of dry unit weight (or dry density if expressed in terms of mass per unit volume) achieved after compaction in the field to $g_{d\max}$
PI	plasticity index
LL	liquid limit
m	meter
ft	foot/feet
in	inch/inches
H	height of embankment
S	side slope of embankment; stated as the ratio of horizontal step to vertical step, for instance for 4H:1V embankment, S would be equal to 4
TSA	total stress analysis
ESA	effective stress analysis
TSA,m	modified total stress analysis
UU	unconsolidated-undrained triaxial test
CU	consolidated-undrained triaxial test
FS	factor of safety in slope stability analysis
Sr	saturation ratio / saturation degree of soil specimen
f_{UU}	total stress friction angle of soil material obtained from UU triaxial test, unit: degrees
C_{UU}	total stress cohesion of soil material obtained from UU triaxial test, unit: kPa
E_{UU}	modulus of elasticity of soil material obtained from UU triaxial test, unit: kPa

f'	effective stress friction angle of soil material obtained from CU triaxial test, unit: degrees
C'	effective stress cohesion of soil material obtained from CU triaxial test, unit: kPa
E_{CU}	modulus of elasticity of soil material obtained from CU triaxial test, unit: kPa
s_{cell}	all-around cell pressure in a UU triaxial test, also known as confining pressure
s'_{C}	effective consolidation pressure in a CU triaxial test
s_{df}	peak or maximum deviator stress
ν	Poisson's ratio

CHAPTER 1: INTRODUCTION

1.1 Introduction and Background

This dissertation investigates the suitability of a performance-based design for the selection and placement of borrow soils for the highway embankments. Performance of the embankments is mainly related to two concerns: slope stability and deformation. Each of these two concerns should be reviewed under different types of material properties: undrained behavior conditions, and drained behavior conditions. Moreover, it is useful to take into account immediate and long-term deformation characteristics. This study also presents a review of state-of-practice of the embankment material selection specifications and embankment construction specifications. At the end of document, recommendations are made for material selection (based on the AASHTO soil classes) and construction practices. After this short explanation about the current study, a brief background about highway embankments is presented in the rest of this section.

Embankment refers to a mass of earthen material that is placed in specific layers and compacted for the purpose of raising the grade of a roadway (or railway) above the level of the existing surrounding ground surface and for providing a suitable and strong foundation for the upper layers of the roadway. A typical highway section ideally consists of the upper road sections (i.e., pavement, base and subbase), subgrade, embankment, and the underlying foundation. Figure 1.1 depicts a typical section of the highway embankment which shows subgrade, embankment, and foundation. Embankment height, and embankment side slope (horizontal step versus vertical step) are also depicted in this figure.

The subgrade is shown as an independent layer in this figure (not part of the embankment). In reality, the subgrade is a layer that is considered semi-infinite. In other words, the subgrade is the same as the embankment. In practice however, many of the highway embankment standard specifications require that the upper few feet of an embankment be built at higher compaction levels and/or with material of higher quality (Hassani et al. 2017). For the purpose of this research, this upper section is referred to as "subgrade" and is considered an independent layer from the embankment. In other words, the scope of this study does not include pavement and subgrade. Furthermore, the foundation soil is assumed to be adequately compacted and competent, so that it does not influence slope stability or deformation performance of the highway embankment.

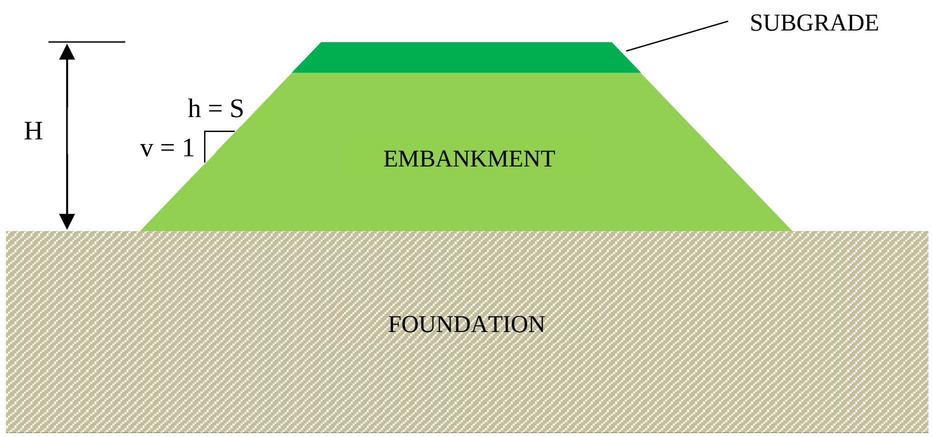

Figure 1.1. Schematic section of a highway embankment

Design of highway embankments involves several considerations such as geotechnical investigation of the foundation, geometry design, assessment and selection of the candidate borrow soil, and considerations for placement and construction procedures. It is noted that out of these factors, geotechnical investigation of the foundation is out of the scope of this study. The rest of items in the mentioned list will be discussed briefly in the following.

The embankment geometry may be simply defined by the height and side slope. Most of the agencies consider embankments higher than 40 ft or 50 ft as high embankments (NCHRP 1971). Concerns regarding high embankments are out of the scope of this research. In highway embankment practice, slopes as steep as 2H:1V are common, but in this research, 1H:1V slope will also be considered. Selected numerical values for the side slope and the height of embankments considered in this study are reviewed in upcoming chapters.

Regarding selection of the borrow material, standards usually specify that the soil meets some qualifications, including but not limited to the soil gradation, Atterberg limits (PI and LL), maximum organic content, and being capable of achieving a certain minimum dry density in the field (Hassani et al. 2017). These specifications are reviewed in the literature review chapter.

Specifications regarding the embankment construction try to address the following three questions:

- How shall embankments be placed?
- What is the acceptable range of moisture content in the field?
- How shall embankments be built and compacted?

In the standards for embankment construction, the first question in this list is usually addressed with the concept of lift thickness, the second question is dealt with by moisture control specifications, and the third question is addressed by means of compaction control specifications. However, after reviewing the literature, specifications regarding embankment material selection and embankment construction were found to vary significantly among agencies.

Dealing with the subject of highway embankments, failures and different mechanisms should be addressed as well. Failures of the embankments can be divided into two main categories: deep-seated failure and shallow failure. A deep-seated failure refers to a case in which the critical slip surface passes through both embankment and foundation. In such cases, the problem usually starts with the foundation as it is softer than the embankment and deforms more than the embankment under the self-weight and service loads. On the other hand, if the critical slip surface passes through only the body of embankment, it will be categorized as a shallow failure. According to Khan et al. (2015), shallow failure is a major issue for slopes constructed with high-plastic clayey soil. It is reminded that the scope of this study considers only failures and settlements related to compacted embankment, not due to poor foundation soil conditions.

1.2 Problem Statement and Research Objectives

Although extensive knowledge and research is available about highway embankments, there are still ambiguities regarding some aspects of these structures, such as material selection criteria; shallow slope failures; best performance-based design practices; and long-term performance of these soil structures.

Among the agencies dealing with highway embankments, there are few which set specifications regarding material selection. However, it can be seen that requirements on the Atterberg limits are more prevalent than those of related to the gradation. Specifications of the Atterberg limits are stated in terms of plasticity index (PI) and liquid limit (LL). Table 1.1 presents a summary of states specifying Atterberg limits as material selection criteria. In fact, a trend to limit the PI (or generally Atterberg limits) of soil material to a maximum value can be seen among the standard specifications. This concept is schematically illustrated on a Casagrande chart in Figure 1.2. It seems this type of specification has caused some issues such as construction delays and cost overruns. However, specifying a threshold Atterberg limit is thought to be a measure for controlling the long-term deformation of embankment material (based on an instance stated in Samtani and Nowatzki 2006a). Authenticity of this approach and further consequences of this specification need to be investigated.

Table 1.1. Summary of states specifying Atterberg limits as material selection criteria (from Hassani et al. 2017)

State	Reference	Specification
Delaware	Delaware DOT (2016)	LL of borrow ≤ 40
Louisiana	Louisiana DOT (2016)	11 ≤ PI ≤ 25
North Carolina	North Carolina DOT (2012)	PI ≤ 15 for coastal area; PI ≤ 25 for Piedmont and Western area
Ohio	Ohio DOT (2016)	LL < 65
Pennsylvania	Pennsylvania DOT (2016)	for soil (fine-grained portion): LL < 65; if 41 < LL < 65: PI ≥ LL-30
Texas	Texas DOT (2014)	LL ≤ 45, PI ≤ 15 for granular material
Washington	Washington DOT (2016)	if 12.1 ≤ P200 ≤ 35, PI ≤ 6 if 35.1 < P200, PI = 0

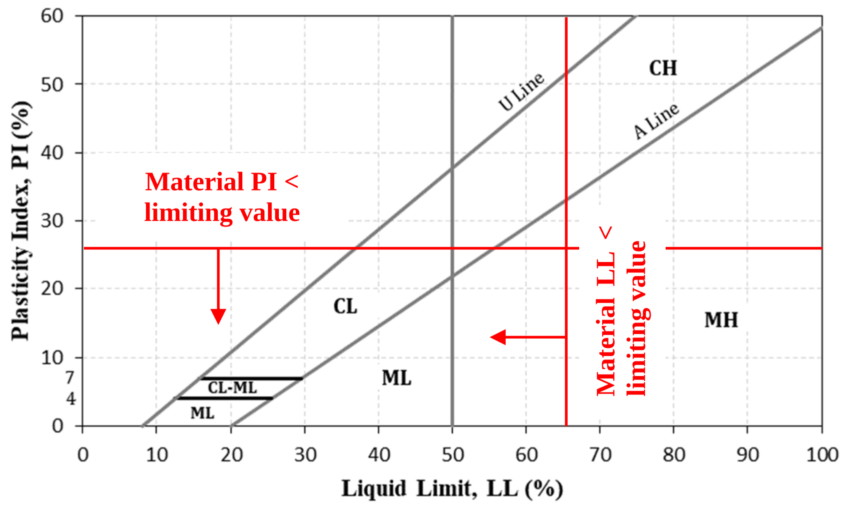

Figure 1.2. Casagrande chart schematically showing common type of specification set by some agencies

As it will be discussed in the literature review chapter, shallow slope failure is a common form of failure for the highway embankments. Figure 1.3 shows longitudinal cracking at North Carolina I-540. These cracks on the surface of the embankment are usually accompanied by bulging of the side slope or toe, and eventually lead to a surficial failure. The soil at this site is highly plastic silt with LL= 58 and PI= 21. The longitudinal cracking issue happened despite the fact that the soil material met the local material selection standards (Hassani et al. 2017; North Carolina DOT 2000). This case will be reviewed in more detail in the in the literature review chapter.

However, if the material selection criteria are fully met, minimum factor of safety (FS) against sliding is observed, and settlement of embankments is in the acceptable range, why are these failures seen commonly in the field? This is one of the paramount questions this study tries to address.

Figure 1.3. Longitudinal cracking at NC I-540 at Davis Drive (Pilipchuk 2008)

Specifying dry unit weight of the compacted soil seems to be almost the only design criterion for highway embankments set by many agencies. This fact along with the state-of-practice of highway embankment design procedure is addressed in the rest of this section.

During the construction of embankments, field observation and quality control are usually performed by means of measuring dry unit weight in the field and comparing it with the maximum dry unit weight ($g_{d\max}$) that can be achieved in a standard laboratory compaction test. This observation is usually performed using a parameter called relative compaction (RC) which is defined as the ratio of dry unit weight (or dry density if expressed in terms of mass per unit volume) achieved after compaction in the field to the $g_{d\max}$. For instance, a minimum RC of 95% is a common construction specification followed by many agencies. The concept of relative compaction (RC) is demonstrated in Figure 1.4a. Figure 1.4a also shows a compaction curve, features of the optimum point (that is $g_{d\max}$ and optimum moisture content [OMC]), and zero air voids line. Needless to say that we are borrowing the well-known compaction concept from Ralph Proctor (Proctor 1933).

It is noted that the energy level which is considered as a comparison basis and is utilized to obtain $g_{d\max}$, is also significant since a compaction test may be performed at two different energy levels of Standard Proctor or Modified Proctor. Standard Proctor and Modified Proctor compaction tests are respectively described by AASHTO T 99 (AASHTO 2015a) and AASHTO T 180 (AASHTO 2015b).

Traditional quality control of embankment construction is depicted in Figure 1.4. Figure 1.4a shows the basic approach for embankment compaction control. In this figure are two curves and one shaded area. The lower curve is a typical compaction curve and the upper curve is the dry unit weight of the soil sample assuming 100% saturation (zero air voids line). The zero air voids curve is in fact an upper limit on the moisture content-dry unit weight domain. The shaded area is an acceptable zone based on a minimum RC of 95%.

Some agencies only require that the RC must be higher than a minimum value, without considering specific range for placement moisture content (Figure 1.4a). While, as shown in Figure 1.4b, other agencies specify a range for placement moisture content besides achieving a minimum RC.

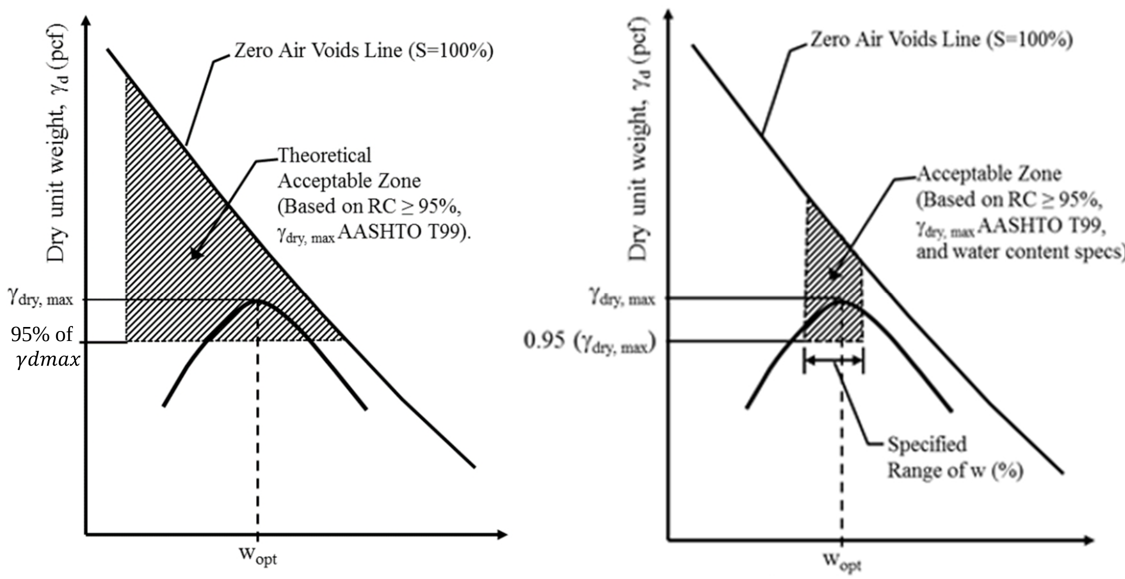

(a) without specified placement moisture content (b) with specified placement moisture content

Figure 1.4. Two types of specifications for compaction of highway embankments
(adopted from Janardhanam and Pando 2015)

We just stated that embankment construction specifications for the most part consist of either setting a minimum value of RC without moisture control, or setting a minimum value of RC along with moisture control. In either case of the two mentioned conventional embankment compaction/placement quality control, no information is examined regarding the embankment slope stability and/or the embankment allowable settlement. This lack of information might be a critical shortcoming of the current design approach.

Addressing the stated concerns and shortcomings would require an "Experimental and Computational Study of Performance of Highway Embankments"[1]. Based on the statement of the problem, the main objectives of this study may be listed as the following five items. The five main objectives are addressed throughout the dissertation and might be referred to using the assigned numbers. Moreover, at the end of Chapter 3 research

[1] Title of this dissertation

tasks as well as the connection between research objectives and research tasks are presented.

1. Review of the standards and literature in terms of embankment material selection criteria and embankment construction specifications;

2. Investigation of the slope stability of highway embankments under the two states of undrained and drained;

3. Investigation of the deformation characteristics of highway embankments under both undrained and drained conditions, as well as long-term deformation characteristics of highway embankments;

4. Investigation of the possibility of new material selection criteria and new acceptance zones on moisture content-dry unit weight domain according to the performance-based design approach;

5. Verification of specifications set by a number of agencies regarding Atterberg limits (PI and LL) and gradation as material selection criteria.

1.3 Organization of Dissertation

This document consists of eight chapters and nine appendices. In Chapter 1, an introduction about highway embankments and a statement of the problem are respectively presented and discussed. The literature review is represented in Chapter 2 where topics such as review of specifications regarding highway embankment material selection, specifications on highway embankment construction, case histories of road and highway embankment failure, specifications on highway embankment design, and creep of compacted soils are discussed.

Chapter 3 presents the governing research methodology. At the end of chapter, extended research objectives and tasks, and their relationship with each other are presented as well. Laboratory testing procedure and results are given in Chapter 4. This includes results for index tests, compaction tests, unconsolidated-undrained triaxial compression tests, consolidated-undrained triaxial compression tests, and one-dimensional creep compression tests.

In Chapters 5 and 6, slope stability analysis and deformation analysis are discussed, respectively. Each chapter first explains the approach, then presents the results. Chapter 7 presents the final acceptance cases.

Chapter 8 brings the document to the end with the summary, conclusions, and recommendations for future work. In addition, the nine appendices at the end of the document provide more details and supporting information about the topics discussed in this research.

CHAPTER 2: LITERATURE REVIEW

2.1 Introduction

An extensive literature review has been carried out to cast light on different aspects of this research, namely: i) review of specifications regarding highway embankment material selection and embankment construction, ii) specifications regarding highway embankment design (slope stability and settlement), iii) case histories of road and highway embankment slope failures, and iv) creep of compacted soils.

At the end of chapter, summary of literature review and identified knowledge gaps concludes the chapter.

2.2 Review of Specifications for Highway Embankments

This research study entails a proposed performance-based methodology for the selection and placement of borrow soils for highway construction. Thus, it is necessary to review the commonly used specifications for selection, construction, and design of highway embankments. Reviewing this information will also help us to find any possible gap or shortcoming which exists in the current standards dealing with highway embankments. Therefore, this section presents a summary of the findings of a state-of-the-practice study performed as part of a NCDOT funded project that was the basis of this doctoral research. A synopsis of the state-of-the-practice study by Hassani et al. (2017) is presented in Appendix A. In addition, this section also presents specifications related to the design of highway embankments, including specifications regarding minimum factor of safety for slope stability, and specifications regarding settlement of the highway embankments. The following subsections will present the key lessons related to the specifications regarding material selection, specifications regarding embankment placement and construction, and specifications regarding embankment design.

2.2.1 Summary of Specifications Regarding Material Selection

Reviewed components regarding material selection include material gradation/classification, and Atterberg limits. The readers are referred to the Appendix A for detailed information about this topic.

2.2.1.1 Requirements on Material Gradation

Only a few of the agencies have minor requirements set for material gradation. These include Colorado, Ohio, Rhode Island, South Carolina and Utah. In all cases, these requirements are very general; for instance, South Carolina (South Carolina DOT 2007) specifies that A-7 group soil shall not be used. Figure 2.1 shows states imposing requirements on gradation.

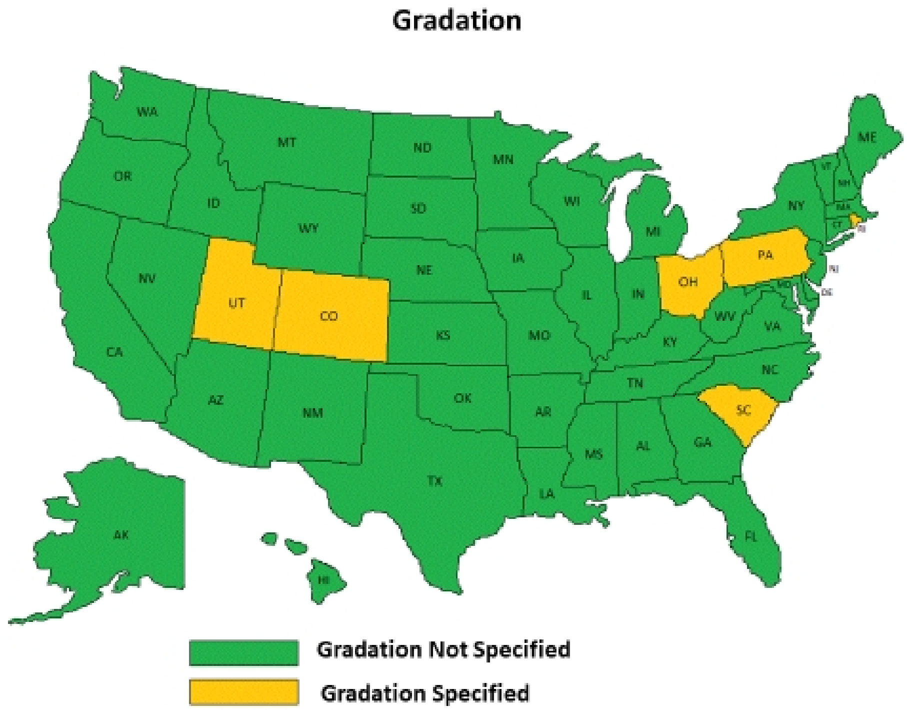

Figure 2.1. States imposing requirements on gradation as material selection criterion (from Hassani et al. 2017)

2.2.1.2 Requirements on Material Atterberg Limits

Seven states including Delaware, Louisiana, North Carolina, Ohio, Pennsylvania, Texas and Washington have specifications on the Atterberg limits required for the material used in embankments. Figure 2.2 shows states imposing requirements for Atterberg limits. Among these states we can mention North Carolina: current specifications require that the plasticity index stay below 15% for coastal area, and below 25% for Piedmont and Western

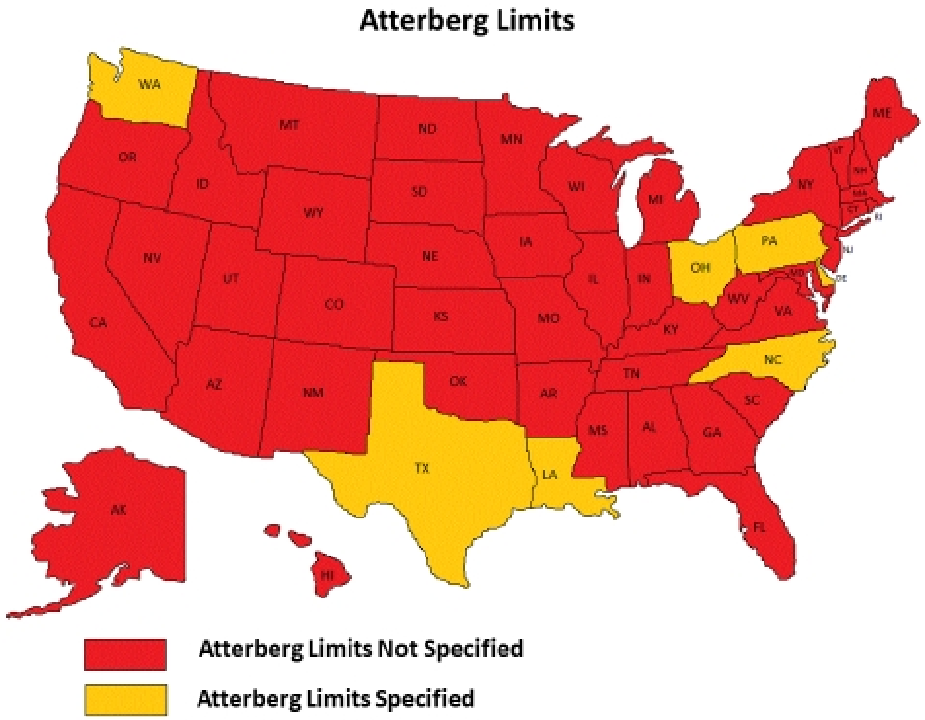

areas.

Figure 2.2. States imposing requirements on Atterberg limits as borrow material selection criteria

(from Hassani et al. 2017)

Table 2.1 summarizes information for U.S. states which use Atterberg limits as embankment material selection criteria.

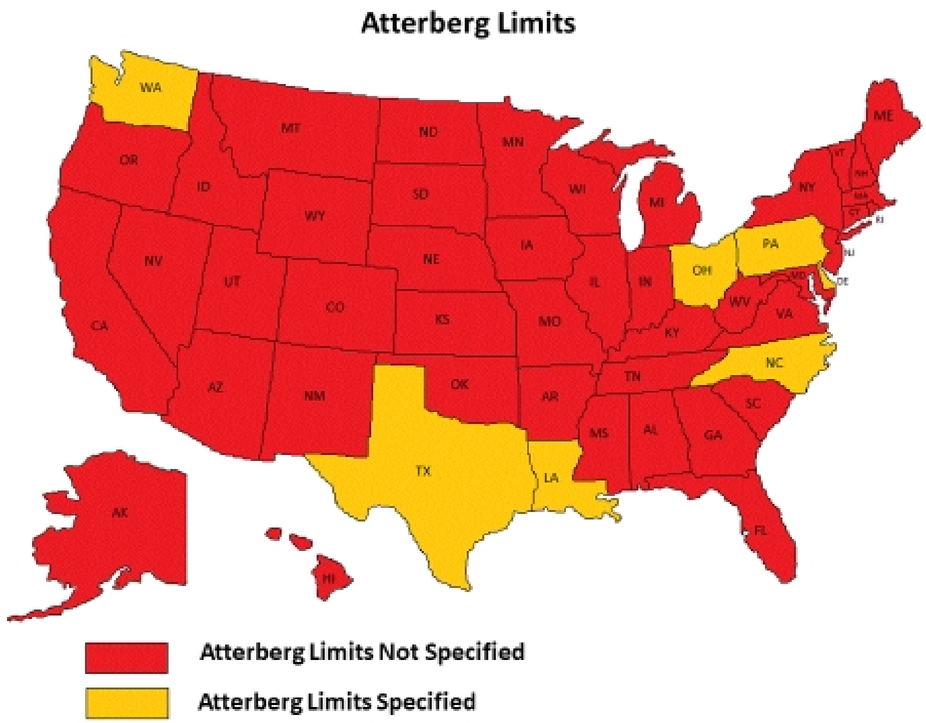

Figure 2.2. States imposing requirements on Atterberg limits as borrow material selection criteria (from Hassani et al. 2017)

Table 2.1. Summary of states specifying Atterberg limits as material selection criteria (from Hassani et al. 2017)

State	Reference	Specification
Delaware	Delaware DOT (2016)	LL of borrow ≤ 40
Iowa	Iowa DOT (2015)	PI > 10, for select cohesive soils
Louisiana	Louisiana DOT (2016)	11 ≤ PI ≤ 25
North Carolina	North Carolina DOT (2012)	PI ≤ 15 for coastal area; PI ≤ 25 for Piedmont and Western area
Ohio	Ohio DOT (2016)	LL < 65
Pennsylvania	Pennsylvania DOT (2016)	for soil (fine-grained portion): LL < 65; if 41 < LL < 65, PI ≥ LL-30
Texas	Texas DOT (2014)	LL ≤ 45, PI ≤ 15 for granular material
Washington	Washington DOT (2016)	if 12.1 ≤ P200 ≤ 35, PI ≤ 6 if 35.1 < P200, PI = 0

Moreover, in a document by Samtani and Nowatzki (2006a) which provides guidelines regarding material selection for structural backfill for bridge abutments, the authors specify limiting the PI of the structural backfill to 10%. The PI is limited to this value to control the long-term deformations.

2.2.2 Summary of Specifications Regarding Construction

In this section a review of the specifications and requirements set by different agencies regarding highway embankment construction is presented. Reviewed components regarding construction include any requirements on minimum field dry unit weight and relative compaction (RC), moisture control, and lift thickness. The synopsis presented in Appendix A will include detailed information about this topic.

2.2.2.1 Requirements on Minimum Field Dry Unit Weight and Relative Compaction

Nine states (Colorado, Delaware, Georgia, Indiana, Maryland, Michigan, Ohio, Pennsylvania and South Carolina) have specifications limiting the minimum dry unit weight of material placed in highway embankment. Reader is referred to Appendix A for detailed information.

The majority of states require achieving a minimum relative compaction specified with respect to a laboratory standard compaction test, such as Standard Proctor (AASHTO T 99) or Modified Proctor (AASHTO T 180).

Of all the fifty states reviewed, thirty-three (33) states somehow state that maximum laboratory dry unit weight ($g_{d\max}$) shall be obtained in accordance with AASHTO T 99, that is Standard Proctor energy. Twenty three (23) of these states necessitate reaching exactly the minimum relative compaction of 95%, while others range from minimum RC of 90% to 102%. FHWA [FHWA (2006)] and AASHTO [AASHTO (2012)] also require compacting embankments to RC ≥ 95% while $g_{d\max}$ obtained at standard energy level. This fact may justify the high number of states sticking to AASHTO T 99. Table 2.2 summarizes compaction energy level distribution among states and Figure 2.3 shows compaction energy level specifications by each state across the U.S.

Table 2.2. Summary of compaction energy required by states (from Hassani et al. 2017)

Energy Level	Number of States
Standard Proctor	33
Modified Proctor	8
Standard/Modified Proctor	5
roller controlled	2
not mentioned	2

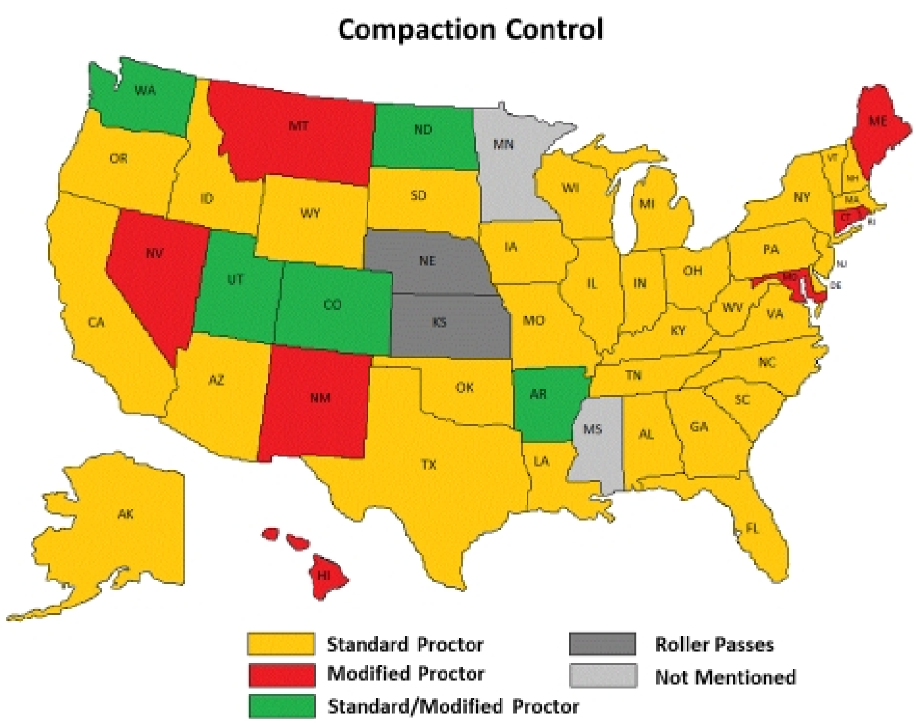

Figure 2.3. Compaction energy specifications by state (from Hassani et al. 2017)

2.2.2.2 Requirements on Moisture Content Control

Twenty seven (27) states have specified some kind of criteria as the moisture content control. These requirements are in most of cases as an acceptable range for placement moisture content. The requirements differ based on the material gradation, Atterberg limits of material, moisture content of material itself, and level or energy of compaction. Ten (10) states have specified acceptable moisture content in the range of ±2% of optimum moisture content.

2.2.2.3 Requirements on Lift Thickness

A lift thickness of 8" in loose state is required by 31 states, while two of the agencies require same 8" lift thickness but measured after compaction. Majority of the states consider lift thickness in loose state. It is noted that maximum accepted lift thickness is 12", while the minimum is 4" loose measurement in Washington that is for the top 2 feet of embankment. Lift thickness specifications requirement is summarized and illustrated in Figure 2.4.

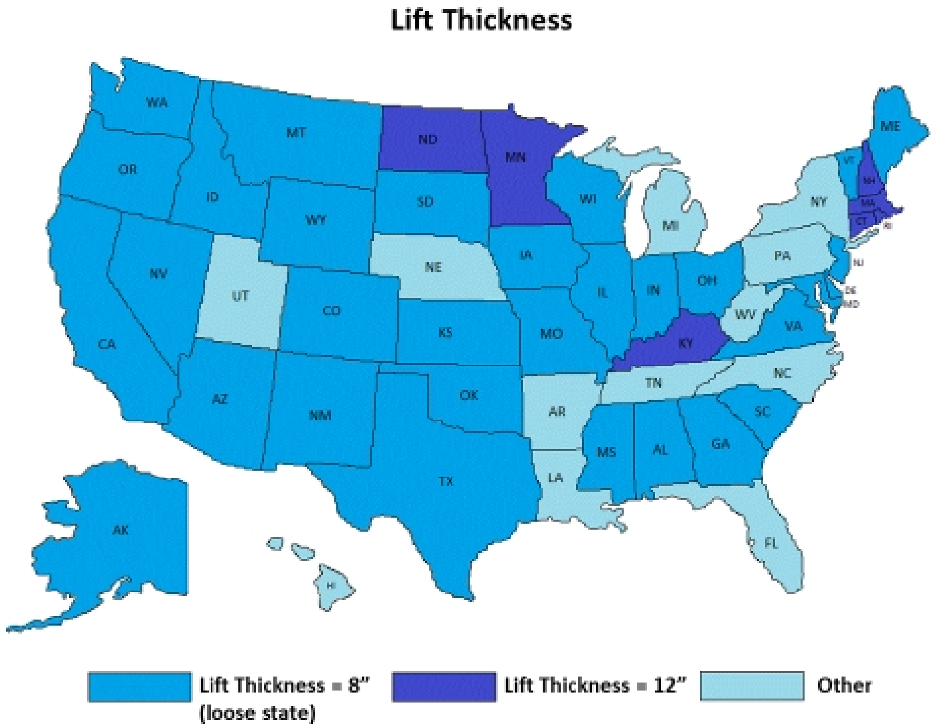

Figure 2.4. Variation of lift thickness specifications by state (from Hassani et al. 2017)

2.2.3 Review of Specifications Regarding Highway Embankment Design

2.2.3.1 Minimum Factor of Safety for Slope Stability

Traditional factors of safety for embankment at the end-of-construction condition are 1.3 to 1.5 (NCHRP 1989). For the purpose of this research project FS=1.3 is selected as the minimum FS for both TSA and ESA conditions.

2.2.3.2 Settlement of Highway Embankments

In the technical literature dealing with highway embankments one can observe that large portion of the available literature focuses on the settlement of embankment foundation and ignores settlement of the embankment itself.

The amount of settlement which is an immediate response to the embankment loading is termed initial settlement. This settlement is compensated during embankment construction, that is when next layers of fill are placed, the embankment is brought up to the design grade level. Thus, initial settlement does not affect the final embankment elevation (Ladd and Foott 1977).

Soriano (2013) states that for high embankments founded on firm ground (hard soils or rocks), long-term settlements and deformations can also cause some problems. This can happen due to creep deformations of the fill material of the embankment.

If post-construction settlements are uniform and are in the order of 0.3 to 0.6 m (1 to 2 ft) during the economic life of a roadway, and occur slowly over a period of time, and do not occur next to a pile-supported structure, they are considered acceptable. If post-construction settlement occurs over a long period of time, it provides the possibility of repair of any pavement distress caused by embankment settlement. The repair could also happen when the pavement is resurfaced. Although rigid pavements have performed well after 0.3 to 0.6 m (1 to 2 ft) of uniform settlement, flexible pavements are usually selected where there is question whether the post-construction settlements are uniform or not. However, some U.S. states utilize a flexible pavement when predicted settlements exceed 150 mm (6 in.) (NCHRP 1975; Stark et al. 2004).

Virginia manual of instructions states that total vertical settlement of embankment fill and underlying native soil shall be less than 2 inches over the initial 20-years, and less than 1 inch over the initial 20-years within 100 ft of bridge abutments (Virginia DOT 2014).

North Carolina DOT (2012) defines the rut as “a surface depression in the wheel path(s) or at the edge of pavement”. Rutting comes from a pavement deformation in any of the pavement layers or in the subgrade, usually caused by consolidation or lateral movement of the materials due to traffic loads. Movement in the mix in hot weather or inadequate compaction during construction is the main cause of rutting. It also reports rutting of 1 inch deep or greater as a severe rut.

Soriano (2013) reports on the geotechnical investigation of the construction of some embankments for the A24 motorway in north of Portugal. Vertical displacements after 22 months of observation have been very small, less than 0.1% of the embankment heights, that means “allowing to forecast a good performance in the future”.

At the end of this section some points about the settlement of highway bridge approaches are presented. These studies at least imply that in other sections of an embankment (which is the subject of the current research project) the settlement can be in the same order or a little more than following values.

NCHRP (1990) suggests a differential settlement of 13 mm (0.5 inch) is likely to require maintenance in highway bridge approaches.

When approach slabs are not used, many scholars [e.g., Zaman et al. 1995; Stark et al. 1995; Long et al. 1998] suggest the allowable differential settlements at the embankment-structure interface to be between 12 and 75mm (0.5 - 3 in.).

Samtani and Nowatzki (2006b) report that according to NCHRP (1983) differential vertical movements of 2 to 4 inches (50 to 100 mm), depending on span length, appear to be acceptable, assuming that approach slabs or other provisions are made to minimize the effects of any differential movements between abutments and approach embankments.

Finally, summary of some of the provided information is presented in Table 2.3. It is noted that the value of one inch (1 in.) is selected as the allowable non-uniform settlement for highway embankments in this research.

Table 2.3. Summary of the literature review on allowable settlement for highway embankments

Reference	Reported/Allowable settlement	Description
NCHRP (1975)	0.3 to 0.6 m (1 to 2 ft)	allowable uniform settlements, but not next to a pile-supported structure;
	150 mm (6 in)	in this case flexible pavement is selected by some U.S. states;
NAVFAC (1986)	0.1-0.2% of H in 3 to 4 years 0.3-0.6% of H in 15 to 20 years	range of secondary compression as a source of embankment settlement; significant only in high embankments; larger values in each range belong to fine-grained plastic soils;
Virginia DOT (2014)	50 mm (2 in)	total vertical settlement; embankment fill and underlying native soil; over the initial 20 years;
	25 mm (1 in)	total vertical settlement; embankment fill and underlying native soil; over the initial 20 years; within 100 ft of bridge abutments;
Khan et al. (2015)	3.8% of H	in a control section which indicated failure; total vertical settlement;
	0.5-1.4% of H	in reinforced sections; total vertical settlement; indicated good performance;
Soriano (2013)	0.1% of H	within 22 months after construction which allows to forecast a good performance in future;
	0.5-1.0% of H	some recommended side slopes; during the first 5-10 years of operation;
North Carolina DOT (2012) *	25 mm (1 in)	considered severe rut in the pavement;
NCHRP (1990) *	13 mm (0.5 inch)	differential settlement for highway bridge approaches;
Zaman et al. 1995; Stark et al. 1995; Long et al. 1998 *	12-75 mm (0.5-3 in)	at embankment-structure interface; when approach slabs are not used;

* Some of the cases mentioned in this table are not directly related to allowable settlement for highway embankments, but they can be used as a guide in this regard.

2.3 Case Histories of Road and Highway Embankment Failure

2.3.1 Introduction and Discussion of Embankment Failure Case Histories

The main purpose of this section is to present a summary of case histories of embankment failures in which the failure surface involves only the highway embankment. Shallow slope failure is a major issue for embankment slopes; particularly for embankment constructed with high plastic clayey soils (Khan et al. 2015).

Review of the literature yielded several case histories of shallow slope failures of highway embankments which will be discussed in the following sections. As mentioned before, these reported slope failure case histories are only for failures through the highway embankment and do not involve any other factors or issues outside the scope of this study, such as issues associated with the embankment foundation.

The third case history in Haywood County, North Carolina is skipped for the purpose of this section as it was mostly triggered due to the acidic runoff from bedrock and other issues related to the foundation of embankment. The studied failures are depicted on the map of Atterberg limits requirements and compaction requirements, respectively. It is noted that these maps were introduced in the sections that reviewed specifications of the highway embankments.

In fact, we are trying to find any possible relationship between failures and imposed requirements by the states. This effort is presented in Figure 2.5 and Figure 2.6. However, it seems reviewing this information does not let us make a strong conclusion about any possible pattern among failures. Of course, in most of the cases failures happen in fields where use Standard Proctor energy as field quality control, but since high percentage (33 out of 50 = 66%) of U.S. states already use standard energy as compaction quality control, we cannot necessarily attribute shallow failures to the locations where use Standard Proctor. The identified case histories are finally summarized in Table 2.4.

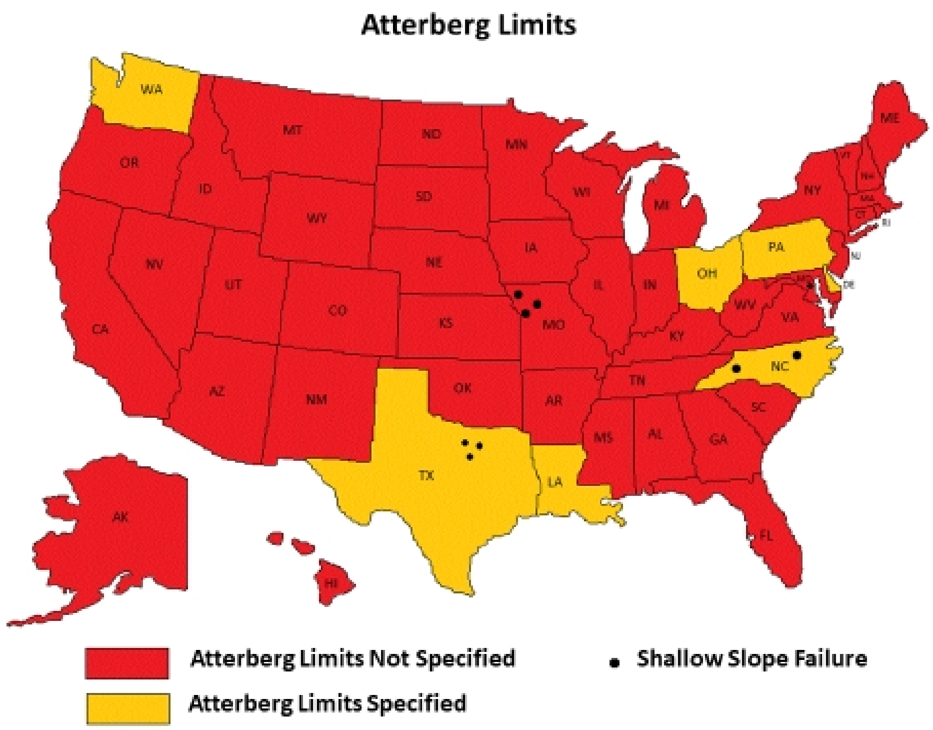

Figure 2.5. Failure cases on the map of Atterberg limits requirements

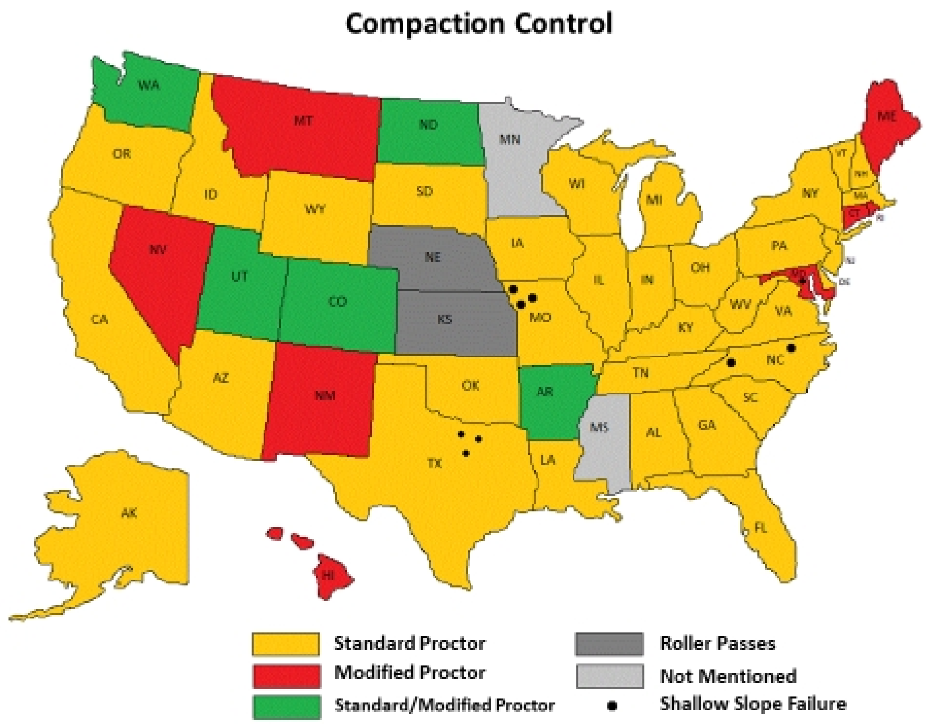

Figure 2.6. Failure cases on the map of compaction requirements

The identified case histories are summarized in Table 2.4. As indicated in this table, the three following reasons may be counted as the main sources of the issue of shallow slope failures. Heavy rainfall events, poor compaction of shoulders of the road in the vicinity of utility cuts, acidic runoff and instability associated with graphitic-sulfidic bedrock. It is noted that out of these three identified reasons, the heavy rainfall events have the largest share as the triggering factor.

Table 2.4 summarizes most important and paramount facts about the case histories. Figure 2.7 (a) and (b) also show distribution of case histories of shallow slope failures presented in this chapter with respect to embankment height and embankment side slope, respectively. The unit for embankment height is feet and the unit for embankment side slope is degrees in these figures. It can be seen that a big portion of reported failures have occurred in embankments higher than 35 ft, and embankments having side slopes between

20° (2.7H:1V) and 30° (1.7H:1V). The following subsections will present a more detailed discussion for each case history listed in Table 2.4.

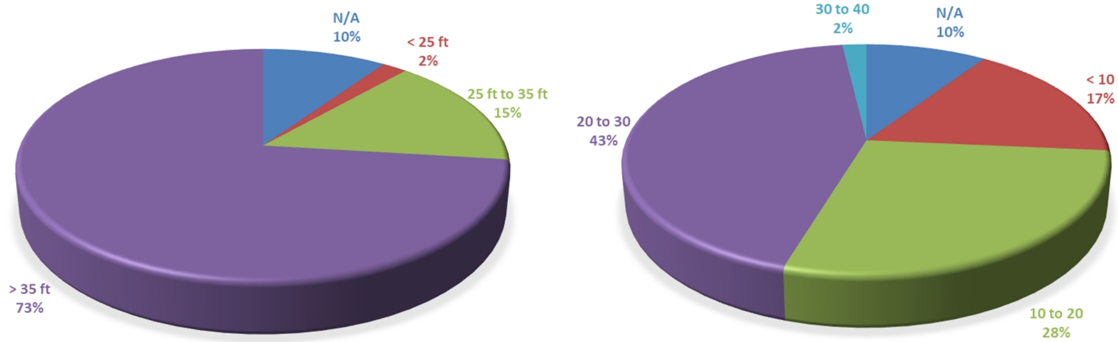

(a) shallow slope failure distribution with embankment height (feet)

(b) shallow slope failure distribution with embankment side slope (degrees)

Figure 2.7. Statistics of case studies of highway embankment shallow slope failure

Table 2.4. Summary of embankment failure case histories

Case history	Reference	n	H	S (slope)	Soil description	Field compaction requirement (construction)	Failure description
I-540 at Davis Drive, NC, inside shoulder	Pilipchuk (2008)	1	16.8 m (55 ft)	2H:1V	MH with LL= 58 and PI= 21	RC ≥ 95%, Standard Proctor	longitudinal cracking caused due to strength loss after wetting-drying cycles
I-540 at Davis Drive, NC, outside shoulder	Santee (2019)	1	16.8 m (55 ft)	2H:1V	MH with LL= 58 and PI= 21	RC ≥ 95%, Standard Proctor	It was 2.1-3.0 m (7-10 ft) deep at worst location; happened after an intense rain event; the failure was repaired by rock plating
Embankment failures from the shoulder of roadway, NC (several cases)	Appalachian Landslide Consultants (2013)	1	N/A	N/A	silty and clayey soil	RC ≥ 95%, Standard Proctor	most common type of road embankment failure seen in western North Carolina; shallow slope failures; poor compaction near utility buried outside shoulders; triggered by rainfall
Maryland investigation (several cases)	Aydilek and Ramanathan (2013)	43	refer to text	refer to text	N/A	RC ≥ 92%, Modified Proctor	50% of failures were on slopes with sand formations, and 39% of slope failures occurred on slopes with gravel formations; majority of failures happened on steep slope angles between 20° (2.7H:1V) and 30° (1.7H:1V); 90% surficial erosion failures; 80% occurred during or after rainfall
U.S. Highway 287, Texas	Khan et al. (2015)	1	9.15 m (30 ft)	3H:1V	high-plastic clayey soil (CH); LL= 48-79 and PL= 25-51; with shrink/swell characteristics	RC ≥ 98%*, Standard Proctor	instrumented equipment showed movement after a rainfall; wetting and drying cycles may have caused the topsoil to soften, resulting in the movement of the slope and causing shoulder cracks; cohesion of soil almost disappears in the fully softened state

Table note: n: number of failures; N/A: not available; * Also depends on the range of soil PI

Table 2.4. Summary of case histories (continued)

Case history	Reference	n	H	S (slope)	Soil description	Field compaction requirement (construction)	Failure description
I-70 Emma field, Missouri	Parra et al. (2003)	1	6.8 m (22 ft)	2.5H:1V	mixed lean and fat clays with scattered cobbles and construction rubble	RC ≥ 95%, Standard Proctor	depth of surficial slides was ranging from 0.9-1.5 m (3-5 ft); control sections failed after higher than normal rainfall; increased pore water pressures at time of failure
I-435 Kansas city field, Missouri	Parra et al. (2003)	1	9.6 m (31.5 ft)	2.2H:1V	lean, soft to medium clay (CL) over stiff to very stiff clay shale (CH)	RC ≥ 95%, Standard Proctor	maximum bending moments of instrumented reinforcing members increased during a period of above average rainfall;
US-36 Stewartsville, Missouri	Loehr and Bowders (2007)	1	8.8 m (29 ft)	2.2H:1V	soft to stiff lean clay (CL) over stiff to very stiff fat clay (CH)	RC ≥ 95%, Standard Proctor	as precipitation increased, both lateral displacement and mobilized bending moment of reinforcing members increased
I-35E Dallas, Texas	Hossain et al. (2017)	1	N/A	N/A	high-plasticity clay with LL= 50-70, and PI≈ 30	RC ≥ 98%*, Standard Proctor	depth of surficial failure speculated to be as much as 2.1m (7ft); bulging and settlement were observed on the slope of embankment; high-plasticity clays normally experience shear strength softening within the first few years after construction due to shrinkage and swelling
SH-183 Fort Worth, Texas	Hossain et al. (2017)	1	N/A	N/A	low- to high- plasticity clay samples with LL= 40-60, and PI= 20-30	RC ≥ 98%*, Standard Proctor	surficial failure and bulging were observed near the crest of slope; tension crack extended up to 3m (10ft)

Table Note: n: number of failures; N/A: not available; * Also depends on the range of soil PI

2.3.2 Longitudinal cracking on I-540 at Davis Drive, North Carolina, Inside Shoulder

This case history occurred at the northbound of Interstate I-540 where a ramp leaves toward the NC-147 expressway. The cracking happened at the highest point of the ramp from I-540 to NC-147 on the inside shoulder, just after the ramp crosses over the Davis Drive. Longitudinal cracking was observed in 2008. Height of the embankment is about 16.8 m (55 ft) with a side slope of 2H:1V (Santee 2019). No problem was seen after the cracks were filled with dirt.

According to the local reports (Pilipchuk 2008), this crack was caused by presence of moisture and collapse of embankment soil due to strength loss after cycles of wetting and drying. Site soil is attributed to be similar to the Test Soil 2 from Lee county of the current research, a highly plastic silt with LL= 58 and PI= 21, which satisfies local material selection criteria. Although this failure is known to be due to the presence of water, this case may provide motivation to undertake a review over material selection specifications. Figure 2.8 shows the longitudinal cracking on I-540 at Davis Drive, North Carolina.

Figure 2.8. Longitudinal cracking on NC I-540 at Davis Drive (Pilipchuk 2008)

2.3.3 Embankment Failure on I-540 at Davis Drive, North Carolina, Outside Shoulder

Reported by the local authorities (Santee 2019), on November 2018 a failure happened on the same place as previous case history, except it was on the outside shoulder of the ramp. The geometry of embankment is also the same. Failure measured about 250 feet long and about 140 feet wide (the slope length). It was 2.1 m to 3.0 m (7-10 ft) deep at worst location. During the failure, lots of material slid down the slope by gravity and help from rainwater. This failure is depicted in Figure 2.9.

The failure occurred around Thanksgiving 2018, after an intense rain event. It is noted that Fall 2018 was a very wet period for the region. The failure was repaired during the Spring and Summer 2019 by rock plating.

Figure 2.9. Failure at outside shoulder of the ramp from I-540 northbound to NC-147 (source: Google Earth)

2.3.4 Debris Flow Failure in Haywood County, North Carolina

In August of 2006 debris flow initiated as an embankment failure on a development road at elevation 4580 ft near the northwest-facing slopes of Eaglenest Ridge in Haywood County, North Carolina. This location is about 2 miles southeast of Maggie Valley and about 500 feet southwest from the end of Summit Drive. The mountain track is 90 ft wide at its widest point. If there was a house at the location where the debris is deposited, it would be destroyed. According to a report by the North Carolina Geological Survey (NCGS 2006), the debris flow was probably triggered because of the heavy rains associated with the remnants of Tropical Storm Ernesto. Field contractors reported 6.5 inches of rain during a 12-hour period prior to the debris flow. The report lists the possible factors leading to the embankment failure as: woody debris and graphitic-sulfidic bedrock fragments in the embankment; a steep embankment slope placed on a steep natural slope overlying a steeply inclined, weathered bedrock surface; and, a possible seepage zone beneath the embankment (NCGS 2006). Some tension cracks of this incident are shown in Figure 2.10.

The bedrock beneath embankment is a graphitic-sulfidic bedrock which seems has been excavated by blasting to construct the road prism. It should be noted that the graphitic-sulfidic bedrock is one of the problematic rock types well-known as prone to acid runoff and instability in embankments (Bryant et al. 2003; Schaeffer and Clawson 1996; Wooten and Latham 2004). Moreover, acidic runoff can decrease the natural pH of stream waters and kill aquatic life.

NCGS geologic and geotechnical experts also had some recommendations to prevent further slope failures and acid runoff in the development area. They proposed two solutions which both neutralize the acidic runoff and improve the stability of the embankment: reconstructing the embankment in compacted lifts treated with lime and limestone; and encapsulating the acidic material in lime and limestone. Of course, it is difficult to establish vegetation on an embankment constructed with graphitic-sulfidic rock material, and most probably vegetation alone will not prevent future slope failures (NCGS 2006).

Figure 2.10. View of cracks in embankment, Haywood County, North Carolina
(source: NCGS 2006)

At the end of reference related to this case history, other examples of the graphitic-sulfidic problematic bedrocks are provided from the same reference (NCGS 2006). In May 2003, Swain County had heavy rains followed by six damaging debris flows, of which five originated in embankments that contained sulfidic rock.

2.3.5 Most Common Type of Road Embankment Failure in Western North Carolina

According to a report by Appalachian Landslide Consultants which was prepared for the Jackson County Planning Department (Appalachian Landslide Consultants 2013), the most common type of road embankment failure seen in western North Carolina is slope failures from the shoulders of the road, as Figure 2.11 illustrates. These are the areas often compacted improperly; sometimes utilities are buried in the outside shoulders and refilled without enough compaction. In such cases, uncompacted soil provides a pathway for water to flow along the utilities or between the more compacted soil of the roadbed and the less compacted soil of the shoulder.

Figure 2.11. Embankment failure from the shoulder of roadway (Appalachian Landslide Consultants 2013)

2.3.6 Embankment Failures in Maryland Reported by Aydilek and Ramanathan (2013)

Aydilek and Ramanathan (2013) reported 48 slope failures in several highway embankments in Maryland. These slope failure cases occurred between 2008 and 2012. They reported that in Maryland which was their study area, majority of these failures took place in slope angles between 20° (2.7H:1V) and 30° (1.7H:1V). They also reviewed statistics of failures versus height of embankment and discovered that majority of failures happened in embankments which had elevations between 30m-90m. Detailed information regarding this study is summarized in Table 2.5. They further noted that among 48 slope failures in highway embankments, 90% were surficial erosion failures, and 80% occurred during or after rainfall. In this study, 50% of slope failures were on slopes with sand formations, and 39% of slope failures occurred on slopes with gravel formations. However, it should be noted that using highly plastic soils as embankment material have been generally accepted as a factor conducive to slope instability (Popescu 1994; Popescu 2002; Aydilek and Ramanathan 2013).

Table 2.5. Summary of information reported by Aydilek and Ramanathan (2013)

Item		Reported value
total number of failures		48
slope angle (degrees)	< 10	10
	10 – 20	15
	20 – 30	22
	30 – 40	1
embankment height (meters)	< 10	6
	10 – 30	11
	30 – 90	27
	90 – 270	4
failure mechanism	surficial failure	90%
lithology or soil type	sand formations	50%
	gravel formations	39%
triggering factor	rainfall	80%

2.3.7 Embankment Failure on U.S. Highway 287, Texas

Khan et al. (2015) reported a slope failure of an embankment located on the southbound slope of U.S. Highway 287 near Midlothian, Texas. This failure which occurred in September 2010 primarily involved surficial slope movements and a cracked shoulder due to rainfall events. Figure 2.12 shows an illustration of the cracked shoulder.

The studied slope consisted of 3H:1V fill slope with a height of 9.15 m (30 ft). The local Eagle Ford formation is composed of residual soils, clay, and weathered shale. Dominant mineral of the soil is montmorillonite which has shrink/swell characteristics. Slope soil was categorized as high-plastic clayey soil (CH), with liquid limit (LL) and plasticity index (PI) of the topsoil ranging between 48-79 and 25-51, respectively.

The researchers constructed three recycled plastic pin (RPP) reinforced sections as long as 15.25 m (50 ft) and left two sections unreinforced as control sections. In this study, it was discovered that instrumented equipment started moving after a rainfall. Moreover, it was seen that control sections had significantly greater settlement (total settlement) at the crest than the reinforced sections. The maximum settlement was 35 cm (3.8% of H) in one of the control sections while reinforced sections had maximum and minimum settlements of 13 cm (1.4% of H) and 5 cm (0.5% of H), respectively.

The failure mechanism could be explained as follows. The highly plastic clay soil having montmorillonite, makes the soil highly susceptible to swelling and shrinkage during wetting and drying cycles. Wright (2005) states that fully softened strengths (which is lower than peak strength) may eventually develop in high-plastic clays, generally in field condition, after exposure to the wetting/drying cycles and provide the governing strength for first-time slides in both excavated and fill slopes. Moreover, it is well known that the cohesion of soil almost disappears in the fully softened state (Wright 2005; Duncan et al. 2014). The wetting and drying cycles may have caused the near-surface soil to soften, resulting in the movement of the slope and causing shoulder cracks. The cracks may have provided an easy path for water to intrude into the slope, which eventually saturated the soil near the crest during rainfall.

Figure 2.12. Surficial movement and cracked shoulder due to rainfall on U.S. Highway 287, Texas [source: Khan et al. 2015]

2.3.8 Embankment Failure on I-70 Emma Field, Missouri

The I70-Emma field case history which was reported by Parra et al. (2003) is located on U.S. Interstate 70 approximately 65 miles west of Columbia, Missouri. As shown in Figure 2.13, the embankment had experienced recurring surficial slides in four areas of the embankment denoted as S1, S2, S3, and S4. Slide areas are also shown in a photograph in Figure 2.14.

Slide areas S1 and S2 were selected for a reinforcement recycled plastic pin (RPP) plan, and slide areas S3 and S4 were left unreinforced as control sections. Reinforcement for slides S1 and S2 was installed during November and December 1999. During spring of 2001, the site experienced higher than normal rainfall. Both control slides (S3 and S4) failed in late Spring of 2001, while only small movements were observed in the stabilized sections.

The slope is an approximately 6.8 m (22 ft) high embankment with 2.5H:1V side slopes (Parra et al. 2003). The embankment soil is composed of mixed lean and fat clays with scattered cobbles and construction rubble. It is noted that depth of the early sliding masses (before stabilization plan) was ranging from approximately 0.9 m (3 ft) to 1.5 m (5 ft).

The continuously screened piezometers and tensiometers (equipment which monitor soil suction) also indicated that increased pore water pressures were observed during Spring 2001, that is when control slides failed. The observed movements from instrumented equipment correspond closely with the rainfall pattern at the site.

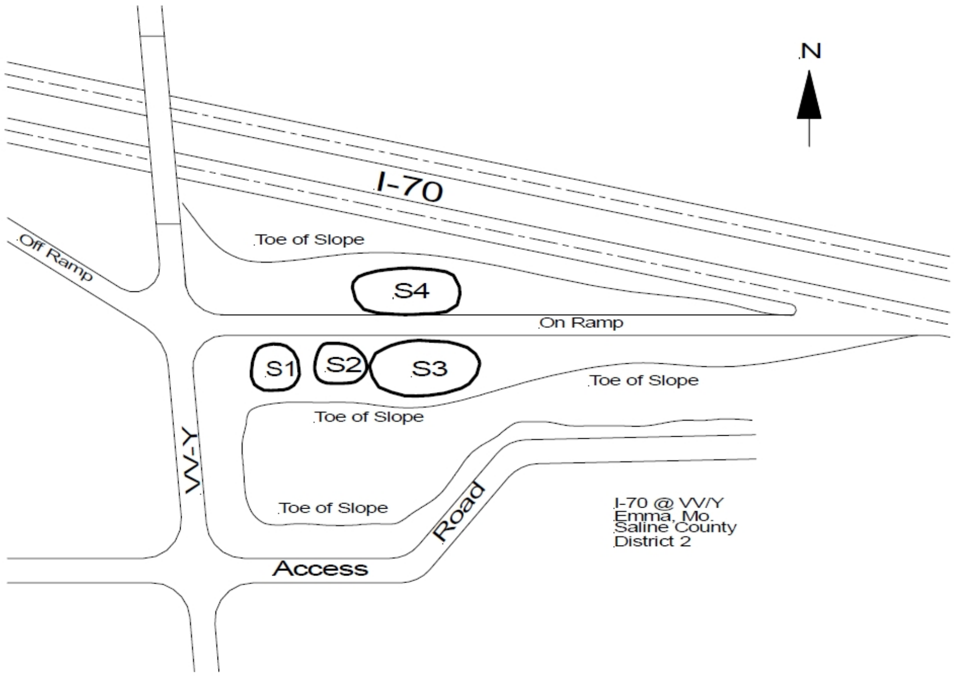

Figure 2.13. Plan view of I-70 Emma field recurring surficial failures (from Parra et al. 2003)

Figure 2.14. South side of embankment at I-70 Emma field showing slide areas S1 (left), S2 (center), and S3 (right) (from Loehr and Bowders 2007)

2.3.9 Embankment Failure on I-435 Kansas City Field, Missouri

Embankment Failure on the I-435 Kansas City site has been studies by a number of researchers (Parra et al. 2003; Loehr and Bowders 2007; Loehr et al. 2007). This case history which occurred in 2001 is located at the intersection of Interstate 435 and Wornall Road in southern Kansas City, Missouri near the Missouri-Kansas border. The embankment is approximately 9.6 m (31.5 ft) high with side slopes of 2.2H:1V. Failed embankment is shown in Figure 2.15.

The embankment is a zoned-fill embankment consisting of a 1.0 m (3 ft.) to 1.5 m (5 ft) surficial layer of mixed lean to fat clay with soft to medium consistency (CL), overlying a stiffer compacted clay shale (CH). Results of the Atterberg limits tests indicate soils from the surficial layer had liquid limits (LL) ranging from 38 to 51 and plasticity indices (PI) from 16 to 34. The underlying compacted shale layer had LL ranging from 29 to 76 and PI from 12 to 51.

This case history was selected for a stabilization project using recycled plastic pin (RPP); however, before that the embankment had experienced at least two surficial slides along the interface between the upper clay and the lower compacted shale. The most recent slide took out a large amount of the ornamental vegetation as well as 4-6 inches of gardening mulch which were part of an older neighborhood beautification project.

Maximum bending moments in the reinforcing members closely correlate with the movements in the slope. Maximum bending moments increased between April and July 2002 during a period of above average rainfall in the area.

Figure 2.15. Recent slide at I-435 Wornall Road site, June 20, 2001 (Loehr and Bowders 2007)

2.3.10 Excavated Slope Failure on US-36 Stewartsville, Missouri

This slope failure case study is located over the US-36 highway approximately two miles west of the city of Stewartsville. This site was selected for a stabilization project using recycled plastic pin (RPP). Installation of reinforcing members was performed during the period of April 30 to May 7, 2002. This case study has been reported by Loehr et al. (2007) and Loehr and Bowders (2007).

This case study is an excavated slope rather than an embankment fill; and is approximately 8.8 m (29 ft) high with an inclination of 2.2H:1V. The stratigraphy of the slope which resembles the I-435 Kansas City site, consists of a surficial layer of soft to medium clay (most of the surficial samples classified as CL) overlying a stiff to hard fat clay (CL or CH). Laboratory testing on samples taken from this site showed that Atterberg limits for the surficial soils varied substantially. Liquid limits (LL) for the surficial soils ranged from 33 to 69 and plastic limits (PL) varied from 16 to 26; plasticity indices (PI) for these soils ranged from 7 to 44. Atterberg limits for the deeper soils were more consistent, with LL ranging from 41 to 55, PL ranging from 16 to 21, and PI ranging from 21 to 34.

As a common phenomenon for all reinforced slopes of this type, it was observed that as precipitation increased in early 2004, both lateral displacement and mobilized bending moment of reinforcing members increased.

Figure 2.16. Photograph of US-36 Stewartsville site taken after the slide (from Loehr and Bowders 2007)

2.3.11 Embankment Failure on I-35E Near Mockingbird Lane in Dallas, Texas

This case history reported by Hossain et al. (2017) is located along I-35E (Northbound) just before the Mockingbird lane overpass in Dallas, Texas. Investigation of this site started in February 2014.

Results of few disturbed/undisturbed samples obtained from soil boring indicated that the soil type was high-plasticity clayey soil (posing above line A), with LL ranging from 50 to 70, and PI mainly around 30.

As illustrated in Figure 2.17 (a) a crack occurred over the shoulder on I-35E due to surficial movement of the slope. The crack propagated up to 42 ft over the shoulder toward the inside of highway and continued to the edge of bridge abutment. In addition, bulging and settlement were both observed on the slope of embankment (Figure 2.17 b).

The resistivity field test was performed to help the researchers estimate depth of the failed zone. The depth of failure due to the surficial soil movement was speculated to be as much as 2.1 m (7 ft) according to the presence of a high-resistivity zone at same depth. It is noted that resistivity of soil depends on the soil type, moisture conditions and void ratio of the soil. Also, it is noted that due to slope movement, the soil in the failed zone becomes looser, which means higher void ratio and higher resistivity. In contrast, presence of moisture results in low resistivity of the soil (Hossain et al. 2017).

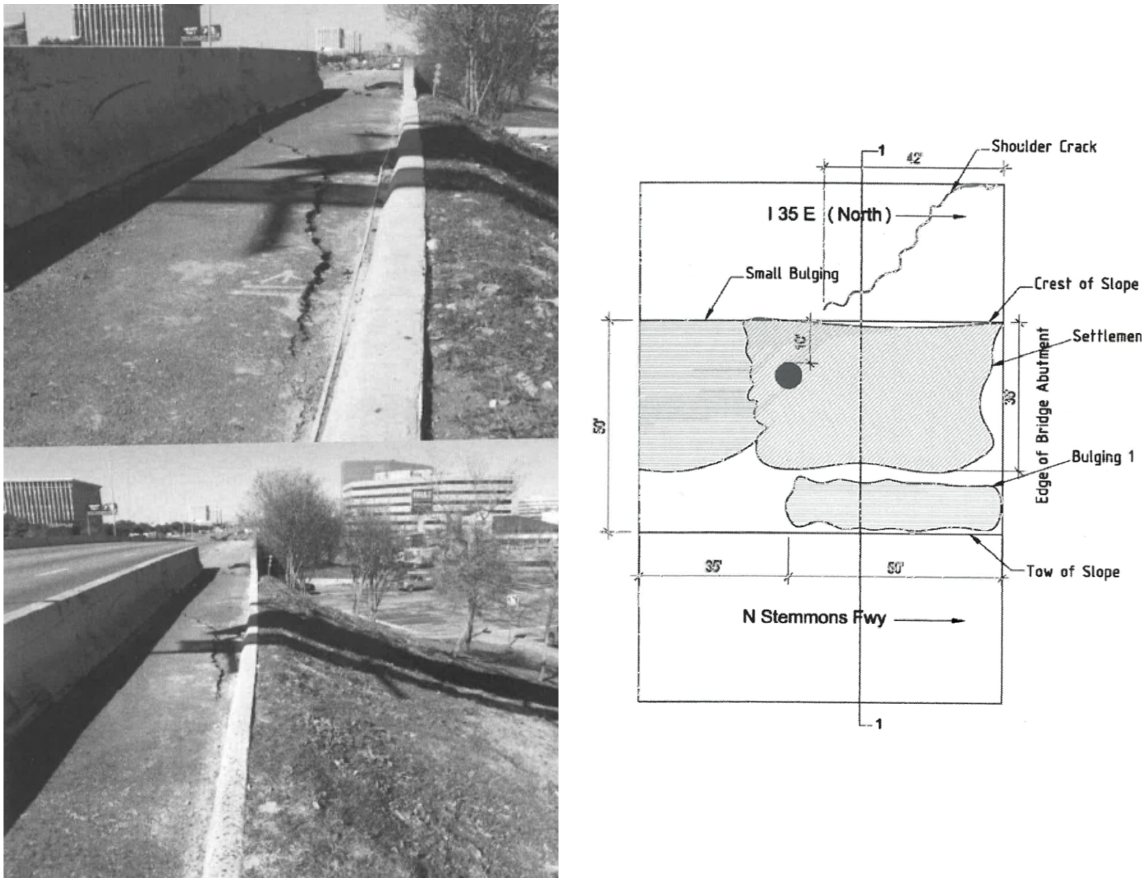

(a) shoulder crack and surficial movement (b) schematic of failure

Figure 2.17. Mockingbird slope failure (Hossain et al. 2017)

It is noted that high-plasticity clays normally experience softening of shear strength within the first few years after construction due to their shrinkage and swelling behavior. Moreover, the small shrinkage cracks may act as a conduit for even more rainwater intrusion and possible saturation of the topsoil of the slope, which may result in the failure of slope.

2.3.12 Embankment Failure on SH-183, Fort Worth, Texas

This case history which was reported by Hossain et al. (2017) is located along SH (state highway) 183, east of the exit ramp from eastbound SH-183 to northbound SH-360, in the north-east corner of Tarrant county, Fort Worth, Texas.

Soil samples taken from site were classified as low- to high- plasticity clay, with LL ranging from 40 to 60, and PI ranging from 20 to 30. Surficial failure and bulging were observed near the crest of slope as depicted in Figure 2.18. Soil resistivity measured using geophysical investigations showed that the tension crack extended up to 3.0 m (10 ft) in depth.

Figure 2.18. Failure of the SH-183 slope (Hossain et al. 2017)

2.4 Creep of Compacted Soils

For the purposes of this research, creep refers to deformation of the soil under constant load. Creep of saturated clays has been studied extensively as part of consolidation behavior of clays. However, it is important to point out that creep in those cases refer to secondary consolidation of a saturated soil that has first undergone a one-dimensional consolidation process.

But in the case of compacted soils an important difference is that the soil is not saturated as shown schematically in Figure 2.19. It can be seen in this figure that, field compacted soils typically fall within a specified acceptance zone (shown as a green rectangle in Figure 2.19; embankment soil is placed with a moisture content within 4% of optimum moisture content (OMC) and usually compacted up to a RC of 95%. All points in this acceptance zone will have a degree of saturation less than 100%.

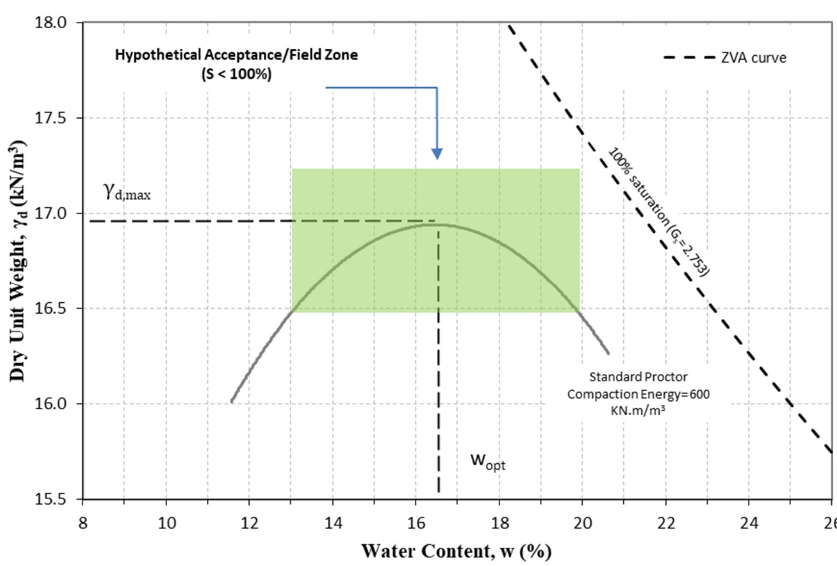

Figure 2.19. Schematic acceptable field compaction zone

Literature review carried out for this section revealed that geotechnical literature is very sparse in terms of creep of unsaturated compacted soils; however, result of this effort is presented as following.

Toriyama (1972) experimented creep characteristics of wet-of-optimum compacted soils under undrained conditions using triaxial apparatus. Confining pressure of these tests were 1 kg/cm^2 (≈ 100 kPa). Soil samples in his study probably were not saturated. According to this study, relationship between creep strain (e) and $\log t$ can be classified into four groups: single straight line, two straight line, a curved line and a straight line, and creep failure. He also found that the rate of creep- $de/d\log t$, is greater for heavily cohesive soil than that of for sandy clay.

Creep stress ratio is defined as $(s_1 - s_3)_c/(s_1 - s_3)_f$ in this study, but since the English script was not available, access to exact definition of parameters was impossible. However, $(s_1 - s_3)_c$ seems to be creep deviator stress and $(s_1 - s_3)_f$ seems to be deviator stress at failure. Creep strain and creep stress ratio are not linearly related, but relationship between $\log e$ and creep stress ratio is approximately linear.

The FHWA Soil an Foundations Reference Manual-Volume I (Samtani and Nowatzki 2006a) has a section that recommends using soils with plasticity index lower than 10 to minimize the long-term deformation of compacted backfill soils. It is pointed out that structural backfill is the material zone that intermediates embankment general section and bridge abutment. It is also recommended to use a layer of structural backfill as thick as 1.5 m (5 ft) beneath abutments on spread footings.

Pagen and Jagannath (1968) studied as-compacted state of four soils using linear viscoelastic strength moduli. Compaction method was drop hammer in this study. The amount of compaction energy and molding moisture content were variant. They used unconfined constant-load creep tests carried out via triaxial cell equipped with two transducers: axial deformation transducer and radial deformation transducer.

The constant-load creep tests loading procedure consisted of initial loading and unloading, each cycle of 5 minutes duration, load magnitude was also equal to a desired particular load. Main loading stage that was used to obtain mechanical properties consisted of 15 minutes duration under load, and 15 minutes in the unload state. Stress levels utilized were relatively low compared to the unconfined compressive strength of soil.

In these tests the elastic creep modulus, E_c, is defined as the constant creep stress divided by the time dependent axial strain at a given time. A sample of the creep modulus values versus moisture content which is for clayey sand is shown in Figure 2.20a. This figure illustrates that there is an optimum moisture content to reach the highest creep modulus. This optimum corresponds to the most desirable state of the compacted soil, that is OMC.

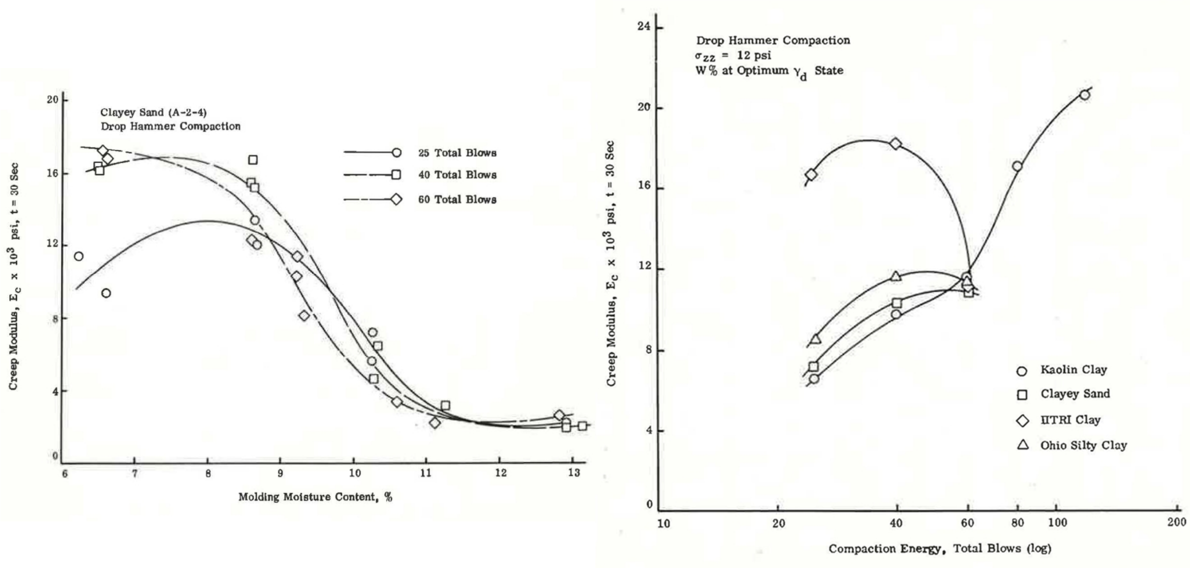

(a) creep modulus vs moisture content for drop hammer compaction

(b) creep modulus vs compaction energy at optimum dry density state

Figure 2.20. Creep modulus vs moisture content and compaction energy (from Pagen and Jagannath 1968)

Their results also showed that maximum dry unit weight and unconfined compressive strength (at optimum dry density) increase by compaction energy. These two relationships are almost linear if compaction energy is plotted in logarithm scale. But the account for variations of creep modulus (E_c) versus compaction energy is slightly different. As shown in Figure 2.20b for the case of three natural soils, 40 blows is the optimum compaction energy. This indicates existence of “over-compaction” for higher energies as they result in samples with lower creep modulus.

Chen (2010) performed one-dimensional compression tests to investigate the settlement characteristics of kaolinite/sand and bentonite/sand specimens. Vertical pressures up to 1300 kPa were used in this study. Soil specimen was selected from the middle of Proctor specimen by trimming compacted Proctor specimen. A load-increment ratio of unity was adopted until each specimen was loaded in stages to a maximum of 1300 kPa. The total loading duration for each load step was selected to be 20 minutes.

In this study it was found that a large amount of compression occurred within the first minute of loading, and only very little compression followed in subsequent minutes. Yoshimi (1958) attributed this initial rapid compression to the following factors: extremely rapid dissipation of excess pore air pressure, and the initial compression of the pore air and soil skeleton.

According to this study, time-compression behavior for specimens compacted at moisture contents other than optimum moisture content were found to be generally similar to that of specimens compacted at the optimum moisture content. Also, the test results clearly showed that the compressibility of the compacted specimens was greatly affected by the compactive energy; the soil compressibility decreased as the compactive effort increased, with the lowest compressibility being observed for specimens that were compacted at the Modified Proctor energy level.

For all Low Energy Proctor and Standard Proctor specimens having 50% clay content, “critical pressure” behavior was observed. This behavior can be characterized by a sudden increase in deformation that occurs when the applied pressure passes beyond a certain value. The observed critical pressure was around 300 kPa which is more or less in the order of reported critical pressures by other researchers (Gradwell and Birrell 1954; Vargas 1953; Sowers 1963). This behavior was attributed to the fabric of these soil specimens in this study. According to Shafiee et al. (2008) the fabric of the 50% clay/sand mixtures are composed of clay as the main body with sand floating in the clay matrix. In the low consolidation pressure range, clay particles which are initially randomly oriented produced a high resistance to deformation (low compressibility). As the consolidation pressure increased, the strains that occurred under loading resulted in higher degree of particle orientation which itself led to a lower resistance to deformation, or in other words higher compressibility (a concept also supported by Seed and Chan 1959).

For the lower clay content mixtures, the compression behavior was mainly controlled by the interaction that occurred between the sand grains, that is for the mixtures having lower clay content, sand grains were the dominant phase in terms of soil structure. As a result, there was no obvious sudden increase in compressibility behavior of mixtures that had a lower clay percentage.

According to this research, kaolinite/sand mixtures exhibited almost the same general trends in terms of compressibility behavior as the bentonite/sand mixtures. As the sand content in soil mixture increased, compressibility was observed to decrease. However, at higher levels of compactive energy, the decrease in compressibility became relatively insignificant. At the Modified Proctor energy level, samples with varying sand content exhibited almost the same degree of compressibility. Moreover, the effect of compactive energy itself is as follows: compactive effort had a significant influence on the observed compressibility. At the same clay/sand mix proportion, the soil became less compressible as the compactive effort increased. Finally, the effect of molding moisture content was observed as follows: with increasing moisture content there is a trend of increase in compressibility; however, this effect is more pronounced in samples with higher clay content.

At the end of this section, Table 2.6 summarizes significant findings of the presented studies.

Table 2.6. Summary of the literature related to creep of compacted soils

Reference	Details of study	Significant findings
Toriyama (1972)	wet-of-optimum compacted specimens; confining pressure of 100 kPa;	could classified 4 groups for relationship between creep strain and log t; greater creep rate for heavily cohesive soil compared to sandy clay;
Samtani and Nowatzki (2006a)	refer to text for definition of structural backfill	to minimize the long-term deformation of compacted backfill soils, use soils with PI lower than 10; use a layer of structural backfill as thick as 1.5m (5ft) beneath abutments on spread footings
Pagen and Jagannath (1968)	compacted specimens; unconfined constant-load creep tests via triaxial cell; loading and unloading were each 15 minutes under low stress levels;	there is an optimum moisture content to reach the highest creep modulus which corresponds to the OMC of compaction curve; existence of over-compaction for higher energies as they result in samples with lower creep modulus
Chen (2010)	compacted kaolinite/sand and bentonite/sand specimens; A load-increment ratio of unity was adopted until each specimen was loaded in stages (each with 20 minutes duration) to a maximum of 1300 kPa;	a large amount of compression occurred within the first minute of loading; the soil compressibility decreased as the compactive effort increased; for Low Energy Proctor and Standard Proctor specimens having 50% clay content, “critical pressure” behavior was observed; for the mixtures having lower clay content, sand grains were the dominant phase in terms of soil structure; as the sand content in soil mixture increased, compressibility was observed to decrease; with increasing moisture content there is a trend of increase in compressibility

2.5 Summary of Literature Review and Identified Knowledge Gaps

At the end of literature review chapter, important facts about the highway embankments that were discovered from the literature, as well as identified knowledge gaps are presented. The current research study tries to cast light on some of these gaps. Relationship of gaps to the particular research objectives is also mentioned; of course, for some of the cases further research is needed.

- Embankment material selection criteria and embankment construction specifications may vary considerably from state to state in the U.S (related to the Objective No. 1).

- The use of PI as material selection criteria for embankments is limited to a few states. In most of the cases, there is a trend in specifying a threshold for the PI of usable material. In the first place, authenticity of this approach needs to be investigated. In the second place, the possibility of unwanted long-term deformations should be investigated when material with PI greater than 10 is used (related to the Objectives No. 1 and 5).

- Traditional field compaction acceptance criteria based on the RC does not provide any information regarding embankment slope stability and/or embankment allowable settlement (related to the Objectives No. 2 and 3, also recommended for future work).

- Slope stability failure through highway embankment alone is not very common. Few cases of failures through embankment, involved shallow or surficial failures and usually induced by heavy rainfall (related to the Objective No. 2).

- Reviewing case history failures which are recently dominated by shallow failure, does not allow us to make any strong conclusion. Most of the failures happen in cases where use Standard Proctor energy as field quality control, but since high percentage of U.S. states (66%) already use standard energy, we cannot necessarily attribute shallow failures to the locations that use Standard Proctor (related to the Objective No. 1).

- Behavior of the instrumented reinforcing members show that failures occur after heavy rainfalls and recorded movements also increase after heavy rainfalls. This will direct us to the study and compare of the behavior of soil samples before saturation versus after saturation (related to the Objectives No. 2 and 3, also recommended for future work).

- Wetting and drying cycles may cause the top layers of soil to soften, crack and finally loose strength and fail. Failure cases are usually thought to be in or close to the saturated state. Thus, investigation of the behavior of saturated samples seems to be a necessary research task (related to the Objectives No. 2 and 3, also recommended for future work).

- Geotechnical literature is very sparse in terms of allowable settlement for the highway embankments. However, after intensive research the value of one inch (1 in.) is selected as the allowable non-uniform deformation/settlement for highway embankments in this research (related to the Objectives No. 3, 4 and 5).

- Review of literature related to the long-term deformation or creep of unsaturated compacted soils revealed that there are not as many references related to this topic. Most of the literature deal with creep of saturated soil samples, or compressibility of soil specimens (related to the Objectives No. 3, also recommended for future work).

In the following chapters this research is described and relevant results is presented to help address the knowledge gaps.

CHAPTER 3: RESEARCH METHODOLOGY

3.1 Introduction

The engineering performance of highway embankments is primarily tied to two design considerations: slope stability and deformation (NCHRP 1971). The first design consideration is usually verified by means of limit equilibrium slope stability analyses and maintaining a minimum factor of safety for stability of all possible critical failure mechanisms. The second design consideration requires that the embankment deformations fall below an allowable tolerance referred to as allowable settlement for highway embankments. The specific requirements for achieving these two design considerations depend on several factors, including the following: embankment height, embankment side slope, material used for construction, construction specifications, actual as-built conditions, foundation conditions and other factors such as drainage control measures, vegetation cover on side slopes, climatic conditions, traffic loading, etc. Under the assumption that the foundation conditions are adequate enough to not influence the above performance design criteria, this research focuses on the embankment material, construction specifications, and geometry of the embankment.

This chapter describes the general research methodology followed in this doctoral research. Also, the chapter presents project research tasks and their connection to the research objectives introduced in Chapter 1.

3.2 General Research Methodology

As mentioned earlier, the performance of highway embankments is primarily associated with two design considerations: slope stability and deformation. In order to meet these two performance criteria, the engineering properties of the compacted candidate soils need to be evaluated as a function of anticipated placement conditions.

As discussed in Chapter 2, the engineering properties of a compacted soil depend on the characteristics of the soil itself (e.g., gradation, plasticity, soil classification), as well as the placement and compaction conditions such as moisture content and dry unit weight. As discussed in the literature review chapter, the engineering properties of the compacted soil of a highway embankment vary depending on the placement moisture content and the as-compacted dry unit weight. Therefore, it is common to specify these two variables in the construction contract specifications. These specifications are often presented in the form of an acceptance region on a dry unit weight versus moisture content space, like the one shown schematically in Figure 3.1. For a given embankment geometry and soil material, each of these performance criteria should be satisfied.

The slope stability performance criterion requires certain engineering properties. The acceptance zone based on slope stability, is shown as a quadrilateral region in Figure 3.1. Similarly, the design consideration of acceptable embankment deformations (short-term and long-term) requires another set of engineering properties that is shown schematically as a different region in Figure 3.1.

The methodology of this research consists of providing guidance on how to propose these two acceptance regions which are required for meeting the two performance criteria.

The intersection of these two regions defines the final acceptance region on the dry unit weight versus moisture content space that complies with both performance criteria. This zone is labeled as Overall Acceptance Zone in Figure 3.1.

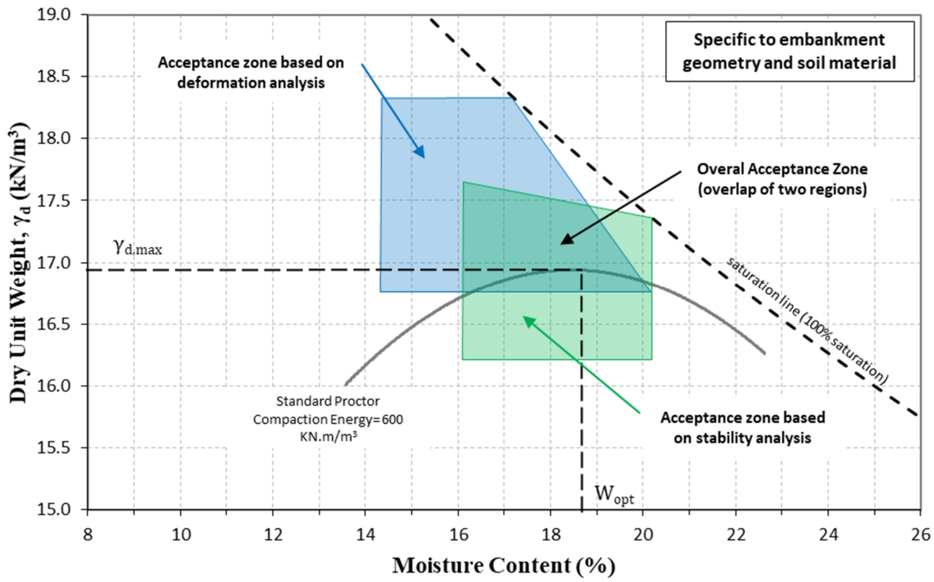

Figure 3.1. Schematic general research methodology; proposed acceptable zone for superimposing criteria based on slope stability criterion and deformation criterion
(modified after Janardhanam and Pando 2015)

The schematic presented in Figure 3.1 shows the general methodology followed in this research. The methodology will be applied to several test soils that are representative of NCDOT field projects in the Piedmont region. The research methodology flowchart is shown in Figure 3.2. This flowchart shows sample selection and laboratory testing as the first two tasks. The laboratory testing program involves obtaining relevant engineering properties for samples compacted at different molding moisture contents and compactive energies. An example of this laboratory testing program is schematically depicted in Figure 3.3 that shows fifteen points on the dry unit weight versus moisture content space. For each of these fifteen compaction conditions, engineering properties are experimentally defined, and analyses relevant to slope stability and deformation are performed to define the final acceptance zone.

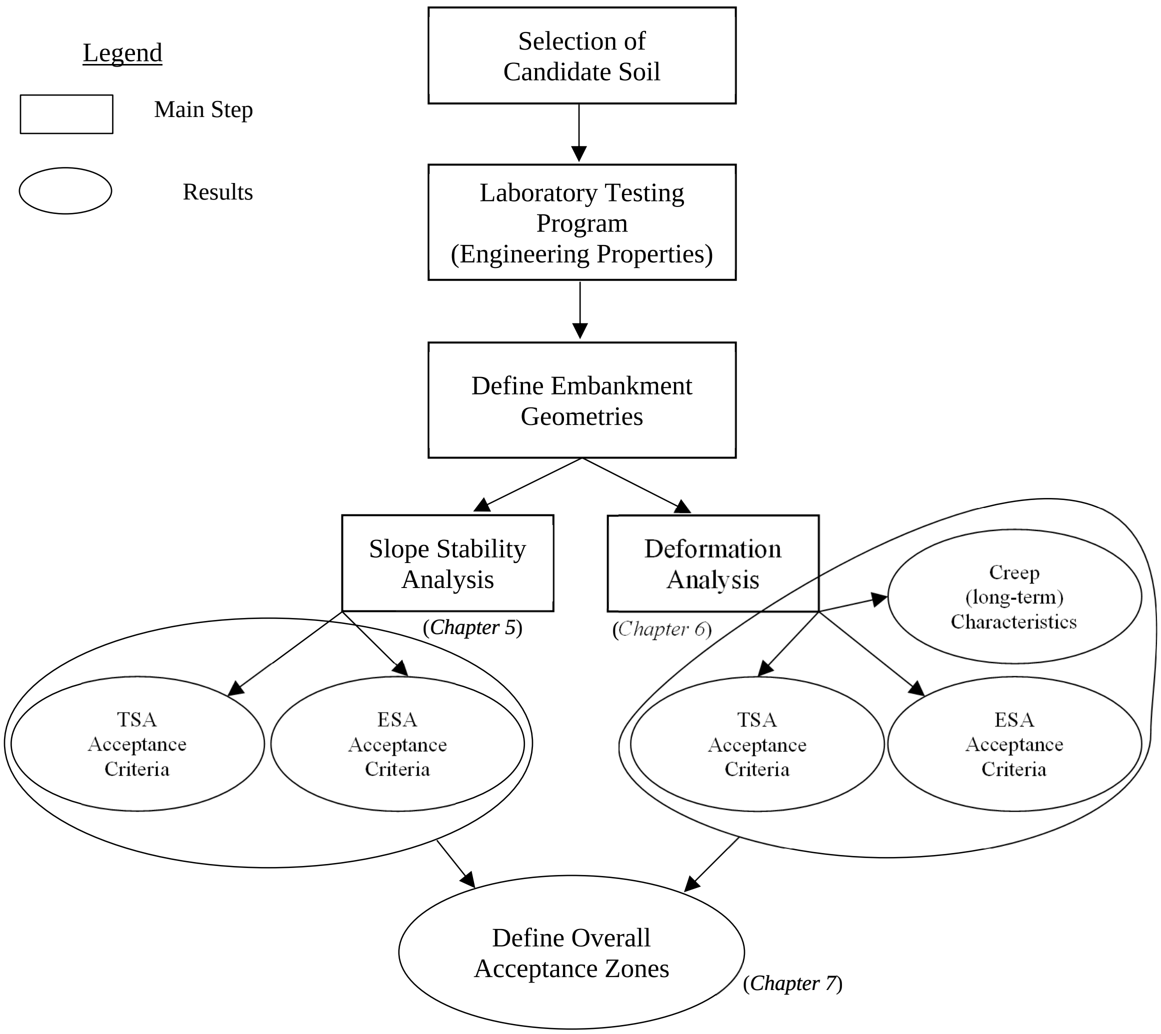

Figure 3.2. Organization flowchart of research

The flowchart of Figure 3.2 also shows the tasks related to slope stability analyses and deformation analyses. For each of these performance criteria, the engineering properties and analyses should be carried out in terms of total stress analysis (TSA) parameters and effective stress analysis (ESA) parameters.

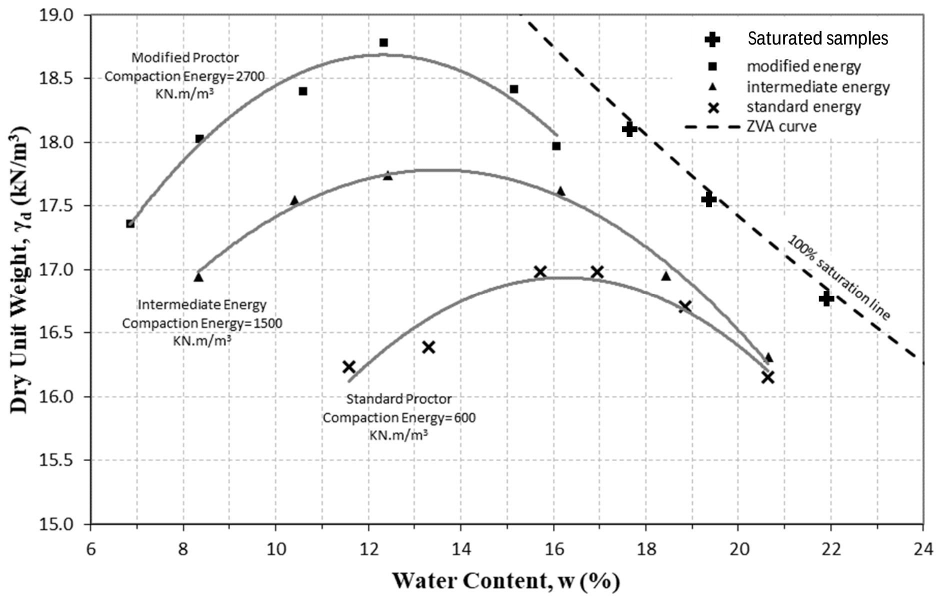

Figure 3.3. Schematic illustration of 15-points method; and saturated soil samples

As shown in Figure 3.2, the next main task is to define the highway embankment geometry. In practice, this task is based on design requirements such as geometric design of road and flood considerations, and usually the specifications stated by AASHTO (1984) is followed. For this research, a total of sixteen embankment geometries are considered. A typical embankment geometry considered in this study is shown in Figure 3.4. Embankment geometries considered for this research are listed in Table 3.1. It is important to note that all analyses for this study assume competent foundation conditions for the embankment. Specifically, the foundation is assumed to be infinitely rigid.

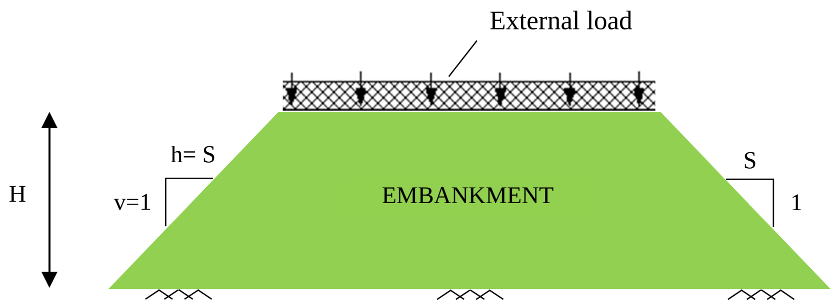

Figure 3.4. Typical embankment section geometry

Table 3.1. Different side slopes and heights considered for embankment geometries

Side slope	Height (ft./m)
1H:1V	10 / 3.00
2H:1V	20 / 6.10
3H:1V	30 / 9.10
4H:1V	40 / 12.20

Following the definition of the highway embankment geometry, and the candidate soil with its corresponding engineering properties, the research flowchart shows analyses that are required for the verification of the two performance criteria. One set of analyses corresponds to the slope stability performance criterion, and the other set corresponds to the deformation performance criterion.

The slope stability analyses are performed for the sixteen geometries and five test soils, using the engineering properties for total stress analysis (TSA) and for effective stress analysis (ESA). The TSA corresponds to short-term conditions that are based on total stress properties. The ESA, on the other hand, corresponds to long-term conditions and requires the use of engineering properties that are based on the effective stresses. More details on these two sets of engineering properties (i.e., TSA and ESA) are provided in Chapter 4.

Similarly, deformation analyses were performed using stress-strain analyses with input properties based on both TSA and ESA parameters. The ESA corresponds to the effective stress deformation properties that represent the embankments under sufficient rainfall infiltration to remove any apparent cohesion associated with suction in the unsaturated compacted soil. This performance criterion also involves evaluation of embankment deformations due to creep.

The superimposition of the two performance criteria, that is slope stability criterion and deformation criterion is the final stage of the research flowchart shown in Figure 3.2. This can be done by overlapping the two individual acceptance zones, as shown in Figure 3.1 which is a topic discussed in Chapter 7.

3.2.1 Embankment Loading

We need to define embankment loading as one of the design parameters. By embankment loading we mean the external load that we need to consider on top of embankment to represent the effect of any external loads after the embankment is brought up to the grade level and built.

According to NCHRP (1971) the design load used to investigate the stability and deformation of an embankment is the weight of the overlying embankment and pavement materials. Traffic loads does not seriously affect embankments except for the upper few feet.

NCHRP report (NCHRP 2004) which deals with geofoam applications in highway embankments has used a uniform surcharge equal to 21.5 kPa (450 lb/ft^2) to model pavement system. To model traffic surcharge, it has also taken values from AASHTO (2002) which is Standard Specifications for Highway Bridges. Based on the AASHTO recommendation of using 0.67 m (2 ft) of an 18.9 kN/m^3 (120 lb/ft^3) soil layer at the top of embankment to represent traffic load, traffic surcharge is 12.6 kPa (263 lb-ft^2). Therefore, the total surcharge representing pavement and traffic would be 21.5 kPa plus 12.6 kPa or 34.1 kPa, which could be rounded up to 35 kPa (730 lb/ft^2).

The value of 35 kPa will be applied as a uniformly distributed load on top of the embankment for both slope stability and deformation analyses in this research.

3.3 Research Tasks

Based on the presented research objectives, and the methodology described in the previous section, a total of nine tasks are defined to perform this study. These nine tasks are listed in Table 3.2.

Table 3.2. Required tasks to accomplish research objectives

Task / Test	Type of task
Task 1: Literature review	Literature review
Task 2: Index tests Task 3: Compaction tests Task 4: Triaxial UU tests Task 5: Triaxial CU tests Task 6: 1D creep compression tests	Laboratory tasks
Task 7: Slope stability analyses Task 8: Deformation analyses Task 9: Definition of overall acceptance zone	Analytical / computational tasks

Having the required tasks presented, Table 3.3 summarizes the connection between research objectives and research tasks.

Table 3.3. Connection between research objectives and defined tasks

<table>
<tr><th>Research Task / Test</th><th colspan="2">Research Objective</th></tr>
<tr><td>Task 1: Literature review</td><td colspan="2">Identification of knowledge gaps</td></tr>
<tr><td>Task 2: Index tests
Task 3: Compaction tests
Task 4: Triaxial UU tests
Task 5: Triaxial CU tests</td><td colspan="2">Definition of engineering properties</td></tr>
<tr><td>Task 4: Triaxial UU tests
Task 7: Slope stability analysis</td><td>embankment slope stability analysis / TSA</td><td rowspan="5">Review of Material Selection Criteria for Highway Embankments</td></tr>
<tr><td>Task 5: Triaxial CU tests
Task 7: Slope stability analysis</td><td>embankment slope stability analysis / ESA</td></tr>
<tr><td>Task 4: Triaxial UU tests
Task 6: 1D creep compression tests
Task 8: Deformation analysis</td><td>embankment deformation analysis / TSA</td></tr>
<tr><td>Task 5: Triaxial CU tests
Task 8: Deformation analysis</td><td>embankment deformation analysis / ESA</td></tr>
<tr><td>Task 9: Definition of overall acceptance zones</td><td></td></tr>
</table>

3.4 Summary

The main methodology used for this dissertation is presented in this chapter. This study's main contribution is evaluating material selection and material placement based on a performance-based design framework. For this study, two performance criteria of slope stability and deformation are considered.

CHAPTER 4: LABORATORY TESTING PROGRAM

4.1 Introduction

This chapter describes the test soils and the methods used in the laboratory testing program designed and performed as part of this doctoral study. The chapter presents the following main sections:

- Description of test soils;
- Compaction test results;
- Unconsolidated-Undrained (UU) triaxial tests;
- Consolidated-Undrained (CU) triaxial tests;
- One-dimensional creep compression tests;
- Summary.

Additional details regarding the laboratory testing program are presented in Appendices B through D with their content summarized as following.

Table 4.1. Summary of appendices related to the laboratory testing program

Appendix	Description
B	Failure lines for Unconsolidated-Undrained triaxial compression tests
C	Failure lines for Consolidated-Undrained triaxial compression tests
D	Calibration of oedometers

4.2 Description of Test Soils

Five test soils from across the Piedmont region of North Carolina were selected for this research. These test soils were picked from NCDOT highway embankment projects that were active at the time of sampling. Figure 4.1 shows the location of the five test soils studied in this research project.

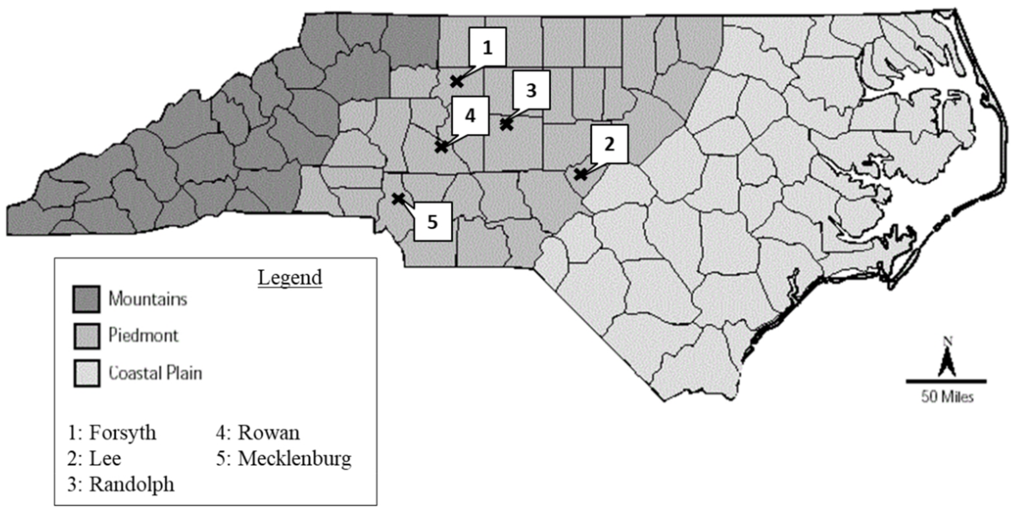

Figure 4.1. Location of Piedmont test soil samples

Upon sampling, we visually examined the five test soils and performed a series of index and classification tests on them. Results of the index tests are summarized in Table 4.2. All procedures performed were in general accordance with the corresponding ASTM standards.

Table 4.2. Index properties of test soils

Property		Soil 1	Soil 2	Soil 3	Soil 4	Soil 5	ASTM No.
	NC County	Forsyth	Lee	Randolph	Rowan	Mecklenburg	-
Classification	USCS	SM	MH	ML	ML	ML	D2487
	AASHTO	A-4 (0)	A-7-6 (28)	A-4 (1)	A-5 (7)	A-5 (5)	D3282
Gradation	Gravel %	5.9	0.0	0.6	1.0	1.6	D422
	Sand %	56.3	1.7	13.9	23.2	28.8	
	Fine %	37.8	98.3	85.5	75.8	69.6	
	Clay %	11.3	41.1	7.2	3.7	7.5	
	D_{50} (μm)	148.7	3.5	19.7	20.7	24.0	
	D_{10} (μm)	1.2	0.2	2.4	3.8	2.4	
	C_u *	189.3	33.6	12.5	7.6	16.9	
	C_c *	5.1	0.5	1.1	1.2	1.4	
Atterberg Limits (%)	LL	30	58	32	48	42	D4318
	PL	28	37	35	42	37	
	PI	2	21	NP *	6	5	
specific gravity	G_S	2.75	2.80	2.71	2.74	2.80	D854

* NP= non-plastic, C_u= coefficient of uniformity, C_c= coefficient of curvature

Representative grain size distribution curves for each test soil are shown in Figure 4.2. These curves include combination of results from sieve analyses and hydrometer test.

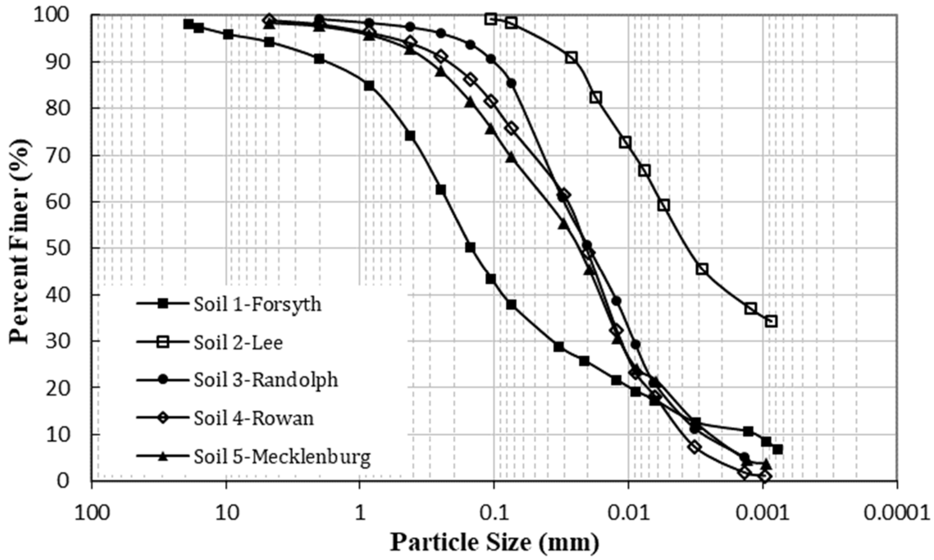

Figure 4.2. Representative gradation curves for test soils

The Atterberg plasticity limits obtained for the test soils are presented in Figure 4.3. This figure shows the Casagrande plasticity chart. Test Soils 1, 4, and 5 fall in a region corresponding to the low plastic silts (ML). Test Soil 2 falls in the region of high plastic silts (MH). As noted in Table 4.2, Test Soil 3 was found to be a non-plastic soil.

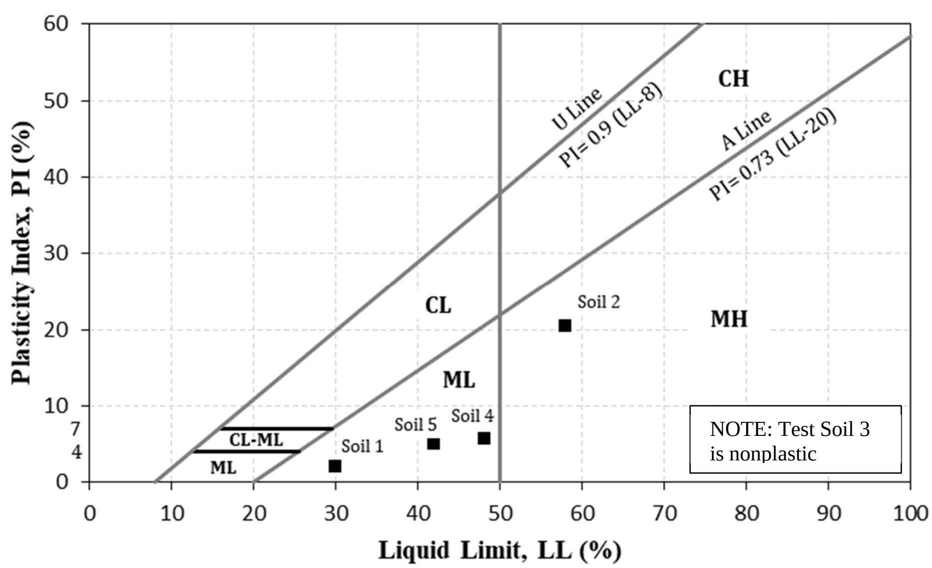

Figure 4.3. Plasticity of test soils on Casagrande chart

Based on the visual-manual inspections (ASTM D2488) and index test results, the following general descriptions could be presented for each test soil:

Test soil 1 (Forsyth county): a light brown silty sand with little clay and few gravel, with plasticity index (PI) as little as 2%. This test soil classified as a SM and an A-4 (0) in the unified soil classification system (USCS) and AASHTO classification system, respectively. A representative photo of this test soil is shown in Figure 4.4a.

Test soil 2 (Lee county): an orange high plastic silt with some clay and trace of sand, with PI equal to 21%. This test soil classified as a MH and an A-7-6 (28) in the unified soil classification system (USCS) and AASHTO classification system, respectively. A representative photo of this test soil is shown in Figure 4.4b.

Test soil 3 (Randolph county): a brownish yellow non-plastic silt with few clay and little gravel and a fluffy structure. This test soil classified as a ML and an A-4 (1) in the unified soil classification system (USCS) and AASHTO classification system, respectively. A representative photo of this test soil is shown in Figure 4.4c.

Test soil 4 (Rowan county): an orange low plastic silt with trace of clay and little sand. This test soil with PI equal to 6 classified as a ML and an A-5 (7) in the unified soil classification system (USCS) and AASHTO classification system, respectively. A representative photo of this test soil is shown in Figure 4.4d.

Test soil 5 (Mecklenburg county): a yellow low plastic silt with few clay and some sand. This test soil with plasticity index (PI) as little as 5%, classified as a ML and an A-5 (5) in the unified soil classification system (USCS) and AASHTO classification system, respectively. A representative photo of this test soil is shown in Figure 4.4e.

(a) Test Soil 1 (Forsyth)

(b) Test Soil 2 (Lee)

(c) Test Soil 3 (Randolph)

(d) Test Soil 4 (Rowan)

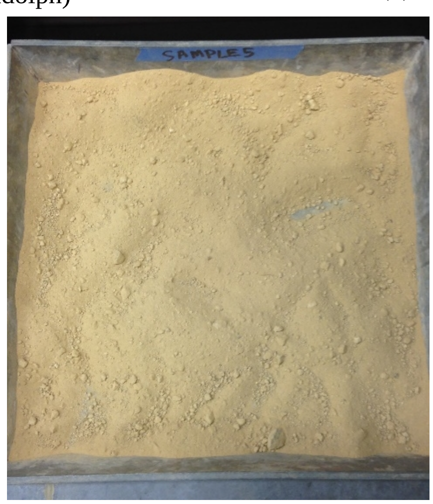

(e) Test Soil 5 (Mecklenburg)

Figure 4.4. Representative photos of research test soils

4.3 Compaction Tests Results

This section presents the compaction test results for the five test soils. For each test soil, compaction tests have been carried out at three energy levels, namely Standard Proctor (ASTM D698), Intermediate Proctor, and Modified Proctor (ASTM D1557).

The compaction tests were performed in general accordance with procedures outlined in the ASTM D698 (Standard Proctor) and ASTM D1557 (Modified Proctor). The tests corresponding to the intermediate energy level were performed using the small compaction mold (with 4 inch inside diameter), the 10 lb rammer with falling height of 18 inch (large rammer) with 3 layers and 23 blows per layer. A summary of the relevant information for each compaction test is presented in Table 4.3. Figure 4.5 depicts representative photos of a compaction test showing the key components such as mold, rammer, and other accessories.

Table 4.3. Summary information for compaction tests

Test series	ASTM	Mold	Rammer weight (lb)	Rammer drop (in)	No. of layers	No. of blows per layer	Compaction energy (KN.m/m3)
Standard Proctor	D698	4 inch	5.5	12	3	25	600
Intermediate Energy	N/A	4 inch	10	18	3	23	1500
Modified Proctor	D1557	4 inch	10	18	5	25	2700

(a) Spatula and tray

(b) Straightedge

(c) Compaction mold with collar

(d) Small and large compaction rammers

(e) Full compaction mold

Figure 4.5. Photos of tools used for compaction tests

In addition to the compaction curve, for each test soil a summary table is presented which lists optimum moisture content (OMC) and maximum dry unit weight obtained for each compaction curve. The results for each test soil are presented in the following subsections.

4.3.1 Compaction Test Results for Test Soil 1

The compaction test results for Test Soil 1 are presented in Figure 4.6 and Table 4.4.

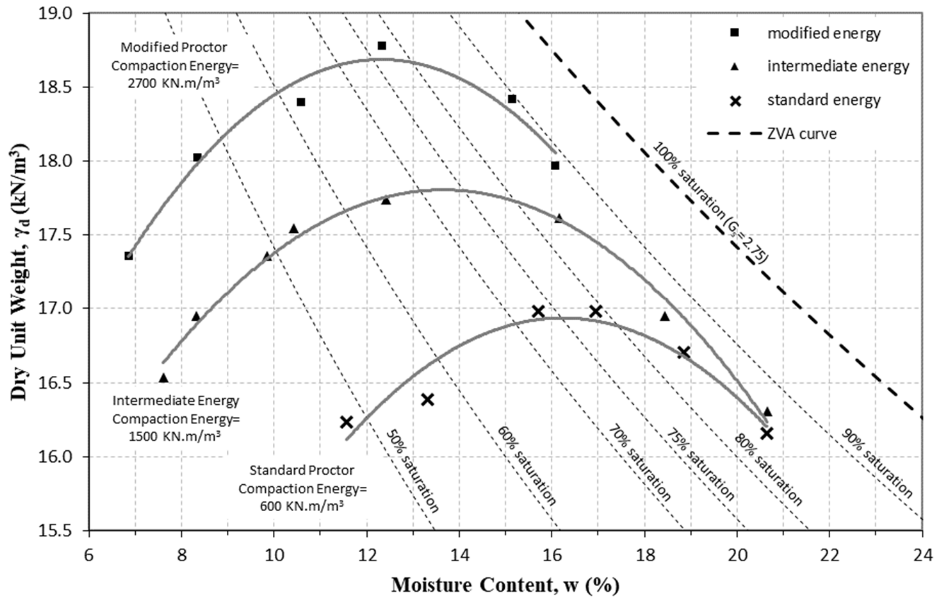

Figure 4.6. Compaction curves for Test Soil 1 at three energy levels

Table 4.4. Summary of compaction test results for Test Soil 1

Test series	Compaction energy (KN.m/m^3)	Optimum moisture content (%)	Maximum dry unit weight (KN/m^3)
Modified Proctor	2700	12.3	18.7
Intermediate Energy	1500	13.9	17.8
Standard Proctor	600	16.3	16.9

For Test Soil 1 the peaks of the three compaction curves are approximately located near the line of 75% saturation.

4.3.2 Compaction Test Results for Test Soil 2

The compaction test results for Test Soil 1 are presented in Figure 4.7 and Table 4.5.

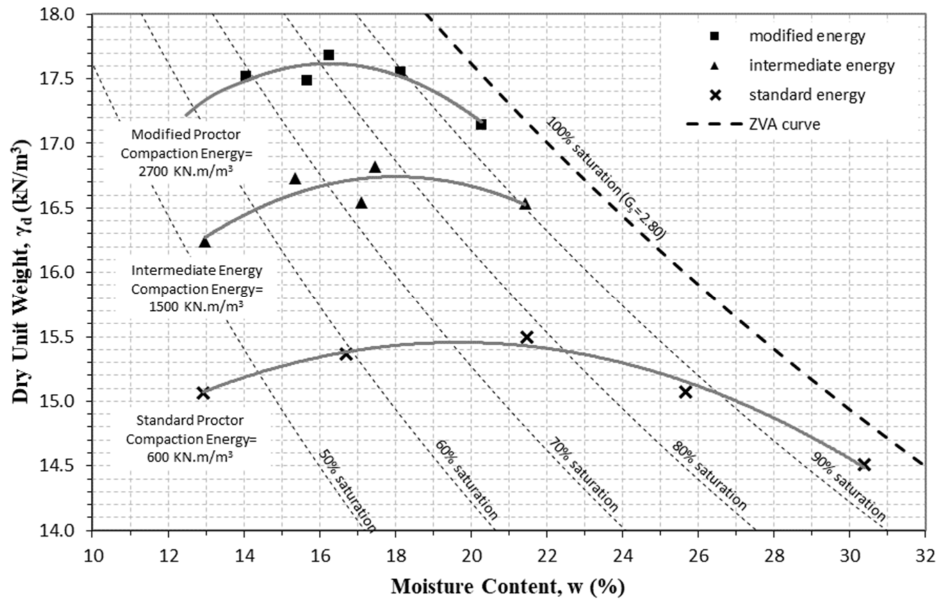

Figure 4.7. Compaction curves for Test Soil 2 at three energy levels

Table 4.5. Summary of compaction test results for Test Soil 2

Test series	Compaction energy (KN.m/m^3)	Optimum moisture content (%)	Maximum dry unit weight (KN/m^3)
Modified Proctor	2700	16.3	17.6
Intermediate Energy	1500	18.0	16.7
Standard Proctor	600	20.0	15.4

It is noted that for Test Soil 2, the peaks of the three compaction curves are located within the lines of 70% saturation and 90% saturation.

4.3.3 Compaction Test Results for Test Soil 3

The compaction test results for Test Soil 1 are presented in Figure 4.8 and Table 4.6.

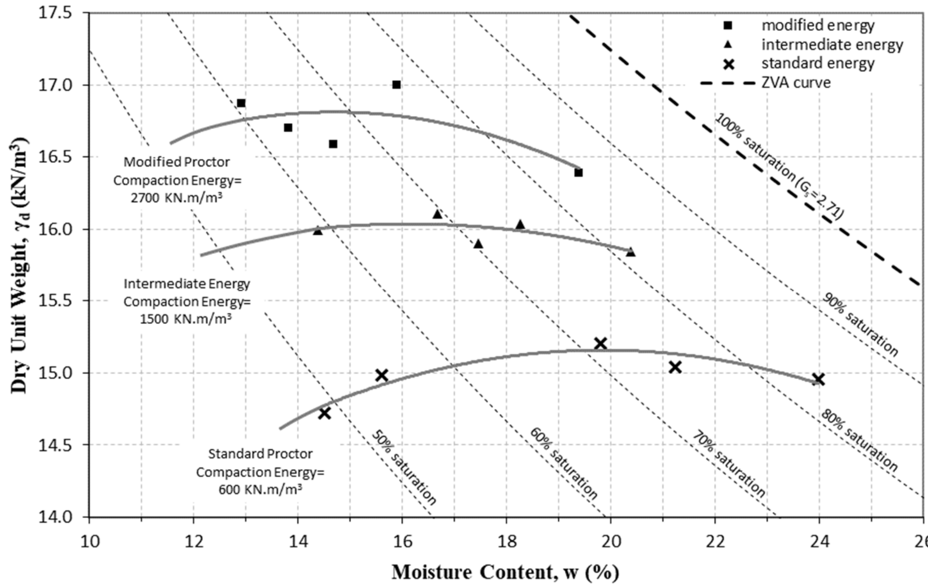

Figure 4.8. Compaction curves for Test Soil 3 at three energy levels

Table 4.6. Summary of compaction test results for Test Soil 3

Test series	Compaction energy (KN.m/m^3)	Optimum moisture content (%)	Maximum dry unit weight (KN/m^3)
Modified Proctor	2700	14.9	16.8
Intermediate Energy	1500	16.1	16.0
Standard Proctor	600	20.0	15.1

For Test Soil 3, the peaks of the three compaction curves are approximately located near the line of 70% saturation.

4.3.4 Compaction Test Results for Test Soil 4

The compaction test results for Test Soil 1 are presented in Figure 4.9 and Table 4.7.

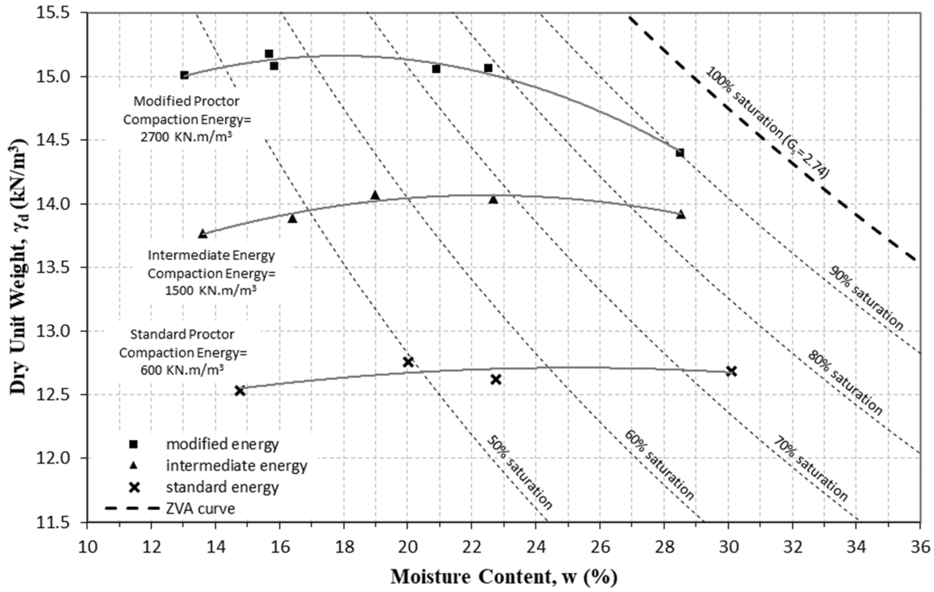

Figure 4.9. Compaction curves for Test soil 4 at three energy levels

Table 4.7. Summary of compaction test results for Test Soil 4

Test series	Compaction energy (KN.m/m^3)	Optimum moisture content (%)	Maximum dry unit weight (KN/m^3)
Modified Proctor	2700	18.0	15.1
Intermediate Energy	1500	22.7	14.1
Standard Proctor	600	25.2	12.7

For Test Soil 4, the peaks of the three compaction curves are located between the lines of 60% saturation and 70% saturation.

4.3.5 Compaction Test Results for Test Soil 5

The compaction test results for Test Soil 1 are presented in Figure 4.10 and Table 4.8.

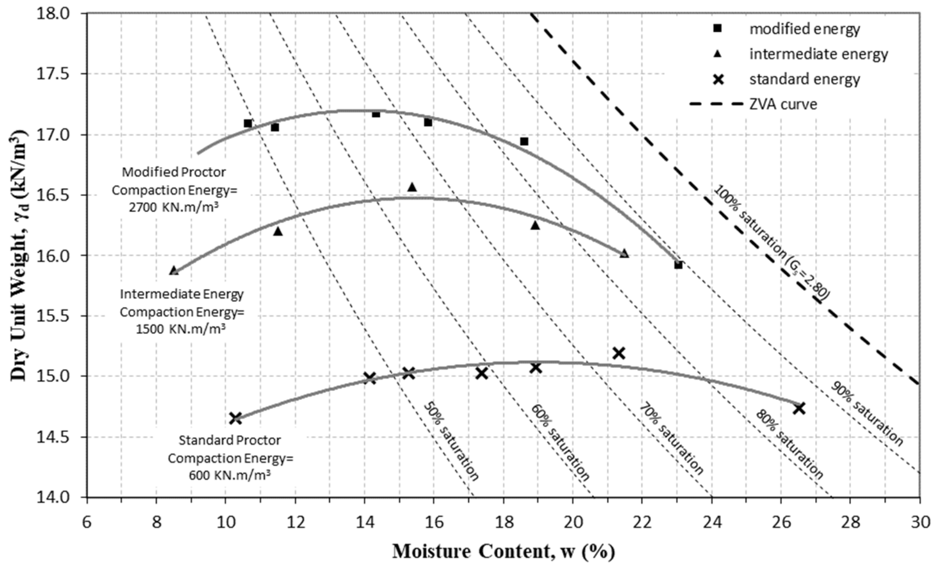

Figure 4.10. Compaction curves for Test Soil 5 at three energy levels

Table 4.8. Summary of compaction test results for Test Soil 5

Test Series	Compaction energy (KN.m/m^3)	Optimum moisture content (%)	Maximum dry unit weight (KN/m^3)
Modified Proctor	2700	14.0	17.2
Intermediate Energy	1500	15.6	16.5
Standard Proctor	600	19.0	15.2

For Test Soil 5, the peaks of the three compaction curves are located between the lines of 60% saturation and 70% saturation, with peaks being very close to the line of 65% saturation.

4.4 Unconsolidated-Undrained Triaxial Compression Tests

4.4.1 Introduction

In order to obtain engineering properties of the compacted soils and to assess the influence of compaction moisture and dry density, a series of UU triaxial tests were performed on the samples prepared at optimum, dry-of-optimum, and wet-of-optimum moisture contents, and compacted at the three energy levels described before. This methodology is often referred to as the 15-points method where 5 points for each of the three levels of compactive energies are tested to assess engineering properties that capture a wide range of different anticipated field conditions in terms of placement moisture content and as-compacted dry unit weight. The following subsections describe the test procedures and then present the preliminary results for the five test soils.

4.4.2 Procedure

Triaxial compression tests under unconsolidated undrained conditions were performed on compacted samples. The triaxial samples were obtained by pushing thin-walled shelby tubes into the compaction molds where the different test soils were compacted using different compaction energies (three levels) and different moisture contents as per the 15-points method described above. The sample preparation procedure is shown in the photos provided in Figure 4.11. The inside diameter of shelby tubes was 35.6 mm (1.4 inch) and the wall diameter was 1.3 mm (0.05 inch). The pushing end was beveled to facilitate the process of pushing. After pushing the tubes, the samples were carefully extruded and initial dimension and weight recorded. The initial moisture content was also measured using the trimmings. To avoid changes in the initial moisture content of sample, soil samples were sealed using plastic wraps.

(a) compaction mold

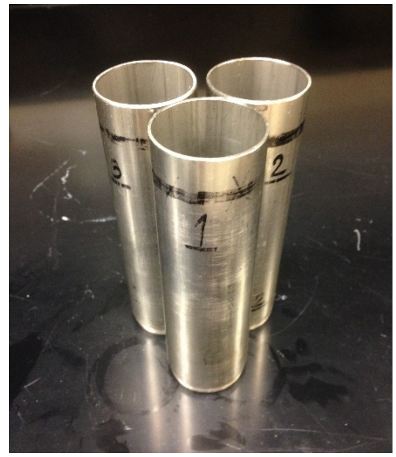

(b) Shelby tubes

(c) pushing tubes into the soil sample

(d) end of pushing

Figure 4.11. Sample preparation for triaxial testing

After sample preparation, the sample is mounted on the pedestal of triaxial device. The UU triaxial tests were performed in general accordance with the ASTM D2850. The triaxial device used for the UU triaxial tests was a Geocomp device which consists of a 8.9 kN (2000 lb) LoadTrac-II reaction frame and two FlowTrac-II systems to control volume and pressure, as shown in Figure 4.12. For more information regarding the triaxial device used, reader is referred to the user manuals of Geocomp company [Geocomp Corporation

2011a; Geocomp Corporation 2011b; Geocomp Corporation 2014]. The triaxial chamber used was adapted to fit a sample pedestal and top cap of 35.6 mm (1.4 inch) to match the diameter of the sample obtained from the shelby tubes described above. Before installation of the sample into the triaxial chamber, filter papers were used on bottom and top of the sample in contact of the soil specimen. Porous stones were used on bottom and top of the sample in contact with the filter papers. It is noted that porous stones were used in dry condition.

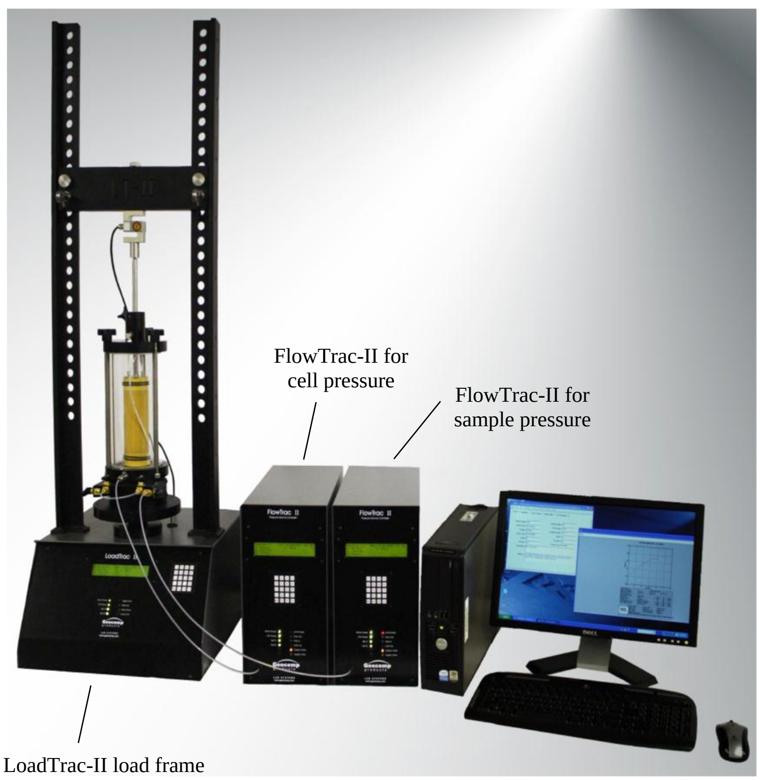

Figure 4.12. LoadTrac-II / FlowTrac-II systems for triaxial tests
(modified after Geocomp Corporation 2011a)

The UU triaxial tests were performed at an axial strain rate of 1%/minute and for confining cell pressures of 25, 50, and 100 kPa. It is noted that for each compaction condition on the moisture content - dry unit weight space, three particular specimens were prepared to allow three UU triaxial tests to be performed at confining cell pressures (σ_{cell}) of 25 kPa, 50 kPa and 100 kPa.

Using the Geocomp triaxial systems, the first stage of each UU triaxial test is the initialization phase where the sample was subjected to a very low cell pressure (10 kPa) to confirm no leakage or sensor errors. After the initialization stage, cell pressure was applied at a rate of 1 kPa/second with no sample drainage allowed to ensure that unconsolidated conditions are satisfied. Following cell pressure application, the sample was sheared under undrained conditions at the constant rate of strain mentioned above. The sample was sheared until a maximum axial strain of 15% or until a well-defined peak deviator stress was observed. The selection of 15% as a limiting value for axial strain has been used by many researchers (Seed and Chan 1959; Seed et al. 1960; ASTM D2850). The final sample conditions, i.e. failure type and failure mode, were recorded for each test and the final moisture content was also measured. The test matrix of all UU triaxial tests performed is reported in Table 4.9 through Table 4.13 corresponding to Test Soil 1 through Test Soil 5, respectively.

Table 4.9. Summary information of UU triaxial testing matrix for Test Soil 1

Molding compactive energy	**Test No.**	**Final w (%)**	**Final γ_d (kN/m^3)**	s_{cell} **(kPa)**
Standard Proctor	S1-UU1	17.4 (OMC + 1.1)	16.5	25
	S1-UU2			50
	S1-UU3			100
Standard Proctor	S1-UU4	15.6 (OMC - 0.7)	17.5	25
	S1-UU5			50
	S1-UU6			100
Standard Proctor	S1-UU7	13.0 (OMC – 3.3)	17.4	25
	S1-UU8			50
	S1-UU9			100
Standard Proctor	S1-UU10	18.9 (OMC + 2.6)	16.5	25
	S1-UU11			50
	S1-UU12			100
Standard Proctor	S1-UU13	13.2 (OMC – 3.1)	15.9	25
	S1-UU14			50
	S1-UU15			100
Standard Proctor	S1-UU16	10.5 (OMC – 5.8)	15.3	25
	S1-UU17			50
	S1-UU18			100
Intermediate Energy	S1-UU19	9.8 (OMC – 4.1)	16.6	25
	S1-UU20			50
	S1-UU21			100
Intermediate Energy	S1-UU22	7.7 (OMC – 6.2)	16.1	25
	S1-UU23			50
	S1-UU24			100
Modified Proctor	S1-UU25	9.3 (OMC – 3.0)	17.5	25
	S1-UU26			50
	S1-UU27			100
Modified Proctor	S1-UU28	7.1 (OMC – 5.2)	17.0	25
	S1-UU29			50
	S1-UU30			100
Modified Proctor	S1-UU31	12.1 (OMC - 0.2)	18.2	25
	S1-UU32			50
	S1-UU33			100
Modified Proctor	S1-UU34	14.5 (OMC + 2.2)	17.8	25
	S1-UU35			50
	S1-UU36			100

Table 4.10. Summary information of UU triaxial testing matrix for Test Soil 2

Molding compactive energy	**Test No.**	**Final w (%)**	**Final γ_d (kN/m^3)**	**s_{cell} (kPa)**
Standard Proctor	S2-UU10	30.2 (OMC + 10.2)	14.5	25
	S2-UU11			50
	S2-UU12			100
Standard Proctor	S2-UU16	25.1 (OMC + 5.1)	15.5	25
	S2-UU17			50
	S2-UU18			100
Standard Proctor	S2-UU19	20.9 (OMC + 0.9)	15.9	25
	S2-UU20			50
	S2-UU21			100
Standard Proctor	S2-UU25	12.5 (OMC – 7.5)	15.4	25
	S2-UU26			50
	S2-UU27			100
Standard Proctor	S2-UU50	16.4 (OMC – 3.6)	16.9	25
	S2-UU51			50
	S2-UU52			100
Intermediate Energy	S2-UU28	15.2 (OMC – 2.8)	17.4	25
	S2-UU29			50
	S2-UU30			100
Intermediate Energy	S2-UU31	21.1 (OMC + 3.1)	16.8	25
	S2-UU32			50
	S2-UU33			100
Intermediate Energy	S2-UU34	17.3 (OMC – 0.7)	17.5	25
	S2-UU35			50
	S2-UU36			100
Intermediate Energy	S2-UU37	12.6 (OMC – 5.4)	17.2	25
	S2-UU38			50
	S2-UU39			100
Modified Proctor	S2-UU4	24.6 (OMC + 8.3)	15.7	25
	S2-UU5			50
	S2-UU6			100
Modified Proctor	S2-UU7	31.2 (OMC + 14.9)	14.4	25
	S2-UU8			50
	S2-UU9			100
Modified Proctor	S2-UU22	19.4 (OMC + 3.1)	17.2	25
	S2-UU23			50
	S2-UU24			100

Table 4.10. Summary information of UU triaxial testing matrix for Test Soil 2 (continued)

Molding compactive energy	**Test No.**	**Final w (%)**	**Final γ_d (kN/m^3)**	**s_{cell} (kPa)**
Modified Proctor	S2-UU47	16.1 (OMC - 0.2)	17.8	25
	S2-UU48			50
	S2-UU49			100
Modified Proctor	S2-UU53	13.6 (OMC – 2.7)	18.4	25
	S2-UU54			50
	S2-UU55			100

Table 4.11. Summary information of UU triaxial testing matrix for Test Soil 3

Molding compactive energy	**Test No.**	**Final w (%)**	**Final γ_d (kN/m^3)**	s_{cell} **(kPa)**
Standard Proctor	S3-UU1	20.7 (OMC + 0.7)	15.5	25
	S3-UU2			50
	S3-UU3			100
Standard Proctor	S3-UU4	21.6 (OMC + 1.6)	15.3	25
	S3-UU5			50
	S3-UU6			100
Standard Proctor	S3-UU7	22.3 (OMC + 2.3)	15.3	25
	S3-UU8			50
	S3-UU9			100
Standard Proctor	S3-UU10	15.9 (OMC - 4.1)	15.4	25
	S3-UU11			50
	S3-UU12			100
Standard Proctor	S3-UU13	14.8 (OMC - 5.2)	15.2	25
	S3-UU14			50
	S3-UU15			100
Intermediate Energy	S3-UU22	14.5 (OMC – 1.6)	16.5	25
	S3-UU23			50
	S3-UU24			100
Intermediate Energy	S3-UU25	15.8 (OMC – 0.3)	16.5	25
	S3-UU26			50
	S3-UU27			100
Intermediate Energy	S3-UU31	17.8 (OMC + 1.7)	16.3	25
	S3-UU33			100
Intermediate Energy	S3-UU37	20.2 (OMC + 4.1)	15.7	25
	S3-UU38			50
	S3-UU39			100
Modified Proctor	S3-UU16	12.5 (OMC – 2.4)	16.7	25
	S3-UU17			50
	S3-UU18			100
Modified Proctor	S3-UU19	15.3 (OMC + 0.4)	16.4	25
	S3-UU20			50
	S3-UU21			100
Modified Proctor	S3-UU28	15.4 (OMC + 0.5)	16.8	25
	S3-UU30			100
Modified Proctor	S3-UU34	19.6 (OMC + 4.7)	16.1	25
	S3-UU35			50
	S3-UU36			100

Table 4.12. Summary information of UU triaxial testing matrix for Test Soil 4

Molding compactive energy	**Test No.**	**Final w (%)**	**Final γ_d (kN/m^3)**	**s_{cell} (kPa)**
Standard Proctor	S4-UU1	44.5 (OMC + 19.3)	11.4	25
	S4-UU2			50
	S4-UU3			100
Standard Proctor	S4-UU4	22.1 (OMC – 3.0)	13.1	25
	S4-UU5			50
	S4-UU6			100
Standard Proctor	S4-UU10	20.1 (OMC – 5.1)	13.3	25
	S4-UU11			50
	S4-UU12			100
Standard Proctor	S4-UU19	29.7 (OMC + 4.5)	13.3	25
	S4-UU20			50
	S4-UU21			100
Standard Proctor	S4-UU28	14.5 (OMC - 10.7)	13.6	25
	S4-UU29			50
	S4-UU30			100
Intermediate Energy	S4-UU13	22.3 (OMC - 0.4)	14.6	25
	S4-UU14			50
	S4-UU15			100
Intermediate Energy	S4-UU22	27.7 (OMC + 5.0)	14.3	25
	S4-UU23			50
	S4-UU24			100
Intermediate Energy	S4-UU31	15.8 (OMC – 6.9)	14.9	25
	S4-UU32			50
	S4-UU33			100
Intermediate Energy	S4-UU37	12.5 (OMC - 10.2)	14.9	25
	S4-UU38			50
	S4-UU39			100
Modified Proctor	S4-UU7	20.0 (OMC + 2.0)	15.1	25
	S4-UU8			50
	S4-UU9			100
Modified Proctor	S4-UU16	22.6 (OMC + 4.6)	15.3	25
	S4-UU17			50
	S4-UU18			100
Modified Proctor	S4-UU25	27.8 (OMC + 9.8)	14.4	
	S4-UU26			
	S4-UU27			

Table 4.12. Summary information of UU triaxial testing matrix for Test Soil 4 (continued)

Molding compactive energy	Test No.	Final w (%)	Final γ_d (kN/m^3)	s_{cell} (kPa)
Modified Proctor	S4-UU34	14.9 (OMC - 3.1)	15.7	25
	S4-UU35			50
	S4-UU36			100
Modified Proctor	S4-UU40	12.5 (OMC - 5.5)	15.4	25
	S4-UU41			50
	S4-UU42			100

Table 4.13. Summary information of UU triaxial testing matrix for Test Soil 5

Molding compactive energy	Test No.	Final w (%)	Final γ_d (kN/m^3)	s_{cell} (kPa)
Standard Proctor	S5-UU1	18.0 (OMC - 1.0)	15.9	25
	S5-UU2			50
	S5-UU3			100
Standard Proctor	S5-UU4	20.8 (OMC + 1.8)	15.5	25
	S5-UU5			50
	S5-UU6			100
Standard Proctor	S5-UU7	15.9 (OMC – 3.1)	15.9	25
	S5-UU8			50
	S5-UU9			100
Standard Proctor	S5-UU19	22.9 (OMC + 3.9)	15.6	25
	S5-UU20			60
	S5-UU21			100
Standard Proctor	S5-UU22	13.7 (OMC – 5.3)	15.8	25
	S5-UU23			50
	S5-UU24			100
Standard Proctor	S5-UU37	14.4 (OMC – 4.6)	14.8	25
	S5-UU38			60
	S5-UU39			150
Standard Proctor	S5-UU40	10.8 (OMC – 8.2)	14.4	25
	S5-UU41			60
	S5-UU42			100
Intermediate Energy	S5-UU10	14.5 (OMC - 1.1)	16.7	25
	S5-UU11			50
	S5-UU12			100
Intermediate Energy	S5-UU13	16.8 (OMC + 1.2)	17	25
	S5-UU15			100
Intermediate Energy	S5-UU16	20.1 (OMC + 4.5)	16.5	25
	S5-UU17			60
	S5-UU18			100
Intermediate Energy	S5-UU25	11.3 (OMC - 4.3)	17.2	25
	S5-UU27			100
Intermediate Energy	S5-UU28	9.4 (OMC – 6.2)	16.8	25
	S5-UU29			50
	S5-UU30			100

Table 4.13. Summary information of UU triaxial testing matrix for Test Soil 5 (continued)

Molding compactive energy	**Test No.**	**Final w (%)**	**Final γ_d (kN/m^3)**	**σ_{cell} (kPa)**
Low Energy	S5-UU31	18.8 (OMC – 0.2)	15.5	25
	S5-UU32			65
	S5-UU33			100
Low Energy	S5-UU34	16.6 (OMC – 2.4)	15.5	25
	S5-UU35			65
	S5-UU36			100

4.4.3 Results of UU Triaxial Tests

This section and subsections present a summary of the results for the UU triaxial tests performed on the five test soils. The results include a summary table and three plots of shear strength parameters (total stress friction angle ϕ_{UU} , total stress cohesion C_{UU}, and elasticity modulus E_{UU}) for each test soil. It is noted that the plots of elasticity modulus belong to the median UU triaxial test with confining pressure equal to $\sigma_{cell} = 50 kPa$. Additional details associated with results of UU triaxial tests can be found in Appendix B.

4.4.3.1 Results of UU Triaxial Tests for Test Soil 1

For Test Soil 1, Figure 4.13 shows total stress friction angle, Figure 4.14 depicts total stress cohesion, and Figure 4.15 illustrates modulus of elasticity.

Table 4.14. Summary information of UU triaxial tests carried out on Test Soil 1

Test No.	Final w (%)	s_{cell} (kPa)	Final g_d (kN/m^3)	f_{UU} (deg)	C_{UU} (kPa)	E_{UU} (MPa)
S1-UU1	17.3	25	15.3			2.9
S1-UU2	16.6	50	17.3	22.6	74.7	3.8
S1-UU3	18.2	100	16.9			4.0
S1-UU4	15.6	25	17.4			8.9
S1-UU5	15.7	50	17.5	34.0	72.8	9.3
S1-UU6	15.6	100	17.8			12.3
S1-UU7	13.0	25	17.1			9.3
S1-UU8	12.7	50	17.6	39.3	69.4	13.8
S1-UU9	13.4	100	17.5			17.8
S1-UU10	19.5	25	16.1			1.1
S1-UU11	18.5	50	16.7	26.7	35.0	2.1
S1-UU12	18.8	100	16.6			2.2
S1-UU13	13.4	25	16.0			11.8
S1-UU14	13.8	50	15.9	32.8	53.3	12.0
S1-UU15	12.3	100	15.8			12.3
S1-UU16	10.7	25	15.2			14.5
S1-UU17	10.2	50	15.2	34.5	46.6	15.6
S1-UU18	10.6	100	15.5			16.2
S1-UU19	9.9	25	16.9			17.0
S1-UU20	9.7	50	16.4	34.1	88.9	19.8
S1-UU21	9.8	100	16.4			21.6
S1-UU22	7.9	25	15.9			14.3
S1-UU23	7.5	50	16.3	44.9	47.5	19.4
S1-UU24	7.8	100	16.1			22.5
S1-UU25	9.0	25	17.4			27.5
S1-UU26	9.4	50	17.5	41.7	152.1	32.2
S1-UU27	9.4	100	17.6			37.1
S1-UU28	7.0	25	17.0			26.4
S1-UU29	7.3	50	17.0	43.9	117.7	27.4
S1-UU30	6.9	100	17.1			36.4
S1-UU31	12.2	25	18.3			22.1
S1-UU32	12.0	50	18.3	34.1	163.0	27.4
S1-UU33	12.1	100	18.0			32.1
S1-UU34	14.8	25	17.6			7.5
S1-UU35	14.8	50	17.8	42.0	54.4	9.5
S1-UU36	13.9	100	18.1			16.5

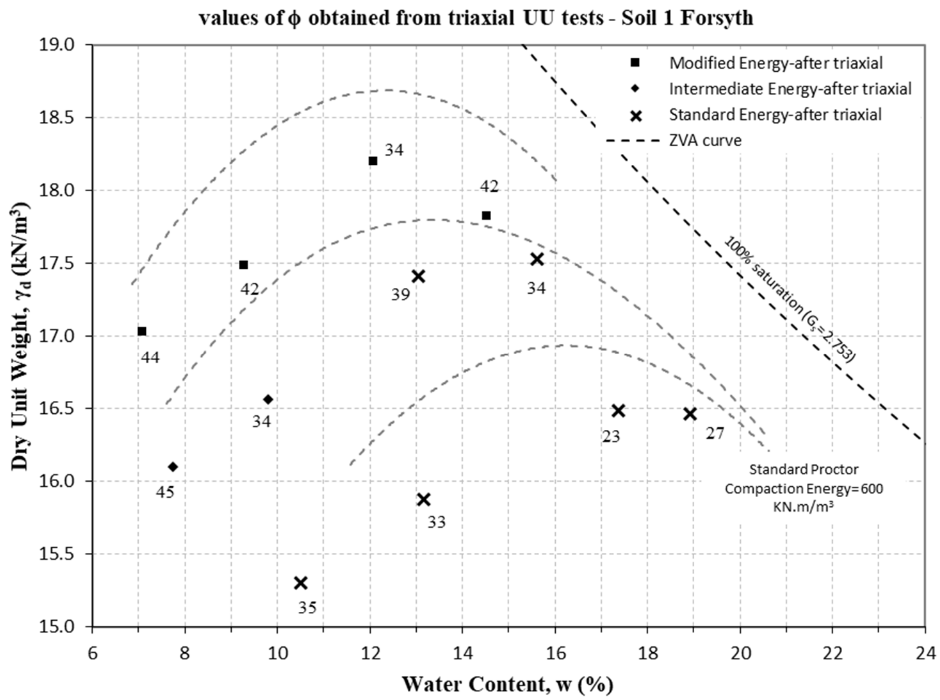

Figure 4.13. Total stress friction angle, f_{UU} (degrees) obtained from UU triaxial tests on Test Soil 1

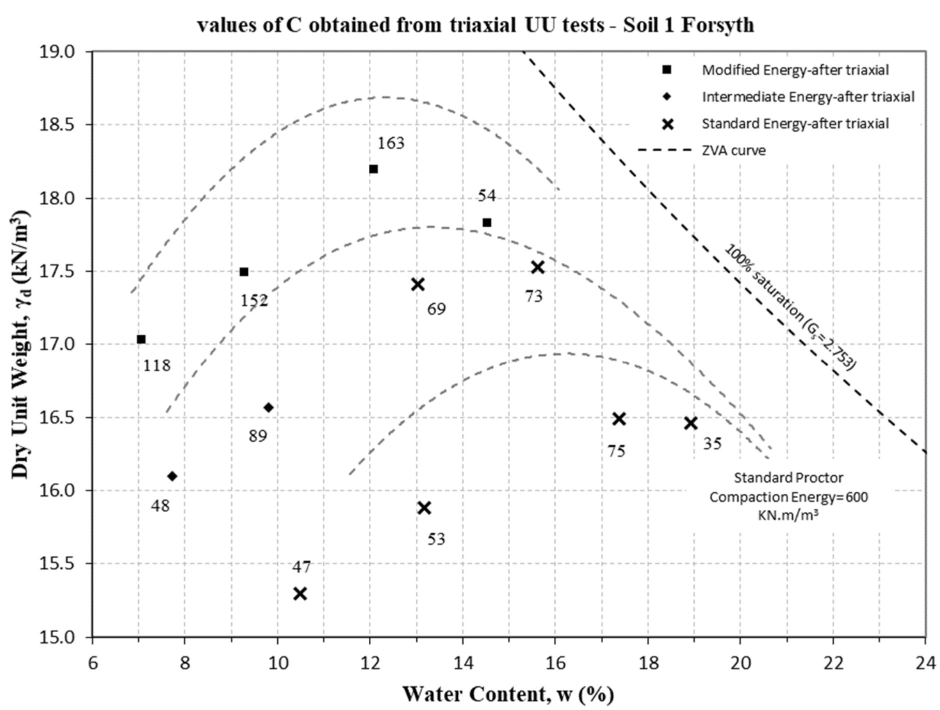

Figure 4.14. Total stress cohesion, C_{UU} (kPa) obtained from UU triaxial tests on Test Soil 1

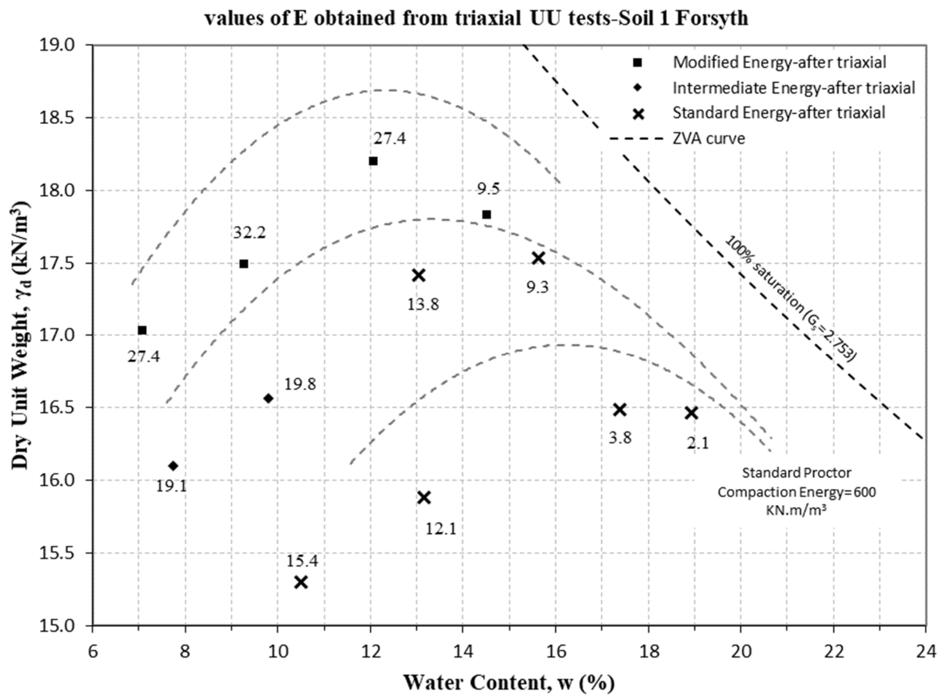

Figure 4.15. Elasticity modulus E_{UU} (MPa) at $s_{cell} = 50\ kPa$ obtained from UU triaxial tests on Test Soil 1

4.4.3.2 Results of UU Triaxial Tests for Test Soil 2

In this section, results of UU triaxial tests carried out on Test Soil 2 (soil sample from Lee County) is presented. The summary table is presented in Table 4.15. After the summary table, three plots have been provided in Figure 4.16, Figure 4.17, and Figure 4.18 which represent total stress friction angle (f_{UU}), total stress cohesion (C_{UU}), and modulus of elasticity (E_{UU}), respectively.

Table 4.15. Summary information of UU triaxial tests carried out on Test Soil 2

Test No.	Final w (%)	s_{cell} (kPa)	Final g_d (kN/m^3)	f_{UU} (deg)	C_{UU} (kPa)	E_{UU} (MPa)
S2-UU4	25.4	25	15.6			4.8
S2-UU5	24.0	50	15.9	35.0	79.0	5.9
S2-UU6	24.5	100	15.7			7.1
S2-UU7	31.7	25	14.8			1.3
S2-UU8	31.0	50	14.3	15.0	45.5	1.5
S2-UU9	30.9	100	14.2			1.7
S2-UU10	31.0	25	14.4			2.0
S2-UU11	29.6	50	14.7	18.0	61.6	2.9
S2-UU12	30.1	100	14.6			3.0
S2-UU16	25.5	25	15.4			7.0
S2-UU17	25.1	50	15.6	28.6	98.3	9.4
S2-UU18	24.8	100	15.6			12.8
S2-UU19	21.0	25	15.8			22.8
S2-UU20	20.8	50	15.9	41.1	89.9	23.0
S2-UU21	20.8	100	16.1			23.2
S2-UU22	20.0	25	17.0			23.7
S2-UU23	19.5	50	17.2	49.1	143.4	26.6
S2-UU24	18.9	100	17.4			32.6
S2-UU25	12.4	25	15.4			22.9
S2-UU26	12.6	50	15.6	38.8	89.3	27.8
S2-UU27	12.6	100	15.2			33.7
S2-UU28	15.4	25	17.5			35.7
S2-UU29	15.0	50	17.3	51.4	118.6	37.1
S2-UU30	15.1	100	17.5			50.6
S2-UU31	21.2	25	16.8			13.5
S2-UU32	21.3	50	16.7	32.2	174.0	15.4
S2-UU33	20.7	100	16.9			17.5
S2-UU34	17.4	25	17.5			28.8
S2-UU35	17.5	50	17.4	36.4	253.9	40.2
S2-UU36	17.1	100	17.5			45.3
S2-UU37	12.9	25	17.2			50.1
S2-UU38	12.6	50	17.2	40.8	243.5	59.0
S2-UU39	12.4	100	17.2			69.5
S2-UU47	16.1	25	17.8			34.7
S2-UU48	16.3	50	18.0	39.2	275.7	38.5
S2-UU49	15.9	100	17.7			51.3

Table 4.15. Summary information of UU triaxial tests carried out on Test Soil 2 (continued)

Test No.	**Final w** (%)	s_{cell} **(kPa)**	**Final** g_d **(kN/m³)**	f_{UU} **(deg)**	C_{UU} **(kPa)**	E_{UU} **(MPa)**
S2-UU50	16.3	25	16.9			40.5
S2-UU51	16.4	50	16.8	34.5	195.9	42.1
S2-UU52	16.4	100	16.9			44.4
S2-UU53	13.4	25	18.3			48.8
S2-UU54	13.6	50	18.5	45.2	326.4	57.3
S2-UU55	13.6	100	18.4			71.7

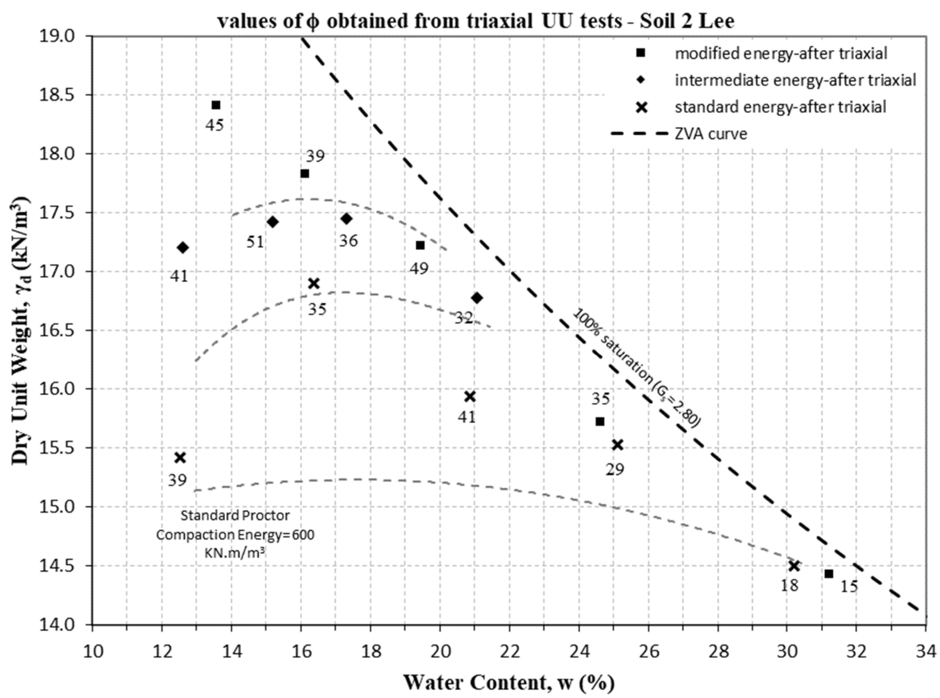

Figure 4.16. Total stress friction angle, f_{UU} (degrees) obtained from UU triaxial tests on Test Soil 2

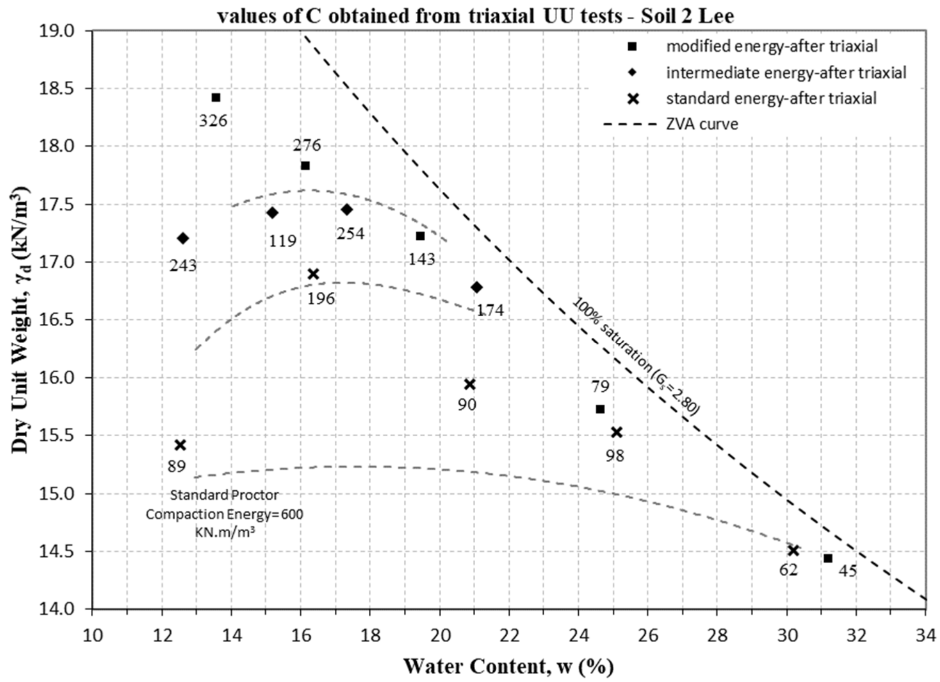

Figure 4.17. Total stress cohesion, C_{UU} (kPa) obtained from UU triaxial tests on Test Soil 2

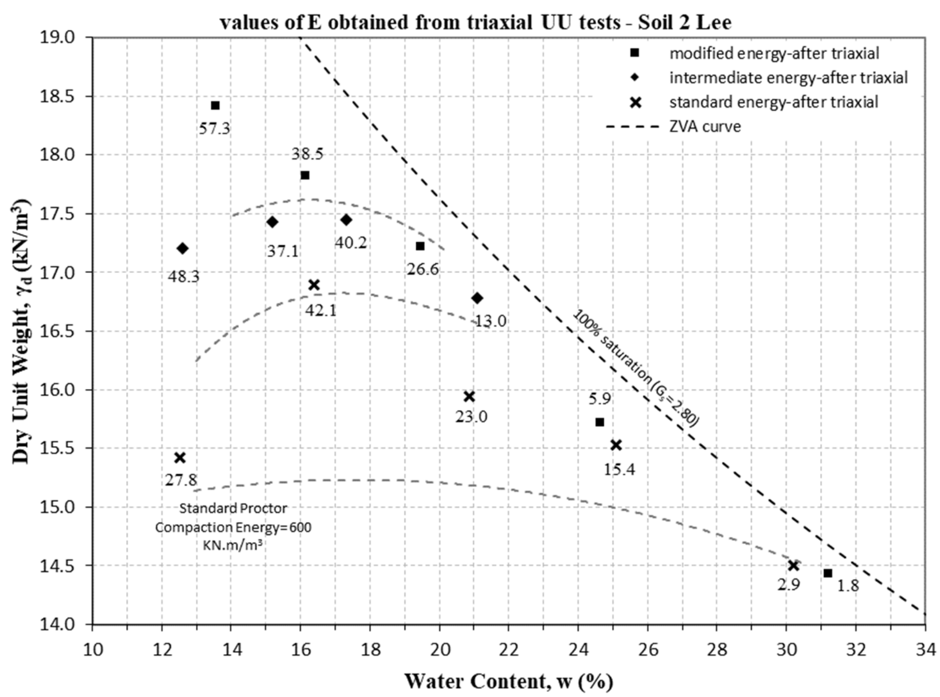

Figure 4.18. Elasticity modulus E_{UU} (MPa) at $s_{cell} = 50\ kPa$ obtained from UU triaxial tests on Test Soil 2

4.4.3.3 Results of UU Triaxial Tests for Test Soil 3

In this section, results of UU triaxial tests carried out on Test Soil 3 (soil sample from Randolph County) is presented. The summary table is presented in Table 4.16. After the summary table, three plots have been provided in Figure 4.19, Figure 4.20, and Figure 4.21 which represent total stress friction angle (f_{UU}), total stress cohesion (C_{UU}), and modulus of elasticity (E_{UU}), respectively.

Table 4.16. Summary information of UU triaxial tests carried out on Test Soil 3

Test No.	Final w (%)	s_{cell} (kPa)	Final g_d (kN/m^3)	f_{UU} (deg)	C_{UU} (kPa)	E_{UU} (MPa)
S3-UU1	22.4	25	15.4			5.6
S3-UU2	19.7	50	15.6	34.5	56.8	7.1
S3-UU3	20.0	100	15.6			9.4
S3-UU4	21.4	25	15.4			4.8
S3-UU5	21.5	50	15.2	33.6	55.0	6.1
S3-UU6	21.8	100	15.3			8.5
S3-UU7	22.2	25	15.3			4.2
S3-UU8	22.7	50	15.3	30.5	65.1	5.5
S3-UU9	22.1	100	15.4			7.2
S3-UU10	16.2	25	15.5			7.2
S3-UU11	15.7	50	15.5	32.0	74.2	8.7
S3-UU12	15.9	100	15.3			11.3
S3-UU13	15.6	25	15.2			7.0
S3-UU14	14.5	50	15.3	30.8	65.2	9.6
S3-UU15	14.2	100	15.2			19.6
S3-UU16	12.6	25	16.3			10.7
S3-UU17	12.4	50	16.9	31.1	136.0	11.7
S3-UU18	12.7	100	16.9			12.7
S3-UU19	15.8	25	16.4			7.2
S3-UU20	15.3	50	16.1	39.6	67.1	9.0
S3-UU21	14.7	100	16.8			11.3
S3-UU22	14.6	25	16.4			8.2
S3-UU23	16.8	50	16.5	36.2	89.5	8.9
S3-UU24	14.4	100	16.6			12.2
S3-UU25	15.7	25	16.4			7.3
S3-UU26	16.0	50	16.4	37.3	73.0	7.9
S3-UU27	15.7	100	16.5			12.3
S3-UU28	15.5	25	16.8	31.9	104.9	6.5
S3-UU30	15.2	100	16.7			9.0
S3-UU31	17.2	25	16.5	32.3	90.5	6.6
S3-UU33	18.4	100	16.2			9.8
S3-UU34	19.7	25	16.0			3.1
S3-UU35	19.5	50	16.2	32.5	79.3	4.0
S3-UU36	19.5	100	16.2			5.0
S3-UU37	20.2	25	15.7			3.0
S3-UU38	19.9	50	15.7	30.3	74.2	4.1
S3-UU39	20.6	100	15.8			5.1

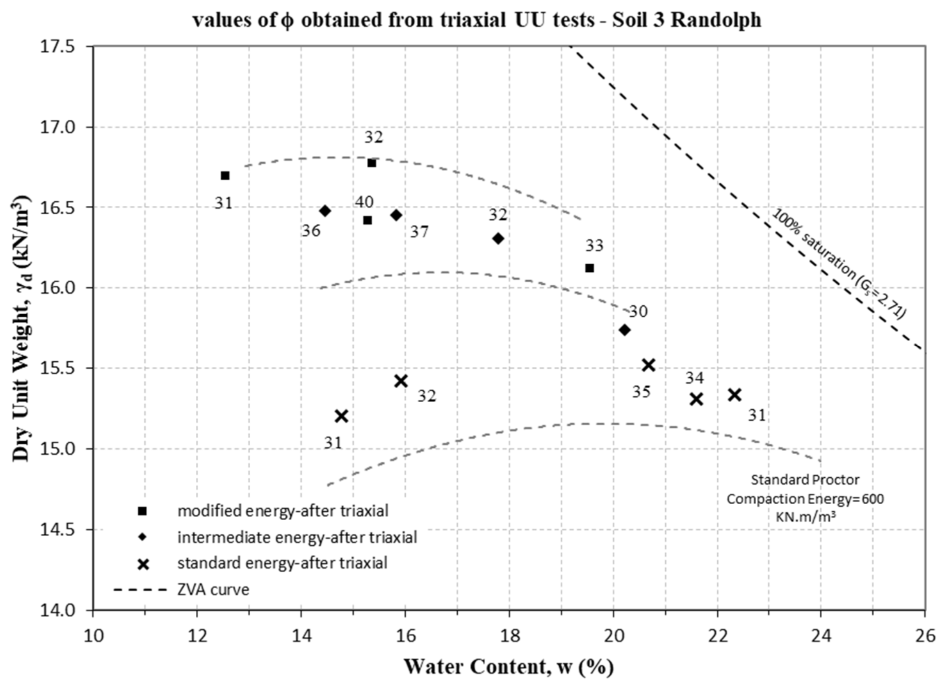

Figure 4.19. Total stress friction angle, f_{UU} (degrees) obtained from UU triaxial tests on Test Soil 3

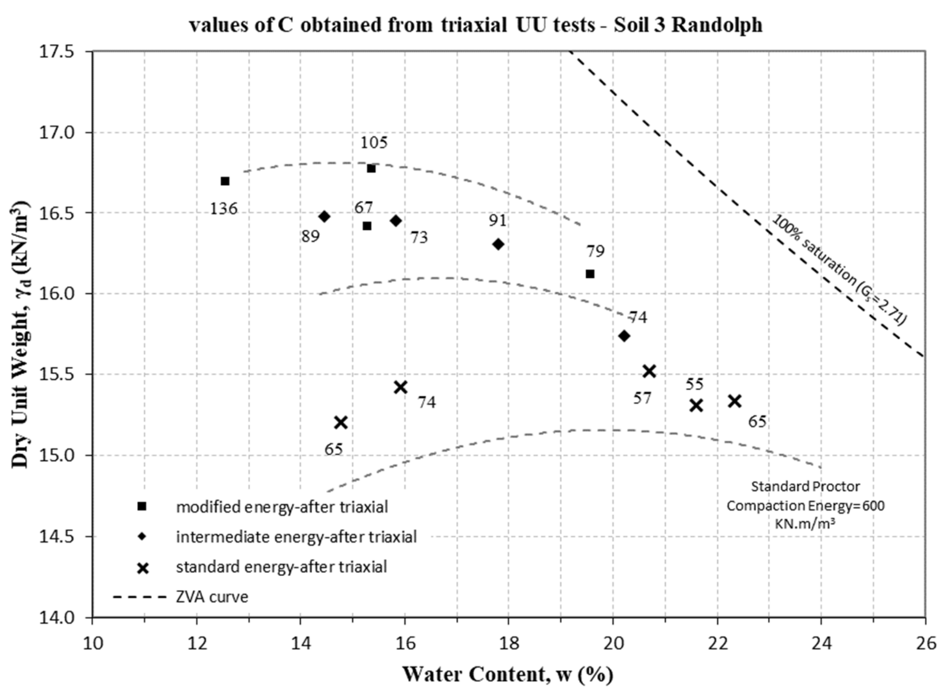

Figure 4.20. Total stress cohesion, C_{UU} (kPa) obtained from UU triaxial tests on Test Soil 3

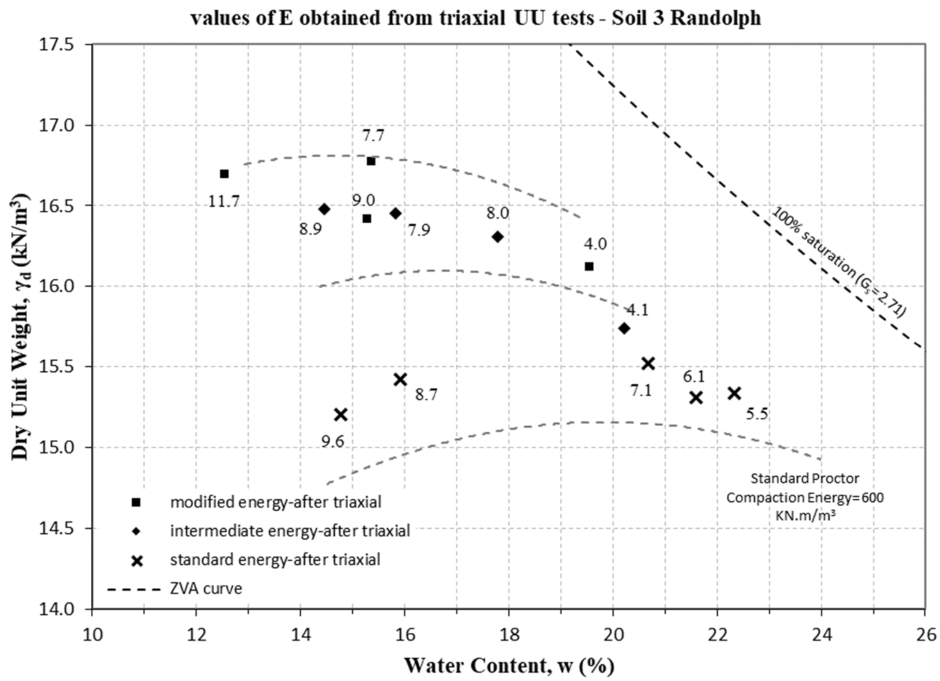

Figure 4.21. Elasticity modulus E_{UU} (MPa) at $s_{cell} = 50\ kPa$ obtained from UU triaxial tests on Test Soil 3

4.4.3.4 Results of UU Triaxial Tests for Test Soil 4

In this section, results of UU triaxial tests carried out on Test Soil 4 (soil sample from Rowan County) is presented. The summary table is presented in Table 4.17. After the summary table, three plots have been provided in Figure 4.22, Figure 4.23, and Figure 4.24 which represent total stress friction angle (f_{UU}), total stress cohesion (C_{UU}), and modulus of elasticity (E_{UU}), respectively.

Table 4.17. Summary information of UU triaxial tests carried out on Test Soil 4

Test No.	**Final w (%)**	s_{cell} **(kPa)**	**Final** g_d **(kN/m^3)**	f_{UU} **(deg)**	C_{UU} **(kPa)**	E_{UU} **(MPa)**
S4-UU1	44.4	25	11.4			1.1
S4-UU2	45.4	50	11.3	26.1	26.5	1.7
S4-UU3	43.7	100	11.6			2.5
S4-UU4	22.2	25	12.9			8.6
S4-UU5	21.9	50	13.1	34.2	68.5	11.5
S4-UU6	22.4	100	13.2			13.9
S4-UU7	20.0	25	15.1			13.6
S4-UU8	19.8	50	15.1	36.5	136.7	15.4
S4-UU9	20.2	100	15.2			17.3
S4-UU10	20.4	25	13.3			8.3
S4-UU11	19.9	50	13.1	32.7	79.3	11.8
S4-UU12	20.0	100	13.4			14.5
S4-UU13	22.5	25	14.6			11.8
S4-UU14	22.2	50	14.5	32.8	120.6	12.8
S4-UU15	22.2	100	14.8			15.4
S4-UU16	22.2	25	15.4			10.8
S4-UU17	22.6	50	15.3	24.5	202.9	12.9
S4-UU18	23.0	100	15.3			14.0
S4-UU19	29.7	25	13.3			6.8
S4-UU20	30.4	50	13.3	30.1	74.3	8.9
S4-UU21	29.1	100	13.4			11.9
S4-UU22	27.0	25	14.4			5.9
S4-UU23	27.5	50	14.4	23.1	134.1	7.0
S4-UU24	28.5	100	14.1			7.9
S4-UU25	27.8	25	14.3			3.6
S4-UU26	27.8	50	14.3	26.9	106.2	4.1
S4-UU27	27.7	100	14.4			5.1
S4-UU28	14.9	25	13.5			12.4
S4-UU29	14.5	50	13.5	33.5	92.5	13.6
S4-UU30	14.0	100	13.7			18.1
S4-UU31	15.8	25	14.9			17.4
S4-UU32	15.9	50	14.7	31.8	153.4	18.9
S4-UU33	15.8	100	15.0			19.8
S4-UU34	15.1	25	15.7			19.9
S4-UU35	14.7	50	15.7	41.6	138.1	21.0
S4-UU36	14.8	100	15.6			22.3

Table 4.17. Summary information of UU triaxial tests carried out on Test Soil 4 (continued)

Test No.	Final w (%)	s_{cell} (kPa)	Final g_d (kN/m^3)	f_{UU} (deg)	C_{UU} (kPa)	E_{UU} (MPa)
S4-UU37	12.7	25	14.7			16.9
S4-UU38	12.5	50	15.0	37.9	138.2	19.2
S4-UU39	12.3	100	15.0			22.2
S4-UU40	12.2	25	15.4			12.4
S4-UU41	12.5	50	15.3	51.4	67.3	21.4
S4-UU42	12.8	100	15.5			23.0

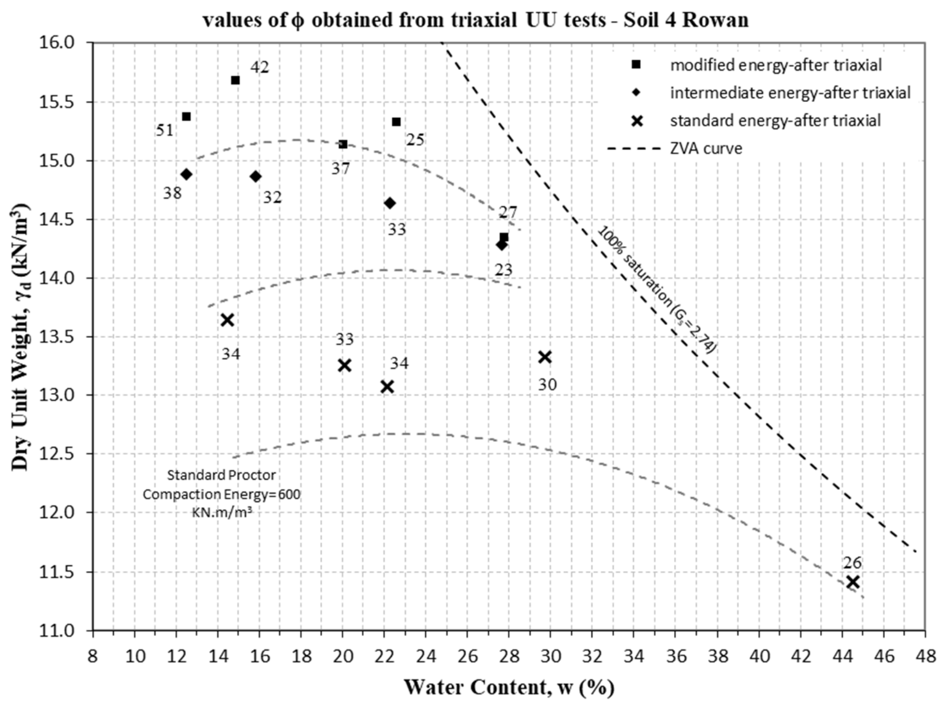

Figure 4.22. Total stress friction angle, f_{UU} (degrees) obtained from UU triaxial tests on Test Soil 4

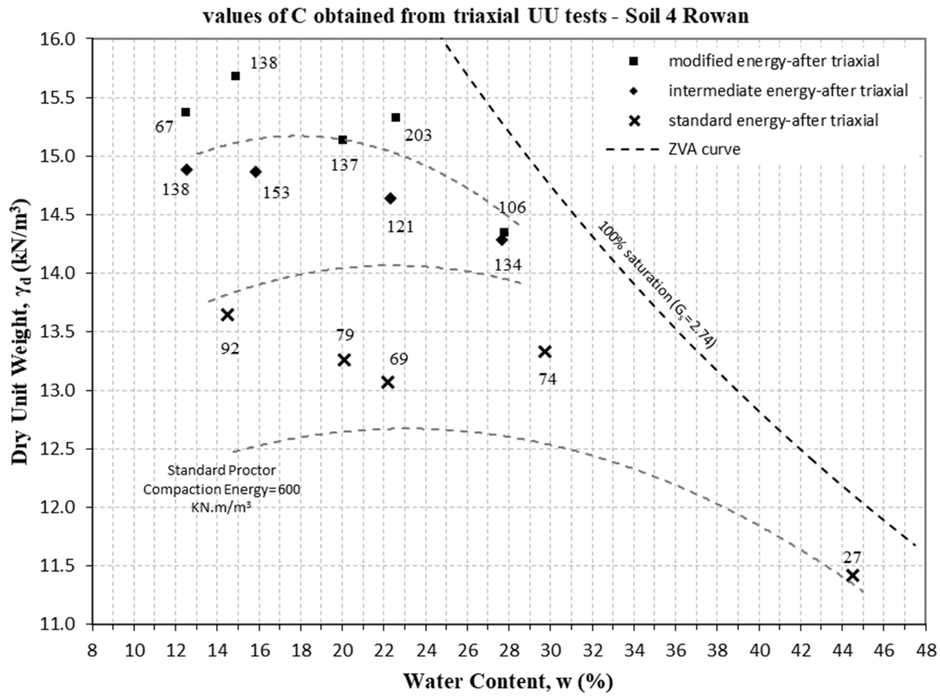

Figure 4.23. Total stress cohesion, c_{UU} (kPa) obtained from UU triaxial tests on Test Soil 4

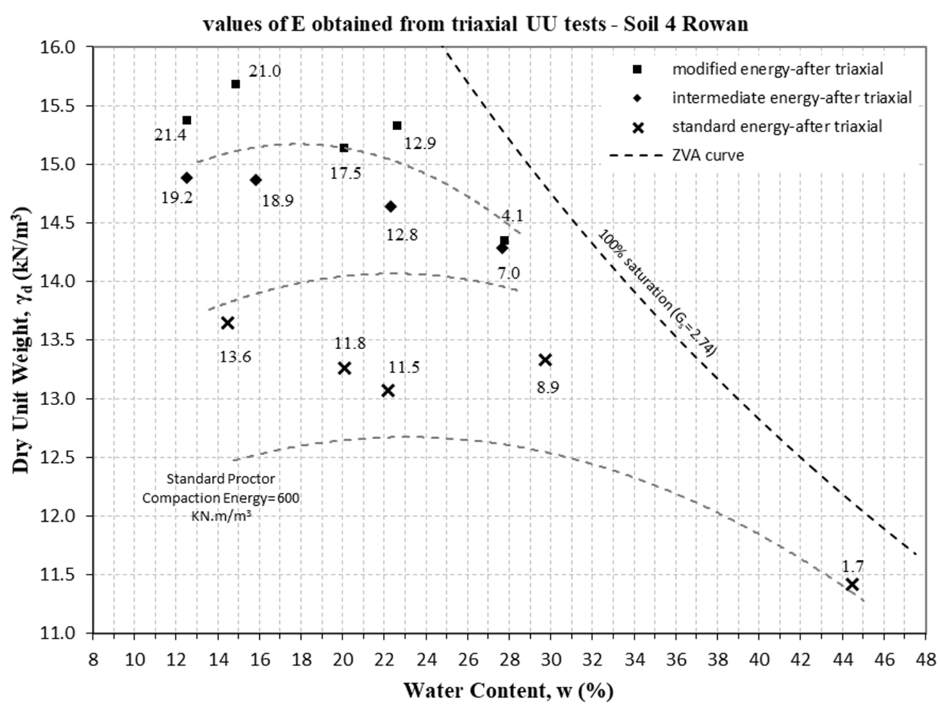

Figure 4.24. Elasticity modulus E_{UU} (MPa) at $s_{cell} = 50\ kPa$ obtained from UU triaxial tests on Test Soil 4

4.4.3.5 Results of UU Triaxial Tests for Test Soil 5

In this section, results of UU triaxial tests carried out on Test Soil 5 (soil sample from Mecklenburg County) will be presented. The summary table is presented in Table 4.18. After the summary table, three plots have been provided in Figure 4.25, Figure 4.26, and Figure 4.27 which represent total stress friction angle (f_{UU}), total stress cohesion (C_{UU}), and modulus of elasticity (E_{UU}), respectively.

Table 4.18. Summary information of UU triaxial tests carried out on Test Soil 5

Test No.	Final w (%)	s_{cell} (kPa)	Final g_d (kN/m^3)	f_{UU} (deg)	C_{UU} (kPa)	E_{UU} (MPa)
S5-UU1	18.2	25	16.0	25.9	93.5	9.3
S5-UU2	18.1	50	15.9			9.7
S5-UU3	17.8	100	15.8			11.6
S5-UU4	21.1	25	15.4	29.0	62.0	6.1
S5-UU5	20.4	50	15.8			8.1
S5-UU6	21.0	100	15.4			9.6
S5-UU7	16.3	25	16.0	30.2	95.1	9.8
S5-UU8	15.5	50	15.9			14.1
S5-UU9	15.8	100	16.0			15.8
S5-UU10	14.6	25	16.7	23.0	148.8	13.3
S5-UU11	14.6	50	16.7			14.2
S5-UU12	14.4	100	16.7			15.1
S5-UU13	16.6	25	16.9	34.4	93.8	7.9
S5-UU15	17.0	100	17.0			13.1
S5-UU16	20.3	25	16.4	28.7	74.8	6.0
S5-UU17	20.2	60	16.5			7.3
S5-UU18	19.9	100	16.6			9.2
S5-UU19	22.8	25	15.6	22.0	85.4	4.7
S5-UU20	23.2	60	15.6			6.0
S5-UU21	22.7	100	15.7			7.2
S5-UU22	13.6	25	15.8	32.5	83.2	12.1
S5-UU23	13.7	50	16.0			13.5
S5-UU24	13.7	100	15.7			14.2
S5-UU25	11.5	25	17.3	29.5	157.8	12.9
S5-UU27	11.2	100	17.0			18.5
S5-UU28	9.3	25	16.3	42.8	90.6	12.0
S5-UU29	9.4	50	16.8			16.1
S5-UU30	9.5	100	17.3			20.5
S5-UU31	18.5	25	15.6	27.5	79.2	8.6
S5-UU32	18.9	65	15.5			9.4
S5-UU33	19.1	100	15.5			10.2
S5-UU34	16.2	25	15.6	25.7	85.6	8.6
S5-UU35	16.8	65	15.4			9.7
S5-UU36	16.7	100	15.5			11.0
S5-UU37	14.4	25	14.7	29.1	60.3	9.4
S5-UU38	14.2	60	15.0			10.3
S5-UU39	14.5	150	14.8			12.2
S5-UU40	10.4	25	14.4	23.5	76.3	10.3
S5-UU41	10.3	60	14.4			11.9
S5-UU42	11.7	100	14.4			13.0

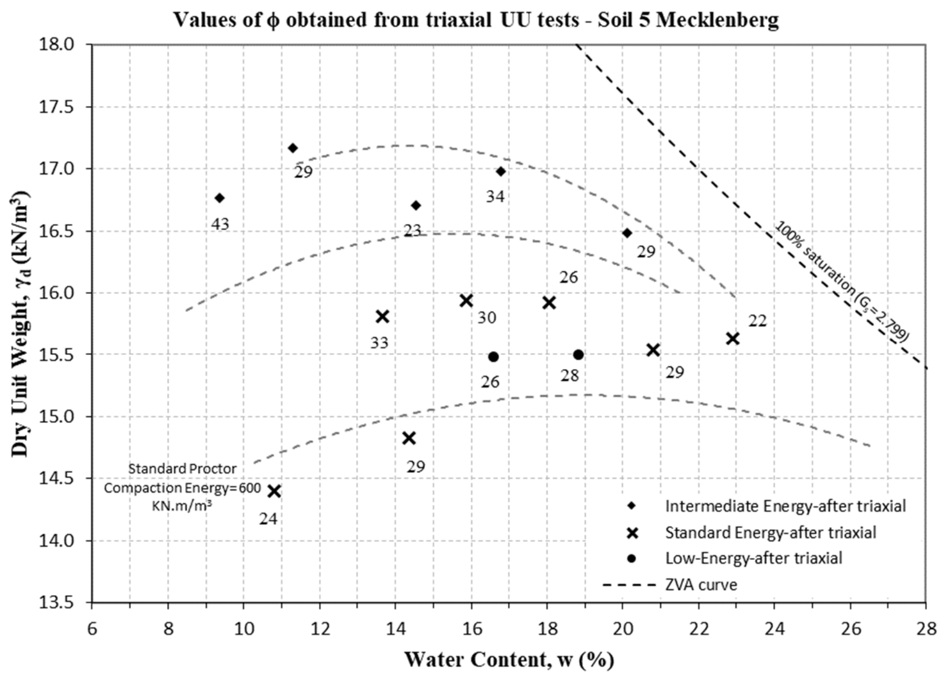

Figure 4.25. Total stress friction angle, f_{UU} (degrees) obtained from UU triaxial tests on Test Soil 5

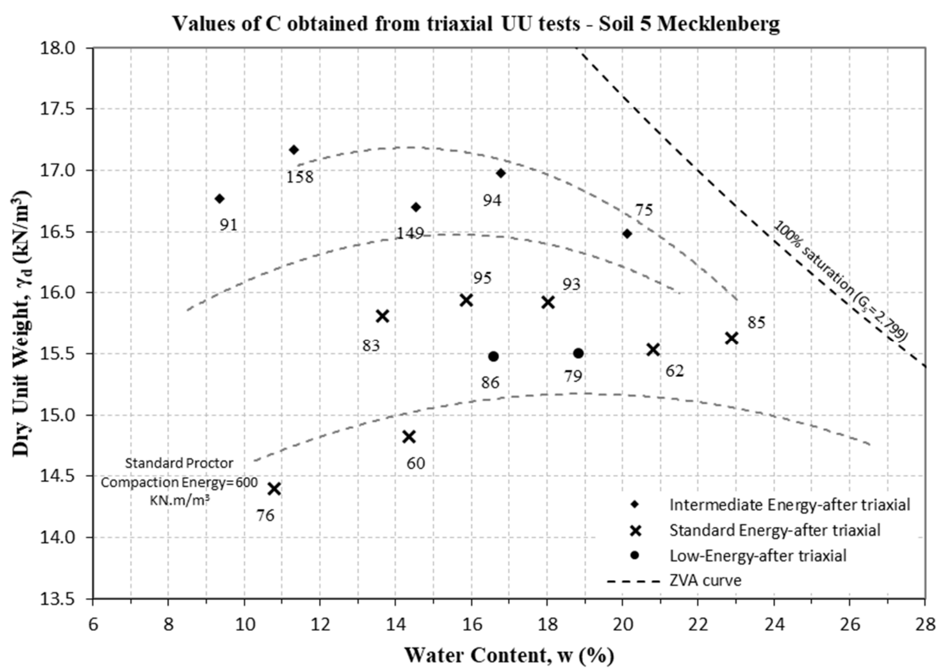

Figure 4.26. Total stress cohesion, C_{UU} (kPa) obtained from UU triaxial tests on Test Soil 5

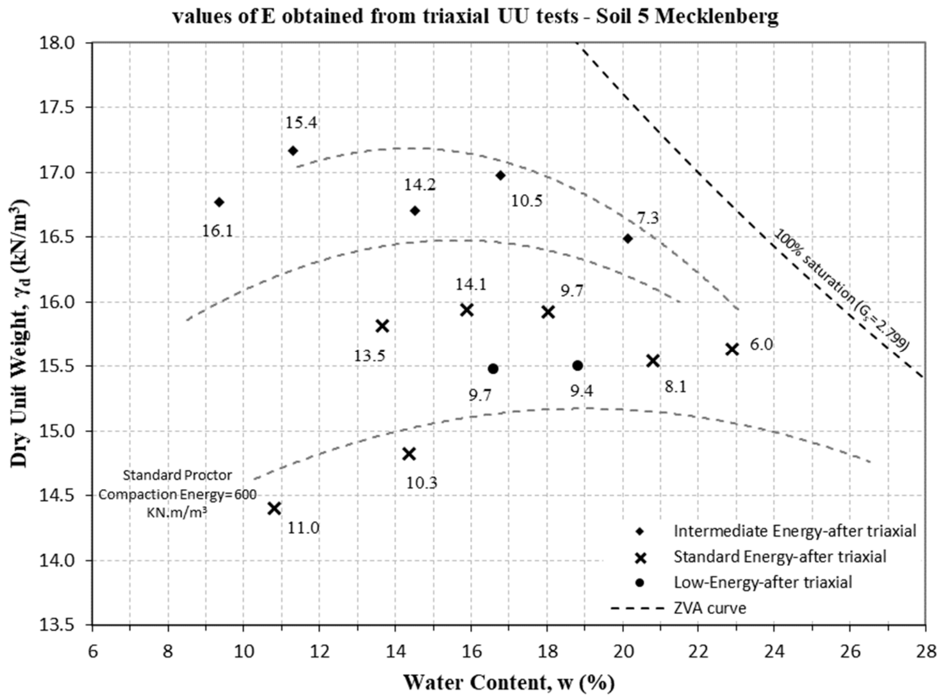

Figure 4.27. Elasticity modulus E_{UU} (MPa) at $s_{cell} = 50\ kPa$ obtained from UU triaxial tests on Test Soil 5

4.5 Consolidated-Undrained Triaxial Compression Tests

4.5.1 Introduction

UU triaxial tests will help to obtain engineering properties of each test soil across the moisture content - dry unit weight space, but not on the saturation line. However, the literature review revealed that one of the dominant types of highway embankment failures is the failure after heavy rainfalls. To study the test soils under this condition, UU triaxial tests will no longer be helpful, as the soil samples are not saturated in these tests. To estimate engineering properties of saturated samples, Consolidated-Undrained triaxial tests have been considered.

4.5.2 Procedure

For the CU triaxial tests, preparation of the specimen and sampling followed exactly the procedure explained for the UU triaxial tests. However, performing the CU triaxial test is different than the UU triaxial test in many aspects. Similar to the UU triaxial, the CU triaxial tests started with an initialization phase where the sample was subjected to a very low cell pressure to confirm no leakage or sensor errors. After the initialization phase, the sample went through a saturation phase. The CU triaxial tests were performed in general accordance with the standard test method ASTM D4767.

Saturation of sample took place by means of increasing cell pressure, then increasing sample pressure (herein called back-pressure) and checking the B-value parameter (Skempton pore pressure coefficient B - Skempton 1954). The pore pressure coefficient B can be simply determined by the equation $B_{value} = \Delta u / \Delta s_3$, where Δu is increase in sample pore pressure due to an increase in cell pressure equal to Δs_3 at each step of the saturation phase. During the saturation phase, effective consolidation pressure (difference between cell pressure and sample pressure) was kept as low as possible. It is also noted that sample pressure was controlled by the FlowTrac-II pump for sample pressure shown in Figure 4.12.

After a high value of B parameter was achieved, consolidation phase started. Effective consolidation pressure (s'_C) was equal to 25 kPa, 50 kPa, and 100 kPa for the three consecutive samples. To simulate field conditions which are inspired by shallow slope failures, low effective consolidation pressures have been used in the consolidation phase.

Following the consolidation phase, the sample was sheared under undrained conditions. The sample was sheared until a maximum axial strain of 15% or until a well-defined peak deviator stress was observed.

For the purpose of this research, failure criterion of generated pore pressure during shear stage equal to zero ($u = 0$) is adopted. According to different researchers, this failure criterion is decent for the following reasons: this criterion results in consistent values of undrained strength ratio with little scatter in the results (Brandon et al. 2006). Also, using this criterion ensures that reliance is not placed on strength that results from negative changes in pore pressure (Torrey 1982).

It is noted that, for each date point, three specimens have been prepared which are compacted at same energy level, and have same moisture content and dry unit weight. Effective consolidation pressure (s'_C) was equal to 25 kPa, 50 kPa, and 100 kPa for the three consecutive samples. Effective stress paths and failure lines associated with the CU triaxial tests have been presented in Appendix C at the end of document.

4.5.3 Results of CU Triaxial Tests

Results of CU triaxial tests are presented in this section. Table 4.19 summarizes essential information associated with the CU triaxial tests. Regarding strength properties (friction angle and cohesion) represented in this table, it is noted that failure criterion of generated pore pressure during shear phase equal to zero (u=0) has been used.

Values of cohesion are also listed in this table. In some few cases where analysis of CU triaxial tests resulted in trivial cohesion value, they are reported zero in this table.

It can be seen that cohesion values are relatively small and negligible, hence one might decide to totally ignore the cohesion component in the effective stress slope stability analysis. It is noted that effective stress slope stability analysis task which will be presented in upcoming chapters, uses CU triaxial tests results as input. However in this research, cohesion component was not neglected for the slope stability purpose, that is, shear strength parameters used for effective stress analyses are as presented in the Table 4.19.

Table 4.19. Summary information of CU triaxial tests

Test No.	Soil ID	molding compactive energy	B_{value}	s'_c (kPa)	initial w (%)	initial g_d (kN/m^3)	before shear w (%)	before shear g_d (kN/m^3)	u=0 failure criterion Ø′ (deg)	u=0 failure criterion C′ (kPa)
S1-CU1	Soil 1	Standard Proctor	0.95	25	15.0	17.5	22.5	16.7	32.5	16.4
S1-CU2			0.89	50						
S1-CU3			0.94	100						
S2-CU1	Soil 2	Standard Proctor	0.96	25	20.6	16.3	35.2	13.8	27.6	3.7
S2-CU3			0.95	100						
S2-CU4	Soil 2	Intermediate Proctor	0.78	25	15.2	18.1	21.6	17.1	29.3	38.5
S2-CU5			0.88	50						
S2-CU6			0.82	100						
S2-CU7	Soil 2	Modified Proctor	0.71	25	14.1	18.5	20.9	17.3	28.6	45.7
S2-CU8			-	50						
S2-CU9			0.64	100						
S3-CU1	Soil 3	Standard Proctor	0.96	25	17.0	14.8	34.7	13.7	30.7	5.0
S3-CU2			0.95	50						
S3-CU3			0.96	100						
S3-CU4	Soil 3	Intermediate Proctor	0.99	25	17.1	16.2	29.7	14.7	37.4	0.0
S3-CU5			0.95	50						
S3-CU6			0.96	100						
S3-CU7	Soil 3	Modified Proctor	0.96	25	12.2	16.5	28.9	14.9	35.9	1.5
S3-CU8			0.95	50						
S3-CU9			0.95	100						

Table 4.19. Summary information of CU triaxial tests (continued)

Test No.	Soil ID	molding compactive energy	B_{value}	s'_C (kPa)	initial w (%)	initial g_d (kN/m^3)	before shear w (%)	before shear g_d (kN/m^3)	u=0 failure criterion f'_{CU}	u=0 failure criterion C'_{CU} (kPa)
S4-CU1	Soil 4	Standard Proctor	0.82	25	22.8	13.4	46.3	11.9	32.4	9.8
S4-CU2			0.98	50						
S4-CU3			0.97	100						
S4-CU4	Soil 4	Intermediate Proctor	0.96	25	18.3	14.5	35.8	13.6	36.2	4.9
S4-CU5			0.96	50						
S4-CU6			0.96	100						
S4-CU7	Soil 4	Modified Proctor	0.97	25	15.7	15.8	34.2	13.9	34.1	14.2
S4-CU9			0.96	100						
S5-CU1	Soil 5	Standard Proctor	0.96	25	13.4	16.1	36.4	13.6	28.8	0.0
S5-CU3			0.95	100						
S5-CU4	Soil 5	Intermediate Proctor	0.95	25	10.9	16.6	32.8	14.3	32.3	3.3
S5-CU5			0.96	50						
S5-CU6			0.95	100						
S5-CU7	Soil 5	Modified Proctor	0.96	25	12.9	17.5	31.8	14.5	43.2	0.0
S5-CU9			0.95	100						

Behavior of the samples in CU triaxial tests was quite interesting. A graph on the moisture content-dry unit weight space is used to show position of the points during the course of CU triaxial test. This type of graph is shown for all test soils respectively in Figure 4.28 through Figure 4.32. This graph actually shows how samples move toward saturation line during the CU triaxial test. Original compaction curves at three energy levels are depicted on this graph as well. Also on this graph value/values of the effective friction angle is written which might be useful for practical purposes, such as slope stability analysis.

Downward move of the points on this type of graph which can be seen for all soil samples, is an indication of swelling. It is reminded that dry unit weight is defined as weight of soil solids (w_s) over total volume of sample. Having w_s constant for a sample during a CU triaxial test, implies that total volume must have increased, due to saturation process. This is a common behavior reported by researchers working with clay/silt soil samples (VandenBerge et al. 2014). It is also noted that to calculate specimen cross-sectional area after consolidation, Method B of ASTM D4767 has been used. It is further noted that equation presented in Method A of this standard never resulted in consistent results.

At the end of this chapter a table is presented which summarizes essential information of particular CU triaxial tests that were carried out in this research.

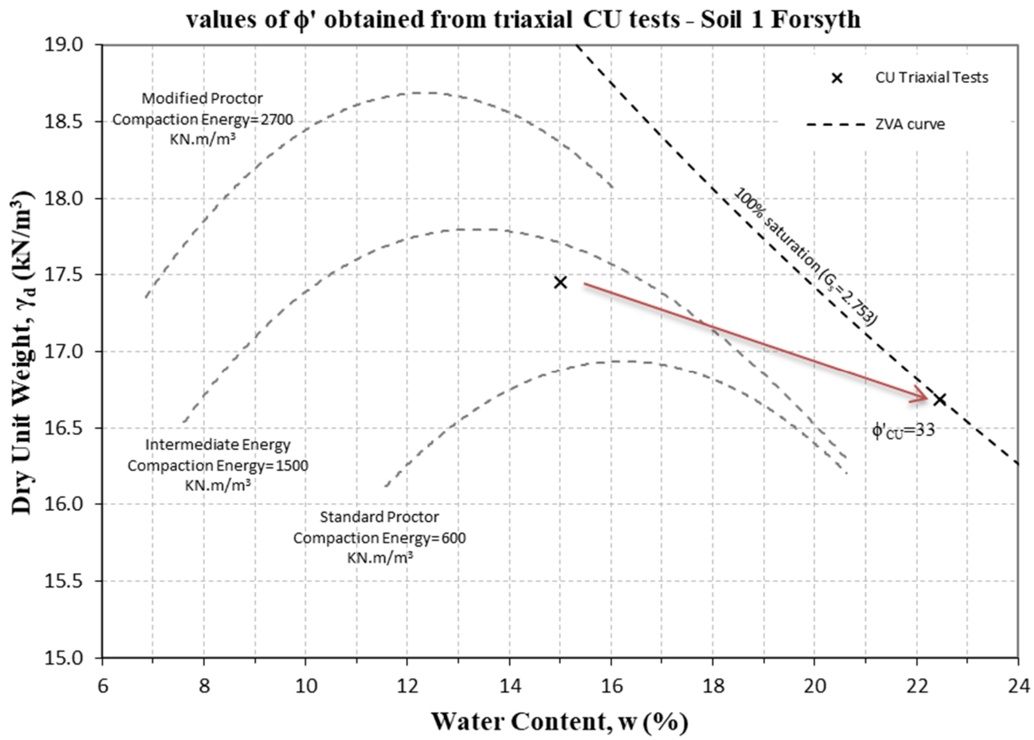

Figure 4.28. Effective stress friction angle, ϕ' obtained from CU triaxial tests - Soil 1

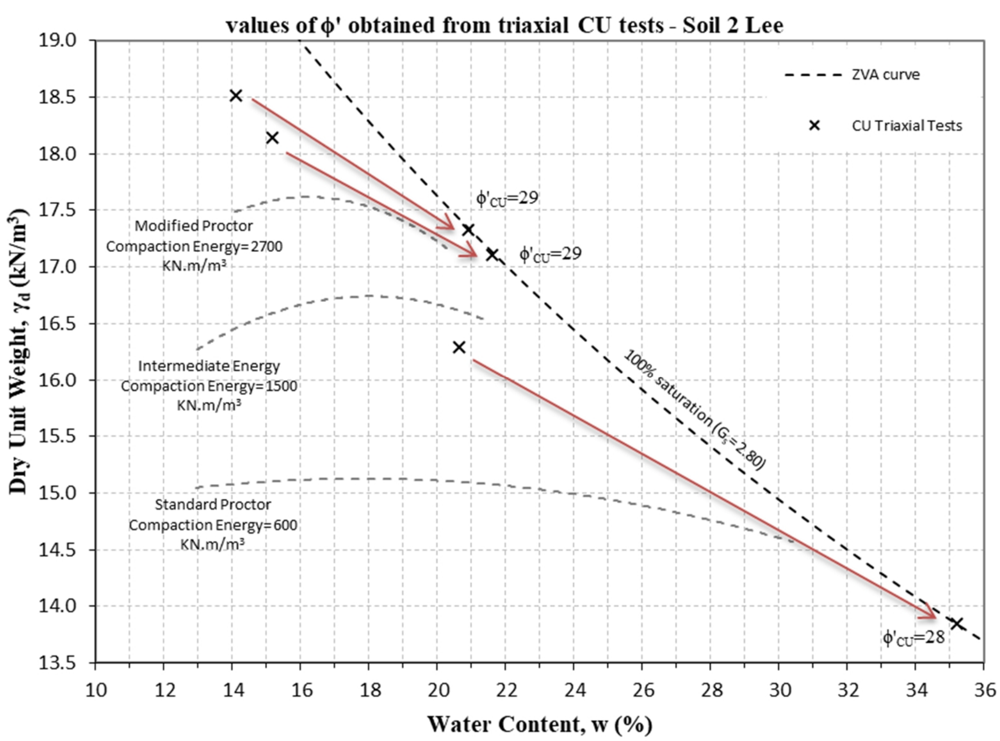

Figure 4.29. Effective stress friction angle, ϕ' obtained from CU triaxial tests - Soil 2

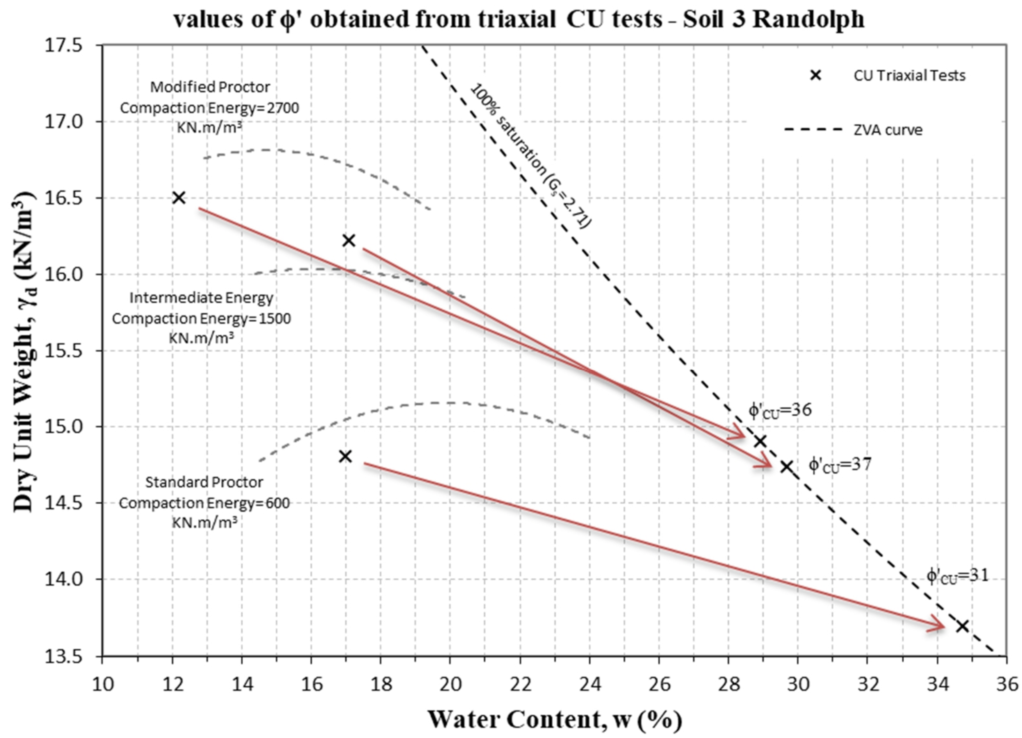

Figure 4.30. Effective stress friction angle, ϕ' obtained from CU triaxial tests - Soil 3

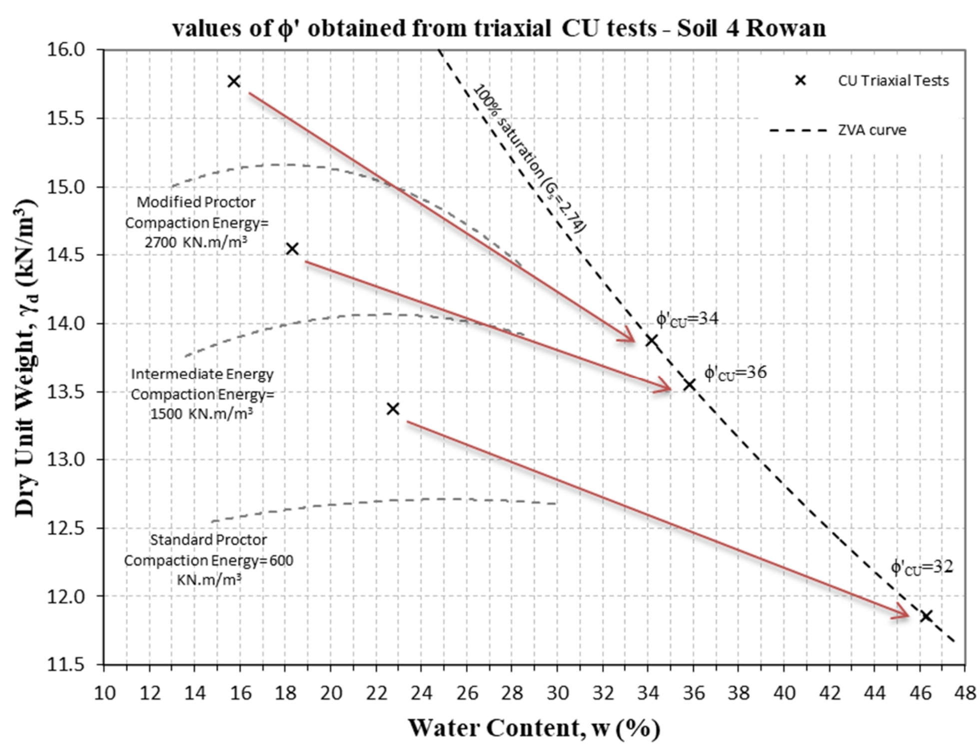

Figure 4.31. Effective stress friction angle, ϕ' obtained from CU triaxial tests - Soil 4

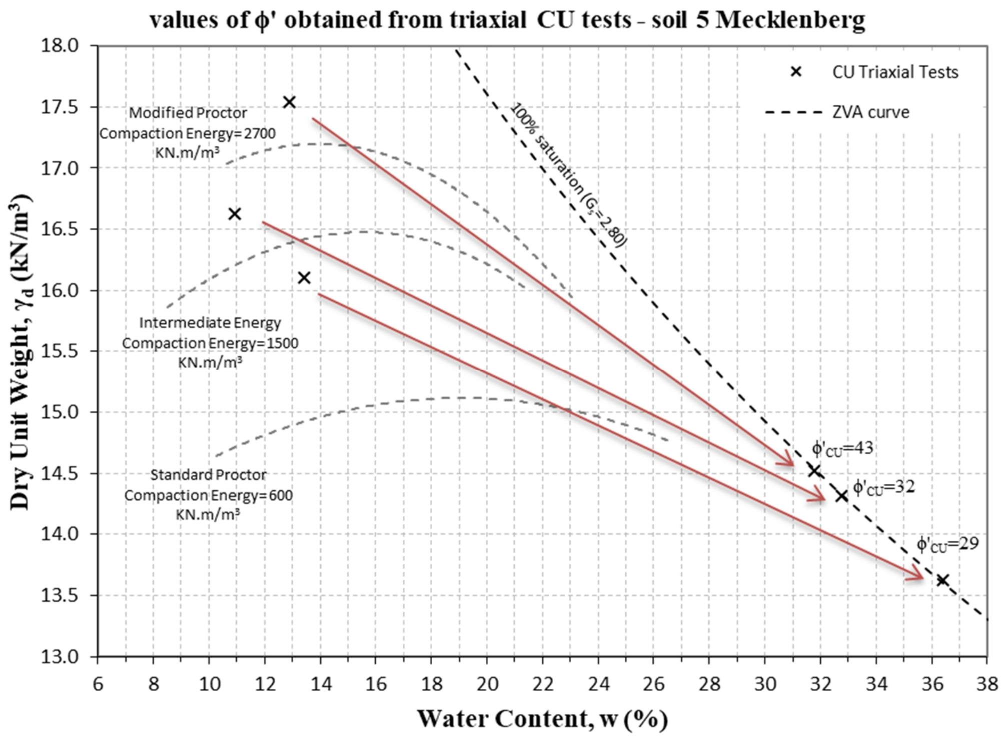

Figure 4.32. Effective stress friction angle, ϕ' obtained from CU triaxial tests - Soil 5

4.5.4 Discussion of CU Triaxial Results versus UU Triaxial Results

It seems effective stress friction angles are same or slightly lower than those of obtained from the total stress analysis. But cohesion terms obtained from the effective stress analysis are noticeably lower than those of from the total stress analysis. Figure 4.33 illustrates differences between effective stress and total stress parameters. This may be due to a concept know as apparent cohesion in the geotechnical literature (Carter and Bentley 1991; Briaud 2013). In an unsaturated soil specimen with occluded air phase, strong suction exists among water molecules which holds soil particles tightly close to each other. As soil specimen becomes saturated, suction disappears and as a result, cohesion and FS associated with that decrease dramatically.

This phenomenon may lead us to think about the need for new type of analyses. For this new analysis, we may decide to ignore the cohesion obtained in a UU triaxial test (C_{UU} in Figure 4.33), resulting in a new Mohr-Coulomb failure envelope that might be used for slope stability analysis. This type of analysis which is called modified total stress analysis will be discussed and reviewed in Chapter 5, Section 5.3.3.

However, as mentioned in Introduction of this chapter one of the dominant types of highway embankment failures is the failure after heavy rainfalls. Hence, to study behavior of saturated soil samples, engineering properties obtained from ESA failure line/envelope (shown in Figure 4.33) will be used.

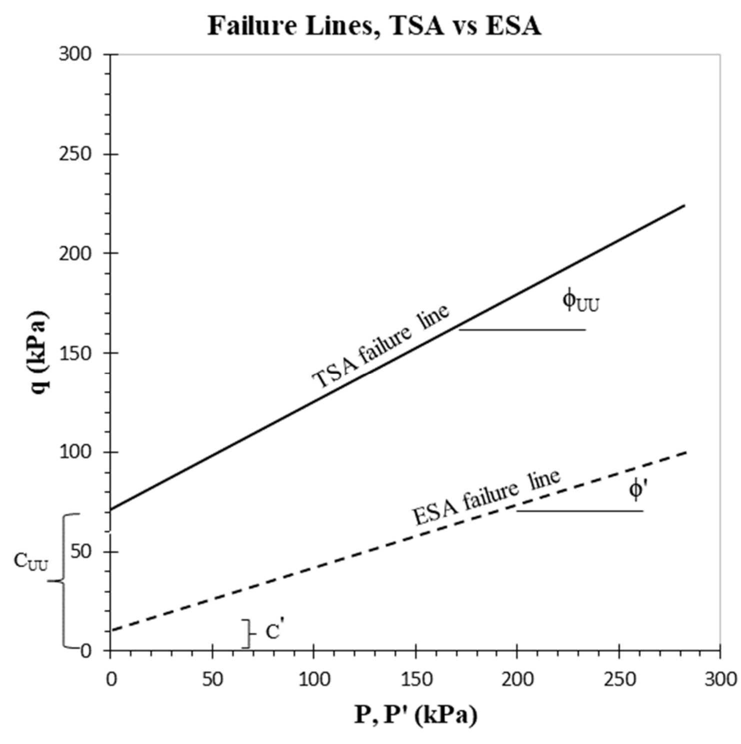

Figure 4.33. TSA failure line vs ESA failure line

4.6 One-Dimensional Creep Compression Tests

4.6.1 Introduction

Besides slope stability and immediate deformation, we could mention another criterion which must be addressed when talking about the performance of highway embankments. This concern is the long-term deformation or "creep" of highway embankment. For the purposes of this research, creep refers to the long-term deformation of soil under a constant load. Creep of saturated clays has been studied extensively as part of the consolidation behavior of clays. However, it is important to point out that in those cases, creep refers to the secondary consolidation of a saturated soil that has first undergone a one-dimensional consolidation phase.

Besides the need to investigate possibility of unacceptable long-term deformation related to soils with high plasticity index, we are also interested to look into the creep characteristics of compacted soils; features such as strain rate and effect of moisture content. Such items has been studied by the "one-dimensional creep compression tests" program. Procedure and initial results of these tests are presented in this chapter, further interpretation of results will be presented in Chapter 6.

4.6.2 Properties of Utilized Soils

Two of the test soils already described in this chapter, Test Soil 2 (from Lee county) and Test Soil 5 (from Mecklenburg county) have been selected for one-dimensional creep compression tests. Detailed index properties of these soil samples were already presented in Table 4.2. The two soil samples selected for testing program of this section, are actually the ones with highest PI (Test Soil 2), and lowest PI (Test Soil 5) among the test soils.

4.6.3 Creep Tests Testing Matrix

A total of 8 tests have been considered to study the creep characteristics of the embankment soils. As stated earlier, Test Soil 2 from Lee County and Test Soil 5 from Mecklenburg County across North Carolina have been selected. Three vertical stresses (σ_V) of 50 kPa, 100 kPa, and 200 kPa have been chosen. This matrix consists of a set of six creep tests, three on each of the test soils, in addition of 2 tests to study the effect of moisture content. To study the effect of moisture content, one test on wet-of-optimum side and another one on dry-of-optimum side of Lee test soil have been considered. Table 4.20 summarizes the testing matrix for this section.

Table 4.20. Testing matrix for creep tests

Test No.	Test Soil ID	Compaction conditions	σ_V (kPa)
Test 1	Test Soil 2	Standard Proctor - OMC	50
Test 2	Test Soil 2	Standard Proctor - OMC	100
Test 3	Test Soil 2	Standard Proctor - OMC	200
Test 4	Test Soil 5	Standard Proctor - OMC	50
Test 5	Test Soil 5	Standard Proctor - OMC	100
Test 6	Test Soil 5	Standard Proctor - OMC	200
Test 7	Test Soil 2	Standard Proctor - OMC+3%	100
Test 8	Test Soil 2	Standard Proctor - OMC-5%	100

4.6.4 Creep Tests Procedure

To investigate long-term settlement characteristics of embankment soils, a series of one-dimensional (1D) compression tests using traditional consolidation devices (also called as oedometer) has been designated.

After breaking clogs and sample preparation (Figure 4.34 a) compaction tests were performed at energy level equal to Standard Proctor with molding moisture contents close to the optimum moisture content (OMC). Figure 4.34 depicts consecutive steps needed to perform a creep test. To obtain oedometer specimen, consolidation ring (the solid ring) was pushed into the compacted soil sample. Unit weight of obtained specimens was monitored and compared with unit weight of the soil inside the compaction mold. Then, solid ring was trimmed off from the soil outside the ring and finial trimming was performed (Figure 4.34 c) to reach the oedometer specimen (Figure 4.34 d). After having the oedometer specimen ready, two filter papers were placed on top and bottom of specimen. It is noted that filter papers were brought to the same moisture content of the soil specimen. Porous stones are components which provide a continuous flow of fluid or gas through the specimen; thus, it was decided to use solid steel discs on top and bottom filter paper instead of the porous stones which are used in the conventional consolidation tests. The non-porous steel disc will help specimen obtain its molding moisture content throughout the long test period, and also will help the vertical stress to transform uniformly across the specimen surface. Solid ring along with filter papers, steel disc and loading pad (Figure 4.34 e) are now placed inside the consolidometer cell.

One-dimensional creep tests discussed in this section, are in essence very long tests. To keep the moisture content of soil specimen constant throughout the test, the consolidometer was placed inside a plastic bag with a piece of moist sponge (Figure 4.34 f). It was seen by try and error that these measures are satisfactory.

(a) sample preparation, breaking clogs, adding water to reach designated moisture

(b) compaction test and pushing the solid ring

(c) trimming off soil outside the oedometer ring

(d) oedometer specimen

(e) placing filter papers on top and bottom, steel disc and loading pad on top of the specimen

(f) oedometer creep test setup

Figure 4.34. Illustration of different steps needed to perform a creep test (one-dimensional compression)

During the testing process, it was observed that consistency of the dial gauges which were used to measure the deformation of soil specimens has paramount influence. For deformation measurement, Mitutoyo dial gauges with 0.0001 inch precision were utilized. It is also noted that, to know the exact loading arm factor, each of the oedometer frames were calibrated in advance. The load factor for oedometers is traditionally acknowledged to be equal to 10. Details of calibration process for the oedometers will be presented in Appendix D.

Figure 4.35 shows dry unit weight of compaction mold specimen versus dry unit weight of the oedometer specimen. This plot may be used as an indication to estimate disturbance level due to sampling process.

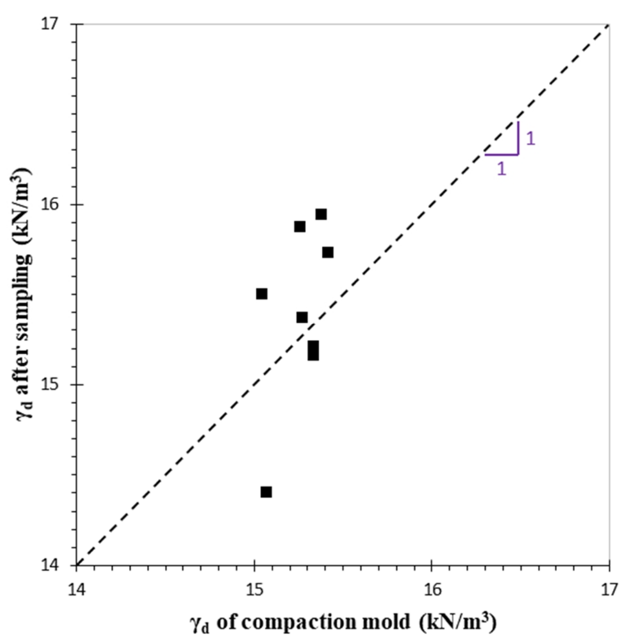

Figure 4.35. Disturbance level due to sampling process

It is noted that one creep test may take as long as one month; hence, importance of a measure to maintain moisture content of the soil specimen cannot be overemphasized.

Using a sponge inside a bag to maintain moisture content of the specimen was observed to be a very effective measure. If the sponge had not been used, or if the sponge did not have enough moisture, the specimens would have ended up with a very low moisture content. It is noted that the sponge must be kept at a moisture content which is much higher than that of for the soil specimen; a moisture content around 100% seemed satisfactory. Figure 4.36 shows variation of moisture content of the test specimens during test period, that is moisture content at the end of creep test versus moisture content after sampling process. It can be seen that these two values are very close to each other for the 8 creep tests presented in this chapter.

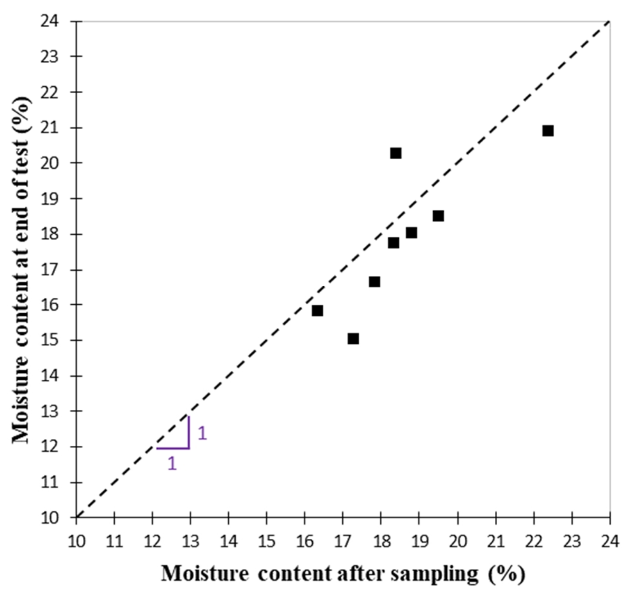

Figure 4.36. Variation of moisture content of all creep test specimens throughout the test

4.6.5 Results of Creep Tests

In this section, results related to the deformation of creep tests will be presented. To hold a consistency among all results, deformation of specimens has been presented in the form of vertical strain. Vertical strain is presented versus time in three different forms of:

natural time, logarithm of time, and square root of time, after that specifications of the graphs will be discussed.

According to the ASTM standard test method for one-dimensional consolidation properties of soils (ASTM D2435), the measured axial deformations shall be corrected for apparatus compressibility whenever the equipment deformation exceeds 0.1% of the initial specimen height or when using filter paper screens. The older version of this standard is slightly different in terms of need for calibration correction; as it states that if the determined calibration exceeds 5% of the measured vertical deformation or if filter paper disks are used in the test, measured vertical deformation must be corrected.

Considering any of the two cases, it was observed that for the creep tests performed for this research, the measured vertical deformation needed correction. To perform calibration tests, the consolidometer was assembled in a similar way for the creep tests, except a hard steel disk replacing the soil specimen. Filter papers were placed on top and bottom of the hard steel disk. Filter papers were moistened to the same degree that they were supposed to present in the actual deformation tests.

Figure 4.37 shows the result of calibration tests for three stress levels used in the creep tests, that is 50 kPa, 100 kPa, and 200 kPa. The amount of calibration correction due to filter papers was seen to be as large as 35% of the uncorrected deformation of soil specimens; thus, confirming the need to perform the calibration correction. In addition, the amount of calibration correction almost did not alter after one week of constant loading. It was decided to use power functions as the fitting curve to calculate the amount of calibration beyond the testing period of one week. Figure 4.37 also shows the power fitting curves.

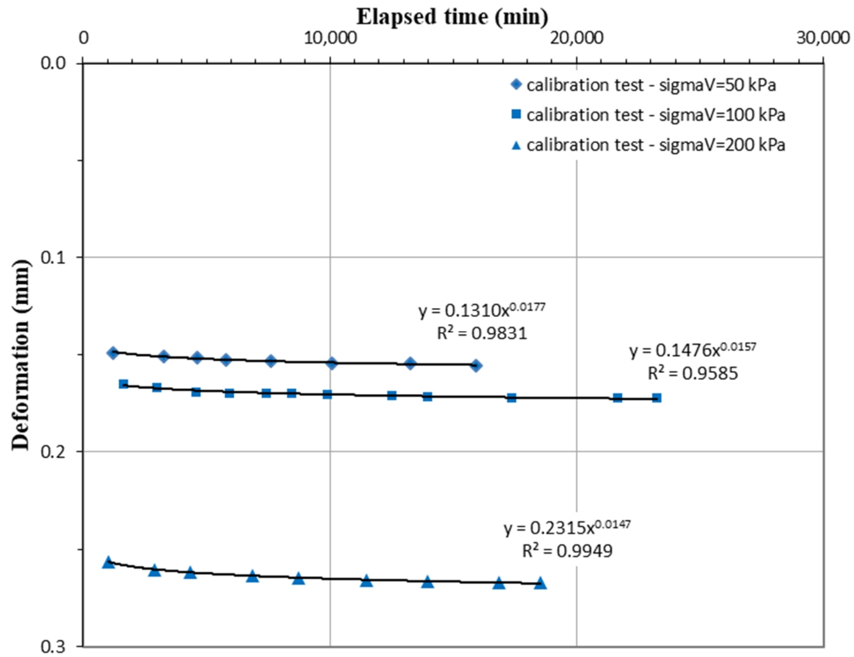

Figure 4.37. Calibration tests results for three stress levels

Figure 4.38 shows vertical strain versus time in natural form. It can be seen that the curves generally consist of two main parts: initial sharp settlement due to immediate response to external loading, followed by a linear section representative of creep deformation. As creep (of any material such as soil, or concrete) is a long-term process, it is usually measured in terms of rate of deformation over time. Hence, the slope of this linear section may be introduced as creep rate ($\dot{\varepsilon}$), which has the unit of percent over time. Creep rate of the tests performed in this section will be discussed later.

The initial part of these curves is related to the compressibility of soil specimens. It is noted that, compressibility characteristics of soil specimens was observed to be highly influenced by sampling method and dry unit weight. The author would like to add that, to find the position of the start point of the curves, a set of strain-hardening tests under similar conditions but with constant rate of strain, was utilized. The rate of application of vertical strain was different and the start point was selected such that it produces a strain rate equal to the actual creep test. However, compressibility characteristics of soil specimens is out of scope of this research.

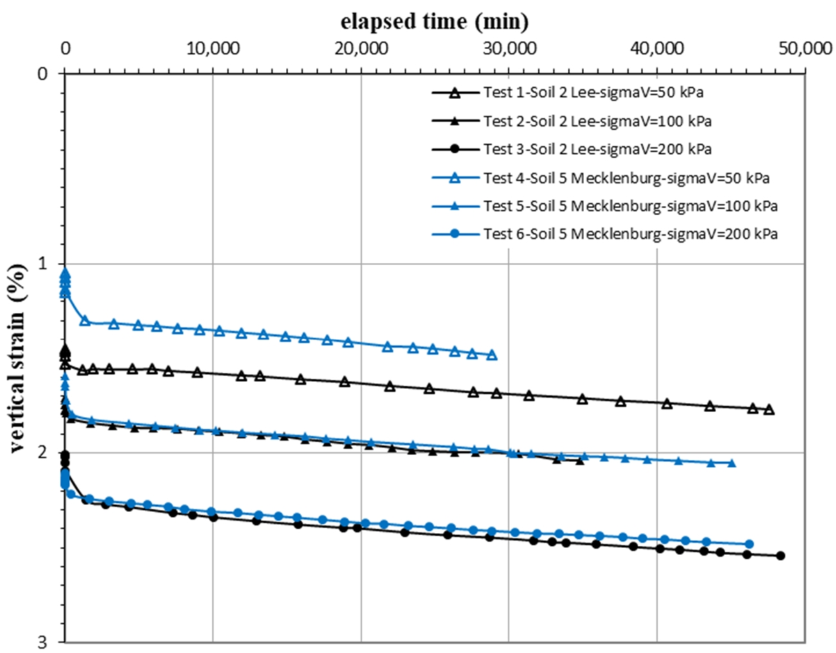

Figure 4.38. Vertical strain versus time

It should be noted that having moisture content of the specimen constant throughout the test is a paramount factor; based on few tests, it was observed that if the moisture content of sample is not kept constant (that is, if it decreases with time), creep rate would be much different (higher) from the actual results. Of course, these tests were considered failed and are not reported in this section.

Figure 4.39 displays vertical strain versus logarithm of time. In this scale, results show a curvature after spending a portion of time (usually more than one week). This behavior is similar to the curvature found in the consolidation curve (void ratio vs log of pressure), which is an indication of the pre-consolidation pressure.

In the square root of time curves, similar to the natural time curves, behavior of samples may be characterized by two phases: initial sharp settlement due to immediate response to external loading, followed by a linear section representative of the creep deformation. Figure 4.40 shows deformation results versus square root of time.

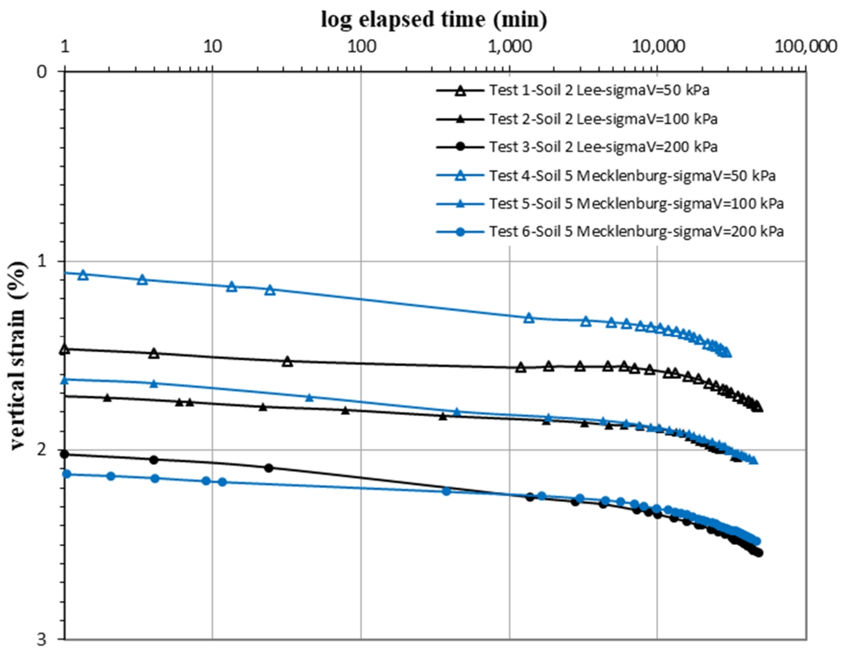

Figure 4.39. Vertical strain versus log of time

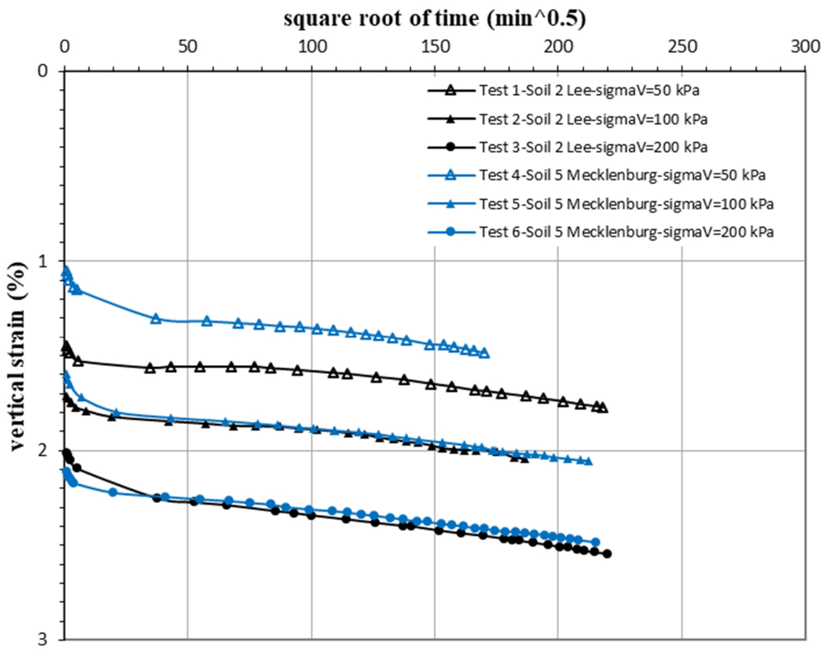

Figure 4.40. Vertical strain versus square root of time

4.7 Summary

Soil samples from across the Piedmont area of North Carolina have been selected for the purpose of this research. This chapter starts with description and index testing results of the five test soils, then proceeds with the procedure and results pertaining to compaction tests, UU triaxial tests, and CU triaxial tests. Information regarding procedure and initial results for the creep compression tests conclude the chapter.

For the UU triaxial tests, rate of the axial strain was equal to 1%/minute. Failure criterion of maximum deviator stress or limiting axial strain of 15%, whichever occurred first was utilized. For the CU triaxial tests, failure criterion of generated pore pressure during shear stage equal to zero has been adopted. Effective stress friction angles are same or slightly lower than those of obtained from the total stress analysis. However, cohesion terms obtained from effective stress analysis are noticeably lower than those of from total stress analysis.

CHAPTER 5: SLOPE STABILITY ANALYSIS

5.1 Introduction

This chapter consists of two main sections: a description of the approach used for the slope stability analyses, and results of the slope stability analyses. Slope stability analyses performed in this research have been carried out for the shear strength parameters obtained from total stresses and effective stresses. For the total stress analyses (TSA) the strength parameters were based on the UU triaxial test results, while for the effective stress analyses (ESA) the strength parameters were based on the CU triaxial test results. In addition, a third type of analyses called modified total stress analyses (TSA,m) have been considered which is based on total stress parameters with neglecting cohesion term. It is noted that slope stability is one of the two performance criteria of the proposed design approach for highway embankments, a topic already discussed in Chapter 3.

5.2 Approach Used for Slope Stability Analyses

The slope stability analyses were carried out using 2D limit equilibrium method based on different methods and procedures. This section describes the general strategies used for the slope stability evaluation of the different embankment geometries built with different test soils having different placement conditions in terms of placement moisture content and compacted dry unit weight.

It is reminded that the scope considers only failures and settlements related to the compacted embankment and not due to poor foundation soil conditions.

To start the slope stability analysis task, one could come up with the idea to input the data into the software and get factors of safety. However, concepts such as critical slip surface, investigation of minimum factor of safety, and mode of failure have received special attention in this research. For this purpose, first a section called "investigation of critical slip surface over the embankment crest" has been studied and significant findings will be presented here. This section is intended to explain and justify the method used for the slope stability analyses.

Embankment sections/geometries were introduced in Chapter 3 where research methodology was presented. Sixteen (16) sections are considered in total for both slope stability analysis task and deformation analysis task. These sections were listed in Table 3.1. Also, external loading on embankment was discussed in Chapter 3.

Slide software (Rocscience, SLIDE version 2018 8.018) has been used to perform slope stability analysis task. It is noted that results of the Slide software have been cross-checked with factor of safety charts (Taylor 1948), as well as another commercial software called GeoStudio-SLOPE/W (Geoslope 2021a).

For the slope stability analyses, five methods of ordinary/Fellenius, Bishop simplified, Janbu corrected, Spencer and Morgenstern-Price were considered. Setting aside the old method of ordinary/Fellenius which gives unreasonably low factors of safety, Spencer method, on average, gives the minimum among the other four and hence will be used. FS from Morgenstern-Price method is in most of the cases equal to or very slightly more than that of from Spencer's.

It is also noted that increasing number of slices which indicates a more accurate analysis, usually tends to slightly increase the value of FS. Number of slices was set equal to 100 in most of the cases, unless the analysis time was unreasonably long which forced us to decrease number of slices to 50.

5.2.1 Investigation of Critical Slip Surface over the Embankment Crest

Values of factor of safety need to be investigated and compared for all geometries as well as all data points. To maintain a consistency among all failure cases, one may decide to consider a constant slip surface for all geometries and all material properties. For example, we could come up with the idea that all slip surfaces start from a point 5 ft beyond the embankment head (crest) and exit from the toe of embankment. But this would be only an assumption; in reality, we need to investigate the location over the crest of embankment where the minimum FS will take place. To further investigate the most appropriate slip surface, a task entitled as "investigation of critical slip surface over the embankment crest" were defined which is discussed in this section very concisely.

To investigate the minimum FS over the crest of embankment, intervals of 5 ft were selected as the offset distance from the edge of crest (i.e. 5ft, 10ft, 15ft, 20ft, and so on from the edge of crest). Predefined slip surfaces were considered such that the start point of each individual slip surface is embankment toe and exit point locates on the crest with the designated offset distance from the edge of crest. However, this type of analysis is called offset analysis in this study.

Alternatively, the well-known critical slip surface search based on the “grid and radius” search was also performed. Conclusion of the “offset analysis” effort may be stated as following.

The factor of safety obtained from the “grid and radius” search method was always lower than that of obtained from the “offset analysis”. Consequently, for each individual geometry and material property, running a global search using the “grid and radius” method seems to be a necessary and even satisfactory step. However, special attention have been given to the geometry of the critical slip surface itself and different modes of failure have been defined based on this fact, which will be discussed later in this chapter.

5.2.2 Infinite or Shallow Slope Stability Analysis

Addressing the methodology for slope stability analysis, special caution must be exercised toward “infinite slope stability”, meaning that FS for the shallow failure should also be investigated. This important task has been carried out; in any case where the FS from the shallow failure was lower than that of from the grid and radius search, the one from shallow failure has been reported. Therefore, for example for any of the 192 cases that was run on Test Soil 1, the minimum FS is being reported.

Figure 5.1 shows the typical geometry of an infinite slope. The required equation to calculate FS for infinite slope stability is proven to be as Equation (5.1).

$$FS = \frac{C}{g_m . z . \sin b . \cos b} + \frac{\tan f}{\tan b} \tag{5.1}$$

where C and f are cohesion and friction angle of soil, z is the depth of failure, g_m is the moist unit weight of soil and b is the slope angle. It is noted that z should not be confused with H, height of embankment, and also z is much smaller than L, length of the shallow slope failure. It is also noted that in case the soil material of a slope is saturated due to a heavy rainfall for example, effective stress strength parameters (C' and f') may be entered into this equation.

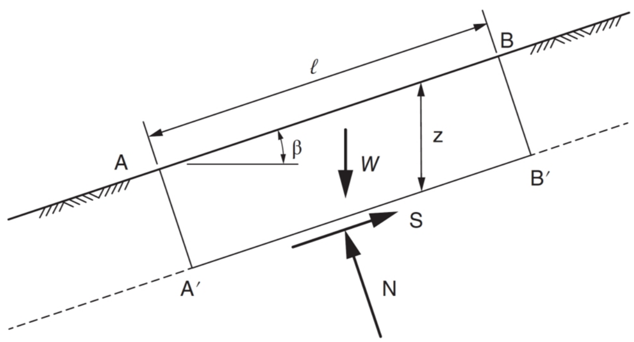

Figure 5.1. Infinite slope stability analysis (adopted from Duncan et al. 2014)

As mentioned in the literature review chapter, the depth of the shallow slope failure varies with soil type and slope geometry, but generally ranges between 0.9 and 2 m (3-7 ft) (Loehr et al. 2007; Briaud 2013). For the purpose of calculations done for shallow slope failure, Z is assumed equal to 1.5m (≈5ft) which seems to be a conservative choice (relatively high Z) as higher values of Z results in lower FS.

5.2.3 Modes of Failure

Different modes of failure which were encountered during slope stability analysis effort of this research will be explained in this section.

Observed modes of failure could be categorized into the following three cases: non-shallow, local, and shallow (same as infinite). Non-shallow failure has a critical slip surface which goes through all the embankment slope and is the result of a global grid search (grid and radius search). We avoid calling this mode of failure "global", as global is a terminology usually referring to a critical slip surface which includes embankment and foundation. As stated earlier in this chapter, this critical slip surface (non-shallow) starts more or less from the embankment toe and cut the embankment crest at a distance from edge. Local failure also is a result of global grid search (grid and radius search), but in this case the critical slip surface does not include all the embankment slope. Finally, shallow or infinite mode refers to the result of using Equation (5.1) with Z being 1.5m. Figure 5.2 schematically illustrates non-shallow slip surface and local slip surface. Shallow slip surface/failure was already depicted in Figure 5.1.

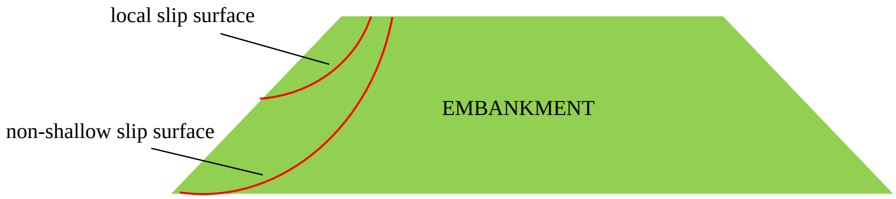

Figure 5.2. Schematic display of non-shallow slip surface and local slip surface

5.3 Results of Slope Stability Analyses

Results of the slope stability analyses will be presented in this section. Results pertaining to the slope stability analyses using total stress parameters, effective stress parameters, and modified total stress parameters have been presented in separately sections.

5.3.1 Total Stress Slope Stability Analysis Using UU Triaxial Parameters

Extensive number of tries/runs are needed for each of the analysis types using either total stress parameters, effective stress parameters, and modified total stress parameters. For example, total number of analyses done for Test Soil 1 at total stress state was 192. It is noted that total number of analyses performed for all test soils at total stress state, that is using UU triaxial parameters was equal to 1072.

Among all the 1072 cases, no cases showed TSA factor of safety lower than the minimum value of 1.3. In many of these cases, the FS was well above the minimum value. To represent an example of such analyses, values of FS along with accepted zone are depicted in Figure 5.3. The figure belongs to Test Soil 1 and for one embankment geometry, that is H=40ft and side slope of 2H:1V. Since the high factors of safety from TSA are not critical, and to save on the volume of this document, detailed information regarding TSA factor of safety is skipped in the dissertation.

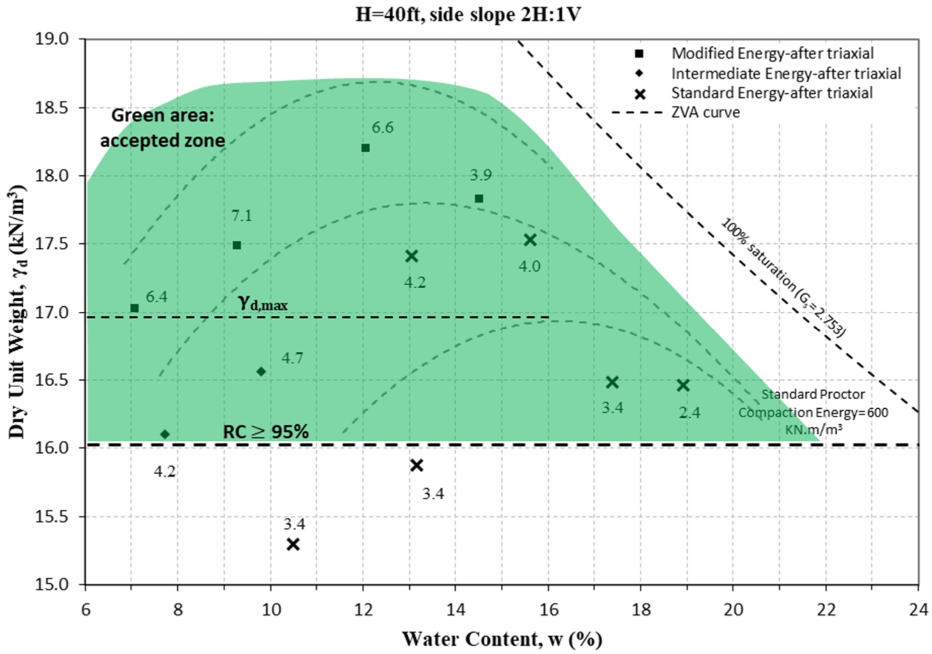

Figure 5.3. Acceptance zone based on total stress slope stability analysis - Test Soil 1 (numbers refer to factor of safety)

The non-shallow failure mode was observed to be the dominant one for the total stress analysis. It is noted that in all the 1072 cases that were run for five test soils using TSA parameters, in only one case the infinite slope (shallow) failure was yielding a FS lower than that of from global/non-shallow failure (grid and radius search). Of course, even for this case both type of factor of safeties were higher than the minimum. This shows that, “for the total stress analysis, shallow failure is never dominant”. This indicates that embankments made with these soil samples are stable right after compaction operation, even if the minimum compactive energy level, that is Standard Proctor is employed.

5.3.2 Effective Stress Slope Stability Analysis Using CU Triaxial Parameters

It is noted that combination of four embankment heights and four side slopes results in 16 embankment sections as listed in Table 3.1. To perform effective stress slope stability analysis, specifications of each data point on figures of the type of Figure 4.29 (points on saturation line) have been attributed to the embankment sections and then effective stress FS has been obtained.

Results of the stability analysis based on ESA parameters were different from those of obtained using TSA parameters, as in the effective stress stability analyses many cases were found to have FS lower than 1.3.

Strength parameters from CU triaxial tests may be mainly characterized by lower cohesion term compared with those of from UU triaxial tests (the concept shown in Figure 4.33). It was seen that as cohesion of soil material decreases, mode of failure shifts from a deep slip surface encompassing all the embankment slope (non-shallow slip surface) to a shallow, small and local one (local slip surface). In addition, for the effective stress analysis many cases were seen where shallow (infinite) failure was the dominant mode of failure.

These facts may lead us to the following statements: "assuming saturation of the highway embankments soil material is possible through their service life, stability (based on ESA parameters) may be crucial". Moreover, "for the effective stress slope stability analysis, shallow failure (infinite) must be checked as there is a high likelihood for this mode of failure".

In addition, it is noted that height of embankment does not play a considerable role in the FS. This might be due of the fact that for the effective stress stability analysis, mode of failure is dominated by the local failure.

Because of the importance and different nature of the FS values associated with effective stress parameters, tables providing detailed information have been presented in Appendix E. It is noted that last column of these tables list mode of failure observed for each specific case. However, Table 5.1 also summarizes important information regarding effective stress slope stability analysis for each test soil in a descriptive way.

Table 5.1. Description of acceptable zones/cases based on effective stress slope stability analysis criterion

Soil sample	Summary points
Test Soil 1 (PI=2) AASHTO class: A-4 (0)	- Even if final dry unit weight* is relatively low, numerical values of the FS for all embankment sections are higher than 1.3. - However, side slope of 1H:1V cannot be recommended. - Non-shallow failure is still the dominant mode of failure.
Test Soil 2 (PI=21) AASHTO class: A-7-6 (28)	- Side slope of 1H:1V is not recommended. - A high final unit weight/dry unit weight might assure an ESA FS even more than 1.3.
Test Soil 3 (PI=NP) AASHTO class: A-4 (1)	- Side slope 1H:1V shall not be used. - Side slope 2H:1V can be tricky and is not recommended. - The cohesion term has nearly vanished, and the local failure is almost the dominant mode of failure. - Many cases of shallow slope failure were dominant.
Test Soil 4 (PI=6) AASHTO class: A-5 (7)	- Side slope 1H:1V seems to be the only problematic section, as other sections yield a FS higher than 1.3 even if the final dry unit weight is not very high.
Test Soil 5 (PI=5) AASHTO class: A-5 (5)	- Side slope 1H:1V shall not be used. - Side slope 2H:1V is not very reliable. - The cohesion term has nearly vanished, and the local failure is almost the dominant mode of failure. - If the embankment compacted with low compactive energy levels such as standard energy, it will fail under rain-induced conditions. - This test soil has the most cases of instability among all.

* Final dry unit weight refers to after saturation and before shear stage, which is applicable to rain-induced conditions.

Finally, it is noted that providing suitable vegetation cover (to reduce infiltration and promote runoff) as well as drainage measures for the highway embankments could be useful in avoiding the detrimental effects of presence of water in the body of embankment. Moreover, the behavior (e.g., shear strength, volumetric behavior, stiffness) of embankment soils may be improved using artificial and biological cementation techniques (e.g., Clough et al. 1981; Nafisi et al. 2019).

5.3.3 Modified Total Stress Slope Stability Analysis Using UU Triaxial Parameters with Neglecting Cohesion

The discussion in Section 4.5.4 of Chapter 4 cast light on the concept of "apparent cohesion". It was stated that as the soil specimen becomes saturated, suction disappears and as a result, cohesion and the FS associated with it decrease dramatically. The decrease in shear strength of fine-grained soils due to either intensive rainfalls or cycles of wetting and drying has been reported by many researchers (Skempton 1984; Day and Axten 1989; Tohari et al. 2007; Hassani et al. 2019; Nobahar et al. 2020). This phenomenon may direct us to define a new set of analyses based on total stress results but without relying on the cohesion term.

This type of analysis is called modified total stress (TSA,m) slope stability analysis in this study and will be presented in this section. The concept which is shown in Figure 5.4 consists of using same friction angle from the UU triaxial test with neglecting cohesion term.

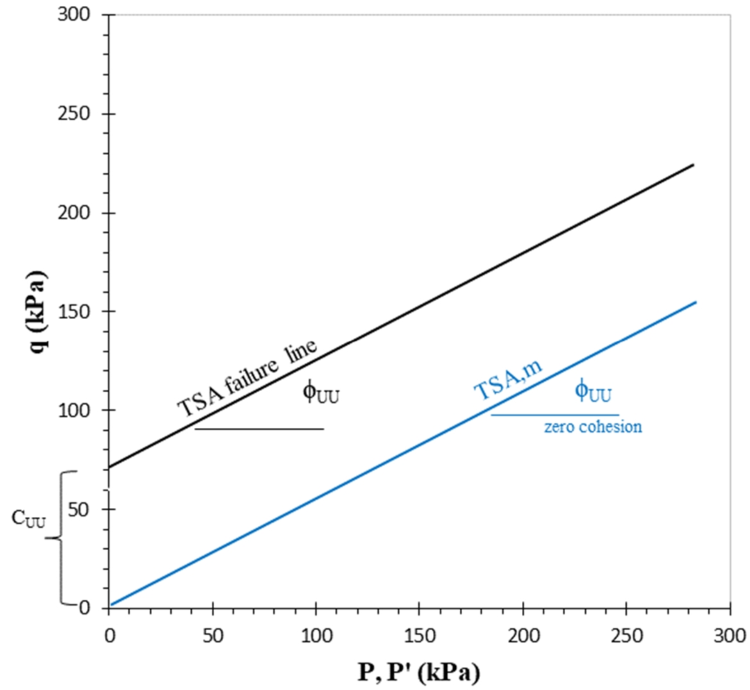

Figure 5.4. Illustration of the concept used for modified total stress analysis

In the remaining of this section, findings related to the modified total stress analysis will be presented.

For the TSA,m lots of cases with FS lower than the minimum of 1.3 were encountered. This fact indicates importance of such an analysis specially for sides of embankment where the soil is subject to drop of strength due to rainwater infiltration.

Also, values of FS associated with the TSA,m were found to be lower than those of from TSA; this was obviously expected due to lack of the cohesion term in the TSA,m versus the TSA.

"Local slip surface" was the dominant mode of failure observed for all the modified total stress analysis cases. That is, the local mode yielded a lower FS than even that of obtained for the infinite slope stability analysis resulted from Equation (5.1) with setting cohesion equal to zero.

Values of factor of safety against sliding associated with the modified total stress analysis were found to be very close to (yet lower than) those of related to the infinite/shallow slope stability analysis based on the TSA,m results. This proximity was almost expected after gaining knowledge on the fact that mode of failure shifts from the non-shallow slip surface to the local slip surface with decreasing cohesion of soil material.

After running analyses for different soil properties and different embankment geometries, acceptance zones based on the modified total stress slope stability analysis may be plotted on the dry unit weight versus moisture content space. For brevity purposes, this type of figures is presented for all test soils but only for one embankment geometry, that is H=40ft and side slope of 2H:1V [1]. Acceptance zones are presented in Figure 5.5 through Figure 5.9 for the five test soils.

Correlation of the accepted zones based on the modified total stress (TSA,m) slope stability analysis with other performance criterion, that is deformation will be discussed in Chapter 7.

[1] Same strategy for representation of results will be followed throughout this document.

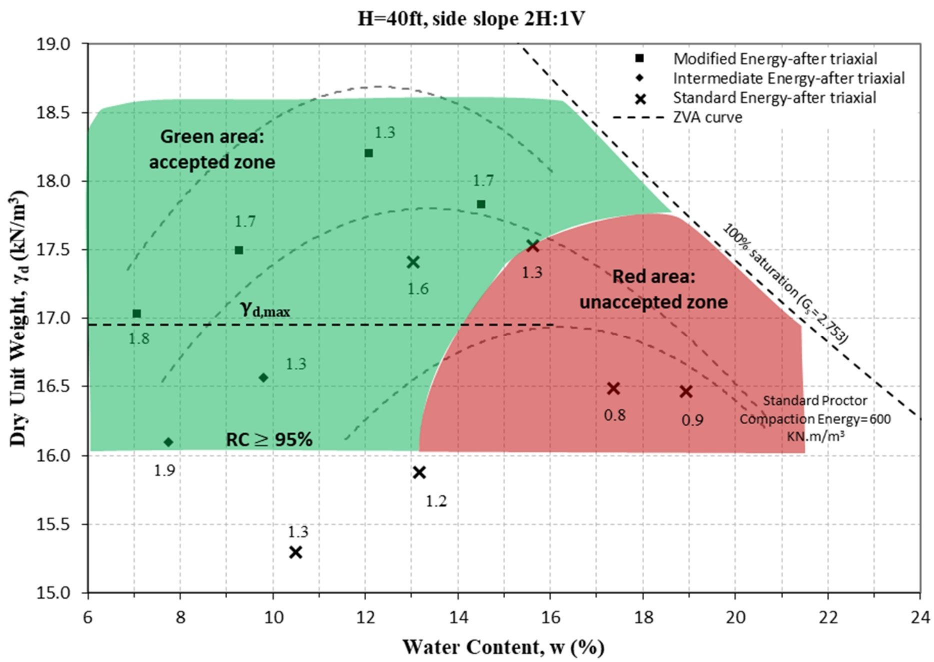

Figure 5.5. Acceptance zone based on modified total stress slope stability analysis - Test Soil 1 (numbers refer to factor of safety)

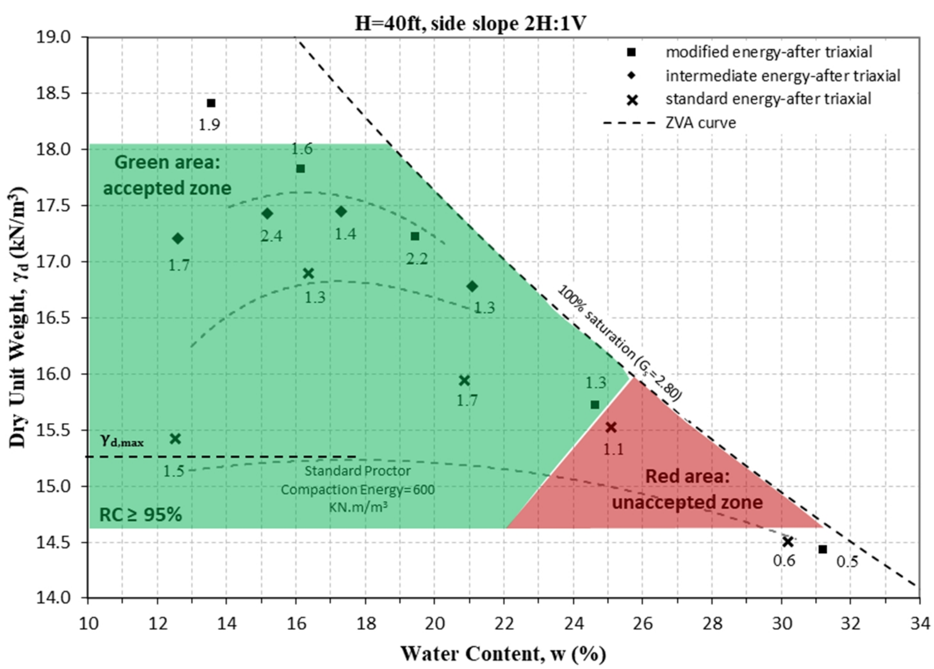

Figure 5.6. Acceptance zone based on modified total stress slope stability analysis - Test Soil 2

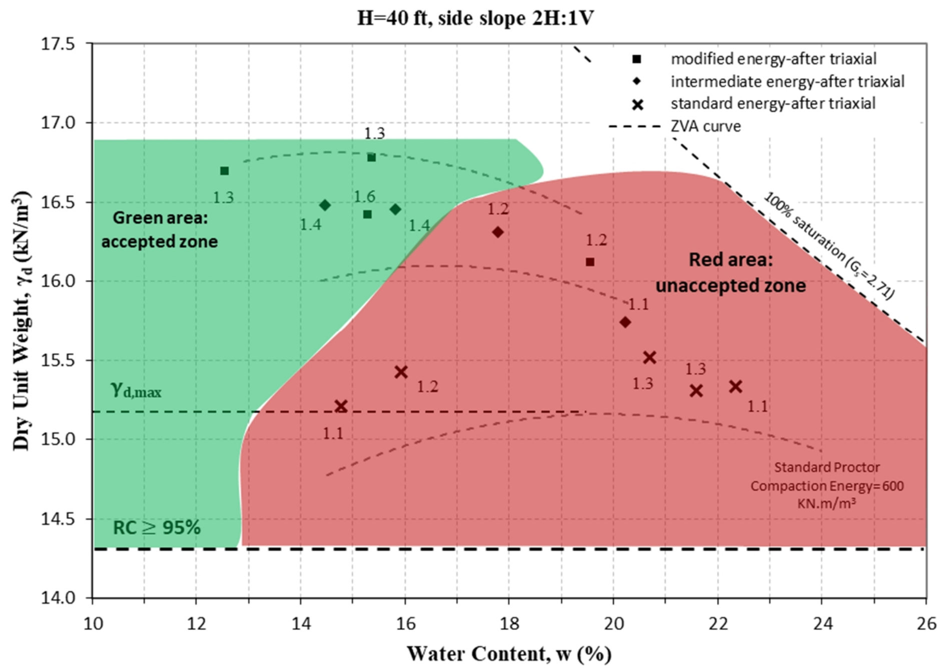

Figure 5.7. Acceptance zone based on modified total stress slope stability analysis - Test Soil 3

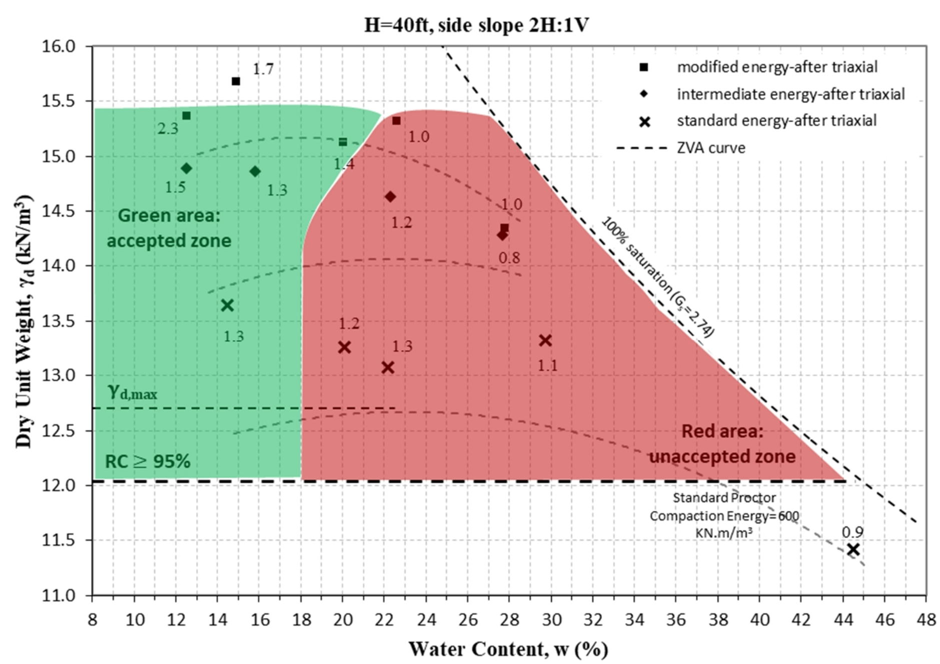

Figure 5.8. Acceptance zone based on modified total stress slope stability analysis - Test Soil 4

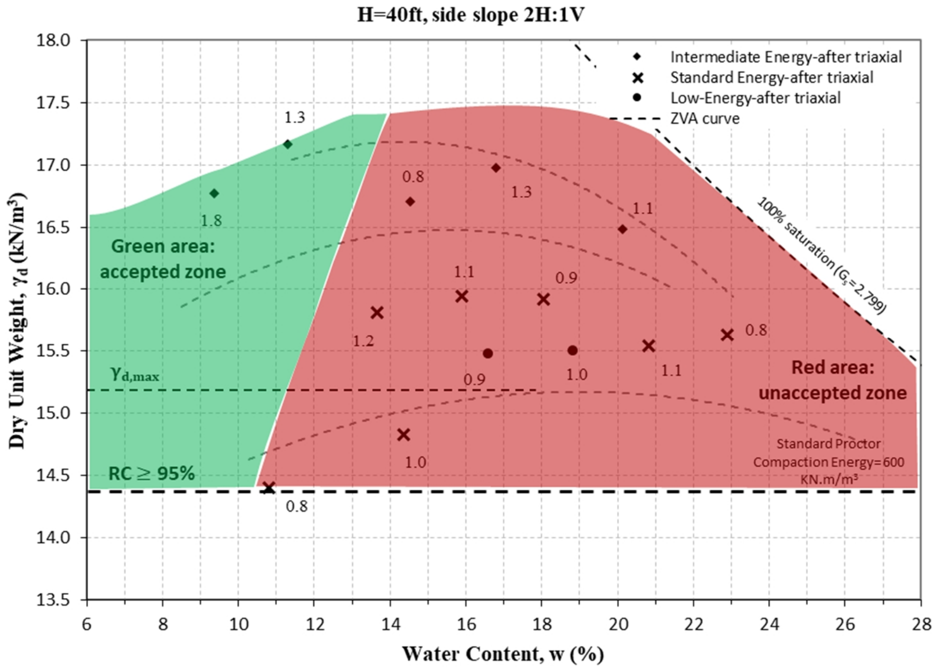

Figure 5.9. Acceptance zone based on modified total stress slope stability analysis - Test Soil 5

Due to the large volume of data, a descriptive table is presented at the end of this section to summarize important information regarding modified total stress slope stability analysis for each test soil. This information can be found in Table 5.2.

Table 5.2. Description of acceptable zones/cases based on modified total stress slope stability analyses criterion

Soil sample	Summary points
Test Soil 1 (PI=2) AASHTO class: A-4 (0)	- Side slope 1H:1V shall not be used regardless of embankment height, compactive energy and MC. - Side slope 2H:1V shall receive special caution (could fall on the border) if test soil is prepared at close to optimum or wet-of-optimum MC for all compactive energy levels. - Points compacted at standard energy with optimum and wet-of-optimum MC are not acceptable, unless for side slope of 4H:1V.
Test Soil 2 (PI=21) AASHTO class: A-7-6 (28)	- Side slope 1H:1V shall not be used regardless of embankment height, compactive energy and MC. - Side slope 2H:1V shall receive special caution (could fall on the border) if test soil is prepared with wet-of-optimum MC at standard and intermediate compactive energy levels. - This test soil has minimum percentage of instability among all.
Test Soil 3 (PI=NP) AASHTO class: A-4 (1)	- Side slope 1H:1V shall not be used regardless of embankment height, compactive energy and MC. - Side slope 2H:1V shall not be used at standard energy and shall receive special caution (could fall on the border) if test soil is prepared at close to optimum or wet-of-optimum MC for intermediate and modified energy levels.
Test Soil 4 (PI=6) AASHTO class: A-5 (7)	- Side slope 1H:1V shall not be used regardless of embankment height, compactive energy and MC. - Side slope 2H:1V shall not be used at standard and intermediate compactive energy levels and shall receive special caution (could fall on the border) if test soil is prepared at wet-of-optimum MC for modified energy level. - Moisture contents above 4% wet-of-optimum is unacceptable for all energy levels and all sections (geometries) except for 4H:1V section which should be investigated.
Test Soil 5 (PI=5) AASHTO class: A-5 (5)	- Side slope 1H:1V shall not be used regardless of embankment height, compactive energy and MC. - Side slope 2H:1V shall not be used at standard and intermediate compactive energy levels, neither for samples prepared at close to optimum and wet-of-optimum MC with modified energy level. Samples prepared at dry-of-optimum MC and compacted with modified energy level should receive special caution (could fall on the border). - Extra caution should be exercised with moisture contents above 4% wet-of-optimum at all compactive energy levels and for all sections. Section 4H:1V stands in a better position in this regard. - This test soil has highest percentage of instability among all.

5.4 Summary

Chapter starts with basics and approach used for the slope stability analysis task. It is noted that slope stability is one of the performance criteria of the new proposed design approach. Results of slope stability analyses based on TSA parameters, ESA parameters, and modified total stress (TSA,m) parameters have been presented separately. Significant results and findings of the chapter are summarized as following.

- Among the 1072 cases reviewed based on TSA parameters, no cases showed a TSA factor of safety lower than the minimum value of 1.3. In many of these cases the FS is well above the minimum value.

- The non-shallow failure mode was observed to be the dominant one for the total stress analysis. This indicates that "for the total stress analysis, shallow failure would never be dominant".

- The two latter findings just mentioned, indicate that embankments made with the tested soil samples are stable right after compaction operation, even if the minimum compactive energy level, that is Standard Proctor is employed.

- For the effective stress stability analysis many cases were found to have FS values lower than 1.3; from which, many cases were seen where shallow failure was the dominant mode of failure.

- Therefore, "for the effective stress slope stability analysis, besides the grid and radius search method, shallow failure must be checked as there is a high likelihood for this mode of failure".

- Slope stability analyses using ESA parameters yielded all the three different modes of failure, that is non-shallow slip surface, local slip surface, and shallow/infinite failure.

- For the effective stress (ESA) and modified total stress (TSA,m) slope stability analyses two descriptive tables have been presented to be used as means of acceptance zone/cases. These two tables may be found in Table 5.1 and Table 5.2, respectively.

CHAPTER 6: DEFORMATION ANALYSIS

6.1 Introduction

In this chapter methodology and basics for deformation analysis of the highway embankment are presented. Deformation is one of the two performance criteria of the new proposed design approach for the highway embankments. Properties of the utilized model and improving strategies of the initial model are introduced in this chapter, then general results associated with deformation will be presented.

In the literature review section, it was noted that the amount of initial settlement which is an immediate response to the embankment self-weight is compensated during embankment construction. However, in this research deformation refers to the amount of immediate deformation due to external pavement and traffic loading. If the immediate deformation is larger than one inch, which is the selected maximum non-uniform allowable settlement for highway embankments, it is considered unacceptable. It is noted that if the post-construction settlements are uniform, they are usually considered acceptable in common practice.

Vertical and horizontal stresses increase with the depth of embankment, this means confining stress increases with depth. This increase in confining stresses might itself affect material properties such as elasticity modulus. This concept has been included in the settlement analyses to come up with suitable models that could absorb change in material properties within the depth.

Embankment deformation is investigated under two conditions: total stress parameters using UU triaxial tests results (TSA), and effective stress parameters using CU triaxial tests results (ESA). Results pertaining to either of these conditions are presented separately.

According to the reports by field experts involved in this project, there has been few cases of cracks on the surface of newly built embankments. These cracks which are mostly toward the sides of embankment, have been observed even as early as construction time, when the embankment is tolerating self-weight load which is due to the accumulative weight of the construction material. However, this new concern could not be addressed using TSA or ESA laboratory testing, as it may be related to the long-term deformation characteristics of the soil material. Thus, there exists a need for one-dimensional creep study of the compacted soil samples. Chapter 4 explained the basics of these tests and this chapter concludes with results and analyses pertaining to those.

6.2 Approach Used for Deformation Analyses

GeoStudio-SIGMA/W software (Geoslope 2021b) has been used to perform deformation analyses of the embankment. The software uses finite element approach to solve geotechnical problems numerically. In finite element method (FEM), usually the following general steps are taken to solve a problem: generating a mesh for the problem, constructing shape functions for individual elements, constructing stiffness matrix for elements, constructing body force matrix for elements, assembly of stiffness matrixes for the whole problem, assembly of body force matrixes for the whole problem, and eventually solving system of equations which leads to finding out displacements at each node. Having nodal displacements, strains then stresses could be determined.

An initial model was developed to help us truly understand the basics behind the deformation calculations, examine the functionality of the computer model, and also to verify output results of the computer model used for the deformation analyses.

6.2.1 Model Properties

Linear elastic is selected as the material model. The simplest SIGMA/W soil model is the linear elastic model in which stresses are directly proportioned to the strains. The proportionality constants are the Young's Modulus, *E*, and Poisson's Ratio, *n* . In a simple three-dimensional form, which includes normal stresses on three planes and shear stress only on xy plane, the stresses and strains may be related to each other by the following equation:

$$\begin{Bmatrix} \sigma_x \\ \sigma_y \\ \sigma_z \\ \tau_{xy} \end{Bmatrix} = \frac{E}{(1+\nu)(1-2\nu)} \begin{bmatrix} 1-\nu & \nu & \nu & 0 \\ \nu & 1-\nu & \nu & 0 \\ \nu & \nu & 1-\nu & 0 \\ 0 & 0 & 0 & \dfrac{1-2\nu}{2} \end{bmatrix} \begin{Bmatrix} \varepsilon_x \\ \varepsilon_y \\ \varepsilon_z \\ \gamma_{xy} \end{Bmatrix} \tag{6.1}$$

Figure 6.1 shows representation of the x, y and z axes that is used for deformation calculations. It can be seen that z axis is defined parallel to the embankment length. Obviously, x and z directions represent horizontal stresses, and any stress in y direction would represent a vertical stress.

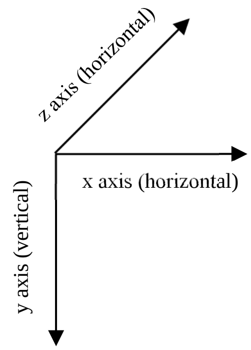

Figure 6.1. Representation of the x, y, and z axes for deformation calculations

System of equations in (6.1) originates from the well-known Hooke’s law (incorporated with the Poisson's law) which is represented in set of Equations (6.2). Starting from system of equations presented in (6.2) and performing a few manipulations, one can reach equations presented in (6.1).

$$\begin{Bmatrix} e_x \\ e_y \\ e_z \\ g_{xy} \end{Bmatrix} = \begin{bmatrix} \frac{s_x}{E} - n\frac{s_y}{E} - n\frac{s_z}{E} \\ -n\frac{s_x}{E} + \frac{s_y}{E} - n\frac{s_z}{E} \\ -n\frac{s_x}{E} - n\frac{s_y}{E} + \frac{s_z}{E} \\ \frac{t_{xy}}{G} \end{bmatrix} \tag{6.2}$$

where G is the material shear modulus which may be obtained using Young's Modulus and Poisson's Ratio as following: $G = \frac{E}{2(1+n)}$. It is noted that for a two-dimensional plane strain analysis, e_z is zero, resulting in having s_z equal to $s_z = n(s_x + s_y)$. This relationship might be proved by setting third equation of (6.2) equal to zero.

In the case of highway embankments the assumption of $e_z = 0$ seems a reasonable selection, as the third dimension (length of embankment) is very long that any deformation in z direction would result in a very infinitesimal strain.

Moreover, reviewing the set of equations presented in (6.1) reveal that when n approaches to 0.5, the system of equations becomes unstable. Of course, under this assumption the volumetric strain moves toward becoming zero. Because of this issue and to avoid numerical problems, in SIGMA/W maximum value for Poisson's ratio is limited to 0.49 (can never be 0.5).

It is reminded that the value of elasticity modulus used in this model is the E_{50}, the modulus of elasticity representing 50% of the maximum deviator stress. It is common in the geotechnical literature to infer stiffness of soil specimens from measurements of the secant modulus E_{50} (Chen 2010; Wiebe et al. 1998). A summary description of the procedure to obtain the elasticity modulus for deformation calculations is presented in Appendix I.

Also, In SIGMA/W, the K_0 condition (lateral earth pressure at rest) may be specified through the Poisson's ratio. In a 2D analysis, K_0 may be obtained using the following equation: $K_0 = n/1 - n$.

6.2.2 Summary Points Related to the Initial Model and Verification of the Computer Model

For development of the initial model, elasticity modulus and unit weight were selected directly from the laboratory results. Figure 6.2 illustrates geometry and other specifications of the initial SIGMA/W model. Traffic and surface pavement load are considered equivalent to a 35 kPa uniformly distributed load which is also depicted in this figure. "Quads and triangles" mesh type with an element size equal to 1m is used for these computer modelings. This combination of mesh type and mesh size generates a reasonable and desirable mesh for the embankment.

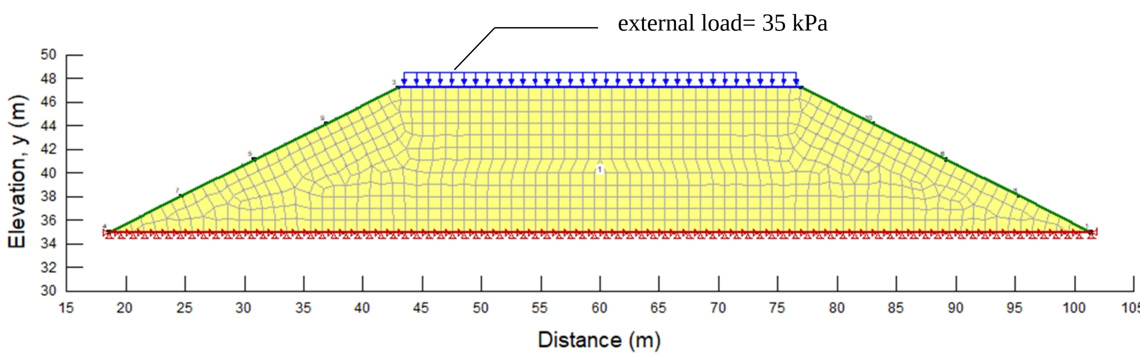

Figure 6.2. Initial embankment model used in SIGMA/W

Maximum settlement of the crest center was equal to 6.9 cm for the initial model. It is noted that the settlement due to embankment self-weight has been zeroed out and does not play any role in this value, in other words, this maximum deformation is only due to the pavement and traffic loading.

Using simplistic engineering rules, the results obtained from the initial model were investigated to verify that the software model is working properly. Four horizontal sections going across the whole width of embankment were selected. These horizontal sections are located at h=0, h=0.25*H, h=0.50*H, and h=0.75*H. It is noted that the depth of embankment is measured along the y-axis direction (refer to Figure 6.1). At each section, total vertical stress at two loading conditions were investigated: in-situ loading condition and step 1 loading condition, which is after application of the uniformly distributed traffic load of 35 kPa. Obviously, the difference between these two loading conditions yield vertical stress due to the traffic loading, which is shown in Figure 6.3 for the four horizontal sections.

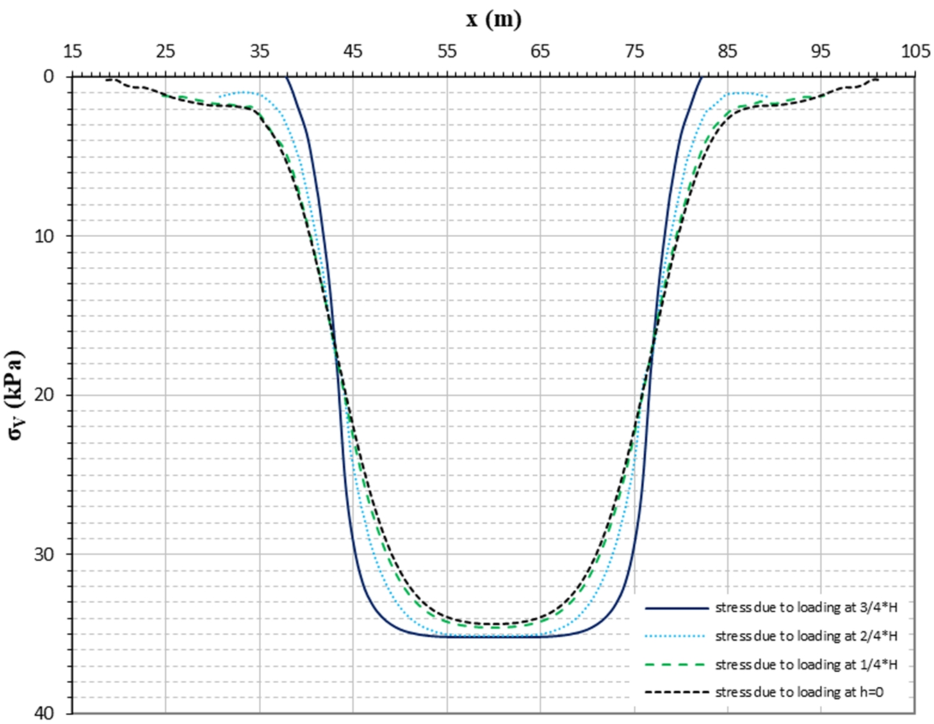

Figure 6.3. Vertical stress due to loading at four horizontal sections

As we expected, the maximum value at all levels is limited to 35 kPa. However, we can interestingly find a block of soil within embankment depth, in which the increase in vertical stress is almost constant and equal to 35 kPa. This block might be defined by the extents of x=50m to x=70m, which encompasses 20m length of embankment. Now let's look into the s_X and s_Z, that is horizontal stresses within this imaginary block.

The profile of horizontal stresses applying on the imaginary soil block - s_X and s_Z versus depth could be obtained. These stresses could be taken equal to their average value without much loss of accuracy; average s_X was equal to 14.5 kPa, and average s_Z was equal to 18.1 kPa. Finally, we encountered a block of soil with properties which are listed in Table 6.1.

Table 6.1. Properties of the selected soil block

Property	Value
length	20 m (from x=50 to x=70)
height	12.2 m (40 ft)
s_Y	35 kPa
s_X	14.5 kPa
s_Z	18.1 kPa
modulus of elasticity, E	3800 kPa
Poisson's ratio, *n*	0.3786

With all this information being available, now we can easily calculate settlement of the soil block. We simply need to consider Equation (6.2) in the following form to calculate ε_y, then the vertical settlement may be determined using Equation (6.3). After plugging in all the parameters, this procedure results in $\Delta H = 7.2\ cm$, which is remarkably close to 6.9 cm, maximum settlement of the crest already calculated by the software.

$$e_y = -n\frac{s_x}{E} + \frac{s_y}{E} - n\frac{s_z}{E} \tag{6.2}$$

$$\Delta H = e_y * H_0 \tag{6.3}$$

6.2.3 Improving Elasticity Modulus Input

The elasticity modulus of embankment material has been selected meticulously; the initial model is improved by the hypothesis of taking into account differences in the elasticity modulus within embankment depth based on the average of horizontal stresses. For brevity of this document this topic is presented only briefly in this section.

Reviewing contours of horizontal stresses- s_X and s_Z, reveals that these stresses increase with depth in an organized fashion. On the other hand, it is established in the geotechnical literature (Lee 1970; Das 2008) that the elasticity modulus of soil increases exponentially with the confining pressure (translated as cell pressure in UU triaxial tests, s_{cell}). This exponentially relationship is shown in Figure 6.4 and Equation (6.4) for a series of UU triaxial tests performed in this research.

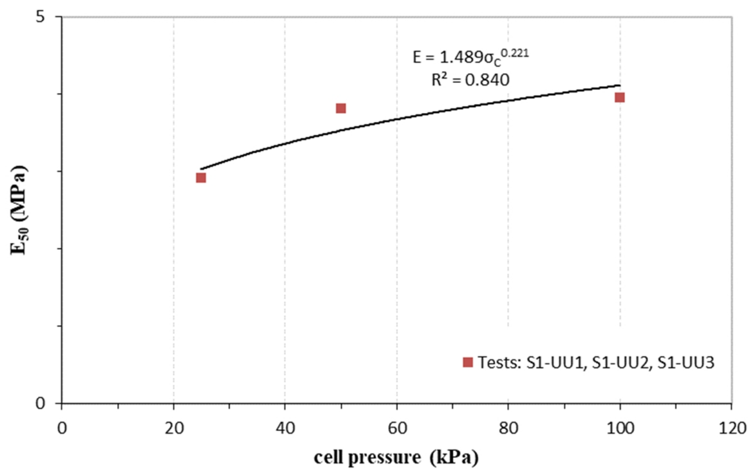

Figure 6.4. Power relationship between elasticity modulus and confining pressure
(pertaining to Test Soil 1: Tests S1-UU1, S1-UU2, S1-UU3)

$$E = a * s_{cell}^{b} \tag{6.4}$$

where E is the elasticity modulus representing 50% of the maximum deviator stress (E_{50}), s_{cell} is the confining or all-around cell pressure applied in the UU triaxial test, and α and β are constants that may be obtained from laboratory results.

The parameter $\sigma_{H,ave} = (\sigma_X + \sigma_Z)/2$ from the computer model which is the average of horizontal stresses represents s_{cell} in the UU triaxial tests. This fact along with the exponential relationship for the elasticity modulus, have been used as two bases for improving the elasticity modulus input into the software. The initial elasticity modulus entered into the model was modified based on a synchronization with output values of $(\sigma_X + \sigma_Z)/2$ obtained from the software itself.

6.2.4 Other Embankment Sections

For embankments with H=40 ft (12.2 m) and H=30 ft (9.1 m), three layers with thicknesses of 0.3H, 0.4H, and 0.3H respectively from bottom to top have been considered. For embankments with H=20 ft (6.1 m) two layers each with 0.5H thickness seemed to be enough to capture variations of material properties within depth, and for embankments with H=10 ft (3 m) only one layer has been considered. Needless to say that, material properties are constant throughout each layer. Figure 6.5 shows embankment sections which are considered to capture variations of the material properties within depth for four different embankment heights.

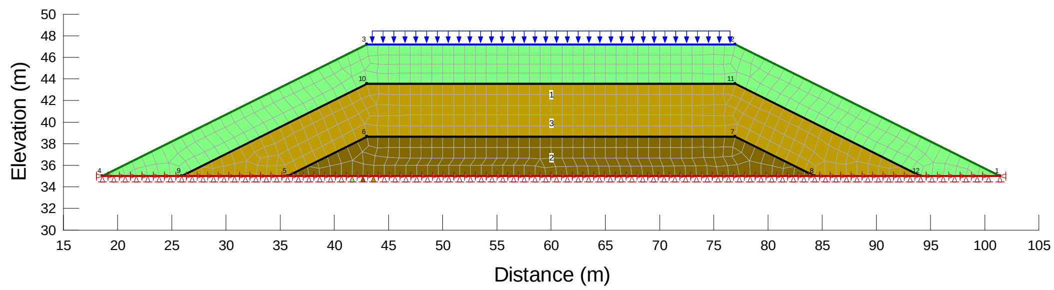

(a) typical modified embankment section for embankments with height= 40 ft (12.2 m) or 30 ft (9.1 m)

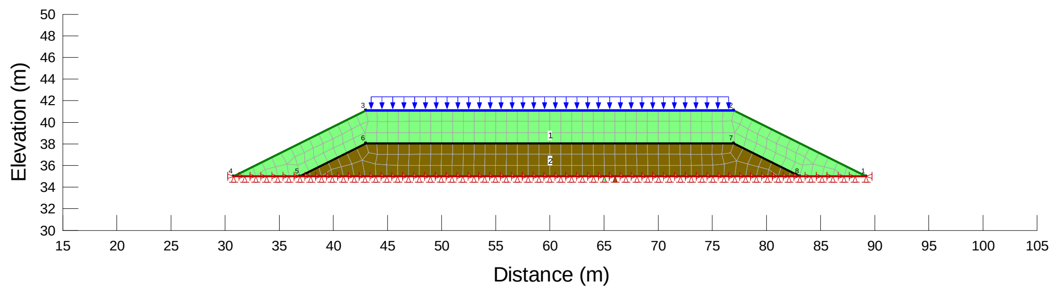

(b) typical modified embankment section for embankments with height= 20 ft (6.1 m)

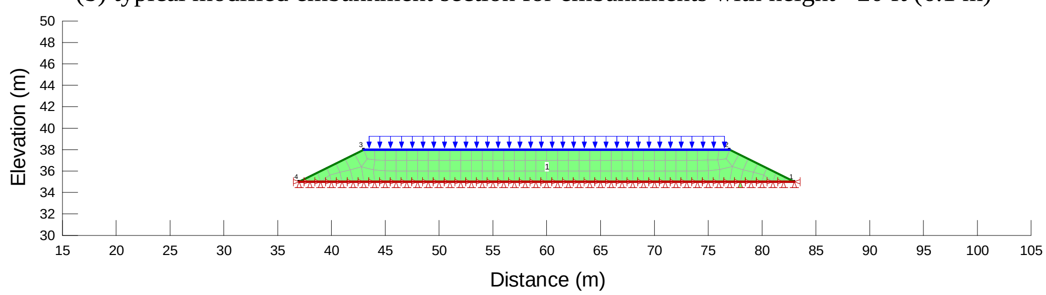

(c) typical embankment section for embankments with height= 10 ft (3.0 m)

Figure 6.5. Typical modified embankment sections for four different heights

6.3 Results of Deformation Analysis

In this section, results of the deformation analyses are presented; deformation analyses results pertaining to the total stress parameters have been separated from those of related to the effective stress parameters.

6.3.1 Total Stress Deformation Analysis Using UU Triaxial Parameters

With the geometric models which take into account differences in elasticity modulus (Figure 6.5), and improving elasticity modulus input based on the average of the horizontal stresses obtained from the model- $(\sigma_X + \sigma_Z)/2$, embankment crest deformation may be calculated for all soil samples and all test points, that is across moisture content-dry unit weight space. Figure 6.6 presents results of Test Soil 1 for an embankment with H=40ft and 2H:1V side slope. Red shaded area shows points that will result in crest deformation larger than one inch- the selected maximum non-uniform allowable settlement for the highway embankments. On the other hand, green shaded area shows the acceptable range. It is reminded that deformation is one of the two performance criteria of the new proposed design approach for the highway embankments. Since the total stress stability was not critical, this area imposed by the total stress deformation performance criterion may be accepted as the final acceptance zone for the TSA.

For brevity purposes, this type of figures is presented for all test soils but only for one embankment geometry, that is H=40ft and side slope of 2H:1V [1]. Acceptance zones are presented in Figure 6.6 through Figure 6.10 for the five test soils. By initial review of these figures, one might conclude that unaccepted zone is smallest for Test Soil 2, a A-7 soil according to the AASHTO category, compared to other soils which are A-4 or A-5 AASHTO class. This might indicate better performance of this soil under total stress conditions.

To represent results of analyses for all the test soils and all the embankment geometric sections, later in this chapter Table 6.3 provides descriptive information regarding acceptable cases based on total stress deformation analysis criterion. In addition,

[1] This strategy for representation of results has been followed throughout the document.

for other test soils and embankment sections, deformation tables presented in Appendix F of this document includes the detailed information.

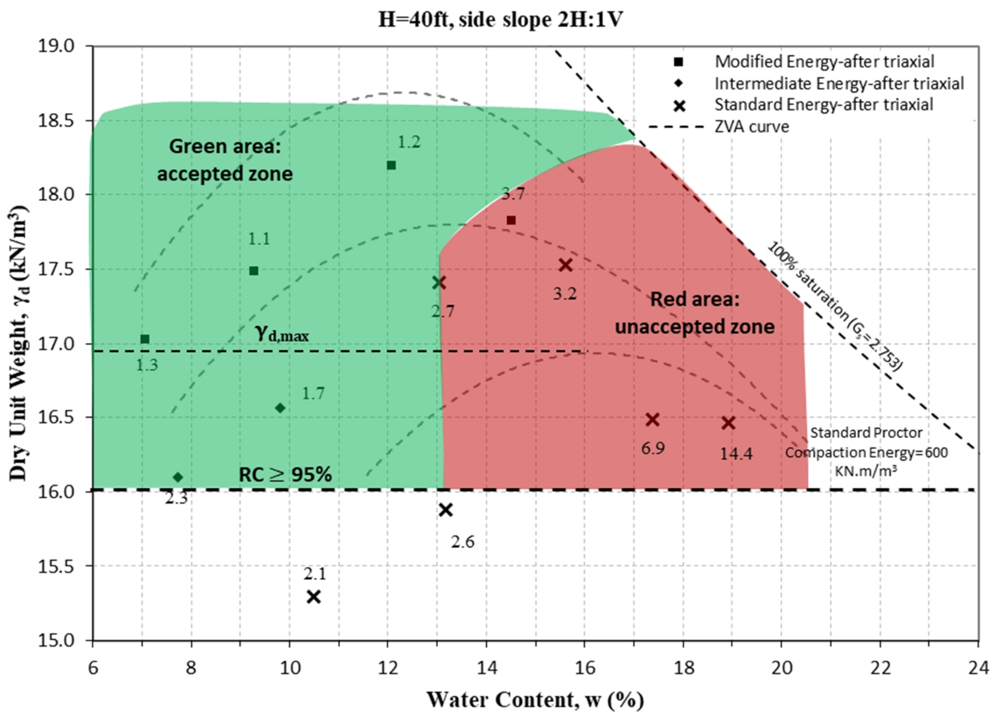

* Figure Note: numbers refer to crest deformation in centimeters
Figure 6.6. Acceptance zone based on deformation TSA – Test Soil 1

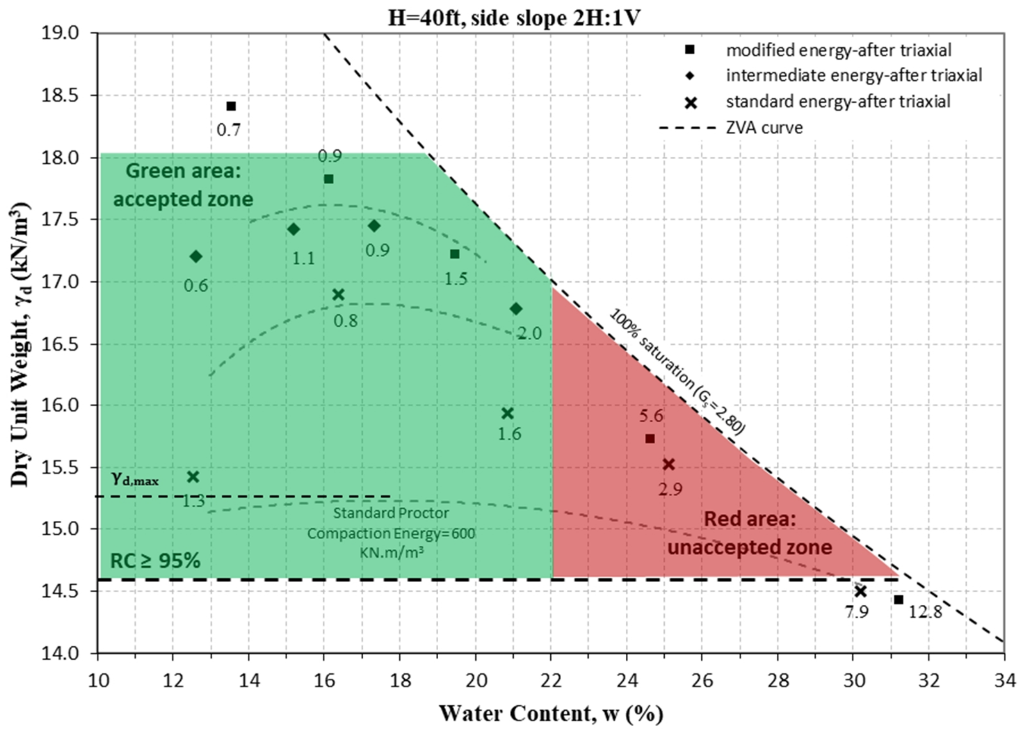

* Figure Note: numbers refer to crest deformation in centimeters

Figure 6.7. Acceptance zone based on deformation TSA – Test Soil 2

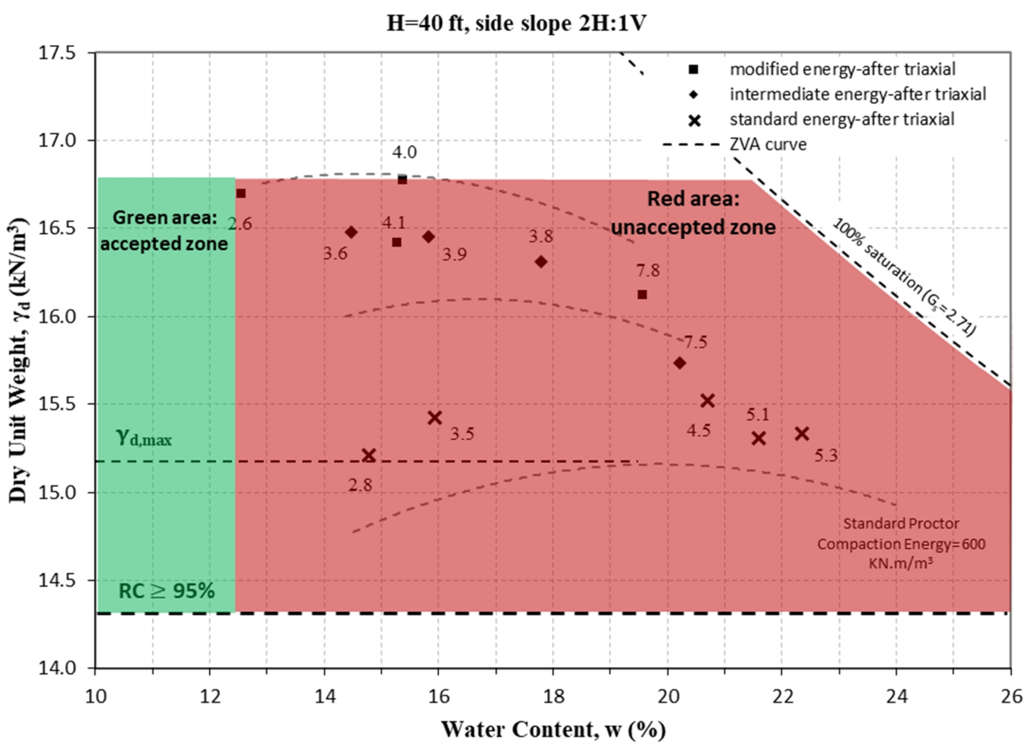

* Figure Note: numbers refer to crest deformation in centimeters

Figure 6.8. Acceptance zone based on deformation TSA – Test Soil 3

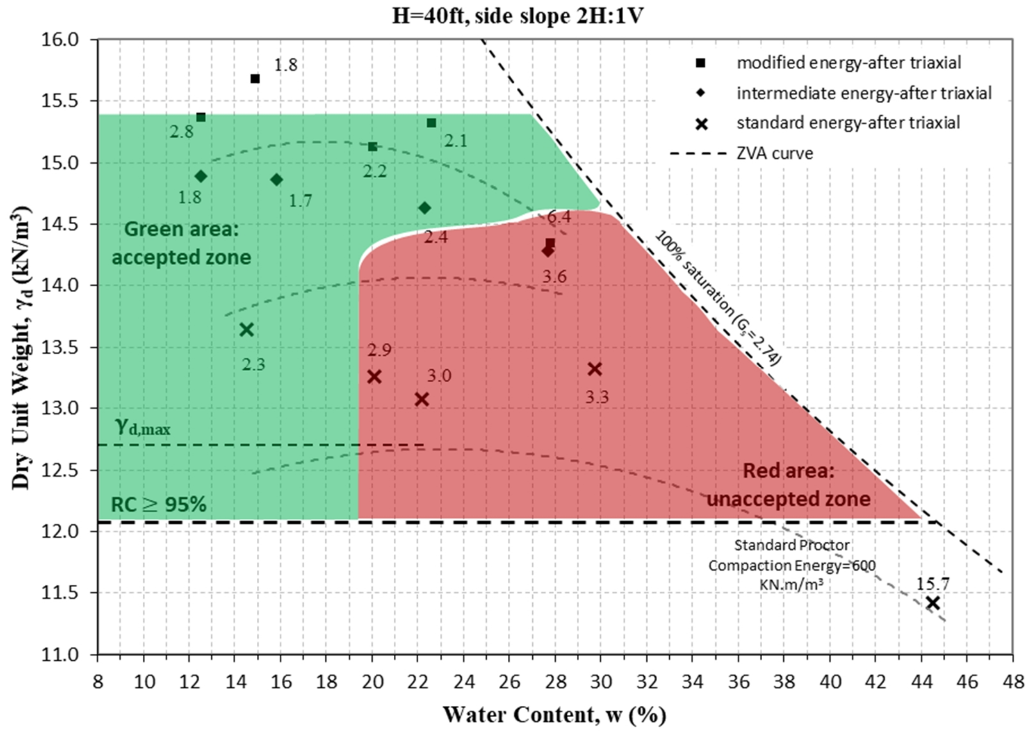

* Figure Note: numbers refer to crest deformation in centimeters

Figure 6.9. Acceptance zone based on deformation TSA – Test Soil 4

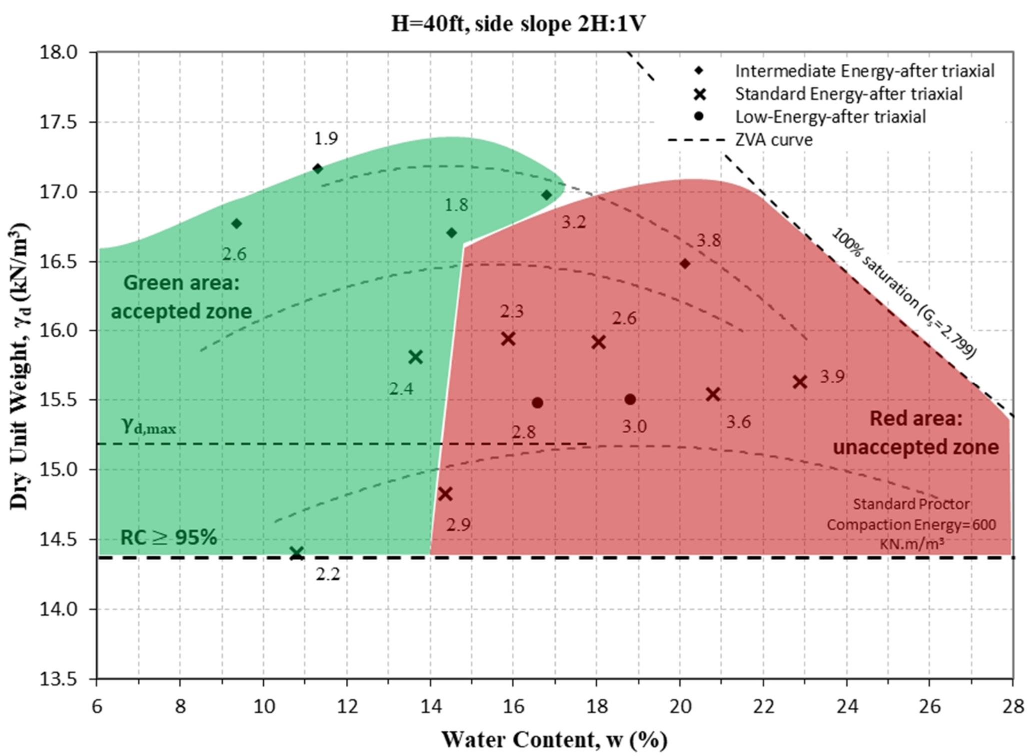

* Figure Note: numbers refer to crest deformation in centimeters

Figure 6.10. Acceptance zone based on deformation TSA – Test Soil 5

Tables in Appendix F provide detailed information of the intensive embankment deformation analyses which have been carried out using total stress parameters. Table 6.2 lists number of deformation analyses which have been done for each test soil.

Table 6.2. Number of deformation analyses done for each soil sample – TSA

Test soil	No. of analyses
Soil 1	192
Soil 2	224
Soil 3	208
Soil 4	224
Soil 5	224

Obviously, the embankment deformation decreases with embankment height. An intensive regression analysis effort was carried out on the results of embankment deformation (following the basic rules found in Gujarati et al. 2009). The regression analysis showed that, embankment deformation generally increases with the embankment height (H) and friction angle of soil (f_{UU}), and decreases with the elasticity modulus of soil (E) and S (larger S means flatter side slope). Of course, effect of the side slope is subtle, and it becomes even less discernible at lower embankment heights. Also, it was observed that as points move from wet-of-optimum to dry-of-optimum, the embankment deformation decreases.

Table 6.3. summarizes huge amount of numerical database and describes acceptable cases based on total stress deformation criterion. It seems helpful to remind that under the TSA conditions, stability criterion was not critical. This indicates that Table 6.3 may serve as the final acceptance zones/cases under the TSA conditions.

Table 6.3. Description of acceptable zones / cases based on total stress deformation analysis criterion (based on 1" limit for non-uniform immediate deformation)

Soil sample	Acceptable cases
Test Soil 1 (PI=2) AASHTO class: A-4 (0)	- For H=40 ft and samples compacted at Standard Proctor, almost all points are not acceptable. - At Standard Proctor, points wet-of-optimum are not acceptable for all embankment sections. At this energy level, points close to optimum need to be investigated. - At Standard Proctor, points dry-of-optimum are acceptable for all sections except H=40 ft. - Even at higher energies, points wet-of-optimum could be problematic.
Test Soil 2 (PI=21) AASHTO class: A-7-6 (28)	- At all energy levels, all points ∓ 5% of optimum are acceptable. - Optimum and dry-of-optimum points at all energy levels are acceptable. - For H=10 ft, regardless of compactive energy and MC, all points are acceptable. - Regardless of compactive energy, MC more than 8% wet-of-optimum is not recommended.
Test Soil 3 (PI=NP) AASHTO class: A-4 (1)	- At Standard Proctor, points wet-of-optimum are not acceptable for almost all sections. - For H=40 ft, regardless of compactive energy and MC, all points are not acceptable. - For H=30 ft, points only drier than 5% of OMC at standard energy and points only drier than 2.5% of OMC at modified energy are acceptable. - For H=20 ft, points dry-of-optimum and close to optimum at modified and intermediate energy are acceptable. But for standard energy only dry-of-optimum points are acceptable. - For H=10 ft, regardless of compactive energy and MC, all points are acceptable. - Many unacceptable cases were observed.
Test Soil 4 (PI=6) AASHTO class: A-5 (7)	- At Standard Proctor, wet-of-optimum points are not recommended for H=40 ft and 30ft; however, for H=40ft points dry-of-optimum are neither recommended. - At Intermediate Proctor and for all sections, points dry-of-optimum are acceptable; however, wet-of-optimum points for H=40 ft and 30 ft are not acceptable. - At Modified Proctor and for all sections, regular points seem to be acceptable. - For H=10 ft and 20 ft regardless of compactive energy and MC all points seem acceptable.
Test Soil 5 (PI=5) AASHTO class: A-5 (5)	- At Standard Proctor and for all sections, points dry-of-optimum are acceptable; however, as they get closer to OMC, they become unacceptable for H=40ft. Wet-of-optimum points are not accepted for H=40 ft and 30ft at this energy level. - At Intermediate Proctor and for all sections, points dry-of-optimum are acceptable; however, for H=40ft points close to optimum and points wet-of-optimum for H=40 ft and 30ft, neither are acceptable.

6.3.2 Effective Stress Deformation Analysis Using CU Triaxial Parameters

Embankment deformation analysis were carried out with the effective stress parameters as well. Tables in the Appendix G provide detailed information of this task. Calculations of the embankment deformation using CU triaxial parameters revealed that, for all test soils (Test Soil 1 through Test Soil 5) and embankment sections, deformation is larger than the limiting value, except for few cases of Test Soil 2 where dry unit weight of the soil sample (before shear stage) were very high. Laboratory results showed that this situation could happen only for the samples initially compacted at Modified Proctor compactive energy or higher. It is noted that for these cases, the FS (associated with ESA) was also higher than the minimum and in the acceptable range. Author would like to remind that Test Soil 2 is the soil sample with highest value of plasticity index (PI=21) among the test soils, with A-7-6 (28) AASHTO classification. This may give grounds to the idea that soils with higher PI perform slightly better under rain-induced infiltration conditions. This also may cast doubt on some state standard specifications that emphasize on bounding the Atterberg limits, such as NCDOT material selection specification of limiting PI to 15% in the North Carolina coastal area. This finding may also reject the specifications that abandon using the A-7 group soil as the embankment material.

Moreover, it is noted that since saturated samples in CU triaxial tests provide lower strength than unsaturated samples in UU triaxial tests, deformation incorporated with them is generally higher.

6.3.3 Results of One-Dimensional Creep Compression

Total of 8 creep tests have been considered to study the creep characteristics of embankment soils. Three vertical stresses (σ_V) of 50 kPa, 100 kPa, and 200 kPa have been chosen for each of the two test soils. Using a sponge inside a bag to maintain moisture content of the specimen was observed to be a very effective innovation to keep moisture content of soil specimen constant throughout the test.

Creep curves generally consisted of two main parts: an initial sharp settlement due to the immediate response to external loading and a linear section representative of the creep deformation.

6.3.3.1 Creep Deformation Curves

Test Soil 5 from Mecklenburg County showed slightly smaller strains in comparison with Test Soil 2 from Lee County. However, the rate of strain was seen to be more or less the same for both. The difference in the PI of tested soils did not indicate any pronounced dissimilarity in the behavior.

While presenting laboratory results of creep tests in chapter 4, we mentioned that in the graph of "strain versus log of time" a curvature is seen after about one week of loading (refer to Figure 4.39). With increasing the deformation since moisture content is constant, unit weight of specimen slightly increases (due to decrease in total volume). A constant moisture content means weight of water phase, hence volume of water phase will be constant. Therefore, decrease in total volume can only take place with decrease in the volume of air phase. However, this situation will cause specimen saturation ratio to increase. The decrease in volume of air phase and increase in saturation ratio, will also affect the volumetric moisture content and will change position of the soil specimen on the volumetric moisture content versus soil suction curve. The author believes the observed point of curvature could be explained with variation in soil suction and concepts of unsaturated soil mechanics.

6.3.3.2 Effect of Soil Moisture Content

Figure 6.11 shows results pertaining to the study of the effect of moisture content. One creep test at wet-of-optimum (Test 7), and one creep test at dry-of-optimum (Test 8) were considered. The wet-of-optimum sample showed a creep rate much higher than the sample compacted at OMC, and the dry-of-optimum sample showed a creep rate slightly lower than that of for the OMC sample. Creep rate of individual tests have been presented in a table in next section. Effect of moisture content on creep rate will be discussed more in next section.

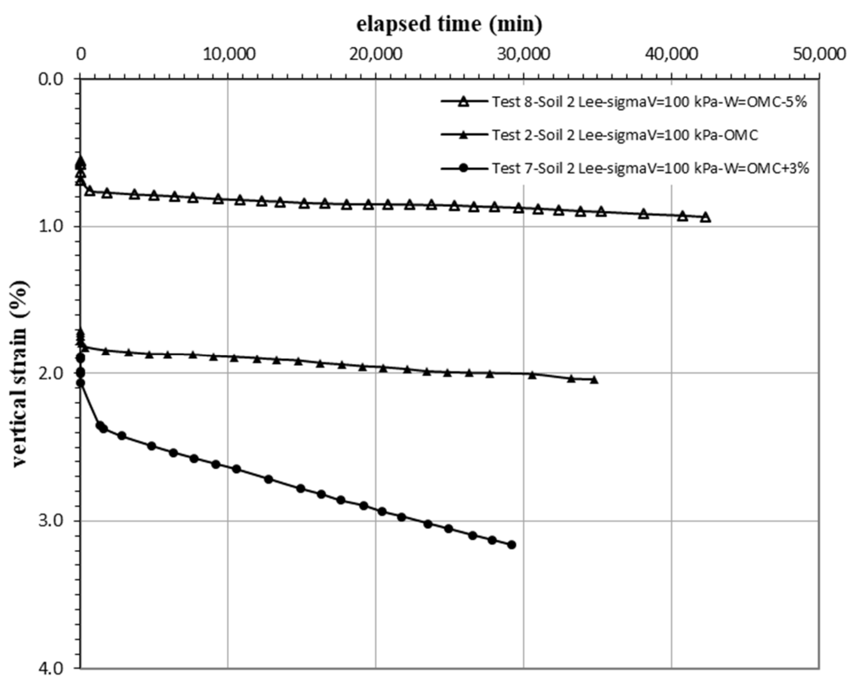

Figure 6.11. Effect of moisture content - Soil 2 (PI=21)

6.3.3.3 Strain Rate Analysis

Strain rate (also called as creep rate) of the one-dimensional deformation tests has been investigated. Vertical strain graphs were presented in three forms in Chapter 4; strain rate of those graphs is introduced in this section as the creep rate. Table 6.4 summarizes information for strain rate of creep tests. Strain rate is presented in two forms of percent per time (%/min) which is obtained from “strain versus time” graphs, and percent per square root of time (%/$\sqrt{min}$) which is obtained from “strain versus square root of time” graphs. Figure 6.12 shows the process to obtain creep rate for one of the tests.

Table 6.4. Strain rate of the one-dimensional creep deformation tests

Test No.	Soil ID	Soil PI	Compaction conditions	σ_V (kPa)	$\dot{\varepsilon}$ (%/min) *	$\dot{\varepsilon}$ (%/$\sqrt{min}$) *
Test 1	Soil 2	21	Standard Proctor - OMC	50	5.15E-06	0.0014
Test 2	Soil 2	21	Standard Proctor - OMC	100	6.10E-06	0.0016
Test 3	Soil 2	21	Standard Proctor - OMC	200	5.86E-06	0.0016
Test 4	Soil 5	5	Standard Proctor - OMC	50	6.64E-06	0.0016
Test 5	Soil 5	5	Standard Proctor - OMC	100	5.30E-06	0.0014
Test 6	Soil 5	5	Standard Proctor - OMC	200	5.22E-06	0.0014
Test 7	Soil 2	21	Standard Proctor - OMC+3%	100	2.86E-05	0.0060
Test 8	Soil 2	21	Standard Proctor - OMC-5%	100	3.58E-06	0.0009

* strain rate belongs to the linear section of the curve

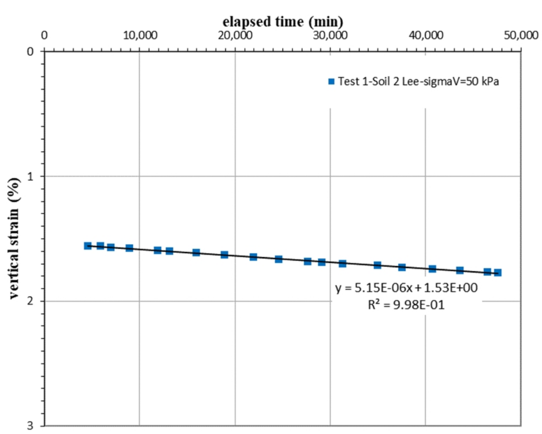

(a) creep rate in natural time

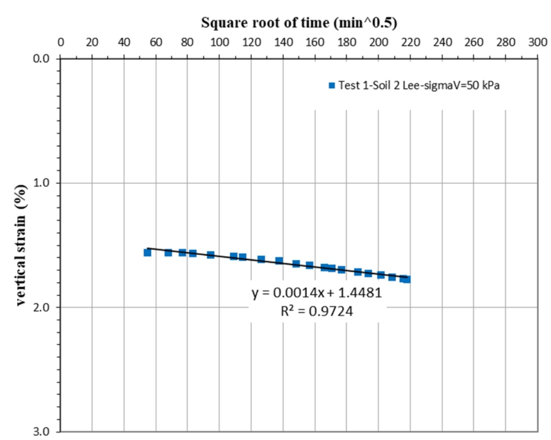

(b) creep rate in square root of time

Figure 6.12. Obtaining creep rate for Test 1 (Soil 2)

The values of strain rate presented in Table 6.4 are valid only if it is guaranteed that the soil has entered into its linear creep behavior. The linear section of creep usually starts after 1 day to 2 days after application of the external load.

There was no strong evidence indicating that Test Soil 2 with higher PI has a higher creep rate. Also, increasing vertical stress (in the range of applied stresses) did not have any significant influence on the creep rate. However, the creep rate was highly influenced by specimen moisture content, as increasing moisture content as little as 3% above the optimum increased the creep rate by a factor of about 5. Decreasing moisture content on the other hand, decreased the creep rate but to a lesser extent. The specimen with moisture content 5% below the OMC, showed a creep rate only 40% lower than the specimen with OMC. The creep rate of 6E-06 %/min may be introduced as a rough number for silty soils compacted at OMC.

If post-construction settlement of embankments is uniform along the length of embankment, they are considered acceptable. However, if non-uniform creep deformation happens, it takes a while before the deformation goes beyond the allowable amount. Table 6.5 summarizes the period of time to reach the allowable deformation of one inch for different embankment heights. This timeframe is based on the rough creep rate of $6*10^{-6}$ %/minute. It is noted that the timeframe presented in this table only takes into account the long-term creep deformation.

Table 6.5. Time needed to reach allowable deformation for different embankment heights

Embankment height H (ft)	Allowable strain (%)	Time (days)
40	0.21	24
30	0.28	32
20	0.42	48
10	0.83	96

6.4 Summary

This chapter opens with methodology and basics used for deformation analysis of the highway embankments. Properties of the utilized model and improving strategies of the initial model were briefly introduced, then results associated with deformation were presented. Embankment deformation has been investigated based on both TSA shear strength parameters and ESA shear strength parameters. For the TSA, acceptable cases are discussed in the form of a descriptive table. Analysis of the results of the one-dimensional creep compression tests which represent long-term deformation of embankments has been presented as well. Significant results and findings of this chapter are summarized as follows.

- Since the total stress slope stability was not critical, the acceptance zone imposed by total stress deformation performance criterion may be regarded as final acceptance zone for the TSA.
- A table (Table 6.3) was presented which provides descriptive information regarding acceptable cases based on the total stress deformation criterion.
- Results of the regression analysis show that, embankment deformation generally increases with the embankment height (H) and friction angle of soil (f_{UU}), and decreases with the elasticity modulus of soil (E) and embankment side slope (S).

Of course, effect of the side slope was subtle, and it becomes even less discernible at lower embankment heights.

- Calculations of the embankment deformation using CU triaxial parameters revealed that for all test soils (Test Soil 1 through Test Soil 5) and embankment sections, deformation was larger than the limiting value, except for few cases of Soil 2 Lee with PI=21 (highest PI among the tested soils) which is a A-7-6 (28) according to AASHTO classification, where dry unit weight of the soil samples (before shear stage) was very high. Laboratory results showed that this situation could happen only for the samples initially compacted at Modified Proctor compactive energy or higher. It is noted that for these cases, the FS (associated with ESA) was also in the acceptable range.

- The finding just mentioned may give grounds to the idea that soils with higher PI such as Test Soil 2 (A-7-6 class), perform slightly better under rain-induced infiltration conditions. This statement is in opposition to the criterion of limiting material PI as material selection that is used by a number of agencies. For example, this may cast doubt on the North Carolina DOT’s material selection specification of limiting PI to 15% in the coastal area. Of course, Test Soil 2 has a PI=21 which still holds this soil in the acceptable range of PI $\leq$ 25 for the Piedmont area of NC. This fact may also reject the specifications that abandon using the A-7 group soil as the embankment material.

- Since saturated samples in CU triaxial tests provide lower strength parameters than unsaturated samples in UU triaxial tests, deformation incorporated with them was generally higher.

- Creep curves generally consist of two main parts: initial sharp settlement due to immediate response to external loading and a linear section representative of creep deformation.

- With respect to the one-dimensional creep compression tests, the difference in the PI of tested soils did not indicate any pronounced dissimilarity in the behavior. There was no strong evidence indicating that Test Soil 2 with higher PI has a higher creep rate. Also, increasing the vertical stress did not have any significant influence on the creep rate. However, the creep rate was highly influenced by the specimen moisture content, as increasing moisture content as little as 3% above the optimum increased the creep rate by a factor of about 5. Decreasing moisture content on the other hand, decreased the creep rate but to a lesser extent. The specimen with moisture content 5% below the OMC, showed a creep rate only 40% lower than the specimen with the OMC. The creep rate of 6E-06 %/min may be introduced as a rough number for the used silty soils compacted at OMC.

CHAPTER 7: FINAL ACCEPTANCE ZONES

7.1 Introduction

As described in Chapter 3, the final proposed acceptable zone consists of superimposing the acceptable zones based on slope stability criterion and deformation criterion (refer to discussion on Figure 1.1). So far, the two former chapters presented different numerous graphs and a number of descriptive tables to define the acceptance zones based on either of the two criteria and different material strength parameters (total stress parameters, effective stress parameters, and modified total stress parameters). This chapter tries to provide an overlap of all these situations.

7.2 Final Acceptance Zones

Superimposition of the acceptable zones based on the slope stability criterion (in terms of the TSA,m) and the deformation criterion (in terms of the TSA) is presented in this chapter. It is noted that specifications regarding the slope stability criterion are mostly associated with the side slope of embankment. On the other hand, specifications regarding the deformation criterion seemed to be generally related to the embankment height, compactive energy utilized, and placement moisture content.

Figure 7.1 shows two red areas; Red area I which is imposed by the slope stability criterion based on modified total stress analysis parameters and Red area II which is imposed by the deformation criterion based on total stress analysis parameters. In this case which belongs to an embankment height H=40ft, side slope of 2H:1V and Test Soil 1, unaccepted area II imposed by the deformation criterion is larger, hence governing the final potential design. The plots for other test soils but same embankment geometry could be seen in Figure 7.2 through Figure 7.5.

After the figures, Table 7.1 presents an overview of superimposition of all acceptable zones / cases in a descriptive manner.

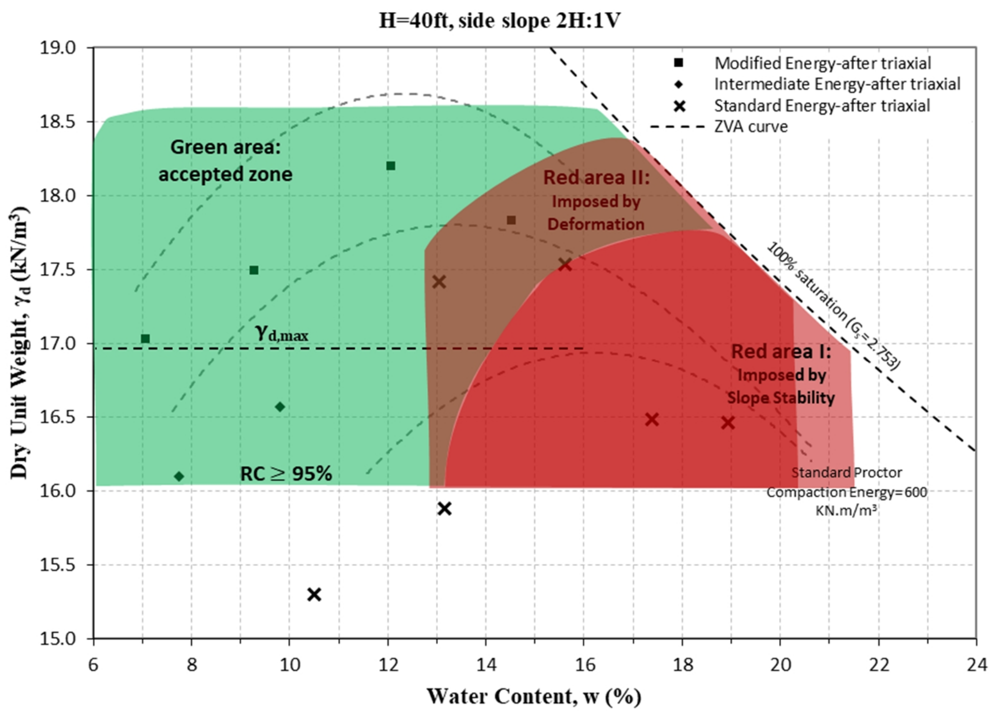

Figure 7.1. Superimposition of acceptance zones – Test Soil 1

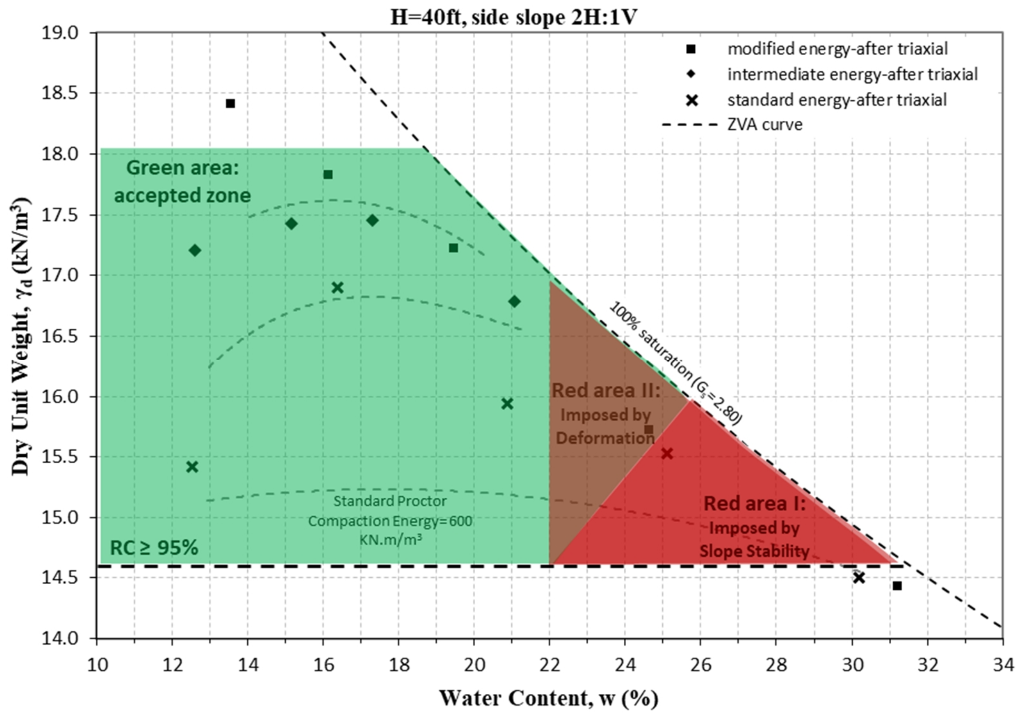

Figure 7.2. Superimposition of acceptance zones – Test Soil 2

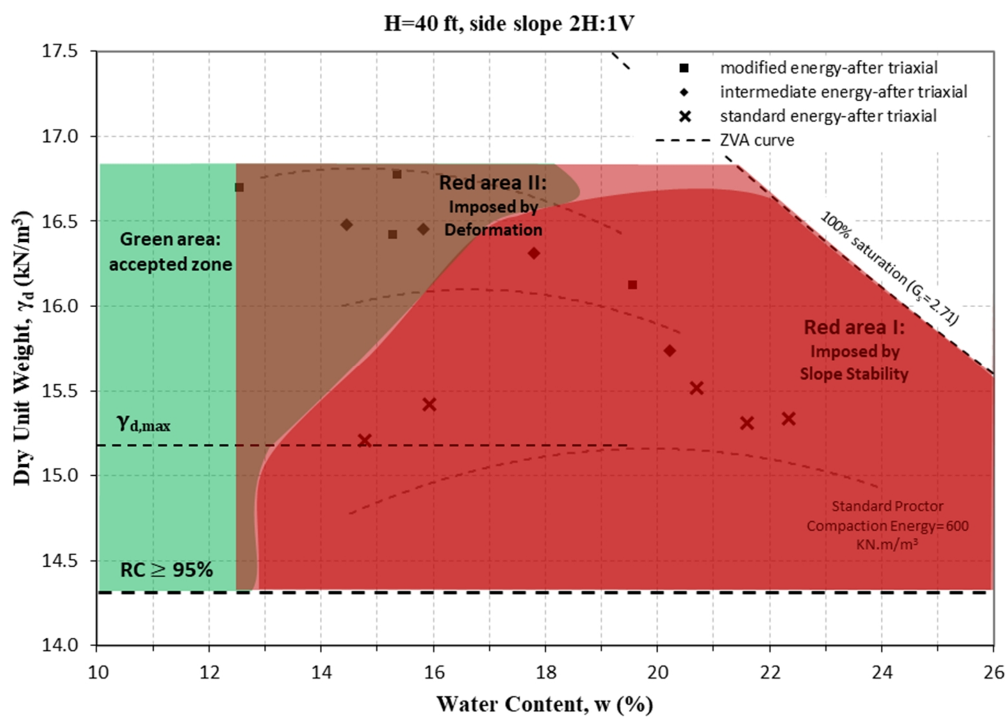

Figure 7.3. Superimposition of acceptance zones – Test Soil 3

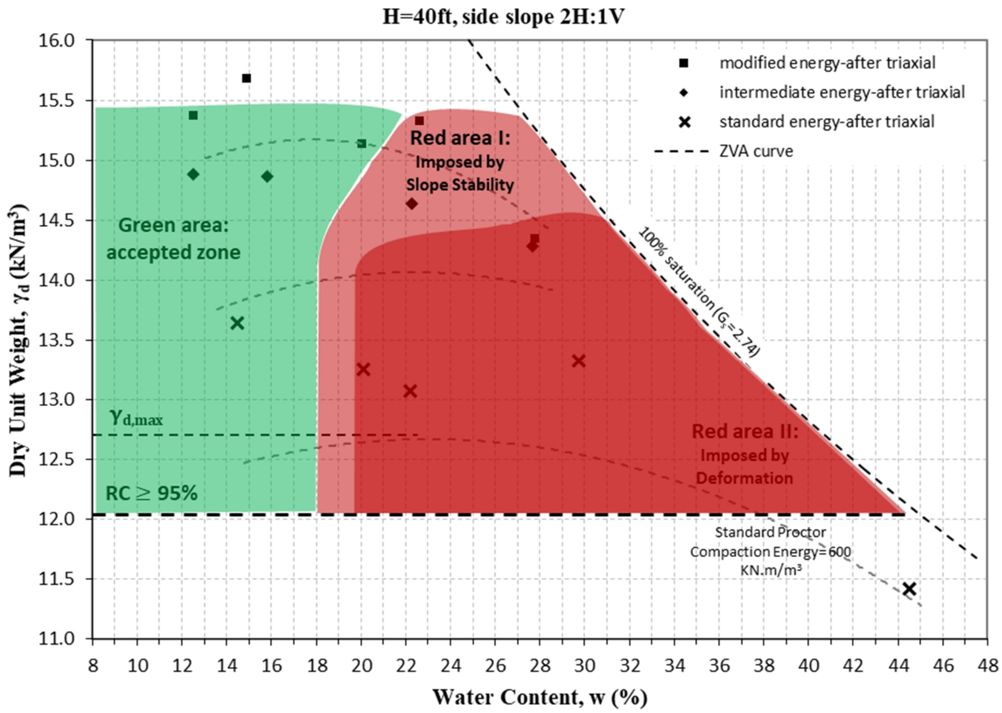

Figure 7.4. Superimposition of acceptance zones – Test Soil 4

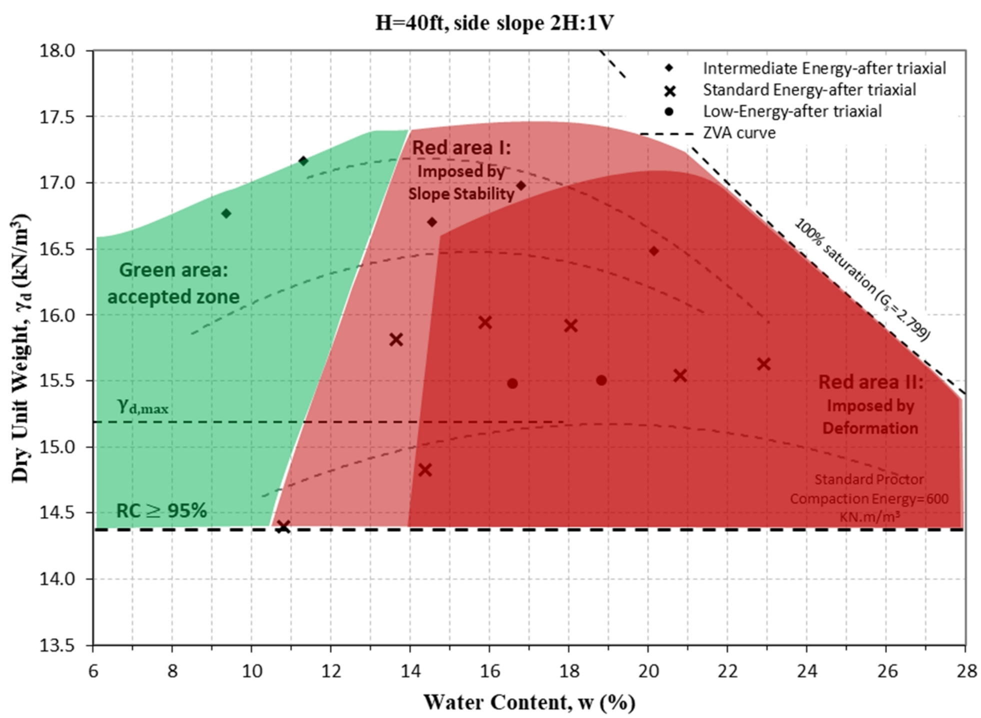

Figure 7.5. Superimposition of acceptance zones – Test Soil 5

Table 7.1. Description of superimposition of acceptable zones / cases based on slope stability and deformation criteria

Soil sample	Acceptable cases	Criterion
Test Soil 1 (PI=2) AASHTO class: A-4 (0)	- Side slope 1H:1V shall not be used regardless of embankment height, compactive energy and MC. - Side slope 2H:1V shall receive special caution (could fall on the border) if test soil is prepared at close to optimum or wet-of-optimum MC for all compactive energy levels. - Points compacted at standard energy with optimum and wet-of-optimum MC are not acceptable, unless for side slope of 4H:1V.	Slope Stability Criterion
	- For H=40 ft and samples compacted at Standard Proctor, almost all points are not acceptable. - At Standard Proctor, points wet-of-optimum are not acceptable for all embankment sections. At this energy level, points close to optimum need to be investigated. - At Standard Proctor, points dry-of-optimum are acceptable for all sections except H=40ft. - Even at higher energies, points wet-of-optimum could be problematic.	Deformation Criterion
Test Soil 2 (PI=21) AASHTO class: A-7-6 (28)	- Side slope 1H:1V shall not be used regardless of embankment height, compactive energy and MC. - Side slope 2H:1V shall receive special caution (could fall on the border) if test soil is prepared with wet-of-optimum MC at standard and intermediate compactive energy levels. - This test soil has minimum percentage of instability among all.	Slope Stability Criterion
	- At all energy levels, all points $\mp$ 5% of optimum are acceptable. - Optimum and dry-of-optimum points at all energy levels are acceptable. - For H=10 ft, regardless of compactive energy and MC, all points are acceptable. - Regardless of compactive energy, MC more than 8% wet-of-optimum is not recommended.	Deformation Criterion
Test Soil 3 (PI=NP) AASHTO class: A-4 (1)	- Side slope 1H:1V shall not be used regardless of embankment height, compactive energy and MC. - Side slope 2H:1V shall not be used at standard energy and shall receive special caution (could fall on the border) if test soil is prepared at close to optimum or wet-of-optimum MC for intermediate and modified energy levels.	Slope Stability Criterion
	- At Standard Proctor, points wet-of-optimum are not acceptable for almost all sections. - For H=40 ft, regardless of compactive energy and MC, all points are not acceptable. - For H=30 ft, points only drier than 5% of OMC at standard energy and points only drier than 2.5% of OMC at modified energy are acceptable. - For H=20 ft, points dry-of-optimum and close to optimum at modified and intermediate energy are acceptable. But for standard energy only dry-of-optimum points are acceptable. - For H=10 ft, regardless of compactive energy and MC, all points are acceptable. - Many unacceptable cases were observed.	Deformation Criterion

Table 7.1. Description of superimposition of acceptable zones / cases based on slope stability and deformation criteria (continued)

Test Soil 4 (PI=6) AASHTO class: A-5 (7)	- Side slope 1H:1V shall not be used regardless of embankment height, compactive energy and MC. - Side slope 2H:1V shall not be used at standard and intermediate compactive energy levels and shall receive special caution (could fall on the border) if test soil is prepared at wet-of-optimum MC for modified energy level. - Moisture contents above 4% wet-of-optimum is unacceptable for all energy levels and all sections (geometries) except for 4H:1V section which should be investigated.	Slope Stability Criterion
	- At Standard Proctor, wet-of-optimum points are not recommended for H=40 ft and 30 ft; however, for H=40ft points dry-of-optimum are neither recommended. - At Intermediate Proctor and for all sections, points dry-of-optimum are acceptable; however, wet-of-optimum points for H=40 ft and 30 ft are not acceptable. - At Modified Proctor and for all sections, regular points seem to be acceptable. - For H=10 ft and 20 ft regardless of compactive energy and MC all points seem acceptable.	Deformation Criterion
Test Soil 5 (PI=5) AASHTO class: A-5 (5)	- Side slope 1H:1V shall not be used regardless of embankment height, compactive energy and MC. - Side slope 2H:1V shall not be used at standard and intermediate compactive energy levels, neither for samples prepared at close to optimum and wet-of-optimum MC with modified energy level. Samples prepared at dry-of-optimum MC and compacted with modified energy level should receive special caution (could fall on the border). - Extra caution should be exercised with moisture contents above 4% wet-of-optimum at all compactive energy levels and for all sections. Section 4H:1V stands in a better position in this regard. - This test soil has highest percentage of instability cases among all.	Slope Stability Criterion
	- At Standard Proctor and for all sections, points dry-of-optimum are acceptable; however, as they get closer to OMC, they become unacceptable for H=40ft. Wet-of-optimum points are not accepted for H=40 ft and 30 ft at this energy level. - At Intermediate Proctor and for all sections, points dry-of-optimum are acceptable; however, for H=40ft points close to optimum and points wet-of-optimum for H=40 ft and 30 ft, neither are acceptable.	Deformation Criterion

7.3 Summary

The chapter presents superimposition of the acceptable zones based on the criterion of slope stability and deformation. Few cases were shown on the dry unit weight versus moisture content space. An elaborate descriptive table completes this information at the end of chapter.

CHAPTER 8: SUMMARY AND CONCLUSIONS

8.1 Summary of Findings

The performance of highway embankments was investigated based on two criteria: slope stability and deformation. Each of these concerns was looked at from two perspectives in terms of material engineering properties: TSA parameters and ESA parameters. In addition to the immediate deformation, long-term deformation of embankment soils was investigated using some laboratory scale creep tests. To find the total stress soil strength properties, a set of unconsolidated-undrained (UU) triaxial compression tests was designed, and to find out effective stress soil strength properties, a set of consolidated-undrained (CU) triaxial compression tests with pore pressure measurements was considered. Table 8.1 summarizes the research workload accomplished for this study. Important findings and conclusions of this study are reviewed in this chapter.

Table 8.1. Performed research workload

Task #	Test / Task description	Number Done
1	literature review	Done
2	sieve analysis	5
	hydrometer	5
	Atterberg limit, PL	6
	Atterberg limit, LL	6
	specific gravity, Gs	7
3	compaction	130
4	UU triaxial	214
5	CU triaxial	41
6	1D creep compression tests	8
7	slope stability analysis	1072 (short-term) + 208 (long-term)
8	deformation analysis	1072 (short-term) + 208 (long-term)
9	regression analysis	Done

Significant results and findings regarding total stress slope stability analyses:

- Among the 1072 cases reviewed based on TSA parameters, no cases showed a TSA factor of safety lower than the minimum value of 1.3. In many of these cases, the FS is well above the minimum value.

- The non-shallow failure mode was observed to be the dominant one for the total stress analysis. This indicates that, for the total stress analysis, shallow failure is never dominant.

- The two latter findings just mentioned, indicate that embankments made with the tested soil samples are stable right after compaction operation, even if the minimum compactive energy level, that is Standard Proctor is employed.

Significant results and findings regarding effective stress slope stability analyses:

- For the effective stress stability analysis many cases were found to have FS values lower than 1.3; from which, many cases were seen where shallow failure was the dominant mode of failure.

- Therefore, for the effective stress slope stability analysis, besides the grid and radius search method, shallow failure must be checked as there is a high likelihood for this mode of failure.

- Slope stability analyses using ESA parameters yielded all the three different modes of failure, that is non-shallow slip surface, local slip surface, and shallow/infinite failure.

- For the effective stress (ESA) slope stability analyses a descriptive table was presented to be used as a means of acceptance zone/cases under this condition. This table tables may be found in Table 5.1.

Significant results and findings regarding slope stability analyses using modified total stress parameters:

- For the slope stability analysis using modified total stress parameters, lots of cases with FS lower than the minimum of 1.3 were encountered.

- A descriptive table was presented to be used as a means of acceptance zone/cases under this condition. This table tables may be found in Table 5.2.

Significant results and findings with respect to the total stress deformation analyses:

- Results of the regression analysis show that, embankment deformation generally increases with the embankment height (H) and friction angle of soil (f_{UU}), and decreases with the elasticity modulus of soil (E) and embankment side slope (S). Of course, effect of the side slope is subtle, and it becomes even less discernible at lower embankment heights.

- A table (Table 6.3) was presented to provide descriptive information regarding acceptable cases based on the total stress deformation criterion.

Significant results and findings with respect to the effective stress deformation analyses:

- Calculations of the embankment deformation using CU triaxial parameters revealed that for all test soils (Test Soil 1 through Test Soil 5) and embankment sections deformation was larger than the limiting value, except for few cases of Test Soil 2 with PI=21 (highest PI among the tested soils) which is a A-7-6 (28) according to AASHTO classification, where dry unit weight of the soil samples (before shear stage) was very high. Laboratory results showed that this situation could happen only for the samples initially compacted at Modified Proctor compactive energy or higher. It is noted that for these cases, the FS (associated with ESA) was also in the acceptable range.

- The finding just mentioned may give grounds to the idea that soils with higher PI, such as Test Soil 2 (A-7-6 class), perform slightly better under rain-induced infiltration conditions. This statement is in opposition to the criterion of limiting material PI as material selection that is used by a number of agencies. For example, this may cast doubt on the North Carolina DOT’s material selection specification of limiting PI to 15% in the coastal area. Of course, Test Soil 2 has a PI=21 which still holds this soil in the acceptable range of PI $\leq$ 25 for the Piedmont area of NC. This fact may also reject the specifications that abandon using the A-7 group soil as the embankment material.

Finally, the most important results and findings related to the performed one-dimensional creep compression tests:

- Creep curves generally consist of two main parts: initial sharp settlement due to immediate response to external loading and a linear section representative of creep deformation.

- The difference in the PI of tested soils did not indicate any pronounced dissimilarity in the behavior. There was no strong evidence indicating that Test Soil 2 with higher PI has a higher creep rate. Also, increasing the vertical stress did not have any significant influence on the creep rate. However, the creep rate is highly influenced by the specimen moisture content, as increasing moisture content as little as 3% above the optimum increased the creep rate by a factor of about 5. Decreasing moisture content on the other hand, decreased the creep rate but to a lesser extent. The specimen with moisture content 5% below the OMC, showed a creep rate only 40% lower than the specimen with the OMC.

- The creep rate of 6E-06 %/min may be introduced as a rough number for the used silty soils compacted at OMC.

8.2 General Conclusions

- Results of this study show that non-uniform deformation service state in terms of total stress parameters along with slope stability service state in terms of TSA,m could control the design. Table 7.1 presents an overview of superimposition of all acceptable zones / cases in a descriptive manner.

- Reported slope stability failures are typically associated with high intensity/duration rainfall incidents. Results of the slope stability analyses in terms of ESA parameters may explain reported shallow rain-induced failures.

- Under the rain-induced conditions, many failures in the form of shallow failure may happen for the embankments constructed with the test soils used in this study.

- Providing suitable vegetation cover as well as drainage measures (to reduce infiltration and promote runoff, respectively) for the highway embankments could be useful in avoiding the detrimental effects of the water presence in the body of embankment.

- Acceptance zone based on RC ≥ 95% with γ_{dmax} obtained using Standard Proctor, for the most part satisfies slope stability and deformation performance service states for the analyzed embankments geometries. However, in segments where the embankment is subject to non-uniform settlements, utilizing higher compactive energies may be useful. Moreover, specifying a range for the placement moisture content may be a possible modification to help keep immediate non-uniform deformations below the allowable value (1 in or 25 mm).

- Results of this study also show that the side slope of 1H:1V must be avoided for highway embankments, and the side slope of 2H:1V is not recommended for weaker soils.

- Placement moisture contents that are more than 8% wet-of-optimum must be avoided. Also, moisture contents more that are than 5% wet-of-optimum are not recommended. Descriptive tables presented in this study provide useful information regarding placement moisture content.

- Among the tested soils, there are two A-4 soils (one silty sand and one low plasticity silt), two A-5 soils (both low plasticity silt), and one A-7-6 soil (high plasticity silt). Of course, according to the AASHTO classification which is represented here in Table 8.2, all test soils used in this study are rated as "fair to poor" as a subgrade. It seems that by moving from left to right over this table, soil materials losing their competence as subgrade is accepted as an engineering rule of thumb[1]. However, contrary to the traditional trend of avoiding A-7 soil class (such as South Carolina DOT), results of this research show that the A-7 used soil performs slightly better than A-4 and A-5 classes. In other words, although Test Soil 2 as an A-7 class with a group index of 28 would be located at the end of this table, performance of this soil as embankment material is evaluated to be better than other test soils.

Table 8.2. AASHTO table for classification of soils and soil-aggregate mixtures (obtained from ASTM D3282)

General Classification	Granular Materials (35 % or less passing No. 200 (75 µm))							Silt-Clay Materials (More than 35 % passing No. 200 (75 µm))			
Group classification	A-1		A-3	A-2				A-4	A-5	A-6	A-7
	A-1-a	A-1-b		A-2-4	A-2-5	A-2-6	A-2-7				A-7-5, A-7-6
Sieve analysis, % passing:											
No. 10 (2.00 mm)	50 max	...	...	...	...	...	...	...	...	...	...
No. 40 (425 µm)	30 max	50 max	51 min	...	...	...	...	...	...	...	...
No. 200 (75 µm)	15 max	25 max	10 max	35 max	35 max	35 max	35 max	36 min	36 min	36 min	36 min
Characteristics of fraction passing No. 40 (425 µm):											
Liquid limit	...		...	40 max	41 min	40 max	41 min	40 max	41 min	40 max	41 min
Plasticity index	6 max		N.P.	10 max	10 max	11 min	11 min	10 max	10 max	11 min	11 min[A]
Usual types of significant constituent materials	Stone Fragments, Gravel and Sand		Fine Sand	Silty or Clayey Gravel and Sand				Silty Soils		Clayey Soils	
General rating as subgrade	Excellent to Good							Fair to Poor			

- Despite the subtle trend of limiting embankment material PI among the agencies and guidelines (such as the North Carolina DOT specification), it seems having a small amount of PI enhances performance in the soil material. This was observed in the silty material; however, the author believes that a similar outcome might be true regarding granular material.

- Atterberg limits are performed only on the portion of the soil that passes No. 40 sieve (0.425mm opening size). Therefore, the relative contribution of this portion of the soil to the properties of the sample as a whole must be considered when using Atterberg limits to evaluate properties of a soil sample as embankment material. For instance, a soil sample with PI=21 and 50% passing No. 40 sieve obviously would perform differently than a soil sample with the same PI but 100% passing No. 40 sieve.

[1] It is noted that role of the subgrade layer is to furnish further support for traffic loads, and moreover, this study is about embankment material but not subgrade.

- We learn great lessons by comparing Test Soil 1 (PI=2) with AASHTO class A-4 as a silty sand (SM), with Test Soil 3 (PI=NP) with AASHTO class A-4 as a low plasticity silt (ML). Although the AASHTO classes are same, it was observed that the silty sand with as little as 2% PI (and obviously more sand-size particles) performed better than the non-plastic silt.

- To further evaluate the results, out of all the analyses conducted for this research we can consider four main sets: TSA FS, TSA deformation, ESA FS, and ESA deformation. Among these categories, TSA FS shows very high values, and ESA deformation reveals weak results, allowing us to ignore these two extreme categories. Table 8.3 provides a ranking index for the test soils used in this study. This table is designed based on the percentage of failures in the categories ESA FS and TSA deformation. This table demonstrates that Test Soil 2, a A-7-6 AASHTO class, has the highest rank. Of course, the table has only comparative application and is not intended to provide an absolute rating for test soils.

Table 8.3. Ranking index for test soils

Test soil	Classification		Test soil rank		
	USCS	AASHTO	ESA FS	TSA deformation	Overall rank
Test Soil 1	SM	A-4 (0)	2	3	2
Test Soil 2	MH	A-7-6 (28)	1	1	1
Test Soil 3	ML	A-4 (1)	4	5	5
Test Soil 4	ML	A-5 (7)	3	3	3
Test Soil 5	ML	A-5 (5)	5	2	4

- The results of this study, which are reflected in Table 8.3, indicate that Test Soil 2 with AASHTO class A-7-6 and PI=21 has the best performance among the test soils under rain induced conditions.

8.3 Recommendations for Future Work

- The study of the highway embankments in this research used laboratory scale testing. Construction of a “test embankment” with same soil samples and monitoring the behavior with field tests and instrumentation could yield valuable results.

- The author expresses that during creep tests on compacted samples many challenges were encountered. Having a setup (probably a humidity chamber) to control and change the moisture content of specimen may be considered.

- Deformation analyses performed in this study used a linear stress-strain model for the soil. Creating a model to simulate non-linear soil behavior could yield valuable results.

REFERENCES

AASHTO (1984), "A Policy on Geometric Design of Highways and Streets," *American Association of State Highway and Transportation Officials*, Washington, DC.

AASHTO (1995), "The Classification of Soils and Soil Aggregate Mixtures for Highway Construction Purposes," M 145,

AASHTO (2002), "Standard Specifications for Highway Bridges," *American Association of State Highway and Transportation Officials*, Washington, DC.

AASHTO (2012), "Standard Specification for Materials for Embankments and Subgrades," AASHTO Designation: M 57, Washington, D.C.

AASHTO (2015a), "Standard Method of Test for Moisture-Density Relations of Soils Using a 2.5-kg (5.5-lb) Rammer and a 305-mm (12-in.) Drop," AASHTO T 99,

AASHTO (2015b), "Standard Method of Test for Moisture-Density Relations of Soils Using a 4.54-kg (10-lb) Rammer and a 457-mm (18-in.) Drop," AASHTO T 180,

Appalachian Landslide Consultants (2013), "Geological/geotechnical report for Jackson County Planning Department," *Appalachian Landslide Consultants, PLLC*, *https://www.jacksonnc.org/_literature_181388/June_2013_ALC_Report*.

ASTM (2003), "Unconsolidated-Undrained triaxial compression test on cohesive soils," D2850, West Conshohocken, PA.

ASTM (2007), "Particle-size analysis of soils," D422, West Conshohocken, PA.

ASTM (2009), "Classification of Soils and Soil-Aggregate Mixtures for Highway Construction Purposes," D3282, West Conshohocken, PA.

ASTM (2009), "Description and Identification of Soils (Visual-Manual Procedure)," D2488, West Conshohocken, PA.

ASTM (2010), "Liquid limit, plastic limit, and plasticity index of soils," D4318, West Conshohocken, PA.

ASTM (2011), "Classification of soils for engineering purposes (unified soil classification system)," D2487, West Conshohocken, PA.

ASTM (2011b), "Consolidated-Undrained triaxial compression test for cohesive soils," D4767, West Conshohocken, PA.

ASTM (2011c), "One-dimensional consolidation properties of soils using incremental loading," D2435, West Conshohocken, PA.

ASTM (2012a), "Laboratory compaction characteristics of soil using modified effort," D1557, West Conshohocken, PA.

ASTM (2012b), "Laboratory compaction characteristics of soil using standard effort," D698, West Conshohocken, PA.

ASTM (2014), "Specific gravity of soil solids by water pycnometer," D854, West Conshohocken, PA.

ASTM (2019), "Laboratory determination of water (moister) content of soil and rock by mass," D2216, West Conshohocken, PA.

Aydilek, A. H., and Ramanathan, R. S. (2013), "Slope failure investigation management system," *Maryland Department of Transportation*, Rep. No.: MD-13-SP009B4N.

Brandon, T. L., Rose, A. T., and Duncan, J. M. (2006), "Drained and undrained strength interpretation for low-plasticity silts," *Journal of Geotechnical and Geoenvironmental Engineering*, 132 (2), 250-257.

Briaud, J. L. (2013), "Geotechnical engineering: unsaturated and saturated soils", *John Wiley & Sons*.

Bryant, L., Mauldon, M., and Mitchell, J. K. (2003), "Geotechnical problems with pyritic rock and soil," *Center for Geotechnical Practice and Research*, Virginia Polytechnic Institute and State University, Blacksburg, Va., 88.

Carter, M., and Bentley, S. P. (1991), "Correlations of soil properties", *Pentech press publishers*.

Chen, Y. (2010), "An experimental investigation of the behavior of compacted clay/sand mixtures," M.Sc. Thesis, Adviser: Meehan C. L., University of Delaware.

Clough, G. W., Sitar, N., Bachus, R. C., and Rad, N. S. (1981), "Cemented sands under static loading," *Geotechnical Engineering Division*, ASCE 107 (GT6).

Das, B. M. (2008), "Advanced Soil Mechanics", Third ed., *Taylor & Francis*.

Day, R. W., and Axten, G. W. (1989), "Surficial stability of compacted clay slopes," *Journal of Geotechnical Engineering*, 115 (4), 577-580.

Delaware DOT (2016), "Standard Specifications for Road and Bridge Construction."

Duncan, J. M., Wright, S. G., and Brandon, T. L. (2014), "Soil strength and slope stability", *John Wiley & Sons*.

FHWA (2006), "Geotechnical Aspects of Pavements," *National Highway Institute*, USDOT, Washington, D.C., Rep. No.: FHWA NHI-05-037.

Geocomp Corporation (2011a), "LoadTrac-II user's manual," Acton, MA, U.S.

Geocomp Corporation (2011b), "FlowTrac-II user's manual," Acton, MA, U.S.

Geocomp Corporation (2014), "Triaxial software user's manual," Acton, MA, U.S.

Geoslope (2021a), "Stability Modeling with GeoStudio," *GEOSLOPE International Ltd.*, www.geoslope.com.

Geoslope (2021b), "Stress-Strain Modeling with GeoStudio," *GEOSLOPE International Ltd.*, www.geoslope.com.

Gradwell, M. W., and Birrell, K. S. (1954), "Physical properties of certain volcanic clays," *New Zealand Journal of Science and Technology*, B36 (2).

Gujarati, D. N., Porter, D. C., and Gunasekar, S. (2009), "Basic Econometrics", 5th ed., *McGraw Hill Education*.

Hassani, M., Pando, M. A., and Janardhanam, R. (2017), "State of Practice of Highway Embankment Construction in the U.S. - A Literature Review of FHWA and USDOTs Requirements for Embankment Material Selection and Embankment Construction," *University of North Carolina at Charlotte*, 56, *https://connect.ncdot.gov/projects/research/Pages/ProjDetails.aspx?ProjectID=2015-05*.

Hassani, M., Pando, M. A., and Janardhanam, R. (2019), "Improvement of Material Criteria for Highway Embankment Construction," *University of North Carolina at Charlotte*, FHWA/NC/2015-05, 215, *https://connect.ncdot.gov/projects/research/Pages/ProjDetails.aspx?ProjectID=2015-05*.

Hossain, S., Khan, S., and Kibria, G. (2017), "Sustainable Slope Stabilisation using Recycled Plastic Pins", *CRC Press, Taylor & Francis Group*.

Iowa DOT (2015), "Engineering Properties of Soil and Rock-Geotechnical Design Manual," *Iowa Department of Transportation*, Rep. No.: 200E-1.

Janardhanam, R., and Pando, M. A. (2015), "Improvement of Material Criteria for Highway Embankment Construction," *University of North Carolina at Charlotte*, Research Proposal: 2015-05.

Khan, M. S., Hossain, S., and Kibria, G. (2015), "Slope Stabilization Using Recycled Plastic Pins," *Performance of Constructed Facilities, ASCE*, 30 (3), 04015054-(1-10).

Ladd, C. C., and Foott, R. (1977), "Foundation design of embankments constructed on varved clays," *U. S. Department of Transportation*, Rep. No.: FHWA TS-77-214.

Lee, K. L. (1970), "Comparison of Plane Strain and Triaxial Tests on Sand," *ASCE, Journal of Soil Mechanics and Foundations Division*, 96 (SM 3), 901-923.

Loehr, J. E., and Bowders, J. J. (2007), "Slope stabilization using recycled plastic pins, phase III," *Missouri Department of Transportation*, Final report, RI98-007D.

Loehr, J. E., Fennessey, T. W., and Bowders, J. J. (2007), "Stabilization of Surficial Slides Using Recycled Plastic Reinforcement," *Transportation Research Record: Journal of the Transportation Research Board*, 1989 (2), 79-87.

Long, J., Olson, S., Stark, T., and Samara, E. (1998), "Differential movement at embankment-bridge structure interface in Illinois," *Transportation Research Record: Journal of the Transportation Research Board*, 1633 53-60.

Louisiana DOT (2016), "Standard Specifications for Roads and Bridges," *Louisiana Department of Transportation and Development*.

Nafisi, A., Safavizadeh, S., and Montoya, B. M. (2019), "Influence of Microbe and Enzyme-Induced Treatments on Cemented Sand Shear Response," *Journal of Geotechnical and Geoenvironmental Engineering*, 145 (9).

NAVFAC (1986), "Foundations and Earth Structures-Design Manual 7.02," *Naval Facilities Engineering Command*.

NCGS (2006), "August 31, 2006 Embankment Failure - Debris Flow at the Cascades Development Haywood County, North Carolina," *North Carolina Geological Survey*.

NCHRP (1971), "NCHRP Synthesis of Highway Practice 8: Construction of Embankments," *Transportation Research Board*, Washington D.C., Rep. No.: Synthesis 8, 38.

NCHRP (1975), "NCHRP Synthesis of Highway Practice 29: Treatment of Soft Foundations for Highway Embankments," *Transportation Research Board, Washington, D.C.*, 25.

NCHRP (1983), "Shallow Foundations for Highway Structures," *NCHRP*, Rep. No.: 107.

NCHRP (1989), "NCHRP Synthesis of Highway Practice 147: Treatment of problem foundations for highway embankments," *Transportation Research Board, Washington, D.C.*, 78.

NCHRP (1990), "NCHRP Synthesis of Highway Practice 159: Design and Construction of Bridge Approaches," *Transportation Research Board, Washington, D.C.*, 45.

NCHRP (2004), "NCHRP Report 529: Guideline and Recommended Standard for Geofoam Applications in Highway Embankments," *Transportation Research Board, Washington, D.C.*, 25.

Nobahar, M., Khan, M. S., and Ivoke, J. (2020), "Combined effect of rainfall and shear strength on the stability of highway embankments made of Yazoo clay in Mississippi," *Geotechnical and Geological Engineering*,2787–2802.

North Carolina DOT (2000), "Interim pavement design procedure," *NC Department of Transportation*, Pavement Management Unit.

North Carolina DOT (2012), "Pavement Condition Survey Manual," *North Carolina Department of Transportation*.

North Carolina DOT (2012), "Standard Specifications for Roads and Structures."

Ohio DOT (2016), "Construction and Material Specifications."

Pagen, C. A., and Jagannath, B. N. (1968), "Mechanical Properties of Compacted Soils," *Highway Research Board*,(235), 13-26.

Parra, J. R., Loehr, J. E., Hagemeyer, D. J., and Bowders, J. J. (2003), "Field Performance of Embankments Stabilized with Recycled Plastic Reinforcement," *Transportation Research Record: Journal of the Transportation Research Board*, 1849 (1), 31-38.

Pennsylvania DOT (2016), "Specifications."

Pilipchuk, J. (2008), "Geotextile for Pavement Stabilization," Presentation by NCDOT, Personal comunication.

Popescu, M. E. (1994), "A suggested method for reporting landslide causes," *Bulletin of the International Association of Engineering Geology*, 50 71-74.

Popescu, M. E. (2002), "Landslide causal factors and landslide remediatial options", *Proc. of 3rd International Conference on Landslides, Slope Stability and Safety of Infra-Structures*, Singapore, pp. 61-81.

Proctor, R. R. (1933), "Fundamental Principles of Soil Compaction," *Engineering News-Record*, 111 (9), 245-248.

Rocscience "SLIDE user manual," http://www.rocscience.com.

Samtani, N. C., and Nowatzki, E. A. (2006a), "Soils and Foundations-Reference Manual, Volume I," *Federal Highway Administration*, Rep. No.: FHWA-NHI–06-088.

Samtani, N. C., and Nowatzki, E. A. (2006b), "Soils and Foundations-Reference Manual, Volume II," *Federal Highway Administration*, Rep. No.: FHWA-NHI–06-089.

Santee, T. (2019), NCDOT, Personal comunication.

Schaeffer, M. F., and Clawson, P. A. (1996), "Identification and treatment of potential acid-producing rocks and water quality monitoring along a transmission line in the Blue Ridge Province, southwestern North Carolina," *Environmental & Engineering Geoscience*, 2 (1), 35-48.

Seed, H. B., and Chan, C. K. (1959), "Structure and strength characteristics of compacted clays," *Journal of the Soil Mechanics and Foundations Division, ASCE*, 85 (SM5), 87-128.

Seed, H. B., Mitchell, J. K., and Chan, C. K. (1960), "The strength of compacted cohesive soils", *Proc. of Research Conference on Shear Strength of Cohesive Soils*, University of Colorado, Boulder, Colorado, pp. 877-964.

Shafiee, A., Tavakoli, H., and Jafari, M. (2008), "Undrained behavior of compacted sand-clay mixtures under monotonic loading paths," *Journal of Applied Sciences*, 8 (18), 3108-3118.

Skempton, A. (1954), "The pore-pressure coefficients A and B," *Geotechnique*, 4 (4), 143-147.

Skempton, A. (1984), "Slope stability of cuttings in brown London clay", *Proc. of Ninth international conference on soil mechanics and foundation engineering*, Tokyo, 3, pp. 261-270.

Soriano, A. (2013), "Embankments and dams, slope stability and landslides: General report", *Proc. of 15th European Conference on Soil Mechanics and Geotechnical Engineering*, Athens, Greece, pp. 171-196.

South Carolina DOT (2007), "Standard Specifications for Highway Construction."

Sowers, G. (1963), "Engineering properties of residual soils derived from igneous and metamorphic rocks", *Proc. of 2nd Panamerican Conference on Soil Mechanics and Foundation Engineering*, Brazil, 1, pp. 39-62.

Stark, T., Arellano, D., Horvath, J., and Leshchinsky, D. (2004), "Geofoam Applications in the Design and Construction of Highway Embankments," *NCHRP*.

Stark, T. D., Olson, S. M., and Long, J. H. (1995), "Differential movement at the embankment/structure interface-mitigation and rehabilitation," *Illinois DOT*, Springfield, Illinois, Rep. No.: LAB-H1 FY93.

Taylor, D. W. (1948), "Fundamentals of soil mechanics", 10 ed., *John Wiley & sons Inc.*, New York.

Texas DOT (2014), "Standard Specifications for Construction and Maintenance of Highways, Streets, and Bridges."

Tohari, A., Nishigaki, M., and Komatsu, M. (2007), "Laboratory rainfall-induced slope failure with moisture content measurement," *Journal of Geotechnical and Geoenvironmental Engineering*, 133 (5), 575-587.

Toriyama, K. (1972), "Creep Study in Compacted Soils," Transactions of The Japanese Society of Irrigation, Drainage and Reclamation Engineering, 1972 (40), 67-72.

Torrey, V. H. (1982), "Laboratory shear strength of dilative silts," *U.S. Army Engineers, Waterways Experiment Station*, Report prepared for the Lower Mississippi Valley Division.

VandenBerge, D. R., Brandon, T., and Duncan, J. (2014), "Triaxial tests on compacted clays for consolidated-undrained conditions," *Geotechnical Testing Journal*, 37 (4), 704-716.

Vargas, M. (1953), "Some engineering properties of residual clay soils occurring in Southern Brazil", *Proc. of 3rd International Conference on Soil Mechanics and Foundation Engineering*, Zurich, 1, pp. 67-71.

Virginia DOT (2014), "Virginia Manual of Instructions-Chapter 3: Geotechnical Engineering," *Virginia Department of Transportation*.

Washington DOT (2016), "Standard Specifications for Road, Bridge and Municipal Construction."

Wiebe, B., Graham, J., Tang, G. X., and Dixon, D. (1998), "Influence of pressure, saturation, and temperature on the behaviour of unsaturated sand-bentonite," *Canadian Geotechnical Journal*, 35 (2), 194-205.

Wooten, R. M., and Latham, R. S. (2004), "Report on the May 5–7, 2003 debris flows on slopes underlain by sulfidic bedrock of the Wehutty, Nantahala, and Copper Hill Formations, Swain County, North Carolina," *North Carolina Geological Survey*, 20.

Wright, S. G. (2005), "Evaluation of soil shear strengths for slope and retaining wall stability analyses with emphasis on high plasticity clays," *Federal Highway Administration*, Rep. No.: FHWA/TX-06/5-1874-01-1.

Yoshimi, Y. (1958), "One-dimensional compression of partially saturated soil," Ph.D. Dissertation, Norhtwestern University.

Zaman, M., Laguros, J. G., and Jha, R. K. (1995), "Statistical models for identification of problematic bridge sites and estimation of approach settlements," *Oklahoma Department of Transportation*, FHWA/OK 94(02), 110.

APPENDIX A: A Synopsis of State-of-the-Practice Review of Specifications Regarding Highway Embankment Material Selection and Highway Embankment Construction

A.1. Review of Specifications Regarding Highway Embankment Material Selection

In this synopsis a review of the specifications and requirements set by different agencies regarding highway embankment material selection is presented. Reviewed components regarding material selection include material gradation / classification, and Atterberg limits. Material presented in this section are mainly obtained from a comprehensive report by Hassani et al. (2017).

A.1.1. Requirements on Material Gradation

After intensive review of the state standards it is noted that only a few of them have minor requirements set for material gradation. These include Colorado, Ohio, Rhode Island, South Carolina and Utah. In all cases, these requirements are very general; for instance, South Carolina specifies that A-7 group soil shall not be used. Pennsylvania also sets some requirements only for the fine-grained portion of the embankment material. Figure A.1 shows states imposing requirements on gradation.

All states mention a maximum allowable particle size suitable for the upper layers of embankment. They usually forbid using particles larger than 4 to 6 inches in the upper 1 or 2 feet, and also disallow use of large rock fragments and stones in the top few feet of the highway embankment.

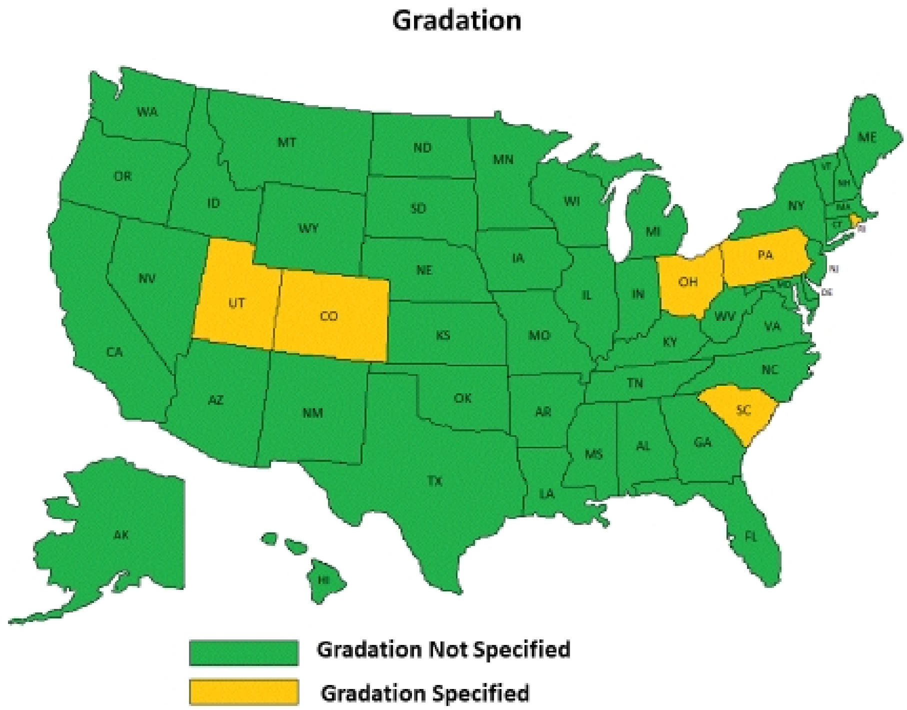

Figure A.1. States imposing requirements on gradation as material selection criterion (from Hassani et al. 2017)

A.1.2. Requirements on Material Atterberg Limits

Seven states including Delaware, Louisiana, North Carolina, Ohio, Pennsylvania, Texas and Washington have specifications on the Atterberg limits required for the material used in embankments. Figure A.2 shows states imposing requirements for Atterberg limits.

Instead of setting a maximum plasticity index, Delaware has specified a maximum liquid limit of 40%. Louisiana sets a minimum PI of 11% and a maximum of 25% for what they classify as usable soil for embankment construction. North Carolina's current specifications require that the plasticity index stay below 15% for coastal area, and below 25% for Piedmont and western area. Pennsylvania specifies that embankment material can consist of both fine-grained portion and granular portion, then it states some conditions regarding gradation, and Atterberg limits of the fine-grained portion which are listed in

Table A.1. In Texas, for a material to be considered as granular the following shall hold: LL ≤ 45, PI ≤ 15. Texas also correlates acceptable relative compaction to the PI of the soil being compacted. In Washington, as borrow material becomes finer, the PI shall be limited to a lower value. This state is probably one of the strictest states with PI = 0 for material having more than 35.1% passing No. 200 sieve. Table A.1 summarizes information for U.S. states agencies which use Atterberg limits as embankment material selection criteria.

Samtani and Nowatzki (2006a) provide guidelines regarding material selection for structural backfill for bridge abutments. In this document, the authors specify limiting the PI of the structural backfill to 10%. The PI is limited to this value to control long-term deformations. Of course, this document is among the federal guidelines and can not be counted in the category of states standards.

Of course, in some specific portions of the embankment, like bridge approaches, or for the select borrow which is usually of higher quality than common borrow, plasticity index requirement may be stricter. However, requirements pertaining to the bridge approaches or to the select borrow are not covered in this synopsis.

Table A.1. Summary of states specifying Atterberg limits as material selection criteria (Hassani et al. 2017)

State	Reference	Specification
Delaware	Delaware DOT (2016)	LL of borrow $\leq$ 40
Iowa	Iowa DOT (2015)	PI > 10, for select cohesive soils
Louisiana	Louisiana DOT (2016)	11 $\leq$ PI $\leq$ 25
North Carolina	North Carolina DOT (2012)	PI $\leq$ 15 for coastal area; PI $\leq$ 25 for Piedmont and Western area
Ohio	Ohio DOT (2016)	LL < 65
Pennsylvania	Pennsylvania DOT (2016)	for soil (fine-grained portion): LL < 65; if 41 < LL < 65, PI $\geq$ LL-30
Texas	Texas DOT (2014)	LL $\leq$ 45, PI $\leq$ 15 for granular material
Washington	Washington DOT (2016)	if 12.1 $\leq P_{200} \leq$ 35, PI $\leq$ 6 if 35.1 < P_{200}, PI = 0

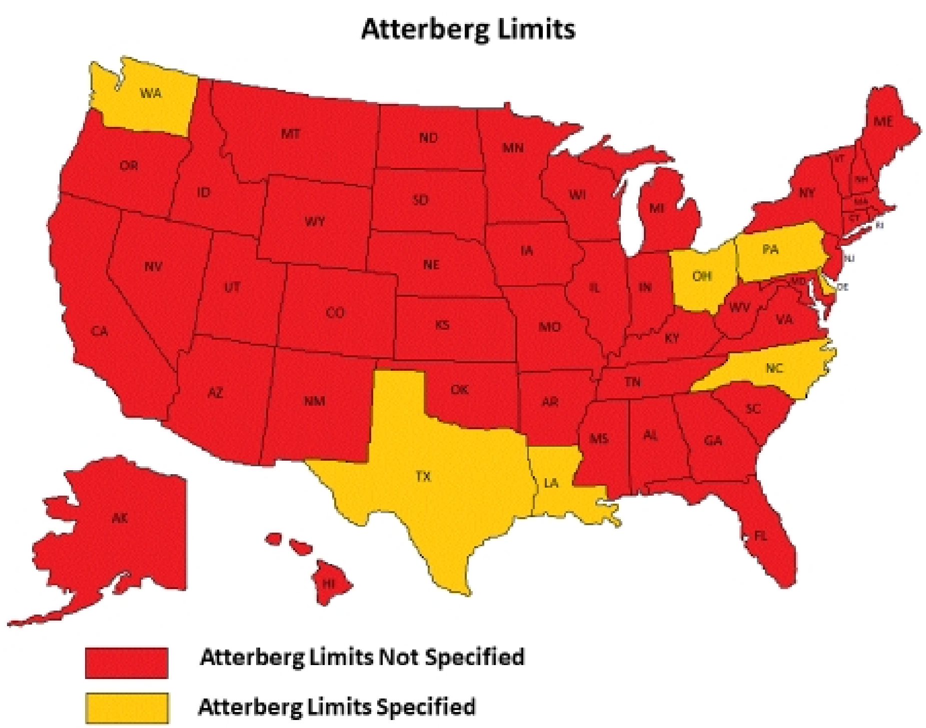

Figure A.2. States imposing requirements on Atterberg limits as borrow material selection criteria (from Hassani et al. 2017)

A.2. Review of Specifications Regarding Highway Embankment Construction

In the second section of this synopsis a review of the specifications and requirements set by different agencies regarding highway embankment construction is presented. Reviewed components regarding construction include any requirements on minimum field dry unit weight and relative compaction (RC), moisture control, and lift thickness.

A.2.1. Requirements on Minimum Field Dry Unit Weight and Relative Compaction

Nine states (Colorado, Delaware, Georgia, Indiana, Maryland, Michigan, Ohio, Pennsylvania and South Carolina) have specifications limiting the minimum dry unit weight of material placed in highway embankment. Of these states, Colorado, Delaware, Georgia, Indiana and Ohio limit the dry unit weight to a minimum value of 90 lbs/ft^3. Michigan and Pennsylvania limit the unit weight to a minimum of 95 lbs/ft^3. Maryland and South Carolina limit the minimum unit weight to 100 lbs/ft^3.

The majority of states require achieving a minimum relative compaction specified with respect to a laboratory standard compaction test, such as Standard Proctor (AASHTO T 99) or Modified Proctor (AASHTO T 180). Of course, a vast number of states use local standards, which represent AASHTO standards with a level of minor modification.

Of all the 50 states reviewed, 33 states somehow state that maximum laboratory dry unit weight ($g_{d\max}$) shall be obtained in accordance with AASHTO T 99, which uses Standard Proctor energy. Twenty three (23) of these states necessitate reaching exactly the minimum relative compaction of 95%, while others range from minimum RC of 90% to 102%. FHWA [FHWA (2006)] and AASHTO [AASHTO (2012)] also require compacting embankments to RC ≥ 95% while $g_{d\max}$ obtained at standard energy level. This fact may justify the high number of states sticking to AASHTO T 99. Number of states accepting AASHTO T 180, Modified Proctor energy, is equal to eight. Half of them require minimum RC of exactly 95% while others range within 90% to 95%.

Five of the states combine standard and modified energy in quality control process, correlating level of compacting energy to factors like material gradation or selected minimum RC in the plans. Two states of Kansas and Nebraska test the quality of embankment compaction according to the roller status. Compaction is considered accomplished by them for example when tamping feet of the roller walks out of the surface, or when a specific number of passes is obtained. No information regarding compaction energy level could be found for the two states of Minnesota and Mississippi. They have only stated relative compaction level. Table A.2. summarizes compaction energy level distribution among states and Figure A.3. shows compaction energy level specifications by each state across the U.S.

Table A.2. Summary of compaction energy required by states (from Hassani et al. 2017)

Energy Level	Number of States
Standard Proctor	33
Modified Proctor	8
Standard/Modified Proctor	5
roller controlled	2
not mentioned	2

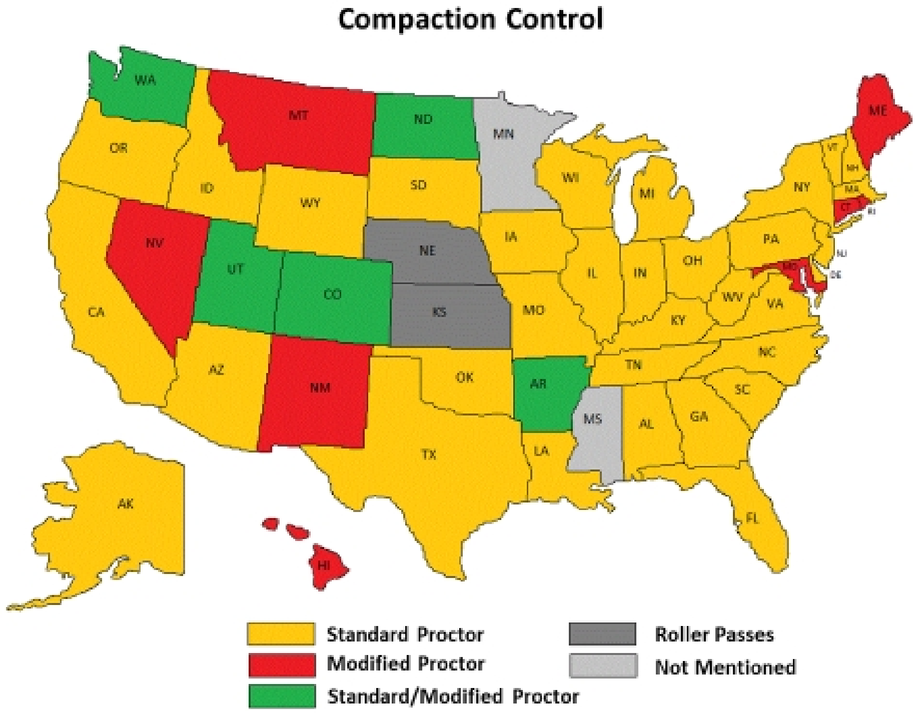

Figure A.3. Compaction energy specifications by state (from Hassani et al. 2017)

A.2.2. Requirements on Moisture Content Control

Twenty seven (27) states have specified some kind of criteria as the moisture content control. These requirements are in most of cases as an acceptable range for placement moisture content. The requirements differ based on the material gradation, Atterberg limits of material, moisture content of material itself, and level or energy of compaction.

Ten (10) states have specified acceptable moisture content in the range of ±2% of optimum moisture content. This high number of states seems to be related to the same specification set by Federal and AASHTO standards.

Twenty three (23) states have not specified any to directly designate moisture content of the embankment layers. Of course, all of them imply that material moisture content shall be in a range that minimum field density requirement is achievable.

A.2.3. Requirements on Lift Thickness

A lift thickness of 8” in loose state is required by 31 states, while two of the agencies require same 8” lift thickness but measured after compaction. Majority of the states consider lift thickness in loose state as only five states of Florida (6” or 12” depending on gradation), Maryland (8”), Pennsylvania (6”/8” for granular material), Rhode Island (12”), West Virginia (6”) set lift thickness requirement measured after compaction. Only Indiana uses a compound lift placement measurement as 6” after compaction and 8” in loose state.

It is noted that maximum accepted lift thickness is 12”, while the minimum is 4” loose measurement in Washington that is for the top 2 feet of embankment. Depending on material gradation, compaction class or position of layer, some states have different placing layer thicknesses.

All states have mentioned lift thickness as an easy to use and whole number, whether loose or compacted, except the New York state. For the New York state, lift thickness shall be obtained via charts with the load per wheel of compacting equipment as input. Lift thickness specifications requirement is summarized and illustrated in Figure A.4. This figure shows 7 states having lift thicknesses equal to 12”; out of which only Rhode Island referring to compacted state and the rest indicating loose state.

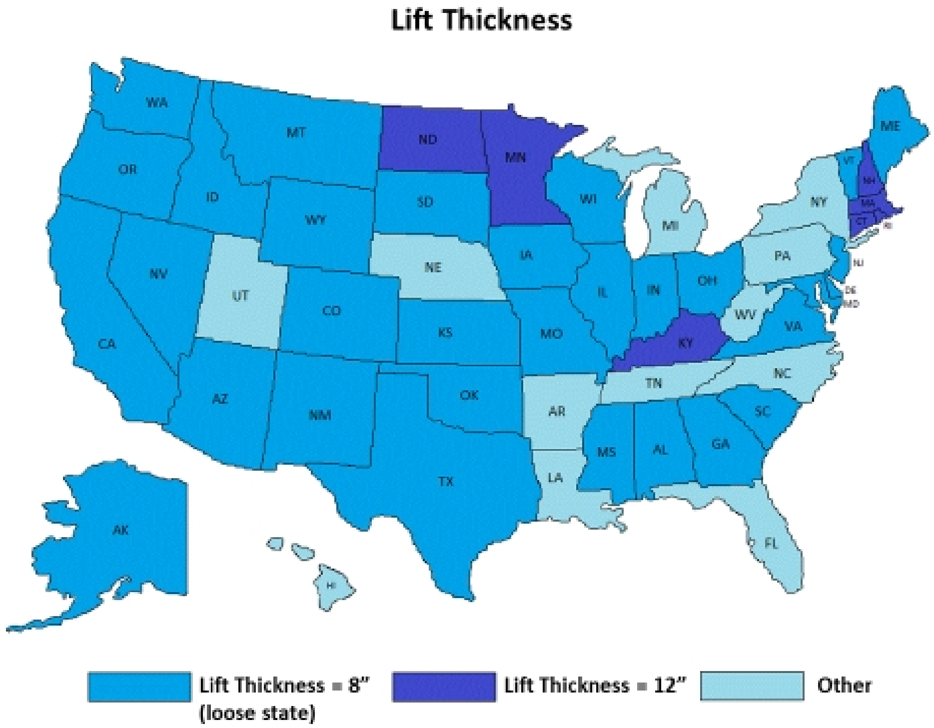

Figure A.4. Variation of lift thickness specifications by state (from Hassani et al. 2017)

APPENDIX B: Failure Lines for Unconsolidated-Undrained Triaxial Tests

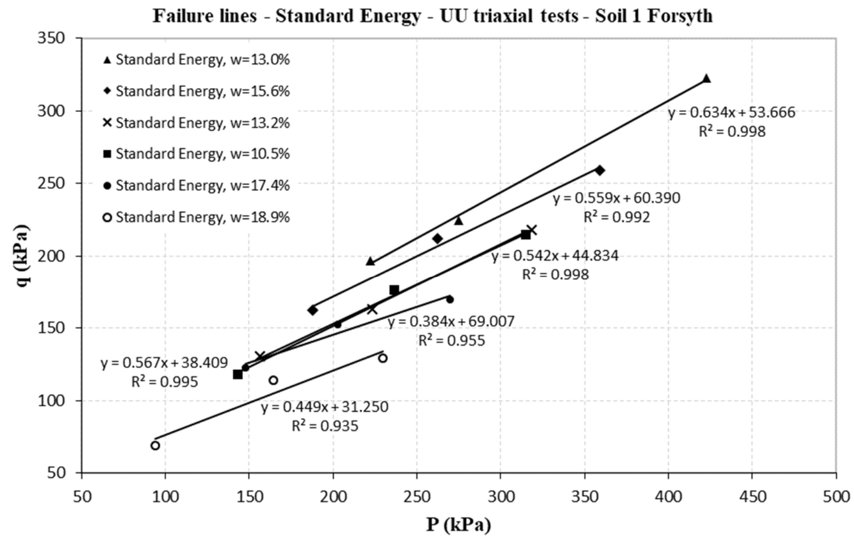

Figure B.1. Failure lines, standard energy, UU triaxial tests, Soil 1

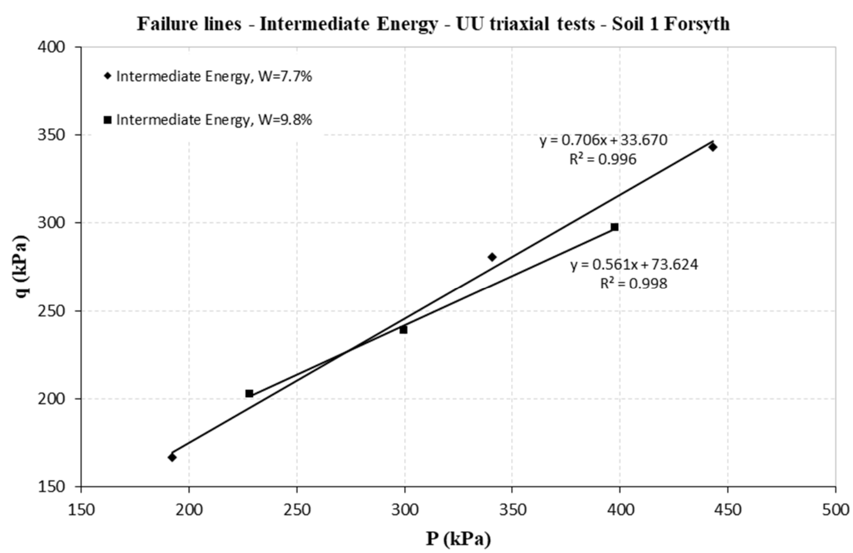

Figure B.2. Failure lines, intermediate energy, UU triaxial tests, Soil 1

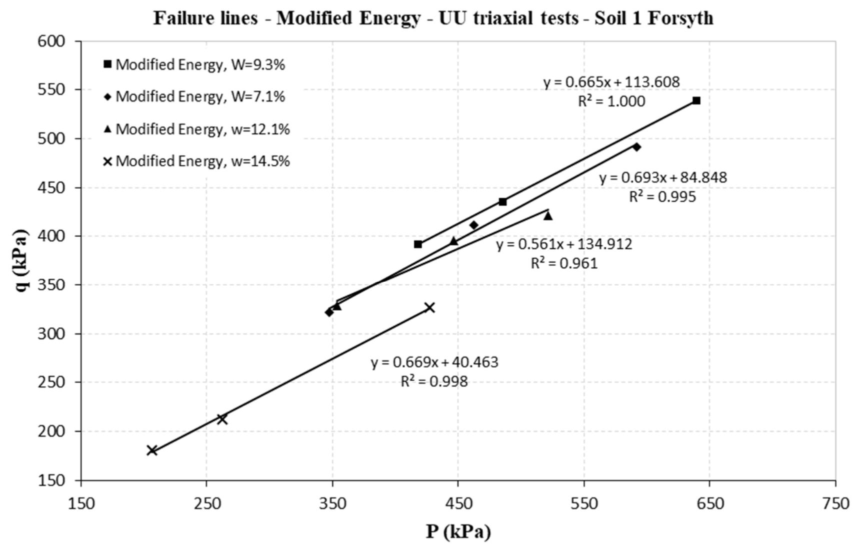

Figure B.3. Failure lines, modified energy, UU triaxial tests, Soil 1

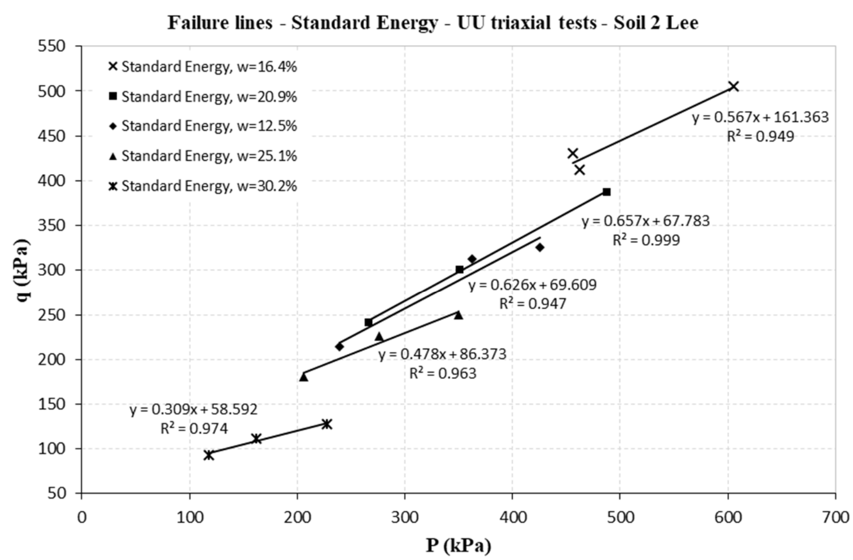

Figure B.4. Failure lines, standard energy, UU triaxial tests, Soil 2

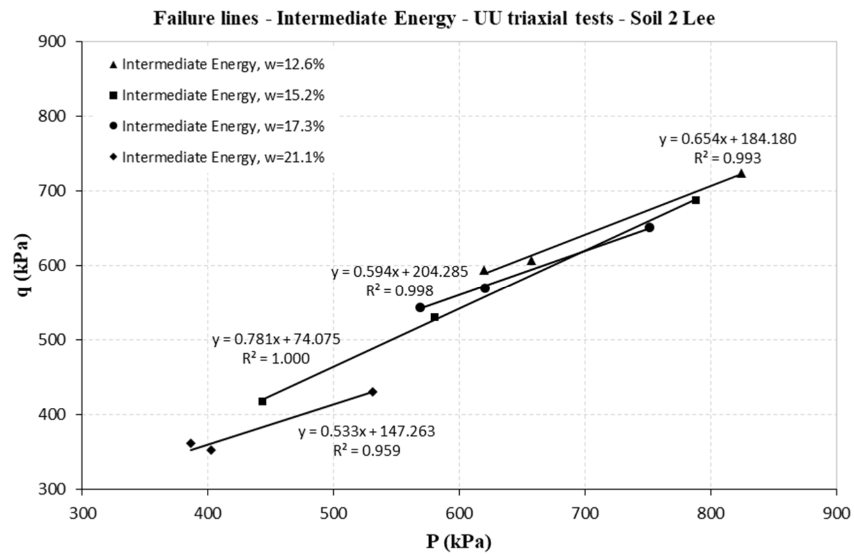

Figure B.5. Failure lines, intermediate energy, UU triaxial tests, Soil 2

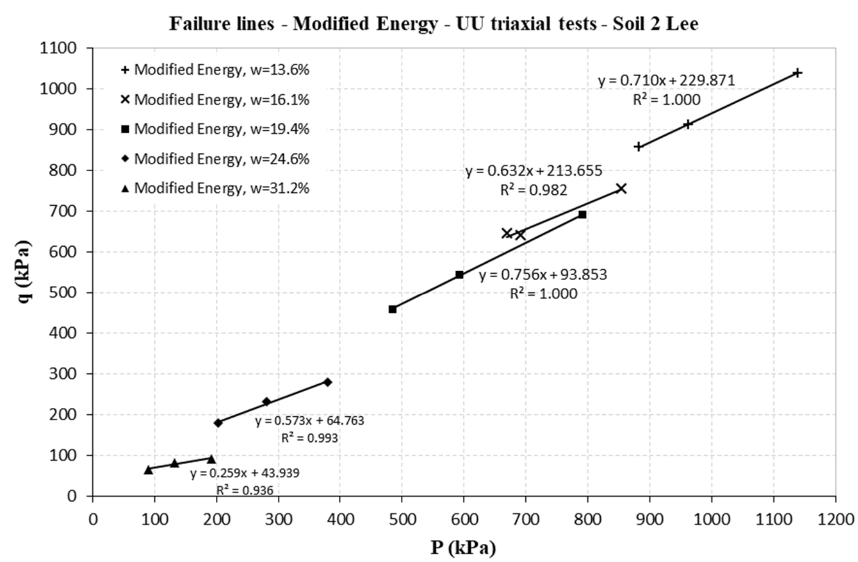

Figure B.6. Failure lines, modified energy, UU triaxial tests, Soil 2

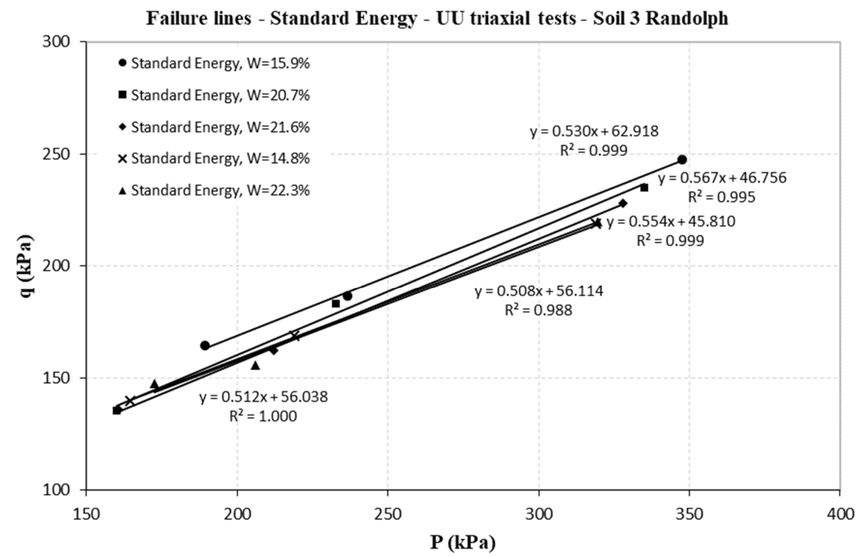

Figure B.7. Failure lines, standard energy, UU triaxial tests, Soil 3

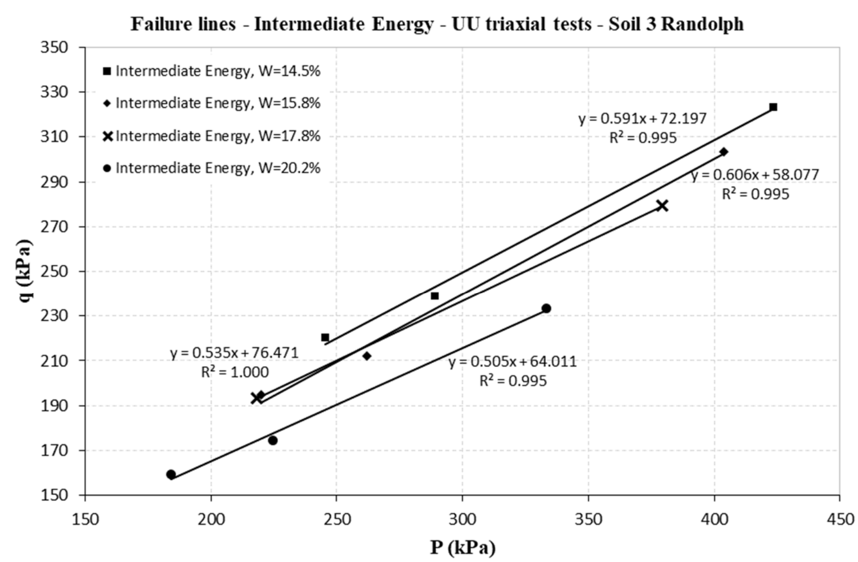

Figure B.8. Failure lines, intermediate energy, UU triaxial tests, Soil 3

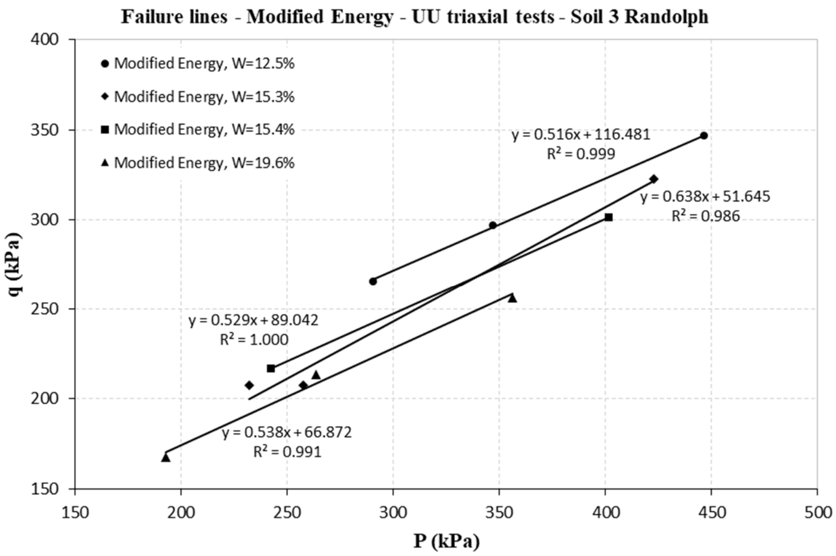

Figure B.9. Failure lines, modified energy, UU triaxial tests, Soil 3

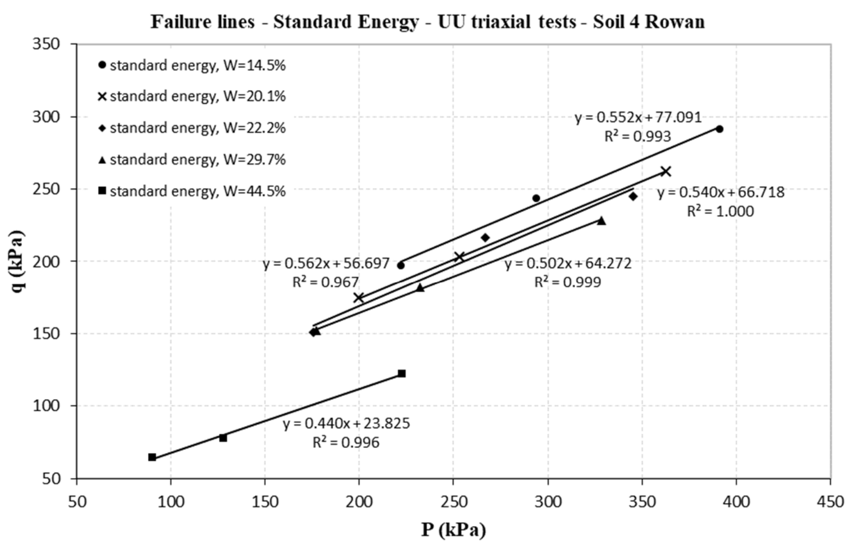

Figure B.10. Failure lines, standard energy, UU triaxial tests, Soil 4

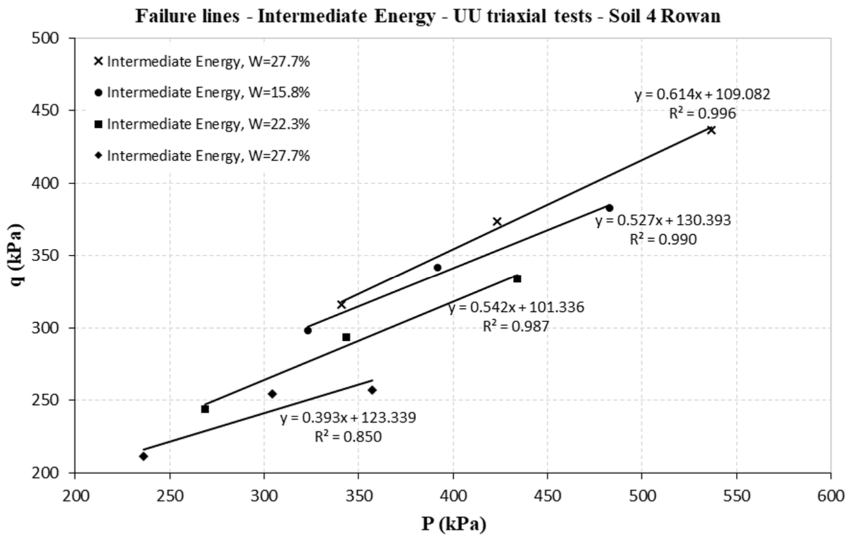

Figure B.11. Failure lines, intermediate energy, UU triaxial tests, Soil 4

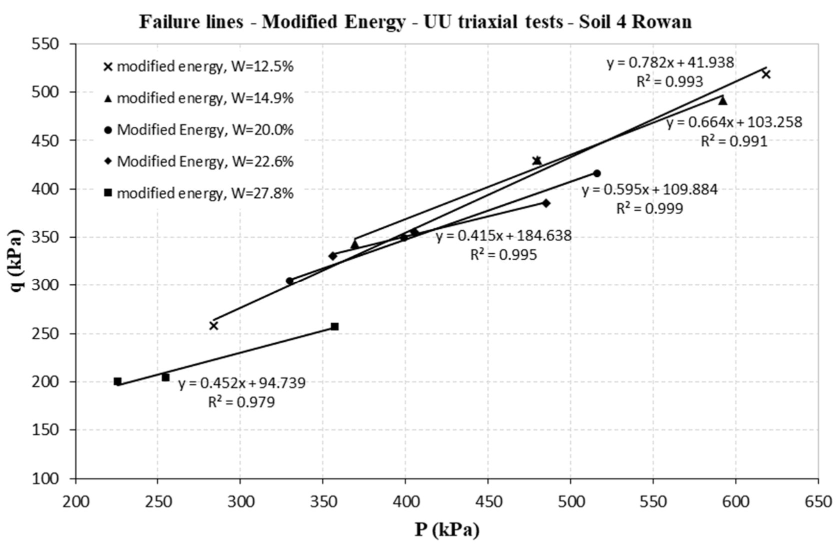

Figure B.12. Failure lines, modified energy, UU triaxial tests, Soil 4

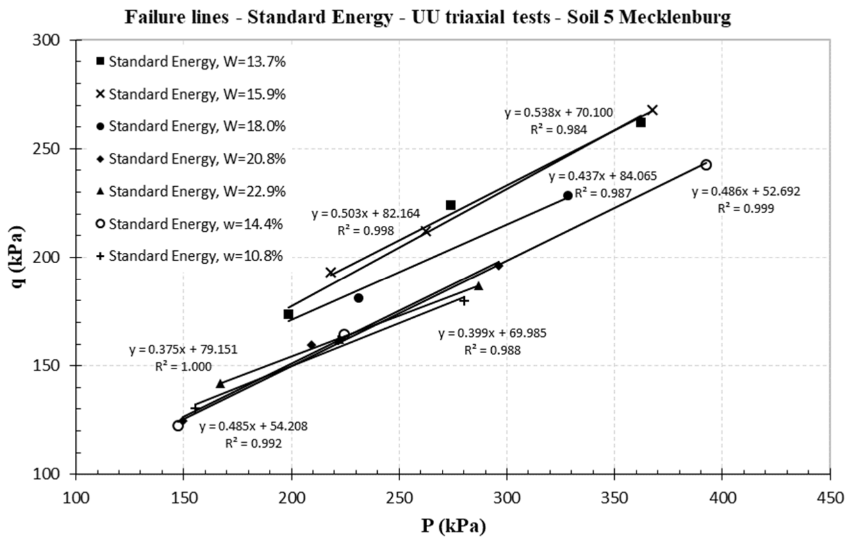

Figure B.13. Failure lines, standard energy, UU triaxial tests, Soil 5

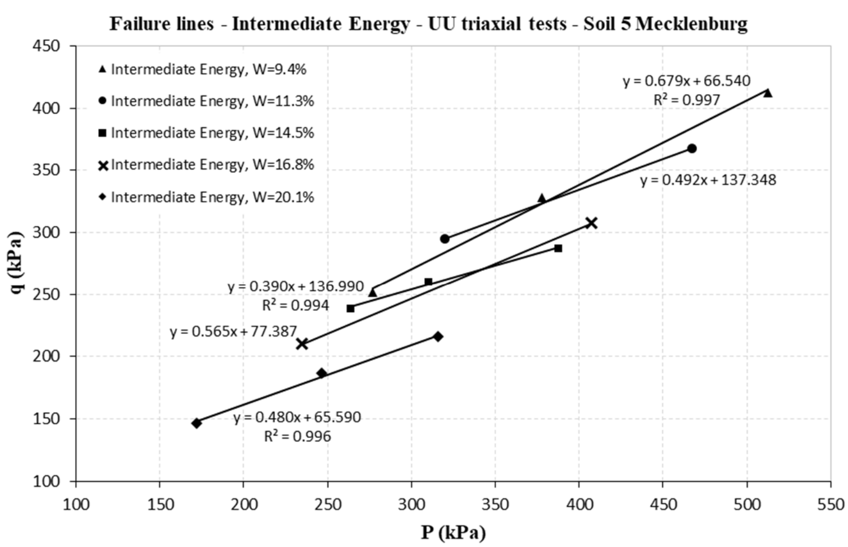

Figure B.14. Failure lines, intermediate energy, UU triaxial tests, Soil 5

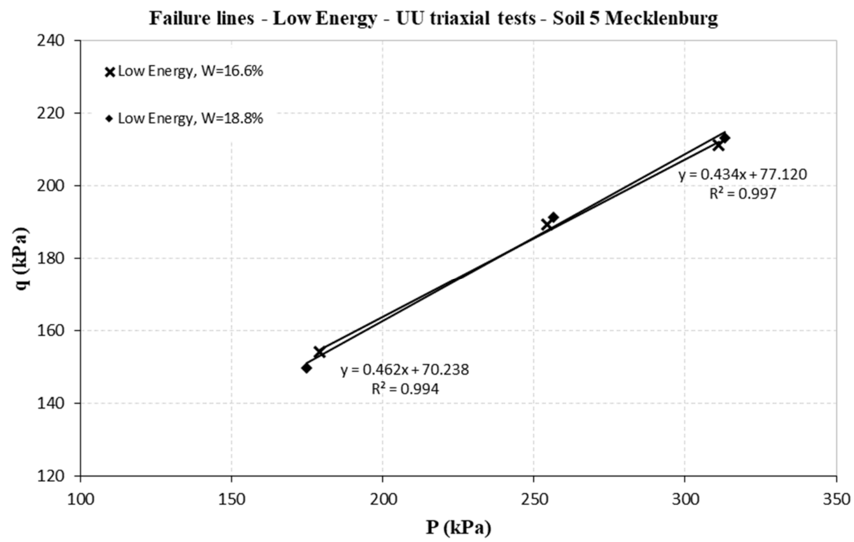

Figure B.15. Failure lines, low energy, UU triaxial tests, Soil 5

APPENDIX C: Failure Lines for Consolidated-Undrained Triaxial Tests

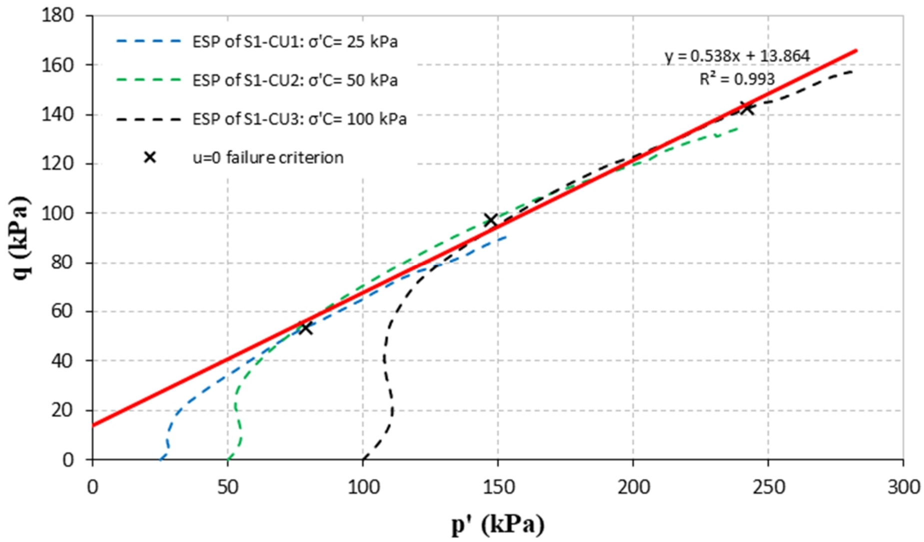

Figure C.1. Effective stress paths and failure line for CU tests on Soil 1 - samples compacted at standard energy

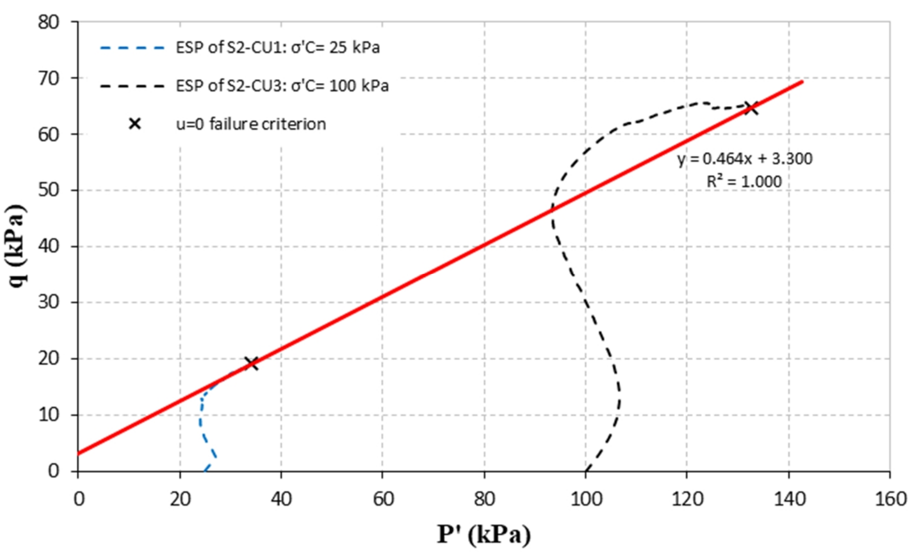

Figure C.2. Effective stress path and failure line for CU tests on Soil 2 - samples compacted at standard energy

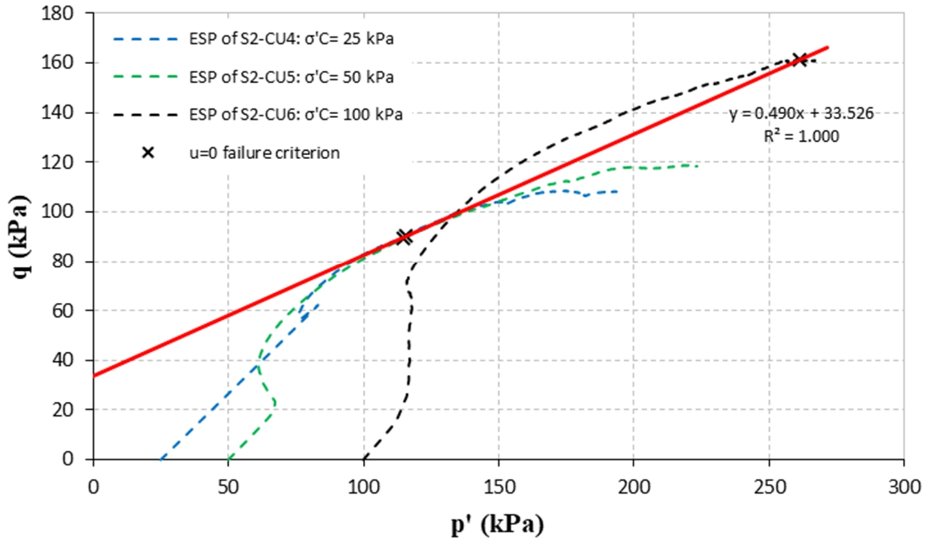

Figure C.3. Effective stress path and failure line for CU tests on Soil 2 - samples compacted at intermediate energy

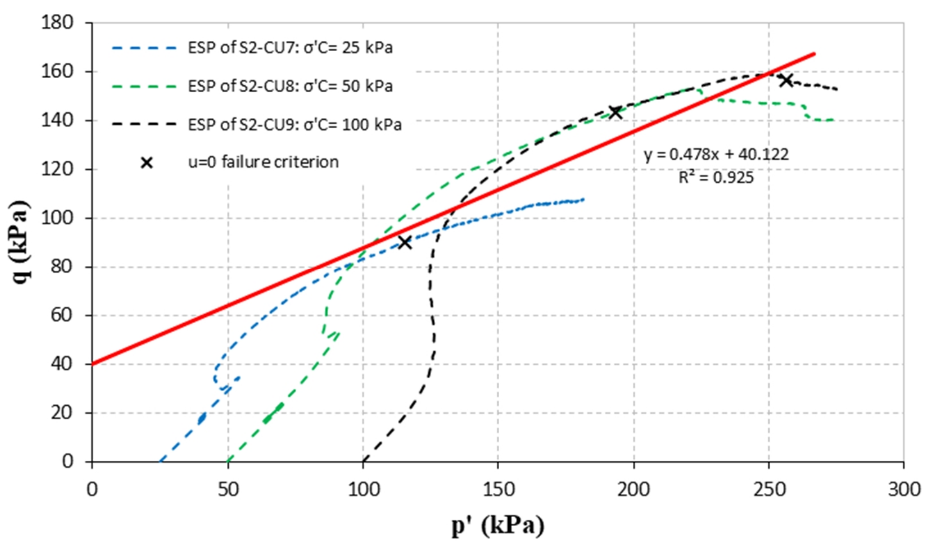

Figure C.4. Effective stress path and failure line for CU tests on Soil 2 - samples compacted at modified energy

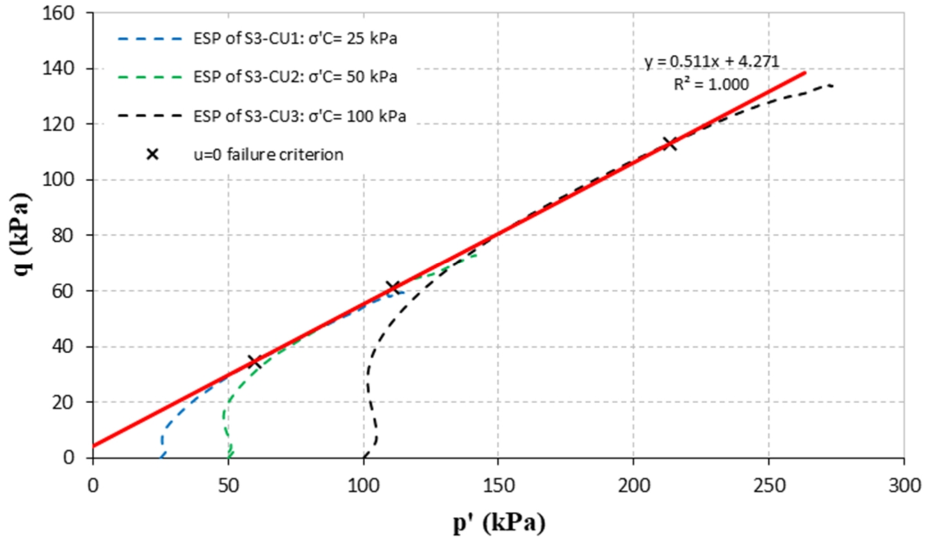

Figure C.5. Effective stress path and failure line for CU tests on Soil 3 - samples compacted at standard energy

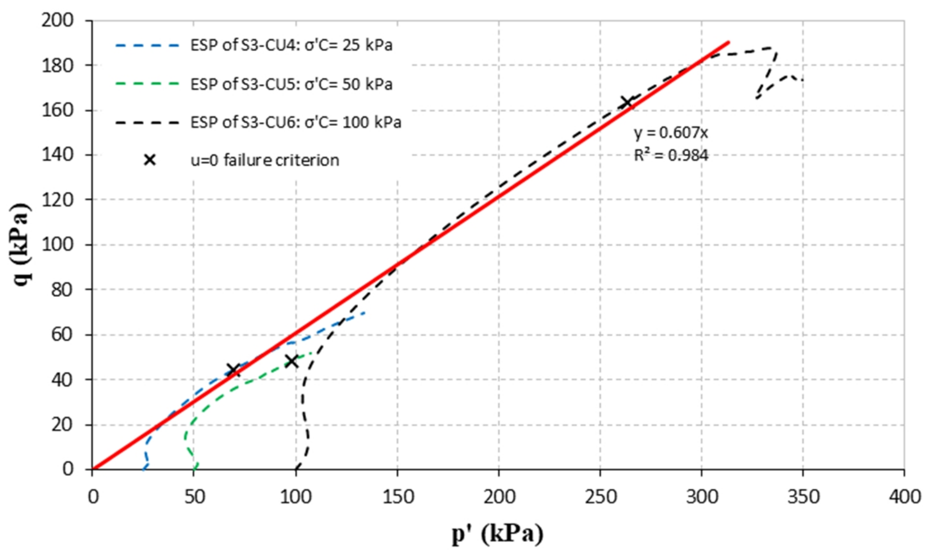

Figure C.6. Effective stress path and failure line for CU tests on Soil 3 - samples compacted at intermediate energy

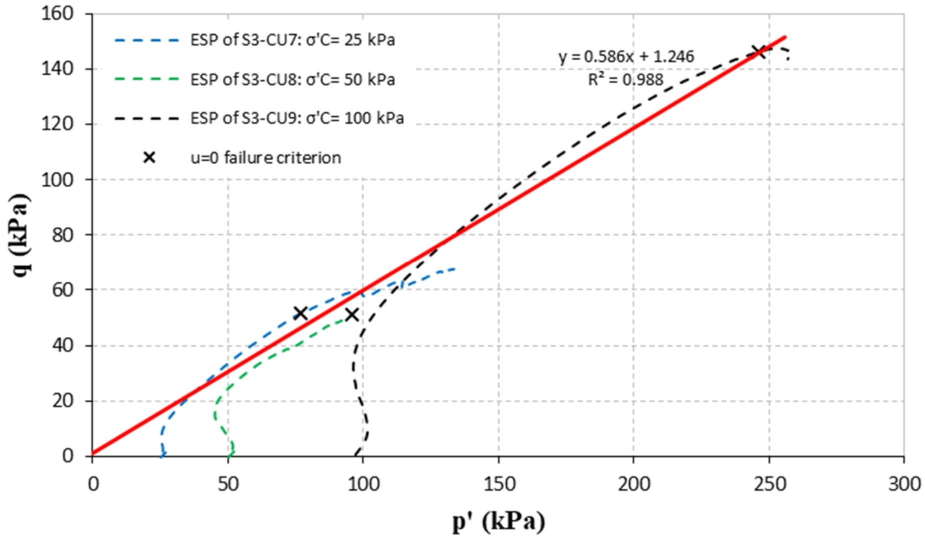

Figure C.7. Effective stress path and failure line for CU tests on Soil 3 - samples compacted at modified energy

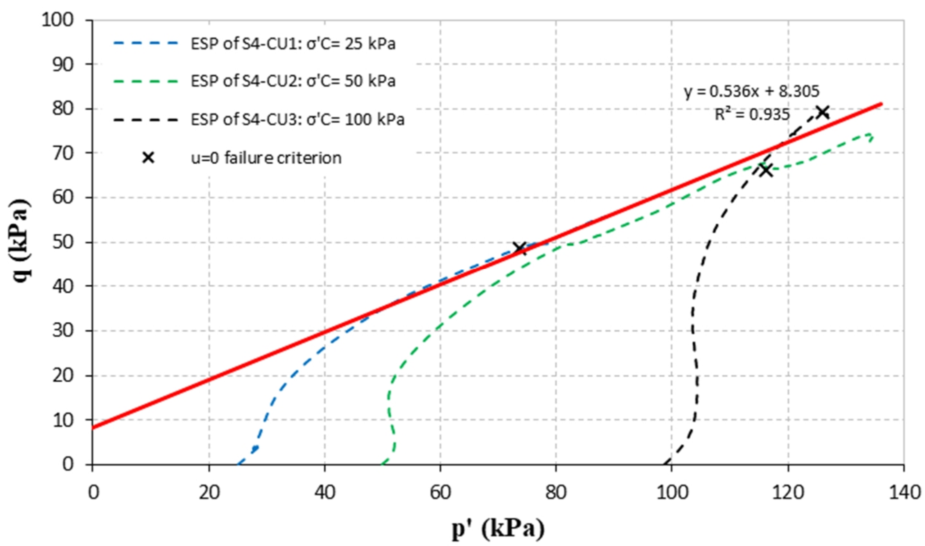

Figure C.8. Effective stress path and failure line for CU tests on Soil 4 - samples compacted at standard energy

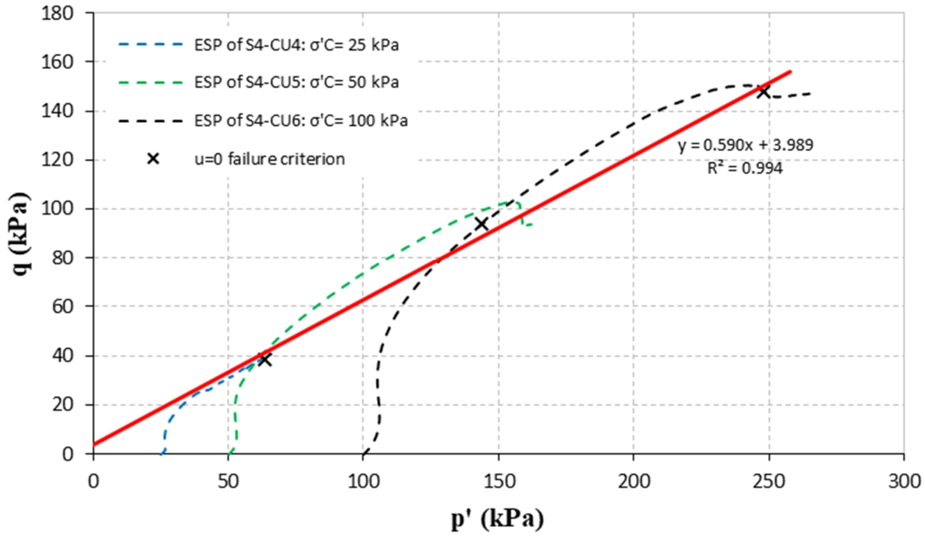

Figure C.9. Effective stress path and failure line for CU tests on Soil 4 - samples compacted at intermediate energy

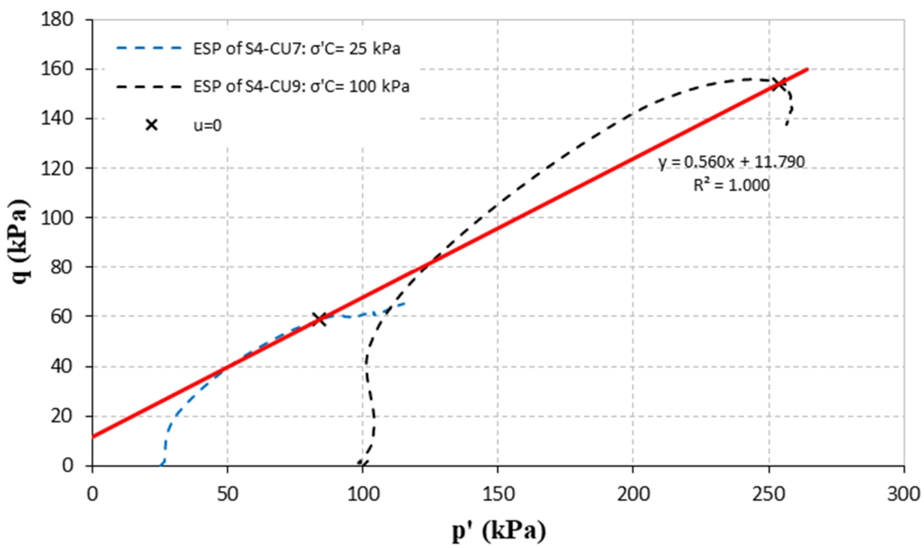

Figure C.10. Effective stress path and failure line for CU tests on Soil 4 - samples compacted at modified energy

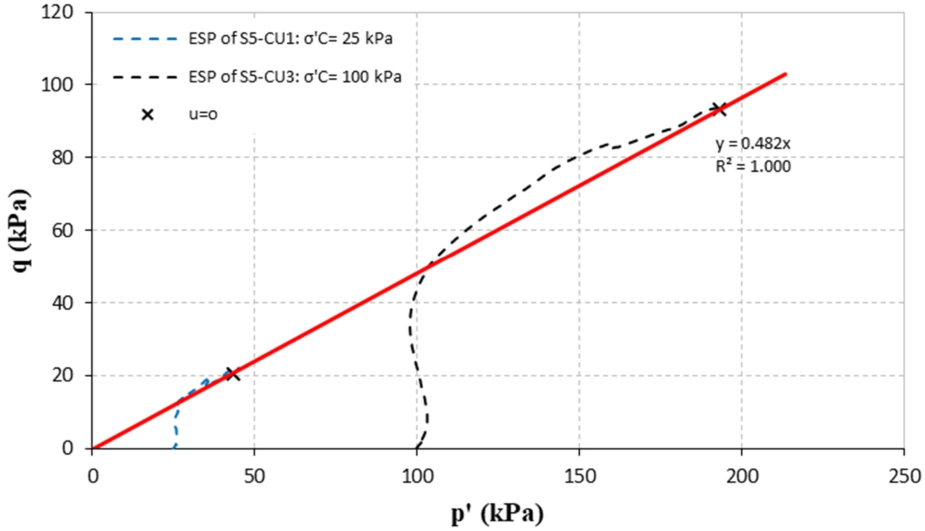

Figure C.11. Effective stress path and failure line for CU tests on Soil 5 - samples compacted at standard energy

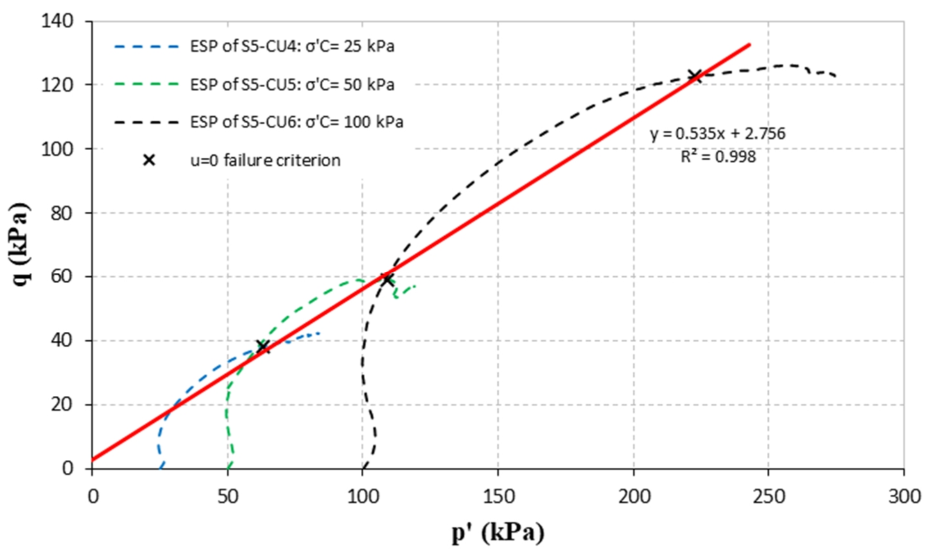

Figure C.12. Effective stress path and failure line for CU tests on Soil 5 - samples compacted at intermediate energy

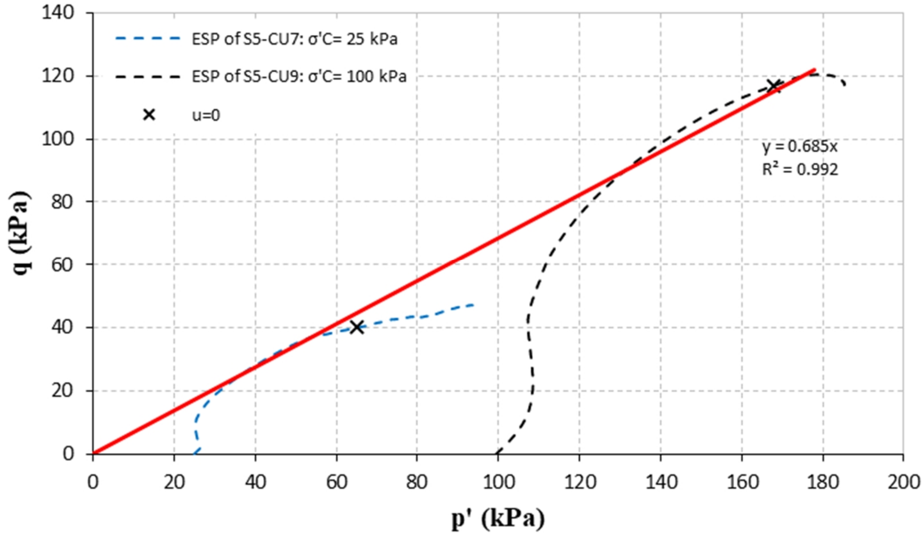

Figure C.13. Effective stress path and failure line for CU tests on Soil 5 - samples compacted at modified energy

APPENDIX D: Calibration of Oedometers

It is traditionally accepted that the load factor for the oedometers is equal to 10, meaning that the force applied to the specimen is 10 times higher than the dead weights placed on the dead weight stand. However, this assumption is investigated in this section and results are discussed. Figure D.1. shows a typical conventional consolidation device which is also called oedometer in the geotechnical jargon.

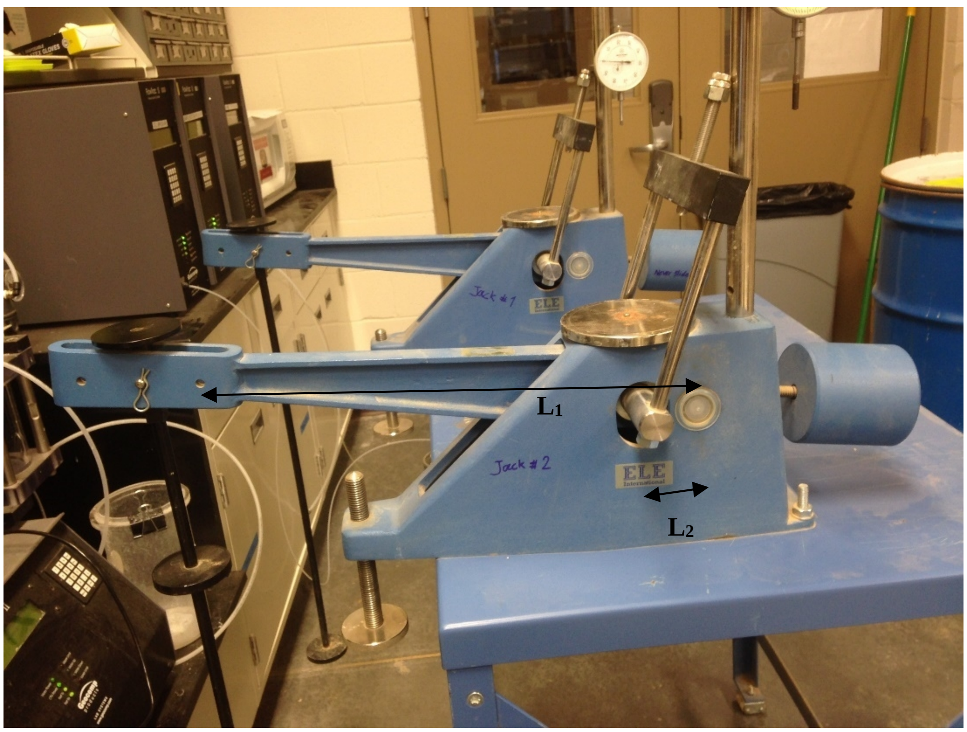

Figure D.1. Conventional consolidation device

It is noted that the calibration process presented here is done while the dead weight stand was placed in the second hole of the arm. In addition, during the process of calibration, oedometer arm was checked to be horizontal by means of a level (spirit level). The basis for the calibration process is that we assumed at horizontal position the front moments are being balanced by rear moments. Front moments are coming from the weight of the front part of oedometer arm, the weight of dead weight stand, and the weight of the loading frame. And the rear moments result from the weight of counterweight.

It should be noted that the ratios of L_1/L_2 was measured and are reported as 9 (=18”/2”), 10 (=20”/2”) and 11 (=22”/2”) respectively for the three holes from right to left. L_1 and L_2 are moment arms which are shown in Figure D.1. However, given that for the calibration purpose the stand was places in the second hole, we expect the load factor to be very close to 10.

Results of the calibration process are presented in Figure D.2 and Figure D.3. Applied load under the loading frame was measured using a load cell. As it can be seen from these figures, load factors are 9.977 and 9.923 for oedometer #1 and oedometer #2, respectively. However, it is noted that these factors are close enough to the factory default number of 10 which is conventionally used for the second hole of arm.

In the calculation process, the load that was used as applied load on the soil sample is calculated from the regression line shown in these two figures. For example, for oedometer #1 the applied load would be equal to 9.977*dead weight - 0.204 in kg unit.

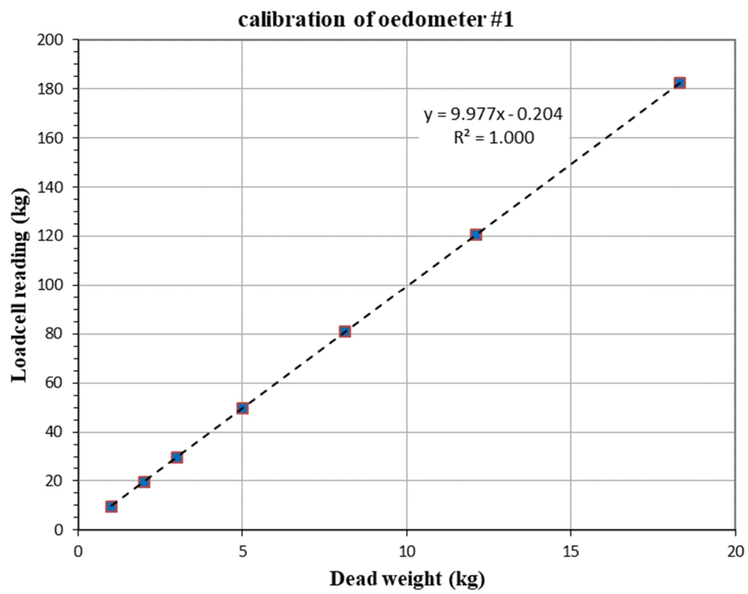

Figure D.2. Calibration graph for oedometer #1

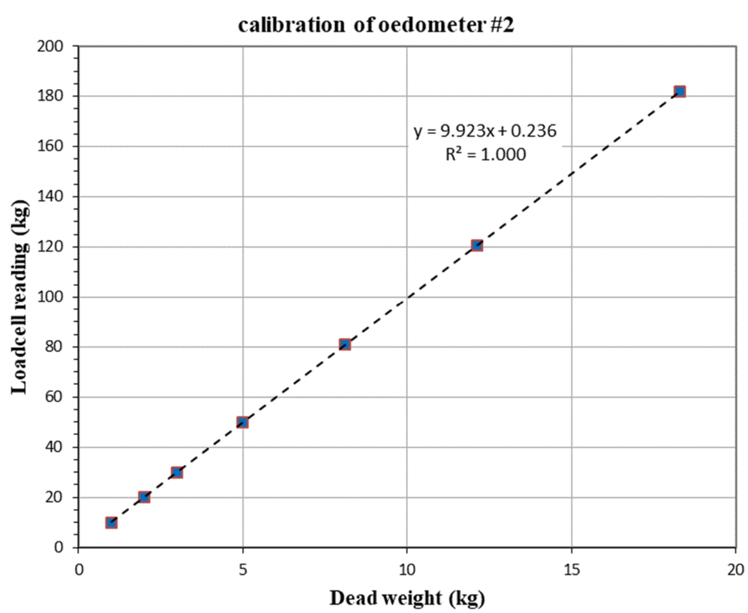

Figure D.3. Calibration graph for oedometer #2

APPENDIX E: Tables for Factor of Safety Against Instability Based on Effective Stress Analysis (CU Triaxial Parameters)

E1: FS Tables for Test Soil 1 – Effective Stress Slope Stability Analysis (CU Triaxial Parameters)

Table E.1. Factor of safety for Test Soil 1 based on ESA parameters

Tests ID	w (%)	$g_d (kN/m^3)$	S (%)	f' (deg)	C' (kPa)	H (m)	slope	Minimum FS	Mode of failure
S1-CU1 S1-CU2 S1-CU3	22.5	16.7	≈ 100	33	16	12.2	1H:1V	1.3	non-shallow
							2H:1V	2.1	non-shallow
							3H:1V	2.8	non-shallow
							4H:1V	3.6	non-shallow
						9.1	1H:1V	1.4	non-shallow
							2H:1V	2.2	non-shallow
							3H:1V	3.0	non-shallow
							4H:1V	3.7	non-shallow
						6.1	1H:1V	1.6	non-shallow
							2H:1V	2.4	non-shallow
							3H:1V	3.2	non-shallow
							4H:1V	3.9	non-shallow
						3.0	1H:1V	1.7	shallow
							2H:1V	2.6	shallow
							3H:1V	3.5	non-shallow
							4H:1V	3.9	local

E2: FS Tables for Test Soil 2 – Effective Stress Slope Stability Analysis (CU Triaxial Parameters)

Table E.2. Factor of safety for Test Soil 2 based on ESA parameters

Tests ID	w (%)	$g_d (kN/m^3)$	S (%)	f' (deg)	C' (kPa)	H (m)	slope	Minimum FS	Mode of failure
S2-CU1 S2-CU3	35.2	13.8	≈ 100	28	4	12.2	1H:1V	0.8	non-shallow
							2H:1V	1.3	non-shallow
							3H:1V	1.9	non-shallow
							4H:1V	2.4	non-shallow
						9.1	1H:1V	0.8	shallow
							2H:1V	1.4	shallow
							3H:1V	1.9	local
							4H:1V	2.3	local
						6.1	1H:1V	0.8	shallow
							2H:1V	1.4	shallow
							3H:1V	1.8	local
							4H:1V	2.1	local
						3.0	1H:1V	0.8	shallow
							2H:1V	1.4	shallow
							3H:1V	1.7	local
							4H:1V	1.9	local

Table E.2. Factor of safety for Test Soil 2 based on ESA parameters (continued)

Tests ID	w (%)	$g_d (kN/m^3)$	S (%)	f' (deg)	C' (kPa)	H (m)	slope	Minimum FS	Mode of failure
S2-CU4 S2-CU5 S2-CU6	21.6	17.1	≈ 100	29	38	12.2	1H:1V	1.7	non-shallow
							2H:1V	2.5	non-shallow
							3H:1V	3.3	non-shallow
							4H:1V	4.1	non-shallow
						9.1	1H:1V	2.0	non-shallow
							2H:1V	2.8	non-shallow
							3H:1V	3.7	non-shallow
							4H:1V	4.5	non-shallow
						6.1	1H:1V	2.3	non-shallow
							2H:1V	3.3	non-shallow
							3H:1V	4.2	non-shallow
							4H:1V	5.0	non-shallow
						3.0	1H:1V	3.0	non-shallow
							2H:1V	4.1	non-shallow
							3H:1V	5.1	non-shallow
							4H:1V	5.9	non-shallow

Table E.2. Factor of safety for Test Soil 2 based on ESA parameters (continued)

Tests ID	w (%)	$g_d (kN/m^3)$	S (%)	f' (deg)	C' (kPa)	H (m)	slope	Minimum FS	Mode of failure
S2-CU7 S2-CU8 S2-CU9	20.9	17.3	≈ 100	29	46	12.2	1H:1V	1.9	non-shallow
							2H:1V	2.8	non-shallow
							3H:1V	3.6	non-shallow
							4H:1V	4.4	non-shallow
						9.1	1H:1V	2.2	non-shallow
							2H:1V	3.1	non-shallow
							3H:1V	4.0	non-shallow
							4H:1V	4.9	non-shallow
						6.1	1H:1V	2.6	non-shallow
							2H:1V	3.6	non-shallow
							3H:1V	4.6	non-shallow
							4H:1V	5.6	non-shallow
						3.0	1H:1V	3.4	shallow
							2H:1V	4.7	shallow
							3H:1V	5.7	non-shallow
							4H:1V	6.7	local

E3: FS Tables for Test Soil 3 – Effective Stress Slope Stability Analysis (CU Triaxial Parameters)

Table E.3. Factor of safety for Test Soil 3 based on ESA parameters

Tests ID	w (%)	$g_d (kN/m^3)$	S (%)	f' (deg)	C' (kPa)	H (m)	slope	Minimum FS	Mode of failure
S3-CU1 S3-CU2 S3-CU3	34.7	13.7	≈ 100	31	5	12.2	1H:1V	0.9	non-shallow
							2H:1V	1.5	non-shallow
							3H:1V	2.2	non-shallow
							4H:1V	2.8	non-shallow
						9.1	1H:1V	1.0	non-shallow
							2H:1V	1.6	non-shallow
							3H:1V	2.2	non-shallow
							4H:1V	2.7	local
						6.1	1H:1V	1.0	shallow
							2H:1V	1.6	shallow
							3H:1V	2.1	local
							4H:1V	2.5	local
						3.0	1H:1V	1.0	shallow
							2H:1V	1.6	shallow
							3H:1V	2.0	local
							4H:1V	2.2	local

Table E.3. Factor of safety for Test Soil 3 based on ESA parameters (continued)

Tests ID	w (%)	$g_d (kN/m^3)$	S (%)	f' (deg)	C' (kPa)	H (m)	slope	Minimum FS	Mode of failure
S3-CU4 S3-CU5 S3-CU6	29.7	14.7	≈ 100	37	0	12.2	1H:1V	0.7	local
							2H:1V	1.4	local
							3H:1V	2.1	local
							4H:1V	2.7	local
						9.1	1H:1V	0.7	local
							2H:1V	1.4	local
							3H:1V	2.0	local
							4H:1V	2.6	local
						6.1	1H:1V	0.7	local
							2H:1V	1.3	local
							3H:1V	1.8	local
							4H:1V	2.2	local
						3.0	1H:1V	0.6	local
							2H:1V	1.1	local
							3H:1V	1.5	local
							4H:1V	1.8	local

Table E.3. Factor of safety for Test Soil 3 based on ESA parameters (continued)

Tests ID	w (%)	$g_d (kN/m^3)$	S (%)	f' (deg)	C' (kPa)	H (m)	slope	Minimum FS	Mode of failure
S3-CU7 S3-CU8 S3-CU9	28.9	14.9	≈ 100	36	2	12.2	1H:1V	0.8	shallow
							2H:1V	1.6	shallow
							3H:1V	2.3	local
							4H:1V	2.9	local
						9.1	1H:1V	0.8	shallow
							2H:1V	1.6	shallow
							3H:1V	2.2	local
							4H:1V	2.7	local
						6.1	1H:1V	0.8	shallow
							2H:1V	1.6	local
							3H:1V	2.0	local
							4H:1V	2.5	local
						3.0	1H:1V	0.8	shallow
							2H:1V	1.4	local
							3H:1V	1.8	local
							4H:1V	2.0	local

E4: FS Tables for Test Soil 4 – Effective Stress Slope Stability Analysis (CU Triaxial Parameters)

Table E.4. Factor of safety for Test Soil 4 based on ESA parameters

Tests ID	w (%)	$g_d (kN/m^3)$	S (%)	f' (deg)	C' (kPa)	H (m)	slope	Minimum FS	Mode of failure
S4-CU1 S4-CU2 S4-CU3	46.3	11.9	≈ 100	32	10	12.2	1H:1V	1.1	non-shallow
							2H:1V	1.8	non-shallow
							3H:1V	2.5	non-shallow
							4H:1V	3.2	non-shallow
						9.1	1H:1V	1.2	non-shallow
							2H:1V	1.9	non-shallow
							3H:1V	2.6	non-shallow
							4H:1V	3.3	non-shallow
						6.1	1H:1V	1.3	non-shallow
							2H:1V	2.1	non-shallow
							3H:1V	2.7	non-shallow
							4H:1V	3.2	local
						3.0	1H:1V	1.4	shallow
							2H:1V	2.2	shallow
							3H:1V	2.8	local
							4H:1V	3.0	local

Table E.4. Factor of safety for Test Soil 4 based on ESA parameters (continued)

Tests ID	w (%)	$g_d (kN/m^3)$	S (%)	f' (deg)	C' (kPa)	H (m)	slope	Minimum FS	Mode of failure
S4-CU4 S4-CU5 S4-CU6	35.8	13.6	≈ 100	36	5	12.2	1H:1V	1.1	non-shallow
							2H:1V	1.8	non-shallow
							3H:1V	2.6	non-shallow
							4H:1V	3.2	local
						9.1	1H:1V	1.1	shallow
							2H:1V	1.9	non-shallow
							3H:1V	2.6	local
							4H:1V	3.1	local
						6.1	1H:1V	1.1	shallow
							2H:1V	1.9	shallow
							3H:1V	2.4	local
							4H:1V	2.8	local
						3.0	1H:1V	1.1	shallow
							2H:1V	1.9	shallow
							3H:1V	2.2	local
							4H:1V	2.5	local

Table E.4. Factor of safety for Test Soil 4 based on ESA parameters (continued)

Tests ID	w (%)	$g_d (kN/m^3)$	S (%)	f' (deg)	C' (kPa)	H (m)	slope	Minimum FS	Mode of failure
S4-CU7 S4-CU9	34.2	13.9	≈ 100	34	14	12.2	1H:1V	1.3	non-shallow
							2H:1V	2.1	non-shallow
							3H:1V	2.9	non-shallow
							4H:1V	3.6	non-shallow
						9.1	1H:1V	1.4	non-shallow
							2H:1V	2.2	non-shallow
							3H:1V	3.0	non-shallow
							4H:1V	3.8	non-shallow
						6.1	1H:1V	1.6	non-shallow
							2H:1V	2.4	non-shallow
							3H:1V	3.2	non-shallow
							4H:1V	3.9	local
						3.0	1H:1V	1.7	shallow
							2H:1V	2.6	shallow
							3H:1V	3.4	non-shallow
							4H:1V	3.7	local

E5: FS Tables for Test Soil 5 – Effective Stress Slope Stability Analysis (CU Triaxial Parameters)

Table E.5. Factor of safety for Test Soil 5 based on ESA parameters

Tests ID	w (%)	$g_d (kN/m^3)$	S (%)	f' (deg)	C' (kPa)	H (m)	slope	Minimum FS	Mode of failure
S5-CU1 S5-CU3	36.4	13.6	≈ 100	29	0	12.2	1H:1V	0.5	local
							2H:1V	1.1	local
							3H:1V	1.5	local
							4H:1V	2.0	local
						9.1	1H:1V	0.5	local
							2H:1V	1.0	local
							3H:1V	1.5	local
							4H:1V	1.9	local
						6.1	1H:1V	0.5	local
							2H:1V	0.9	local
							3H:1V	1.3	local
							4H:1V	1.6	local
						3.0	1H:1V	0.5	local
							2H:1V	0.8	local
							3H:1V	1.1	local
							4H:1V	1.3	local

Table E.5. Factor of safety for Test Soil 5 based on ESA parameters (continued)

Tests ID	w (%)	$g_d (kN/m^3)$	S (%)	f' (deg)	C' (kPa)	H (m)	slope	Minimum FS	Mode of failure
S5-CU4 S5-CU5 S5-CU6	32.8	14.3	≈ 100	32	3	12.2	1H:1V	0.8	non-shallow
							2H:1V	1.5	non-shallow
							3H:1V	2.1	local
							4H:1V	2.6	local
						9.1	1H:1V	0.9	shallow
							2H:1V	1.5	non-shallow
							3H:1V	2.0	local
							4H:1V	2.5	local
						6.1	1H:1V	0.9	shallow
							2H:1V	1.5	local
							3H:1V	1.9	local
							4H:1V	2.3	local
						3.0	1H:1V	0.9	shallow
							2H:1V	1.5	local
							3H:1V	1.7	local
							4H:1V	2.0	local

Table E.5. Factor of safety for Test Soil 5 based on ESA parameters (continued)

Tests ID	w (%)	$g_d (kN/m^3)$	S (%)	f' (deg)	C' (kPa)	H (m)	slope	Minimum FS	Mode of failure
S5-CU7 S5-CU9	31.8	14.5	≈ 100	43	0	12.2	1H:1V	0.9	local
							2H:1V	1.8	local
							3H:1V	2.6	local
							4H:1V	3.4	local
						9.1	1H:1V	0.9	local
							2H:1V	1.7	local
							3H:1V	2.5	local
							4H:1V	3.2	local
						6.1	1H:1V	0.9	local
							2H:1V	1.6	local
							3H:1V	2.2	local
							4H:1V	2.8	local
						3.0	1H:1V	0.8	local
							2H:1V	1.4	local
							3H:1V	1.8	local
							4H:1V	2.2	local

APPENDIX F: Deformation Tables Based on Total Stress Analysis (UU Triaxial Parameters)

F1: Deformation Tables for Test Soil 1 – Total Stress Analysis (UU Triaxial Parameters)

Table F.1. Embankment crest deformation for Test Soil 1 - TSA

Tests ID	w (%)	$g_d (kN/m^3)$	S (%)	f_{UU} (deg)	C_{UU} (kPa)	ν	E_{50} (MPa)	H (m)	slope	crest deformation (cm)
S1-UU1 S1-UU2 S1-UU3	17.4	16.5	82.3	23	75	0.3786	2.916 3.816 3.960	12.2	1H:1V	7.11
									2H:1V	6.90
									3H:1V	6.76
									4H:1V	6.78
								9.1	1H:1V	5.35
									2H:1V	5.27
									3H:1V	5.16
									4H:1V	5.15
								6.1	1H:1V	3.66
									2H:1V	3.59
									3H:1V	3.58
									4H:1V	3.56
								3.0	1H:1V	1.89
									2H:1V	1.86
									3H:1V	1.86
									4H:1V	1.86

Table F.1. Embankment crest deformation for Test Soil 1 - TSA (continued)

Tests ID	w (%)	$g_d (kN/m^3)$	S (%)	f_{UU} (deg)	C_{UU} (kPa)	ν	E_{50} (MPa)	H (m)	slope	crest deformation (cm)
S1-UU4 S1-UU5 S1-UU6	15.6	17.5	79.7	34	73	0.3056	8.934 9.267 12.348	12.2	1H:1V	3.22
									2H:1V	3.17
									3H:1V	3.15
									4H:1V	3.15
								9.1	1H:1V	2.44
									2H:1V	2.43
									3H:1V	2.42
									4H:1V	2.42
								6.1	1H:1V	1.73
									2H:1V	1.71
									3H:1V	1.71
									4H:1V	1.70
								3.0	1H:1V	0.91
									2H:1V	0.91
									3H:1V	0.90
									4H:1V	0.91

Table F.1. Embankment crest deformation for Test Soil 1 - TSA (continued)

Tests ID	w (%)	$g_d (kN/m^3)$	S (%)	f_{UU} (deg)	C_{UU} (kPa)	ν	E_{50} (MPa)	H (m)	slope	crest deformation (cm)
S1-UU7 S1-UU8 S1-UU9	13.0	17.4	65.3	39	69	0.2679	9.290 13.847 17.838	12.2	1H:1V	2.83
									2H:1V	2.70
									3H:1V	2.73
									4H:1V	2.76
								9.1	1H:1V	2.28
									2H:1V	2.28
									3H:1V	2.28
									4H:1V	2.28
								6.1	1H:1V	1.62
									2H:1V	1.62
									3H:1V	1.62
									4H:1V	1.62
								3.0	1H:1V	0.94
									2H:1V	0.94
									3H:1V	0.93
									4H:1V	0.94

Table F.1. Embankment crest deformation for Test Soil 1 - TSA (continued)

Tests ID	w (%)	$g_d (kN/m^3)$	S (%)	f_{UU} (deg)	C_{UU} (kPa)	ν	E_{50} (MPa)	H (m)	slope	crest deformation (cm)
S1-UU10 S1-UU11 S1-UU12	18.9	16.5	81.4	27	35	0.3532	1.142 2.139 2.240	12.2	1H:1V	15.22
									2H:1V	14.62
									3H:1V	14.23
									4H:1V	14.24
								9.1	1H:1V	11.91
									2H:1V	11.77
									3H:1V	11.64
									4H:1V	11.53
								6.1	1H:1V	8.43
									2H:1V	8.29
									3H:1V	8.27
									4H:1V	8.26
								3.0	1H:1V	4.76
									2H:1V	4.73
									3H:1V	4.72
									4H:1V	4.73

Table F.1. Embankment crest deformation for Test Soil 1 - TSA (continued)

Tests ID	w (%)	$g_d (kN/m^3)$	S (%)	f_{UU} (deg)	C_{UU} (kPa)	ν	E_{50} (MPa)	H (m)	slope	crest deformation (cm)
S1-UU13 S1-UU14 S1-UU15	13.2	15.9	51.6	33	53	0.3141	11.766 12.008 12.288	12.2	1H:1V	2.66
									2H:1V	2.60
									3H:1V	2.64
									4H:1V	2.64
								9.1	1H:1V	1.98
									2H:1V	1.97
									3H:1V	1.96
									4H:1V	1.96
								6.1	1H:1V	1.33
									2H:1V	1.32
									3H:1V	1.32
									4H:1V	1.32
								3.0	1H:1V	0.66
									2H:1V	0.66
									3H:1V	0.65
									4H:1V	0.66

Table F.1. Embankment crest deformation for Test Soil 1 - TSA (continued)

Tests ID	w (%)	$g_d (kN/m^3)$	S (%)	f_{UU} (deg)	C_{UU} (kPa)	ν	E_{50} (MPa)	H (m)	slope	crest deformation (cm)
S1-UU16 S1-UU17 S1-UU18	10.5	15.3	37.9	35	47	0.3022	14.539 15.559 16.231	12.2	1H:1V	2.14
									2H:1V	2.10
									3H:1V	2.13
									4H:1V	2.13
								9.1	1H:1V	1.61
									2H:1V	1.60
									3H:1V	1.60
									4H:1V	1.60
								6.1	1H:1V	1.09
									2H:1V	1.09
									3H:1V	1.09
									4H:1V	1.09
								3.0	1H:1V	0.55
									2H:1V	0.55
									3H:1V	0.55
									4H:1V	0.55

Table F.1. Embankment crest deformation for Test Soil 1 - TSA (continued)

Tests ID	w (%)	$g_d (kN/m^3)$	S (%)	f_{UU} (deg)	C_{UU} (kPa)	ν	E_{50} (MPa)	H (m)	slope	crest deformation (cm)
S1-UU19 S1-UU20 S1-UU21	9.8	16.6	42.6	34	89	0.3059	17.034 19.776 21.565	12.2	1H:1V	1.69
									2H:1V	1.70
									3H:1V	1.66
									4H:1V	1.66
								9.1	1H:1V	1.29
									2H:1V	1.29
									3H:1V	1.28
									4H:1V	1.28
								6.1	1H:1V	0.89
									2H:1V	0.89
									3H:1V	0.89
									4H:1V	0.89
								3.0	1H:1V	0.46
									2H:1V	0.46
									3H:1V	0.46
									4H:1V	0.46

Table F.1. Embankment crest deformation for Test Soil 1 - TSA (continued)

Tests ID	w (%)	$g_d (kN/m^3)$	S (%)	f_{UU} (deg)	C_{UU} (kPa)	ν	E_{50} (MPa)	H (m)	slope	crest deformation (cm)
S1-UU22 S1-UU23 S1-UU24	7.7	16.1	31.4	45	48	0.2265	14.296 19.440 22.473	12.2	1H:1V	2.33
									2H:1V	2.30
									3H:1V	2.32
									4H:1V	2.32
								9.1	1H:1V	1.83
									2H:1V	1.83
									3H:1V	1.83
									4H:1V	1.83
								6.1	1H:1V	1.32
									2H:1V	1.32
									3H:1V	1.32
									4H:1V	1.32
								3.0	1H:1V	0.72
									2H:1V	0.72
									3H:1V	0.72
									4H:1V	0.72

Table F.1. Embankment crest deformation for Test Soil 1 - TSA (continued)

Tests ID	w (%)	$g_d (kN/m^3)$	S (%)	f_{UU} (deg)	C_{UU} (kPa)	ν	E_{50} (MPa)	H (m)	slope	crest deformation (cm)
S1-UU25 S1-UU26 S1-UU27	9.3	17.5	47.0	42	152	0.2486	27.529 32.222 37.121	12.2	1H:1V	1.17
									2H:1V	1.10
									3H:1V	1.16
									4H:1V	1.17
								9.1	1H:1V	0.91
									2H:1V	0.91
									3H:1V	0.91
									4H:1V	0.91
								6.1	1H:1V	0.64
									2H:1V	0.64
									3H:1V	0.64
									4H:1V	0.64
								3.0	1H:1V	0.34
									2H:1V	0.34
									3H:1V	0.34
									4H:1V	0.34

Table F.1. Embankment crest deformation for Test Soil 1 - TSA (continued)

Tests ID	w (%)	$g_d (kN/m^3)$	S (%)	f_{UU} (deg)	C_{UU} (kPa)	ν	E_{50} (MPa)	H (m)	slope	crest deformation (cm)
S1-UU28 S1-UU29 S1-UU30	7.1	17.0	33.2	44	118	0.2339	26.436 27.388 36.450	12.2	1H:1V	1.33
									2H:1V	1.30
									3H:1V	1.33
									4H:1V	1.33
								9.1	1H:1V	1.02
									2H:1V	1.02
									3H:1V	1.02
									4H:1V	1.02
								6.1	1H:1V	0.72
									2H:1V	0.72
									3H:1V	0.72
									4H:1V	0.72
								3.0	1H:1V	0.39
									2H:1V	0.39
									3H:1V	0.39
									4H:1V	0.39

Table F.1. Embankment crest deformation for Test Soil 1 - TSA (continued)

Tests ID	w (%)	$g_d (kN/m^3)$	S (%)	f_{UU} (deg)	C_{UU} (kPa)	ν	E_{50} (MPa)	H (m)	slope	crest deformation (cm)
S1-UU31 S1-UU32 S1-UU33	12.1	18.2	68.7	34	163	0.3059	22.110 27.449 32.073	12.2	1H:1V	1.19
									2H:1V	1.17
									3H:1V	1.17
									4H:1V	1.17
								9.1	1H:1V	0.91
									2H:1V	0.91
									3H:1V	0.91
									4H:1V	0.91
								6.1	1H:1V	0.64
									2H:1V	0.64
									3H:1V	0.64
									4H:1V	0.64
								3.0	1H:1V	0.34
									2H:1V	0.34
									3H:1V	0.34
									4H:1V	0.34

Table F.1. Embankment crest deformation for Test Soil 1 - TSA (continued)

Tests ID	w (%)	$g_d (kN/m^3)$	S (%)	f_{UU} (deg)	C_{UU} (kPa)	ν	E_{50} (MPa)	H (m)	slope	crest deformation (cm)
S1-UU34 S1-UU35 S1-UU36	14.5	17.8	77.7	42	54	0.2486	7.549 9.513 16.503	12.2	1H:1V	3.73
									2H:1V	3.69
									3H:1V	3.69
									4H:1V	3.69
								9.1	1H:1V	3.12
									2H:1V	3.12
									3H:1V	3.12
									4H:1V	3.12
								6.1	1H:1V	2.36
									2H:1V	2.36
									3H:1V	2.36
									4H:1V	2.34
								3.0	1H:1V	1.41
									2H:1V	1.41
									3H:1V	1.41
									4H:1V	1.41

F2: Deformation Tables for Test Soil 2 – Total Stress Analysis (UU Triaxial Parameters)

Table F.2. Embankment crest deformation for Test Soil 2 - TSA

Tests ID	w (%)	$g_d (kN/m^3)$	S (%)	f_{UU} (deg)	C_{UU} (kPa)	ν	E_{50} (MPa)	H (m)	slope	crest deformation (cm)
S2-UU10 S2-UU11 S2-UU12	30.2	14.5	95.7	18	62	0.4086	2.010 2.868 2.979	12.2	1H:1V	8.33
									2H:1V	7.92
									3H:1V	7.78
									4H:1V	7.74
								9.1	1H:1V	6.20
									2H:1V	6.04
									3H:1V	5.95
									4H:1V	5.92
								6.1	1H:1V	4.29
									2H:1V	4.15
									3H:1V	4.12
									4H:1V	4.06
								3.0	1H:1V	2.21
									2H:1V	2.19
									3H:1V	2.15
									4H:1V	2.15

Table F.2. Embankment crest deformation for Test Soil 2 - TSA (continued)

Tests ID	w (%)	$g_d (kN/m^3)$	S (%)	f_{UU} (deg)	C_{UU} (kPa)	ν	E_{50} (MPa)	H (m)	slope	crest deformation (cm)
S2-UU16 S2-UU17 S2-UU18	25.1	15.5	91.6	29	98	0.3400	6.977 9.430 12.774	12.2	1H:1V	3.07
									2H:1V	2.93
									3H:1V	2.90
									4H:1V	2.89
								9.1	1H:1V	2.32
									2H:1V	2.30
									3H:1V	2.42
									4H:1V	2.30
								6.1	1H:1V	1.69
									2H:1V	1.68
									3H:1V	1.68
									4H:1V	1.68
								3.0	1H:1V	0.94
									2H:1V	0.93
									3H:1V	0.93
									4H:1V	0.93

Table F.2. Embankment crest deformation for Test Soil 2 - TSA (continued)

Tests ID	w (%)	$g_d (kN/m^3)$	S (%)	f_{UU} (deg)	C_{UU} (kPa)	ν	E_{50} (MPa)	H (m)	slope	crest deformation (cm)
S2-UU19 S2-UU20 S2-UU21	20.9	15.9	81.0	41	90	0.2559	22.751 22.989 23.225	12.2	1H:1V	1.57
									2H:1V	1.57
									3H:1V	1.57
									4H:1V	1.57
								9.1	1H:1V	1.16
									2H:1V	1.16
									3H:1V	1.16
									4H:1V	1.16
								6.1	1H:1V	0.78
									2H:1V	0.78
									3H:1V	0.78
									4H:1V	0.78
								3.0	1H:1V	0.39
									2H:1V	0.39
									3H:1V	0.39
									4H:1V	0.39

Table F.2. Embankment crest deformation for Test Soil 2 - TSA (continued)

Tests ID	w (%)	$g_d (kN/m^3)$	S (%)	f_{UU} (deg)	C_{UU} (kPa)	ν	E_{50} (MPa)	H (m)	slope	crest deformation (cm)
S2-UU25 S2-UU26 S2-UU27	12.5	15.4	45.0	39	89	0.2704	22.931 27.799 33.744	12.2	1H:1V	1.30
									2H:1V	1.30
									3H:1V	1.30
									4H:1V	1.30
								9.1	1H:1V	1.02
									2H:1V	1.02
									3H:1V	1.02
									4H:1V	1.02
								6.1	1H:1V	0.73
									2H:1V	0.73
									3H:1V	0.73
									4H:1V	0.73
								3.0	1H:1V	0.39
									2H:1V	0.38
									3H:1V	0.38
									4H:1V	0.38

Table F.2. Embankment crest deformation for Test Soil 2 - TSA (continued)

Tests ID	w (%)	$g_d (kN/m^3)$	S (%)	f_{UU} (deg)	C_{UU} (kPa)	ν	E_{50} (MPa)	H (m)	slope	crest deformation (cm)
S2-UU50 S2-UU51 S2-UU52	16.4	16.9	73.5	35	196	0.2989	40.535 42.094 44.409	12.2	1H:1V	0.78
									2H:1V	0.78
									3H:1V	0.78
									4H:1V	0.78
								9.1	1H:1V	0.58
									2H:1V	0.58
									3H:1V	0.58
									4H:1V	0.58
								6.1	1H:1V	0.40
									2H:1V	0.39
									3H:1V	0.39
									4H:1V	0.39
								3.0	1H:1V	0.20
									2H:1V	0.20
									3H:1V	0.20
									4H:1V	0.20

Table F.2. Embankment crest deformation for Test Soil 2 - TSA (continued)

Tests ID	w (%)	$g_d (kN/m^3)$	S (%)	f_{UU} (deg)	C_{UU} (kPa)	ν	E_{50} (MPa)	H (m)	slope	crest deformation (cm)
S2-UU28 S2-UU29 S2-UU30	15.2	17.4	73.9	51	119	0.1822	35.660 37.086 50.641	12.2	1H:1V	1.09
									2H:1V	1.09
									3H:1V	1.09
									4H:1V	1.09
								9.1	1H:1V	0.86
									2H:1V	0.86
									3H:1V	0.86
									4H:1V	0.86
								6.1	1H:1V	0.61
									2H:1V	0.61
									3H:1V	0.61
									4H:1V	0.61
								3.0	1H:1V	0.33
									2H:1V	0.33
									3H:1V	0.33
									4H:1V	0.33

Table F.2. Embankment crest deformation for Test Soil 2 - TSA (continued)

Tests ID	w (%)	$g_d (kN/m^3)$	S (%)	f_{UU} (deg)	C_{UU} (kPa)	ν	E_{50} (MPa)	H (m)	slope	crest deformation (cm)
S2-UU31 S2-UU32 S2-UU33	21.1	16.8	92.9	32	174	0.3198	13.507 15.390 17.468	12.2	1H:1V	2.01
									2H:1V	1.98
									3H:1V	1.97
									4H:1V	1.97
								9.1	1H:1V	1.53
									2H:1V	1.51
									3H:1V	1.51
									4H:1V	1.51
								6.1	1H:1V	1.05
									2H:1V	1.04
									3H:1V	1.04
									4H:1V	1.04
								3.0	1H:1V	0.55
									2H:1V	0.55
									3H:1V	0.55
									4H:1V	0.55

Table F.2. Embankment crest deformation for Test Soil 2 - TSA (continued)

Tests ID	w (%)	$g_d (kN/m^3)$	S (%)	f_{UU} (deg)	C_{UU} (kPa)	ν	E_{50} (MPa)	H (m)	slope	crest deformation (cm)
S2-UU34 S2-UU35 S2-UU36	17.3	17.5	84.8	36	254	0.2919	28.781 40.247 45.274	12.2	1H:1V	0.88
									2H:1V	0.88
									3H:1V	0.88
									4H:1V	0.88
								9.1	1H:1V	0.69
									2H:1V	0.69
									3H:1V	0.69
									4H:1V	0.69
								6.1	1H:1V	0.50
									2H:1V	0.50
									3H:1V	0.50
									4H:1V	0.50
								3.0	1H:1V	0.27
									2H:1V	0.27
									3H:1V	0.27
									4H:1V	0.27

Table F.2. Embankment crest deformation for Test Soil 2 - TSA (continued)

Tests ID	w (%)	$g_d (kN/m^3)$	S (%)	f_{UU} (deg)	C_{UU} (kPa)	ν	E_{50} (MPa)	H (m)	slope	crest deformation (cm)
S2-UU37 S2-UU38 S2-UU39	12.6	17.2	59.3	41	243	0.2559	50.072 59.010 69.549	12.2	1H:1V	0.63
									2H:1V	0.63
									3H:1V	0.63
									4H:1V	0.63
								9.1	1H:1V	0.49
									2H:1V	0.49
									3H:1V	0.49
									4H:1V	0.49
								6.1	1H:1V	0.35
									2H:1V	0.35
									3H:1V	0.35
									4H:1V	0.35
								3.0	1H:1V	0.18
									2H:1V	0.18
									3H:1V	0.18
									4H:1V	0.18

Table F.2. Embankment crest deformation for Test Soil 2 - TSA (continued)

Tests ID	w (%)	$g_d (kN/m^3)$	S (%)	f_{UU} (deg)	C_{UU} (kPa)	ν	E_{50} (MPa)	H (m)	slope	crest deformation (cm)
S2-UU4 S2-UU5 S2-UU6	24.6	15.7	92.5	35	79	0.2989	4.756 5.928 7.132	12.2	1H:1V	5.58
									2H:1V	5.56
									3H:1V	5.55
									4H:1V	5.55
								9.1	1H:1V	4.34
									2H:1V	4.33
									3H:1V	4.33
									4H:1V	4.33
								6.1	1H:1V	3.11
									2H:1V	3.10
									3H:1V	3.10
									4H:1V	3.09
								3.0	1H:1V	1.68
									2H:1V	1.68
									3H:1V	1.68
									4H:1V	1.68

Table F.2. Embankment crest deformation for Test Soil 2 - TSA (continued)

Tests ID	w (%)	$g_d (kN/m^3)$	S (%)	f_{UU} (deg)	C_{UU} (kPa)	ν	E_{50} (MPa)	H (m)	slope	crest deformation (cm)
S2-UU7 S2-UU8 S2-UU9	31.2	14.4	93.1	15	45	0.4257	1.338 1.515 1.715	12.2	1H:1V	13.50
									2H:1V	12.83
									3H:1V	12.61
									4H:1V	12.50
								9.1	1H:1V	9.84
									2H:1V	9.51
									3H:1V	9.42
									4H:1V	9.33
								6.1	1H:1V	6.60
									2H:1V	6.40
									3H:1V	6.33
									4H:1V	6.30
								3.0	1H:1V	3.33
									2H:1V	3.23
									3H:1V	3.19
									4H:1V	3.19

Table F.2. Embankment crest deformation for Test Soil 2 - TSA (continued)

Tests ID	w (%)	$g_d (kN/m^3)$	S (%)	f_{UU} (deg)	C_{UU} (kPa)	ν	E_{50} (MPa)	H (m)	slope	crest deformation (cm)
S2-UU22 S2-UU23 S2-UU24	19.4	17.2	91.7	49	143	0.1970	23.699 26.555 32.595	12.2	1H:1V	1.52
									2H:1V	1.52
									3H:1V	1.52
									4H:1V	1.52
								9.1	1H:1V	1.20
									2H:1V	1.20
									3H:1V	1.20
									4H:1V	1.20
								6.1	1H:1V	0.87
									2H:1V	0.87
									3H:1V	0.87
									4H:1V	0.87
								3.0	1H:1V	0.46
									2H:1V	0.46
									3H:1V	0.46
									4H:1V	0.46

Table F.2. Embankment crest deformation for Test Soil 2 - TSA (continued)

Tests ID	**w (%)**	$g_d (kN/m^3)$	**S (%)**	f_{UU} **(deg)**	C_{UU} **(kPa)**	**ν**	E_{50} **(MPa)**	**H (m)**	**slope**	**crest deformation (cm)**
S2-UU47 S2-UU48 S2-UU49	16.1	17.8	83.8	39	276	0.2704	34.719 38.456 51.274	12.2	1H:1V	0.87
									2H:1V	0.87
									3H:1V	0.87
									4H:1V	0.87
								9.1	1H:1V	0.67
									2H:1V	0.67
									3H:1V	0.67
									4H:1V	0.67
								6.1	1H:1V	0.48
									2H:1V	0.48
									3H:1V	0.48
									4H:1V	0.48
								3.0	1H:1V	0.26
									2H:1V	0.26
									3H:1V	0.26
									4H:1V	0.26

Table F.2. Embankment crest deformation for Test Soil 2 - TSA (continued)

Tests ID	w (%)	$g_d (kN/m^3)$	S (%)	f_{UU} (deg)	C_{UU} (kPa)	ν	E_{50} (MPa)	H (m)	slope	crest deformation (cm)
S2-UU53 S2-UU54 S2-UU55	13.6	18.4	77.4	45	326	0.2265	48.763 57.319 71.676	12.2	1H:1V	0.67
									2H:1V	0.67
									3H:1V	0.67
									4H:1V	0.67
								9.1	1H:1V	0.53
									2H:1V	0.53
									3H:1V	0.53
									4H:1V	0.53
								6.1	1H:1V	0.38
									2H:1V	0.38
									3H:1V	0.38
									4H:1V	0.38
								3.0	1H:1V	0.21
									2H:1V	0.21
									3H:1V	0.21
									4H:1V	0.21

F3: Deformation Tables for Test Soil 3 – Total Stress Analysis (UU Triaxial Parameters)

Table F.3. Embankment crest deformation for Test Soil 3 - TSA

Tests ID	w (%)	$g_d (kN/m^3)$	S (%)	f_{UU} (deg)	C_{UU} (kPa)	ν	E_{50} (MPa)	H (m)	slope	crest deformation (cm)
S3-UU1 S3-UU2 S3-UU3	20.7	15.5	78.6	35	57	0.3022	5.601 7.118 9.387	12.2	1H:1V	4.65
									2H:1V	4.50
									3H:1V	4.50
									4H:1V	4.50
								9.1	1H:1V	3.61
									2H:1V	3.59
									3H:1V	3.59
									4H:1V	3.59
								6.1	1H:1V	2.59
									2H:1V	2.58
									3H:1V	2.58
									4H:1V	2.58
								3.0	1H:1V	1.41
									2H:1V	1.41
									3H:1V	1.41
									4H:1V	1.41

Table F.3. Embankment crest deformation for Test Soil 3 - TSA (continued)

Tests ID	**w (%)**	$g_d (kN/m^3)$	**S (%)**	f_{UU} **(deg)**	C_{UU} **(kPa)**	**ν**	E_{50} **(MPa)**	**H (m)**	**slope**	**crest deformation (cm)**
S3-UU4 S3-UU5 S3-UU6	21.6	15.3	79.5	34	55	0.3084	4.844 6.113 8.535	12.2	1H:1V	5.17
									2H:1V	5.10
									3H:1V	5.09
									4H:1V	5.08
								9.1	1H:1V	4.07
									2H:1V	4.05
									3H:1V	4.05
									4H:1V	4.05
								6.1	1H:1V	2.94
									2H:1V	2.86
									3H:1V	2.86
									4H:1V	2.86
								3.0	1H:1V	1.62
									2H:1V	1.62
									3H:1V	1.62
									4H:1V	1.62

Table F.3. Embankment crest deformation for Test Soil 3 - TSA (continued)

Tests ID	w (%)	$g_d (kN/m^3)$	S (%)	f_{UU} (deg)	C_{UU} (kPa)	ν	E_{50} (MPa)	H (m)	slope	crest deformation (cm)
S3-UU7 S3-UU8 S3-UU9	22.3	15.3	82.6	31	65	0.3298	4.187 5.483 7.180	12.2	1H:1V	5.42
									2H:1V	5.34
									3H:1V	5.33
									4H:1V	5.32
								9.1	1H:1V	4.25
									2H:1V	4.19
									3H:1V	4.19
									4H:1V	4.18
								6.1	1H:1V	3.01
									2H:1V	2.99
									3H:1V	2.99
									4H:1V	2.99
								3.0	1H:1V	1.67
									2H:1V	1.66
									3H:1V	1.66
									4H:1V	1.66

Table F.3. Embankment crest deformation for Test Soil 3 - TSA (continued)

Tests ID	w (%)	$g_d (kN/m^3)$	S (%)	f_{UU} (deg)	C_{UU} (kPa)	ν	E_{50} (MPa)	H (m)	slope	crest deformation (cm)
S3-UU10 S3-UU11 S3-UU12	15.9	15.4	59.7	32	74	0.3197	7.186 8.652 11.326	12.2	1H:1V	3.54
									2H:1V	3.52
									3H:1V	3.45
									4H:1V	3.45
								9.1	1H:1V	2.76
									2H:1V	2.75
									3H:1V	2.75
									4H:1V	2.75
								6.1	1H:1V	1.94
									2H:1V	1.92
									3H:1V	1.92
									4H:1V	1.92
								3.0	1H:1V	1.05
									2H:1V	1.05
									3H:1V	1.05
									4H:1V	1.05

Table F.3. Embankment crest deformation for Test Soil 3 - TSA (continued)

Tests ID	w (%)	$g_d (kN/m^3)$	S (%)	f_{UU} (deg)	C_{UU} (kPa)	ν	E_{50} (MPa)	H (m)	slope	crest deformation (cm)
S3-UU13 S3-UU14 S3-UU15	14.8	15.2	53.5	31	65	0.3280	7.041 9.597 19.639	12.2	1H:1V	2.82
									2H:1V	2.80
									3H:1V	2.72
									4H:1V	2.72
								9.1	1H:1V	2.30
									2H:1V	2.28
									3H:1V	2.28
									4H:1V	2.28
								6.1	1H:1V	1.72
									2H:1V	1.71
									3H:1V	1.64
									4H:1V	1.64
								3.0	1H:1V	1.04
									2H:1V	1.04
									3H:1V	1.04
									4H:1V	1.04

Table F.3. Embankment crest deformation for Test Soil 3 - TSA (continued)

Tests ID	**w (%)**	$g_d\ (kN/m^3)$	**S (%)**	f_{UU} **(deg)**	C_{UU} **(kPa)**	**ν**	E_{50} **(MPa)**	**H (m)**	**slope**	**crest deformation (cm)**
S3-UU22 S3-UU23 S3-UU24	14.5	16.5	67.5	36	89	0.2903	8.210 8.947 12.162	12.2	1H:1V	3.59
									2H:1V	3.57
									3H:1V	3.57
									4H:1V	3.57
								9.1	1H:1V	2.73
									2H:1V	2.73
									3H:1V	2.72
									4H:1V	2.72
								6.1	1H:1V	1.94
									2H:1V	1.93
									3H:1V	1.93
									4H:1V	1.93
								3.0	1H:1V	1.04
									2H:1V	1.04
									3H:1V	1.04
									4H:1V	1.04

Table F.3. Embankment crest deformation for Test Soil 3 - TSA (continued)

Tests ID	w (%)	$g_d (kN/m^3)$	S (%)	f_{UU}(deg)	C_{UU} (kPa)	ν	E_{50}(MPa)	H (m)	slope	crest deformation (cm)
S3-UU25 S3-UU26 S3-UU27	15.8	16.5	69.6	37	73	0.2826	7.335 7.853 12.289	12.2	1H:1V	3.93
									2H:1V	3.92
									3H:1V	3.92
									4H:1V	3.91
								9.1	1H:1V	3.11
									2H:1V	3.07
									3H:1V	3.07
									4H:1V	3.07
								6.1	1H:1V	2.22
									2H:1V	2.22
									3H:1V	2.21
									4H:1V	2.21
								3.0	1H:1V	1.23
									2H:1V	1.23
									3H:1V	1.23
									4H:1V	1.23

Table F.3. Embankment crest deformation for Test Soil 3 - TSA (continued)

Tests ID	**w (%)**	$g_d (kN/m^3)$	**S (%)**	f_{UU} **(deg)**	C_{UU} **(kPa)**	**ν**	E_{50} **(MPa)**	**H (m)**	**slope**	**crest deformation (cm)**
S3-UU31 S3-UU33	17.8	16.3	76.5	32	91	0.3174	6.623 9.816	12.2	1H:1V	3.83
									2H:1V	3.81
									3H:1V	3.80
									4H:1V	3.80
								9.1	1H:1V	2.96
									2H:1V	2.94
									3H:1V	2.94
									4H:1V	2.94
								6.1	1H:1V	2.09
									2H:1V	2.08
									3H:1V	2.05
									4H:1V	2.05
								3.0	1H:1V	1.12
									2H:1V	1.12
									3H:1V	1.12
									4H:1V	1.12

Table F.3. Embankment crest deformation for Test Soil 3 - TSA (continued)

Tests ID	w (%)	$g_d (kN/m^3)$	S (%)	f_{UU} (deg)	C_{UU} (kPa)	ν	E_{50} (MPa)	H (m)	slope	crest deformation (cm)
S3-UU37 S3-UU38 S3-UU39	20.2	15.7	79.5	30	74	0.3311	3.044 4.081 5.062	12.2	1H:1V	7.53
									2H:1V	7.48
									3H:1V	7.29
									4H:1V	7.28
								9.1	1H:1V	5.75
									2H:1V	5.71
									3H:1V	5.66
									4H:1V	5.66
								6.1	1H:1V	4.11
									2H:1V	4.09
									3H:1V	4.06
									4H:1V	4.06
								3.0	1H:1V	2.24
									2H:1V	2.23
									3H:1V	2.23
									4H:1V	2.23

Table F.3. Embankment crest deformation for Test Soil 3 - TSA (continued)

Tests ID	w (%)	$g_d (kN/m^3)$	S (%)	f_{UU} (deg)	C_{UU} (kPa)	ν	E_{50} (MPa)	H (m)	slope	crest deformation (cm)
S3-UU16 S3-UU17 S3-UU18	12.5	16.7	57.5	31	136	0.3261	10.697 11.727 12.684	12.2	1H:1V	2.63
									2H:1V	2.60
									3H:1V	2.60
									4H:1V	2.60
								9.1	1H:1V	1.97
									2H:1V	1.96
									3H:1V	1.96
									4H:1V	1.96
								6.1	1H:1V	1.35
									2H:1V	1.34
									3H:1V	1.33
									4H:1V	1.33
								3.0	1H:1V	0.69
									2H:1V	0.68
									3H:1V	0.68
									4H:1V	0.68

Table F.3. Embankment crest deformation for Test Soil 3 - TSA (continued)

Tests ID	**w (%)**	g_d **(*kN* / *m*³)**	**S (%)**	f_{UU} **(deg)**	C_{UU} **(kPa)**	**ν**	E_{50} **(MPa)**	**H (m)**	**slope**	**crest deformation (cm)**
S3-UU19 S3-UU20 S3-UU21	15.3	16.4	66.9	40	67	0.2658	7.153 8.988 11.322	12.2	1H:1V	4.06
									2H:1V	4.05
									3H:1V	4.05
									4H:1V	4.05
								9.1	1H:1V	3.24
									2H:1V	3.23
									3H:1V	3.23
									4H:1V	3.23
								6.1	1H:1V	2.35
									2H:1V	2.29
									3H:1V	2.29
									4H:1V	2.29
								3.0	1H:1V	1.26
									2H:1V	1.26
									3H:1V	1.26
									4H:1V	1.26

Table F.3. Embankment crest deformation for Test Soil 3 - TSA (continued)

Tests ID	w (%)	$g_d (kN/m^3)$	S (%)	f_{UU} (deg)	C_{UU} (kPa)	ν	E_{50} (MPa)	H (m)	slope	crest deformation (cm)
S3-UU28 S3-UU30	15.4	16.8	71.2	32	105	0.3202	6.4821 9.0404	12.2	1H:1V	4.02
									2H:1V	4.00
									3H:1V	3.98
									4H:1V	3.98
								9.1	1H:1V	3.08
									2H:1V	3.06
									3H:1V	3.06
									4H:1V	3.06
								6.1	1H:1V	2.16
									2H:1V	2.15
									3H:1V	2.12
									4H:1V	2.12
								3.0	1H:1V	1.14
									2H:1V	1.14
									3H:1V	1.14
									4H:1V	1.14

Table F.3. Embankment crest deformation for Test Soil 3 - TSA (continued)

Tests ID	w (%)	$g_d (kN/m^3)$	S (%)	f_{UU} (deg)	C_{UU} (kPa)	ν	E_{50} (MPa)	H (m)	slope	crest deformation (cm)
S3-UU34 S3-UU35 S3-UU36	19.6	16.1	81.7	33	79	0.3160	3.073 3.962 5.021	12.2	1H:1V	7.84
									2H:1V	7.80
									3H:1V	7.79
									4H:1V	7.78
								9.1	1H:1V	6.35
									2H:1V	6.16
									3H:1V	6.09
									4H:1V	6.08
								6.1	1H:1V	4.42
									2H:1V	4.37
									3H:1V	4.32
									4H:1V	4.32
								3.0	1H:1V	2.40
									2H:1V	2.39
									3H:1V	2.39
									4H:1V	2.39

F4: Deformation Tables for Test Soil 4 – Total Stress Analysis (UU Triaxial Parameters)

Table F.4. Embankment crest deformation for Test Soil 4 - TSA

Tests ID	w (%)	$g_d (kN/m^3)$	S (%)	f_{UU} (deg)	C_{UU} (kPa)	ν	E_{50} (MPa)	H (m)	slope	crest deformation (cm)
S4-UU1 S4-UU2 S4-UU3	44.5	11.4	90.3	26	27	0.3590	1.143 1.667 2.514	12.2	1H:1V	16.54
									2H:1V	15.68
									3H:1V	15.61
									4H:1V	15.58
								9.1	1H:1V	12.68
									2H:1V	12.27
									3H:1V	12.22
									4H:1V	12.22
								6.1	1H:1V	9.19
									2H:1V	9.17
									3H:1V	9.15
									4H:1V	9.04
								3.0	1H:1V	5.15
									2H:1V	5.11
									3H:1V	5.10
									4H:1V	5.11

Table F.4. Embankment crest deformation for Test Soil 4 - TSA (continued)

Tests ID	w (%)	$g_d (kN/m^3)$	S (%)	f_{UU} (deg)	C_{UU} (kPa)	ν	E_{50} (MPa)	H (m)	slope	crest deformation (cm)
S4-UU4 S4-UU5 S4-UU6	22.2	13.1	57.6	34	69	0.3046	8.553 11.466 13.944	12.2	1H:1V	3.08
									2H:1V	3.04
									3H:1V	3.04
									4H:1V	3.04
								9.1	1H:1V	2.37
									2H:1V	2.36
									3H:1V	2.36
									4H:1V	2.36
								6.1	1H:1V	1.68
									2H:1V	1.67
									3H:1V	1.67
									4H:1V	1.67
								3.0	1H:1V	0.91
									2H:1V	0.91
									3H:1V	0.91
									4H:1V	0.91

Table F.4. Embankment crest deformation for Test Soil 4 - TSA (continued)

Tests ID	w (%)	$g_d (kN/m^3)$	S (%)	f_{UU} (deg)	C_{UU} (kPa)	ν	E_{50} (MPa)	H (m)	slope	crest deformation (cm)
S4-UU10 S4-UU11 S4-UU12	20.1	13.3	53.7	33	79	0.3151	8.333 11.786 14.513	12.2	1H:1V	2.95
									2H:1V	2.94
									3H:1V	2.93
									4H:1V	2.93
								9.1	1H:1V	2.31
									2H:1V	2.27
									3H:1V	2.27
									4H:1V	2.27
								6.1	1H:1V	1.65
									2H:1V	1.64
									3H:1V	1.63
									4H:1V	1.63
								3.0	1H:1V	0.91
									2H:1V	0.90
									3H:1V	0.90
									4H:1V	0.90

Table F.4. Embankment crest deformation for Test Soil 4 - TSA (continued)

Tests ID	**w (%)**	$g_d (kN/m^3)$	**S (%)**	f_{UU} **(deg)**	C_{UU} **(kPa)**	**ν**	E_{50} **(MPa)**	**H (m)**	**slope**	**crest deformation (cm)**
S4-UU19 S4-UU20 S4-UU21	29.7	13.3	80.2	30	74	0.3324	6.773 8.872 11.852	12.2	1H:1V	3.39
									2H:1V	3.32
									3H:1V	3.27
									4H:1V	3.27
								9.1	1H:1V	2.65
									2H:1V	2.59
									3H:1V	2.55
									4H:1V	2.55
								6.1	1H:1V	1.89
									2H:1V	1.84
									3H:1V	1.82
									4H:1V	1.82
								3.0	1H:1V	1.04
									2H:1V	1.03
									3H:1V	1.03
									4H:1V	1.03

Table F.4. Embankment crest deformation for Test Soil 4 - TSA (continued)

Tests ID	w (%)	$g_d (kN/m^3)$	S (%)	f_{UU} (deg)	C_{UU} (kPa)	ν	E_{50} (MPa)	H (m)	slope	crest deformation (cm)
S4-UU28 S4-UU29 S4-UU30	14.5	13.6	41.0	34	92	0.3094	12.448 13.614 18.113	12.2	1H:1V	2.29
									2H:1V	2.27
									3H:1V	2.27
									4H:1V	2.27
								9.1	1H:1V	1.75
									2H:1V	1.74
									3H:1V	1.74
									4H:1V	1.74
								6.1	1H:1V	1.22
									2H:1V	1.22
									3H:1V	1.22
									4H:1V	1.22
								3.0	1H:1V	0.65
									2H:1V	0.65
									3H:1V	0.65
									4H:1V	0.65

Table F.4. Embankment crest deformation for Test Soil 4 - TSA (continued)

Tests ID	w (%)	$g_d (kN/m^3)$	S (%)	f_{UU} (deg)	C_{UU} (kPa)	ν	E_{50} (MPa)	H (m)	slope	crest deformation (cm)
S4-UU13 S4-UU14 S4-UU15	22.3	14.6	73.1	33	121	0.3141	11.752 12.805 15.386	12.2	1H:1V	2.43
									2H:1V	2.42
									3H:1V	2.38
									4H:1V	2.38
								9.1	1H:1V	1.84
									2H:1V	1.83
									3H:1V	1.83
									4H:1V	1.83
								6.1	1H:1V	1.28
									2H:1V	1.27
									3H:1V	1.27
									4H:1V	1.27
								3.0	1H:1V	0.67
									2H:1V	0.66
									3H:1V	0.66
									4H:1V	0.66

Table F.4. Embankment crest deformation for Test Soil 4 - TSA (continued)

Tests ID	w (%)	$g_d (kN/m^3)$	S (%)	f_{UU} (deg)	C_{UU} (kPa)	ν	E_{50} (MPa)	H (m)	slope	crest deformation (cm)
S4-UU22 S4-UU23 S4-UU24	27.7	14.3	86.1	23	134	0.3777	5.924 6.956 7.919	12.2	1H:1V	3.72
									2H:1V	3.60
									3H:1V	3.58
									4H:1V	3.58
								9.1	1H:1V	2.78
									2H:1V	2.74
									3H:1V	2.74
									4H:1V	2.74
								6.1	1H:1V	1.91
									2H:1V	1.88
									3H:1V	1.88
									4H:1V	1.86
								3.0	1H:1V	0.98
									2H:1V	0.97
									3H:1V	0.97
									4H:1V	0.97

Table F.4. Embankment crest deformation for Test Soil 4 - TSA (continued)

Tests ID	w (%)	$g_d (kN/m^3)$	S (%)	f_{UU} (deg)	C_{UU} (kPa)	ν	E_{50} (MPa)	H (m)	slope	crest deformation (cm)
S4-UU31 S4-UU32 S4-UU33	15.8	14.9	53.7	32	153	0.3211	17.377 18.872 19.793	12.2	1H:1V	1.68
									2H:1V	1.67
									3H:1V	1.66
									4H:1V	1.66
								9.1	1H:1V	1.26
									2H:1V	1.25
									3H:1V	1.25
									4H:1V	1.25
								6.1	1H:1V	0.86
									2H:1V	0.85
									3H:1V	0.85
									4H:1V	0.85
								3.0	1H:1V	0.43
									2H:1V	0.43
									3H:1V	0.43
									4H:1V	0.43

Table F.4. Embankment crest deformation for Test Soil 4 - TSA (continued)

Tests ID	w (%)	$g_d (kN/m^3)$	S (%)	f_{UU} (deg)	C_{UU} (kPa)	ν	E_{50} (MPa)	H (m)	slope	crest deformation (cm)
S4-UU37 S4-UU38 S4-UU39	12.5	14.9	42.6	38	138	0.2785	16.877 19.181 22.201	12.2	1H:1V	1.84
									2H:1V	1.84
									3H:1V	1.83
									4H:1V	1.83
								9.1	1H:1V	1.41
									2H:1V	1.41
									3H:1V	1.41
									4H:1V	1.41
								6.1	1H:1V	0.99
									2H:1V	0.99
									3H:1V	0.99
									4H:1V	0.98
								3.0	1H:1V	0.51
									2H:1V	0.51
									3H:1V	0.51
									4H:1V	0.51

Table F.4. Embankment crest deformation for Test Soil 4 - TSA (continued)

Tests ID	w (%)	$g_d (kN/m^3)$	S (%)	f_{UU} (deg)	C_{UU} (kPa)	ν	E_{50} (MPa)	H (m)	slope	crest deformation (cm)
S4-UU7 S4-UU8 S4-UU9	20.0	15.1	70.9	37	137	0.2883	13.624 15.364 17.314	12.2	1H:1V	2.22
									2H:1V	2.21
									3H:1V	2.21
									4H:1V	2.21
								9.1	1H:1V	1.69
									2H:1V	1.68
									3H:1V	1.68
									4H:1V	1.68
								6.1	1H:1V	1.17
									2H:1V	1.17
									3H:1V	1.17
									4H:1V	1.17
								3.0	1H:1V	0.61
									2H:1V	0.61
									3H:1V	0.61
									4H:1V	0.61

Table F.4. Embankment crest deformation for Test Soil 4 - TSA (continued)

Tests ID	w (%)	$g_d (kN/m^3)$	S (%)	f_{UU} (deg)	C_{UU} (kPa)	ν	E_{50} (MPa)	H (m)	slope	crest deformation (cm)
S4-UU16 S4-UU17 S4-UU18	22.6	15.3	82.2	25	203	0.3691	10.808 12.888 13.969	12.2	1H:1V	2.11
									2H:1V	2.06
									3H:1V	2.05
									4H:1V	2.05
								9.1	1H:1V	1.58
									2H:1V	1.56
									3H:1V	1.56
									4H:1V	1.56
								6.1	1H:1V	1.09
									2H:1V	1.08
									3H:1V	1.08
									4H:1V	1.07
								3.0	1H:1V	0.56
									2H:1V	0.55
									3H:1V	0.55
									4H:1V	0.55

Table F.4. Embankment crest deformation for Test Soil 4 - TSA (continued)

Tests ID	w (%)	$g_d (kN/m^3)$	S (%)	f_{UU} (deg)	C_{UU} (kPa)	ν	E_{50} (MPa)	H (m)	slope	crest deformation (cm)
S4-UU25 S4-UU26 S4-UU27	27.8	14.4	87.4	27	106	0.3540	3.638 4.114 5.121	12.2	1H:1V	6.52
									2H:1V	6.40
									3H:1V	6.38
									4H:1V	6.38
								9.1	1H:1V	4.92
									2H:1V	4.87
									3H:1V	4.86
									4H:1V	4.86
								6.1	1H:1V	3.46
									2H:1V	3.39
									3H:1V	3.38
									4H:1V	3.38
								3.0	1H:1V	1.80
									2H:1V	1.79
									3H:1V	1.79
									4H:1V	1.79

Table F.4. Embankment crest deformation for Test Soil 4 - TSA (continued)

Tests ID	w (%)	$g_d (kN/m^3)$	S (%)	f_{UU} (deg)	C_{UU} (kPa)	ν	E_{50} (MPa)	H (m)	slope	crest deformation (cm)
S4-UU34 S4-UU35 S4-UU36	14.9	15.7	57.2	42	138	0.2515	19.875 20.985 22.335	12.2	1H:1V	1.75
									2H:1V	1.75
									3H:1V	1.75
									4H:1V	1.75
								9.1	1H:1V	1.32
									2H:1V	1.31
									3H:1V	1.31
									4H:1V	1.31
								6.1	1H:1V	0.90
									2H:1V	0.90
									3H:1V	0.90
									4H:1V	0.90
								3.0	1H:1V	0.45
									2H:1V	0.45
									3H:1V	0.45
									4H:1V	0.45

Table F.4. Embankment crest deformation for Test Soil 4 - TSA (continued)

Tests ID	w (%)	$g_d (kN/m^3)$	S (%)	f_{UU} (deg)	C_{UU} (kPa)	ν	E_{50} (MPa)	H (m)	slope	crest deformation (cm)
S4-UU40 S4-UU41 S4-UU42	12.5	15.4	45.8	51	67	0.1790	12.388 21.370 22.998	12.2	1H:1V	2.82
									2H:1V	2.82
									3H:1V	2.82
									4H:1V	2.82
								9.1	1H:1V	2.28
									2H:1V	2.28
									3H:1V	2.28
									4H:1V	2.28
								6.1	1H:1V	1.67
									2H:1V	1.67
									3H:1V	1.67
									4H:1V	1.67
								3.0	1H:1V	0.97
									2H:1V	0.97
									3H:1V	0.97
									4H:1V	0.97

F5: Deformation Tables for Test Soil 5 – Total Stress Analysis (UU Triaxial Parameters)

Table F.5. Embankment crest deformation for Test Soil 5 - TSA

Tests ID	w (%)	$g_d (kN/m^3)$	S (%)	f_{UU} (deg)	C_{UU} (kPa)	ν	E_{50} (MPa)	H (m)	slope	crest deformation (cm)
S5-UU31 S5-UU32 S5-UU33	18.8	15.5	68.3	28	79	0.3498	8.553 9.908 10.210	12.2	1H:1V	3.04
									2H:1V	2.99
									3H:1V	2.98
									4H:1V	2.98
								9.1	1H:1V	2.26
									2H:1V	2.24
									3H:1V	2.23
									4H:1V	2.23
								6.1	1H:1V	1.55
									2H:1V	1.54
									3H:1V	1.53
									4H:1V	1.53
								3.0	1H:1V	0.78
									2H:1V	0.78
									3H:1V	0.78
									4H:1V	0.78

Table F.5. Embankment crest deformation for Test Soil 5 - TSA (continued)

Tests ID	**w (%)**	$g_d(kN/m^3)$	**S (%)**	f_{UU} **(deg)**	C_{UU} **(kPa)**	**ν**	E_{50} **(MPa)**	**H (m)**	**slope**	**crest deformation (cm)**
S5-UU34 S5-UU35 S5-UU36	16.6	15.5	60.0	26	86	0.3614	8.560 9.969 10.982	12.2	1H:1V	2.84
									2H:1V	2.78
									3H:1V	2.76
									4H:1V	2.76
								9.1	1H:1V	2.13
									2H:1V	2.09
									3H:1V	2.08
									4H:1V	2.08
								6.1	1H:1V	1.46
									2H:1V	1.44
									3H:1V	1.43
									4H:1V	1.43
								3.0	1H:1V	0.75
									2H:1V	0.74
									3H:1V	0.74
									4H:1V	0.74

Table F.5. Embankment crest deformation for Test Soil 5 - TSA (continued)

Tests ID	**w (%)**	$g_d(kN/m^3)$	**S (%)**	f_{UU} **(deg)**	C_{UU} **(kPa)**	**ν**	E_{50} **(MPa)**	**H (m)**	**slope**	**crest deformation (cm)**
S5-UU1 S5-UU2 S5-UU3	18.0	15.9	69.8	26	93	0.3602	9.316 9.691 11.566	12.2	1H:1V	2.71
									2H:1V	2.64
									3H:1V	2.64
									4H:1V	2.63
								9.1	1H:1V	2.02
									2H:1V	1.99
									3H:1V	1.98
									4H:1V	1.98
								6.1	1H:1V	1.38
									2H:1V	1.36
									3H:1V	1.36
									4H:1V	1.36
								3.0	1H:1V	0.70
									2H:1V	0.70
									3H:1V	0.70
									4H:1V	0.70

Table F.5. Embankment crest deformation for Test Soil 5 - TSA (continued)

Tests ID	**w (%)**	$g_d(kN/m^3)$	**S (%)**	f_{UU} **(deg)**	C_{UU} **(kPa)**	**ν**	E_{50} **(MPa)**	**H (m)**	**slope**	**crest deformation (cm)**
S5-UU4 S5-UU5 S5-UU6	20.8	15.5	76.0	29	62	0.3399	6.089 8.112 9.580	12.2	1H:1V	3.73
									2H:1V	3.63
									3H:1V	3.62
									4H:1V	3.62
								9.1	1H:1V	2.89
									2H:1V	2.79
									3H:1V	2.79
									4H:1V	2.79
								6.1	1H:1V	2.00
									2H:1V	1.99
									3H:1V	1.98
									4H:1V	1.98
								3.0	1H:1V	1.09
									2H:1V	1.08
									3H:1V	1.08
									4H:1V	1.08

Table F.5. Embankment crest deformation for Test Soil 5 - TSA (continued)

Tests ID	w (%)	$g_d (kN/m^3)$	S (%)	f_{UU} (deg)	C_{UU} (kPa)	ν	E_{50} (MPa)	H (m)	slope	crest deformation (cm)
S5-UU7 S5-UU8 S5-UU9	15.9	15.9	61.6	30	95	0.3320	9.815 14.077 15.843	12.2	1H:1V	2.31
									2H:1V	2.26
									3H:1V	2.26
									4H:1V	2.26
								9.1	1H:1V	1.80
									2H:1V	1.75
									3H:1V	1.74
									4H:1V	1.74
								6.1	1H:1V	1.27
									2H:1V	1.24
									3H:1V	1.24
									4H:1V	1.24
								3.0	1H:1V	0.69
									2H:1V	0.68
									3H:1V	0.68
									4H:1V	0.68

Table F.5. Embankment crest deformation for Test Soil 5 - TSA (continued)

Tests ID	w (%)	$g_d (kN/m^3)$	S (%)	f_{UU} (deg)	C_{UU} (kPa)	ν	E_{50} (MPa)	H (m)	slope	crest deformation (cm)
S5-UU19 S5-UU20 S5-UU21	22.9	15.6	84.8	22	85	0.3850	4.654 6.931 7.156	12.2	1H:1V	4.03
									2H:1V	3.85
									3H:1V	3.78
									4H:1V	3.77
								9.1	1H:1V	3.04
									2H:1V	2.90
									3H:1V	2.89
									4H:1V	2.88
								6.1	1H:1V	2.11
									2H:1V	2.05
									3H:1V	2.05
									4H:1V	2.05
								3.0	1H:1V	1.12
									2H:1V	1.10
									3H:1V	1.09
									4H:1V	1.09

Table F.5. Embankment crest deformation for Test Soil 5 - TSA (continued)

Tests ID	w (%)	$g_d (kN/m^3)$	S (%)	f_{UU} (deg)	C_{UU} (kPa)	ν	E_{50} (MPa)	H (m)	slope	crest deformation (cm)
S5-UU22 S5-UU23 S5-UU24	13.7	15.8	52.0	33	83	0.3155	12.097 14.106 14.186	12.2	1H:1V	2.38
									2H:1V	2.35
									3H:1V	2.35
									4H:1V	2.35
								9.1	1H:1V	1.78
									2H:1V	1.77
									3H:1V	1.77
									4H:1V	1.77
								6.1	1H:1V	1.22
									2H:1V	1.21
									3H:1V	1.21
									4H:1V	1.21
								3.0	1H:1V	0.62
									2H:1V	0.62
									3H:1V	0.62
									4H:1V	0.62

Table F.5. Embankment crest deformation for Test Soil 5 - TSA (continued)

Tests ID	w (%)	$g_d (kN/m^3)$	S (%)	f_{UU} (deg)	C_{UU} (kPa)	ν	E_{50} (MPa)	H (m)	slope	crest deformation (cm)
S5-UU37 S5-UU38 S5-UU39	14.4	14.8	47.2	29	60	0.3395	9.438 10.357 12.200	12.2	1H:1V	2.89
									2H:1V	2.85
									3H:1V	2.83
									4H:1V	2.82
								9.1	1H:1V	2.16
									2H:1V	2.14
									3H:1V	2.13
									4H:1V	2.12
								6.1	1H:1V	1.48
									2H:1V	1.46
									3H:1V	1.46
									4H:1V	1.46
								3.0	1H:1V	0.75
									2H:1V	0.75
									3H:1V	0.75
									4H:1V	0.75

Table F.5. Embankment crest deformation for Test Soil 5 - TSA (continued)

Tests ID	w (%)	$g_d (kN/m^3)$	S (%)	f_{UU} (deg)	C_{UU} (kPa)	ν	E_{50} (MPa)	H (m)	slope	crest deformation (cm)
S5-UU40 S5-UU41 S5-UU42	10.8	14.4	33.4	24	76	0.3754	10.308 11.942 13.011	12.2	1H:1V	2.27
									2H:1V	2.22
									3H:1V	2.21
									4H:1V	2.20
								9.1	1H:1V	1.68
									2H:1V	1.67
									3H:1V	1.66
									4H:1V	1.65
								6.1	1H:1V	1.15
									2H:1V	1.13
									3H:1V	1.13
									4H:1V	1.13
								3.0	1H:1V	0.58
									2H:1V	0.58
									3H:1V	0.58
									4H:1V	0.58

Table F.5. Embankment crest deformation for Test Soil 5 - TSA (continued)

Tests ID	w (%)	$g_d (kN/m^3)$	S (%)	f_{UU} (deg)	C_{UU} (kPa)	ν	E_{50} (MPa)	H (m)	slope	crest deformation (cm)
S5-UU10 S5-UU11 S5-UU12	14.5	16.7	63.2	23	149	0.3785	13.260 14.241 15.150	12.2	1H:1V	1.82
									2H:1V	1.79
									3H:1V	1.78
									4H:1V	1.77
								9.1	1H:1V	1.35
									2H:1V	1.33
									3H:1V	1.32
									4H:1V	1.32
								6.1	1H:1V	0.91
									2H:1V	0.90
									3H:1V	0.89
									4H:1V	0.89
								3.0	1H:1V	0.45
									2H:1V	0.45
									3H:1V	0.45
									4H:1V	0.45

Table F.5. Embankment crest deformation for Test Soil 5 - TSA (continued)

Tests ID	w (%)	$g_d (kN/m^3)$	S (%)	f_{UU} (deg)	C_{UU} (kPa)	ν	E_{50} (MPa)	H (m)	slope	crest deformation (cm)
S5-UU13 S5-UU14	16.8	17.0	76.2	34	94	0.3031	7.933 13.119	12.2	1H:1V	3.26
									2H:1V	3.15
									3H:1V	3.11
									4H:1V	3.11
								9.1	1H:1V	2.51
									2H:1V	2.49
									3H:1V	2.49
									4H:1V	2.45
								6.1	1H:1V	1.81
									2H:1V	1.79
									3H:1V	1.79
									4H:1V	1.79
								3.0	1H:1V	0.99
									2H:1V	0.99
									3H:1V	0.99
									4H:1V	0.99

Table F.5. Embankment crest deformation for Test Soil 5 - TSA (continued)

Tests ID	w (%)	$g_d (kN/m^3)$	S (%)	f_{UU} (deg)	C_{UU} (kPa)	ν	E_{50} (MPa)	H (m)	slope	crest deformation (cm)
S5-UU16 S5-UU17 S5-UU18	20.1	16.5	84.7	29	75	0.3421	6.005 7.555 9.158	12.2	1H:1V	3.90
									2H:1V	3.79
									3H:1V	3.78
									4H:1V	3.77
								9.1	1H:1V	2.96
									2H:1V	2.94
									3H:1V	2.93
									4H:1V	2.93
								6.1	1H:1V	2.10
									2H:1V	2.08
									3H:1V	2.07
									4H:1V	2.07
								3.0	1H:1V	1.12
									2H:1V	1.12
									3H:1V	1.12
									4H:1V	1.12

Table F.5. Embankment crest deformation for Test Soil 5 - TSA (continued)

Tests ID	w (%)	$g_d (kN/m^3)$	S (%)	f_{UU} (deg)	C_{UU} (kPa)	ν	E_{50} (MPa)	H (m)	slope	crest deformation (cm)
S5-UU25 S5-UU27	11.3	17.2	52.8	29	158	0.3369	12.869 18.531	12.2	1H:1V	1.91
									2H:1V	1.87
									3H:1V	1.86
									4H:1V	1.86
								9.1	1H:1V	1.45
									2H:1V	1.42
									3H:1V	1.42
									4H:1V	1.42
								6.1	1H:1V	1.01
									2H:1V	1.00
									3H:1V	1.00
									4H:1V	1.00
								3.0	1H:1V	0.54
									2H:1V	0.53
									3H:1V	0.53
									4H:1V	0.53

Table F.5. Embankment crest deformation for Test Soil 5 - TSA (continued)

Tests ID	**w (%)**	$g_d (kN/m^3)$	**S (%)**	f_{UU} **(deg)**	C_{UU} **(kPa)**	**ν**	E_{50} **(MPa)**	**H (m)**	**slope**	**crest deformation (cm)**
S5-UU28 S5-UU29 S5-UU30	9.4	16.8	41.3	43	91	0.2430	12.045 16.050 20.479	12.2	1H:1V	2.58
									2H:1V	2.56
									3H:1V	2.55
									4H:1V	2.55
								9.1	1H:1V	2.02
									2H:1V	2.01
									3H:1V	2.01
									4H:1V	2.01
								6.1	1H:1V	1.48
									2H:1V	1.48
									3H:1V	1.46
									4H:1V	1.46
								3.0	1H:1V	0.80
									2H:1V	0.80
									3H:1V	0.80
									4H:1V	0.80

APPENDIX G: Deformation Tables for Effective Stress Analysis (CU Triaxial Parameters)

G1: Deformation Tables for Test Soil 1 – Effective Stress Analysis (CU Triaxial Parameters)

Table G.1. Embankment crest deformation for Test Soil 1 - ESA

Tests ID	w (%)	$g_d (kN/m^3)$	S (%)	f' (deg)	C' (kPa)	ν	E_{50} (MPa)	H (m)	slope	crest deformation (cm)
S1-CU1 S1-CU2 S1-CU3	22.5	16.7	≈ 100	33	16	0.3160	1.399 2.663 4.213	12.2	1H:1V	12.92
									2H:1V	12.37
									3H:1V	12.08
									4H:1V	12.07
								9.1	1H:1V	10.80
									2H:1V	10.27
									3H:1V	10.12
									4H:1V	10.11
								6.1	1H:1V	7.89
									2H:1V	7.51
									3H:1V	7.51
									4H:1V	7.50
								3.0	1H:1V	4.91
									2H:1V	4.89
									3H:1V	4.89
									4H:1V	4.89

G2: Deformation Tables for Test Soil 2 – Effective Stress Analysis (CU Triaxial Parameters)

Table G.2. Embankment crest deformation for Test Soil 2 - ESA

Tests ID	w (%)	$g_d (kN/m^3)$	S (%)	f' (deg)	C' (kPa)	ν	E_{50} (MPa)	H (m)	slope	crest deformation (cm)
S2-CU1 S2-CU3	35.2	13.8	≈ 100	28	4	0.3490	1.843 6.246	12.2	1H:1V	8.68
									2H:1V	8.09
									3H:1V	7.97
									4H:1V	7.65
								9.1	1H:1V	6.59
									2H:1V	6.48
									3H:1V	6.48
									4H:1V	6.45
								6.1	1H:1V	5.07
									2H:1V	5.01
									3H:1V	5.01
									4H:1V	4.98
								3.0	1H:1V	3.15
									2H:1V	3.04
									3H:1V	3.04
									4H:1V	3.04

Table G.2. Embankment crest deformation for Test Soil 2 - ESA (continued)

Tests ID	w (%)	$g_d (kN/m^3)$	S (%)	f' (deg)	C' (kPa)	ν	E_{50} (MPa)	H (m)	slope	crest deformation (cm)
S2-CU4 S2-CU5 S2-CU6	21.6	17.1	≈ 100	29	38	0.3377	3.677 5.279 7.585	12.2	1H:1V	5.47
									2H:1V	5.22
									3H:1V	5.20
									4H:1V	5.03
								9.1	1H:1V	4.18
									2H:1V	4.11
									3H:1V	4.10
									4H:1V	4.09
								6.1	1H:1V	3.08
									2H:1V	3.02
									3H:1V	3.02
									4H:1V	3.01
								3.0	1H:1V	1.76
									2H:1V	1.75
									3H:1V	1.75
									4H:1V	1.75

Table G.2. Embankment crest deformation for Test Soil 2 - ESA (continued)

Tests ID	w (%)	$g_d (kN/m^3)$	S (%)	f' (deg)	C' (kPa)	ν	E_{50}(MPa)	H (m)	slope	crest deformation (cm)
S2-CU7 S2-CU8 S2-CU9	20.9	17.3	≈ 100	29	46	0.3430	5.378 10.174 12.972	12.2	1H:1V	3.16
									2H:1V	2.94
									3H:1V	2.93
									4H:1V	2.93
								9.1	1H:1V	2.40
									2H:1V	2.37
									3H:1V	2.37
									4H:1V	2.36
								6.1	1H:1V	1.82
									2H:1V	1.78
									3H:1V	1.78
									4H:1V	1.77
								3.0	1H:1V	1.06
									2H:1V	1.05
									3H:1V	1.05
									4H:1V	1.05

G3: Deformation Tables for Test Soil 3 – Effective Stress Analysis (CU Triaxial Parameters)

Table G.3. Embankment crest deformation for Test Soil 3 - ESA

Tests ID	w (%)	$g_d (kN/m^3)$	S (%)	f' (deg)	C' (kPa)	ν	E_{50} (MPa)	H (m)	slope	crest deformation (cm)
S3-CU1 S3-CU2 S3-CU3	34.7	13.7	≈ 100	31	5	0.3284	1.440 2.207 4.823	12.2	1H:1V	12.77
									2H:1V	12.11
									3H:1V	12.11
									4H:1V	12.10
								9.1	1H:1V	10.75
									2H:1V	10.15
									3H:1V	10.13
									4H:1V	9.97
								6.1	1H:1V	7.96
									2H:1V	7.48
									3H:1V	7.47
									4H:1V	7.46
								3.0	1H:1V	4.82
									2H:1V	4.80
									3H:1V	4.80
									4H:1V	4.80

Table G.3. Embankment crest deformation for Test Soil 3 - ESA (continued)

Tests ID	**w (%)**	$g_d (kN/m^3)$	**S (%)**	f' **(deg)**	C' **(kPa)**	**ν**	E_{50} **(MPa)**	**H (m)**	**slope**	**crest deformation (cm)**
S3-CU4 S3-CU5 S3-CU6	29.7	14.7	≈ 100	37	0	0.2821	1.591 1.632 4.590	12.2	1H:1V	16.89
									2H:1V	16.83
									3H:1V	16.20
									4H:1V	15.99
								9.1	1H:1V	14.27
									2H:1V	13.72
									3H:1V	13.70
									4H:1V	13.43
								6.1	1H:1V	10.85
									2H:1V	10.21
									3H:1V	10.21
									4H:1V	10.21
								3.0	1H:1V	6.40
									2H:1V	6.39
									3H:1V	6.39
									4H:1V	6.39

Table G.3. Embankment crest deformation for Test Soil 3 - ESA (continued)

Tests ID	w (%)	$g_d (kN/m^3)$	S (%)	f' (deg)	C' (kPa)	ν	E_{50} (MPa)	H (m)	slope	crest deformation (cm)
S3-CU7 S3-CU8 S3-CU9	28.9	14.9	≈ 100	36	2	0.2928	1.627 2.625 4.203	12.2	1H:1V	13.88
									2H:1V	13.33
									3H:1V	13.17
									4H:1V	13.17
								9.1	1H:1V	11.09
									2H:1V	10.89
									3H:1V	10.88
									4H:1V	10.54
								6.1	1H:1V	8.34
									2H:1V	8.20
									3H:1V	8.20
									4H:1V	8.19
								3.0	1H:1V	5.13
									2H:1V	5.12
									3H:1V	5.12
									4H:1V	5.12

G4: Deformation Tables for Test Soil 4 – Effective Stress Analysis (CU Triaxial Parameters)

Table G.4. Embankment crest deformation for Test Soil 4 - ESA

Tests ID	w (%)	$g_d (kN/m^3)$	S (%)	f' (deg)	C' (kPa)	ν	E_{50} (MPa)	H (m)	slope	crest deformation (cm)
S4-CU1 S4-CU2 S4-CU3	46.3	11.9	≈ 100	32	10	0.3169	2.482 3.154 5.018	12.2	1H:1V	9.77
									2H:1V	9.42
									3H:1V	9.40
									4H:1V	9.39
								9.1	1H:1V	7.61
									2H:1V	7.41
									3H:1V	7.40
									4H:1V	7.32
								6.1	1H:1V	5.58
									2H:1V	5.52
									3H:1V	5.52
									4H:1V	5.51
								3.0	1H:1V	3.15
									2H:1V	3.14
									3H:1V	3.14
									4H:1V	3.14

Table G.4. Embankment crest deformation for Test Soil 4 - ESA (continued)

Tests ID	w (%)	$g_d (kN/m^3)$	S (%)	f' (deg)	C' (kPa)	ν	E_{50} (MPa)	H (m)	slope	crest deformation (cm)
S4-CU4 S4-CU5 S4-CU6	35.8	13.6	≈ 100	36	5	0.2908	2.433 3.493 5.994	12.2	1H:1V	9.95
									2H:1V	9.88
									3H:1V	9.87
									4H:1V	9.61
								9.1	1H:1V	8.00
									2H:1V	7.86
									3H:1V	7.85
									4H:1V	7.85
								6.1	1H:1V	5.85
									2H:1V	5.83
									3H:1V	5.83
									4H:1V	5.83
								3.0	1H:1V	3.57
									2H:1V	3.56
									3H:1V	3.56
									4H:1V	3.56

Table G.4. Embankment crest deformation for Test Soil 4 - ESA (continued)

Tests ID	**w (%)**	$g_d (kN/m^3)$	**S (%)**	f' **(deg)**	C' **(kPa)**	**ν**	E_{50} **(MPa)**	**H (m)**	**slope**	**crest deformation (cm)**
S4-CU7 S4-CU9	34.2	13.9	≈ 100	34	14	0.3056	2.306 5.322	12.2	1H:1V	9.81
									2H:1V	9.46
									3H:1V	9.45
									4H:1V	9.44
								9.1	1H:1V	7.78
									2H:1V	7.74
									3H:1V	7.53
									4H:1V	7.44
								6.1	1H:1V	5.79
									2H:1V	5.76
									3H:1V	5.72
									4H:1V	5.72
								3.0	1H:1V	3.35
									2H:1V	3.34
									3H:1V	3.34
									4H:1V	3.34

G5: Deformation Tables for Test Soil 5 – Effective Stress Analysis (CU Triaxial Parameters)

Table G.5. Embankment crest deformation for Test Soil 5 - ESA

Tests ID	w (%)	$g_d (kN/m^3)$	S (%)	f' (deg)	C' (kPa)	ν	E_{50} (MPa)	H (m)	slope	crest deformation (cm)
S5-CU1 S5-CU3	36.4	13.6	≈ 100	29	0	0.3412	1.632 4.056	12.2	1H:1V	11.36
									2H:1V	10.93
									3H:1V	10.77
									4H:1V	10.78
								9.1	1H:1V	8.83
									2H:1V	8.59
									3H:1V	8.56
									4H:1V	8.50
								6.1	1H:1V	6.50
									2H:1V	6.45
									3H:1V	6.43
									4H:1V	6.43
								3.0	1H:1V	3.89
									2H:1V	3.87
									3H:1V	3.87
									4H:1V	3.87

Table G.5. Embankment crest deformation for Test Soil 5 - ESA (continued)

Tests ID	w (%)	$g_d (kN/m^3)$	S (%)	f' (deg)	C' (kPa)	ν	E_{50} (MPa)	H (m)	slope	crest deformation (cm)
S5-CU4 S5-CU5 S5-CU6	32.8	14.3	≈ 100	32	3	0.3174	1.422 2.466 4.437	12.2	1H:1V	13.68
									2H:1V	12.48
									3H:1V	12.31
									4H:1V	12.30
								9.1	1H:1V	11.00
									2H:1V	10.32
									3H:1V	10.32
									4H:1V	10.27
								6.1	1H:1V	7.98
									2H:1V	7.93
									3H:1V	7.92
									4H:1V	7.91
								3.0	1H:1V	4.93
									2H:1V	4.92
									3H:1V	4.92
									4H:1V	4.92

Table G.5. Embankment crest deformation for Test Soil 5 - ESA (continued)

Tests ID	w (%)	$g_d (kN/m^3)$	S (%)	f' (deg)	C' (kPa)	ν	E_{50}(MPa)	H (m)	slope	crest deformation (cm)
S5-CU7 S5-CU9	31.8	14.5	≈ 100	43	0	0.2395	1.447 4.007	12.2	1H:1V	19.37
									2H:1V	19.07
									3H:1V	19.07
									4H:1V	19.06
								9.1	1H:1V	15.71
									2H:1V	15.41
									3H:1V	15.41
									4H:1V	15.40
								6.1	1H:1V	12.12
									2H:1V	12.11
									3H:1V	12.11
									4H:1V	12.11
								3.0	1H:1V	7.61
									2H:1V	7.61
									3H:1V	7.61
									4H:1V	7.61

APPENDIX H: Sensitivity Analysis of Deformation Calculations

A brief sensitivity analysis on maximum crest settlement of embankment is presented in this appendix. Investigated parameters include size of the mesh, mesh type, and Poisson's ratio. This appendix is in line with "deformation analysis" chapter.

Effect of Size of the Mesh

In the original analysis, the mesh size was selected equal to 1m. Table H.1 summarizes information regarding effect of mesh size on the maximum settlement of crest. As it could be anticipated, as size of mesh increases maximum settlement decreases but the change is not very significant.

Table H.1. Effect of mesh size on maximum deformation of crest

mesh size (m)	max. deformation of crest (cm)
1	6.88
2	6.87
5	6.84
10	6.62

Effect of Type of Mesh

As stated in the "deformation analysis" chapter, mesh type was selected quads & triangles in the original analysis. Table H.2 lists different types of available meshes in the software as well as their effect on the maximum settlement of crest. As expected, it is obvious that the influence is not very considerable.

Table H.2. Effect of mesh type on maximum deformation of crest

Mesh type	max. deformation of crest (cm)
triangles only	6.88
quads & triangles	6.88
rectangular grid of quads	6.88
triangular grid of quads / triangles	6.90

Effect of Poisson's Ratio

Contrary to mesh size and mesh type, Poisson's ratio seems to be more influential factor in the analysis process. Table H.3 presents effect of Poisson's ratio on maximum settlement of crest, and Figure H.1 depicts same information. It can be seen that with increase in Poisson's ratio vertical settlement decreases dramatically. Highlighted number in the table was used in the original model. It was selected such that it results in a K_0 value in agreement with laboratory results/empirical equations.

On the other hand, it was seen that the amount of heave increases with increasing Poisson's ratio. This latter seems reasonable as increase in Poisson's ratio means more lateral deformation on the sides of embankment. This fact also results in more heave on those spots. In fact, as Poisson's ratio get closer to 0.5 volumetric strain approaches zero, with ε_z already being zero as a result of 2D plain strain analysis, higher lateral strain/deformation must indicate lower vertical strain/deformation.

Table H.3. Effect of Poisson's ratio on maximum settlement of crest

Poisson's ratio	max. settlement of crest (cm)
0.30	8.7
0.35	7.6
0.3786	6.9
0.40	6.3
0.45	4.8
0.49	3.3

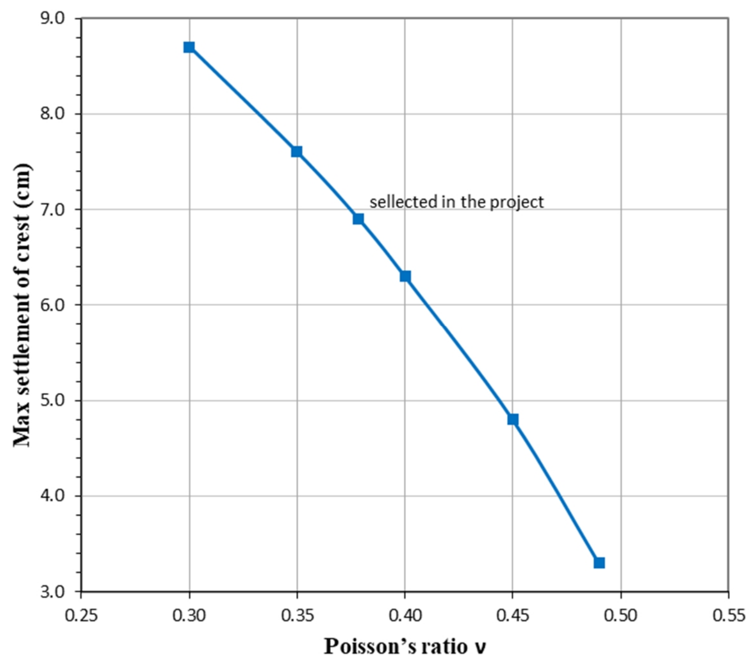

Figure H.1. Effect of Poisson's ratio on maximum settlement of crest

APPENDIX I: Procedure to Obtain Elasticity Modulus for Deformation Considerations

Elasticity modulus of the soil is a parameter that is representative of the soil strength and bearing capacity. This parameter is also required for deformation analyses. Elasticity modulus can be obtained from different laboratory tests including UU triaxial tests. Figure I.1 shows a typical stress-strain curve from a UU triaxial compression test. According to Das (2008), different elasticity moduli may be defined as follows:

- Initial tangent modulus, E_i
- Tangent modulus at a given stress level, E_t
- Secant modulus at a given stress level, E_s

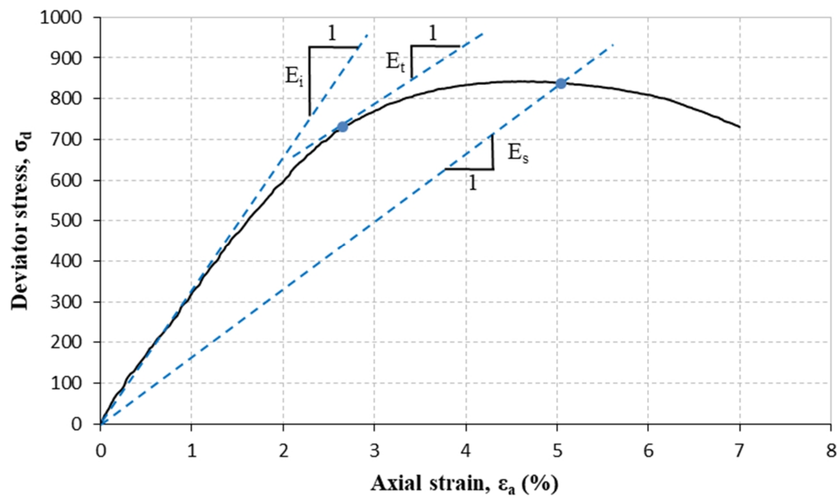

Figure I.1. Schematic definition of different soil moduli from triaxial test results (modified after Das 2008)

According to Das (2008), when the modulus of elasticity for a given soil is quoted in ordinary geotechnical problems, it is meant to be the secant modulus from zero to about half the maximum / failure deviator stress ($\frac{1}{2} * s_{df}$) which is denoted by E_{50}. Definition of E_{50} is schematically depicted in Figure I.2. In the geotechnical literature it is common to infer stiffness of soil specimens from measurements of the secant modulus E_{50} (Chen 2010; Wiebe et al. 1998). Hence, in this research E_{50} has been used for engineering properties, and deformation calculations in both TSA and ESA. That is, the modulus of elasticity which is presented throughout this document and is obtained either from the UU triaxial tests (E_{UU}), or from the CU triaxial tests (E_{CU}) is from the type of E_{50} that just introduced. It is noted that the parameter E_{50} itself is a function of some variables such as specimen moisture content, specimen dry unit weight, soil type, cell pressure and so on.

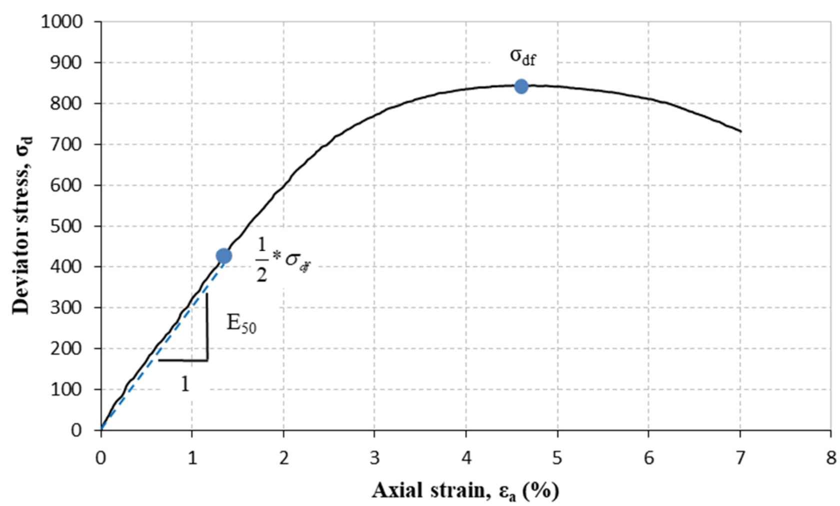

Figure I.2. Schematic definition of E_{50}- commonly used in ordinary geotechnical problems as soil modulus of elasticity